INFORMATION TO USERS

This manuscript has been reproduced from the microfilm master. UMI films the text directly from the original or copy submitted. Thus, some thesis and dissertation copies are in typewriter face, while others may be from any type of computer printer.

The quality of this reproduction is dependent upon the quality of the copy submitted. Broken or indistinct print, colored or poor quality illustrations and photographs, print bleedthrough, substandard margins, and improper alignment can adversely affect reproduction.

In the unlikely event that the author did not send UMI a complete manuscript and there are missing pages, these will be noted. Also, if unauthorized copyright material had to be removed, a note will indicate the deletion.

Oversize materials (e.g., maps, drawings, charts) are reproduced by sectioning the original, beginning at the upper left-hand corner and continuing from left to right in equal sections with small overlaps.

Photographs included in the original manuscript have been reproduced xerographically in this copy. Higher quality 6" x 9" black and white photographic prints are available for any photographs or illustrations appearing in this copy for an additional charge. Contact UMI directly to order.

Bell & Howell Information and Learning
300 North Zeeb Road, Ann Arbor, MI 48106-1346 USA

UMI®
800-521-0600

VARIABLE SOURCE AREA MODELING IN URBAN AREAS

By

CATERINA VALEO, B.Sc., B.A.Sc., M.Eng.

A Thesis

Submitted to the School of Graduate Studies

in Partial Fulfilment of the Requirements

for the Degree

Doctor of Philosophy

McMaster University

VARIABLE SOURCE AREA MODELING IN URBAN AREAS

DOCTOR OF PHILOSOPHY (1998)
(Civil Engineering)

McMaster University
Hamilton, Ontario

TITLE: Variable Source Area Modeling in Urban Areas

AUTHOR: Caterina Valeo, B.Sc., B.A.Sc. (Toronto), M.Eng. (McMaster)

SUPERVISOR: Professor I. K. Tsanis

NUMBER OF PAGES: xxiv, 302, A.47

ABSTRACT

A variable source area model called TOPMODEL was modified to incorporate urban areas in both the topographic index and the mechanism of surface runoff generation. The revised model was applied to a small catchment in the Hamilton-Wentworth area. A Geographic Information System was utilized to delineate the Ancaster Creek Catchment and produce Digital Elevation Models (DEM). FORTRAN programs in conjunction with the DEM were used to compute topographic indices that explicitly accounted for urban areas. Additional FORTRAN programs were modified to determine flow rates from this semi-urbanized catchment. Model testing was conducted in three phases: 1) a study of aggregation and scale effects using a partially revised model (TOPURBAN v. 1) on three separate time periods; 2) a fully revised model (TOPURBAN v. 2) tested on six time periods; 3) comparisons between a conventional Hortonian flow model and TOPURBAN v. 2.

Ten different DEM sizes were used to compute topographic indices and TOPURBAN v. 1 was applied during the snow-free period of a wet, dry and median year. Four separate parameters were optimized. The results indicated that three of the four calibrated parameters varied only slightly with DEM size but the hydraulic conductivity increased with increasing grid cell size. Twenty-one statistics were computed to evaluate TOPURBAN v. 1's performance for predicting flow with regard to DEM size. The statistics indicated that the DEM size of 50 m produces the most optimum conditions for the best TOPURBAN v. 1 performance. TOPURBAN v. 1 was later modified to create TOPURBAN v. 2 which better accounted for the storage in urban areas that was not considered in version 1. The new version added an additional calibration parameter and was tested on 6 data series in total. TOPURBAN v. 2 increased Nash and Sutcliffe Efficiency by anywhere from 2% to 8%. This increase proves that TOPURBAN v. 2 is a suitable model for combining urban areas into a hillslope hydrology scheme.

TOPURBAN v.2 was compared to the conventional Hortonian-Flow model QualHYMO, on all 6 continuous series, on two single events, and on the regional storm. TOPURBAN v. 2 out-performed QualHYMO in the single event tests and in the continuous series simulations by anywhere from 20% - 80% in Nash and Sutcliffe Efficiency. Estimates of peak flow rate for the regional storm were within roughly 35% of the estimate provided by MacLaren Plansearch Ltd. in the Spencer Creek Watershed Study that included the Ancaster Creek Catchment.

ACKNOWLEDGMENTS

This work could not have been completed without the assistance of many individuals and organizations. Firstly, I would like to thank those agencies that funded this work: The National Science and Engineering Research Council of Canada, and the Ontario Graduate Scholarship Program. I would also like to thank McMaster University and the Department of Civil Engineering for providing the infrastructure to conduct this work.

I am indebted to Dr. S. M. A. Moin and Dr. J. Vlachopoulos of my supervisory committee. Dr. Moin's technical expertise was invaluable as well as his insight, interest and guidance, which were always helpful. I am also very grateful to Dr. Vlachopoulos, who was always accommodating and always knew just what questions to ask. I would also like to ask the members of my defense committee: Dr. J. Marsalek, Dr. J. Drake, Dr. L. King and Dr. M.K. Woo.

There are a number of people who provided free data and advice. I would like to thank Tony Horvat of the Hamilton Conservation Authority for providing rain gauge data and many useful notes; Mark Stirrup of the Regional Municipality of Hamilton-Wentworth for additional rain gauge data; Susan Saunders of Environment Canada for providing hydrometric data; Marinus Abrahamse of Environment Canada for his insight and assistance; and Brian Bishop of Philips Environmental Planning.

I would also like to mention a particular trio from CIS: Todd Pfaff, Patricia Monger and Mark Hollamby-Lane. Thanks for all the assistance and for your prompt service on both major and minor problems. Thanks also to Gail Britton and Debbie Smaluck for their administrative support during my graduate student career.

I would also like to acknowledge the contributions to my academic development by

several professors in the Department of Civil Engineering. I must make particular mention of Dr. A. Ghobarah and Dr. J. C. Wilson. Thank you for all your support.

I have had the good fortune of meeting some wonderfully supportive friends that have provided wisdom, many laughs and good company. A million thanks go to Patricia Barker, John Copp, Aaron (K'Plah!) Farrell, Grace Ferracuti, Prosenjit Mitra, Huihua Shen, Kathie Siriunas and Jian Wu. I would in particular like to thank Pearl Zheng for making my experience at McMaster a joy to look back on. You're an awesome badminton player and a great friend. I would also like to thank Anne Siriunas for her financial support during some tougher times.

Lastly, I would like to thank my wonderful husband Kristofer Siriunas who encouraged and supported me through years of highs and lows. Thank you Gorgeous.

TABLE OF CONTENTS

LIST OF FIGURES

LIST OF TABLES

LIST OF SYMBOLS, FUNCTIONS AND ABBREVIATIONS

Symbols

English Alphabet (uppercase followed by lowercase letters)

A	drainage area (m^2 or km^2)
A_c	fraction of catchment area contributing to saturation excess overland flow
Ac	variable source area (m^2)
A_i	surface area of column i (m^2)
A_i'	upslope area draining into cell i (m^2)
A_s	cross-sectional surface area of flow (m^2)
ABS_i^t	initial abstraction from impervious area at time t (mm)
ABS_p^t	initial abstraction from pervious area at time t (mm)
API^t	Antecedent Precipitation Index at time t (mm)
API_k	Antecedent Precipitation Index constant
B	channel surface width (m)
B_W	watershed parameter in Williams and Hahn Unit Hydrograph method
C	soil water capacity (m^{-1})
CN	Curve Number
$CN(X_p)$	Curve Number related to exceedence probability X_p
D	duration of rainfall (hr)
D_{avg}	average absolute difference between observed and predicted rainfall during rain events (%)
D_{ji}	distance between gauge j and cell i (m)
D_{max}	average absolute difference between observed and predicted rainfall during rain events (%)
D_{min}	average absolute difference between observed and predicted rainfall during rain events (%)
E	Nash and Sutcliffe Efficiency
Ea_i^t	actual evapotranspiration of column i at time t (m/hr)
Ep^t	potential evapotranspiration of at time t (m/hr)
ET	total evapotranspiration (m)
ET_o	reference (potential) evapotranspiration (m/day)
F	objective function (m^2)
F_o	no model value of F (m^2)
F_{CHV}	calibration factor for channel flow velocity

F_{RV}	calibration factor for overland flow velocity
F(t)	cumulative infiltration (cm)
G	subsurface through flow (m)
G_f	soil heat flux ($Mjm^{-2}d^{-1}$)
H(x,y,t)	saturated zone thickness (m)
HT	elevation drop from catchment divide to outlet (m)
I	total interception (mm)
I^τ	inflow to urban storage at time τ (mm/hr)
K	hydraulic conductivity (m/hr or cm/hr)
$K(S_i^t)$	hydraulic conductivity as a function of saturation deficit of column i at time t (m/hr)
$K(\theta,z)$	hydraulic conductivity as a function of soil moisture content θ and depth z (m/hr)
Ko	catchment average saturated hydraulic conductivity at the surface (m/hr)
Ko_i	saturated hydraulic conductivity at the surface for column i (m/hr)
$K_x(x,y)$	unsaturated hydraulic conductivity in x direction (m/hr)
$K_y(x,y)$	unsaturated hydraulic conductivity in y direction (m/hr)
L	hydraulic length of longest drainage path (km)
L_s	twice the length of streams (m)
N	number of points in series
N_c	number of downslope neighbouring cells of a cell
N_E	number of elements in catchment for RDS method
N_P	number of test points
N_R	number of rain gauges in RDS method
N_{RV}	number of flow path segments
N_{nac}	total number of $\ln(a/\tan\beta)_i$ classes
O	reservoir outflow (m^3/s)
O_{nN}	outflow from last reservoir (m^3/s)
$\bar{P}$	areal average precipitation across the catchment (m/hr or mm/hr)
P	total precipitation (m/hr or mm/hr or m)
P_a	atmospheric pressure (mbar)
P_e	excess precipitation (m/hr or mm/hr or inches)
P_i	rainfall observed at gauge i (m)
P^t	rainfall at time t (m/hr)
P^τ	rainfall at time τ (m/hr)
Q	discharge (m/hr or cms)
Qb^t	total baseflow at time t (m/hr or m^3/hr or m^3/s)

Q_b^t	baseflow in QualHYMO (cms)
Q_{min}	user specified minimum baseflow (cms)
Q_o	initial flowrate (m/hr or m^3/hr)
$Q_{obs}(t)$	observed discharge at time t (m/hr or m^3/hr)
Qov^t	total overland flow at time t (m/hr or m^3/hr)
Q_p	peak discharge (m/hr, cfs, m^3/s)
Q_p^t	discharge rate in pervious areas (cms)
$Q_{pred}(t)$	predicted discharge at time t (m/hr or m^3/hr)
Q_{uS}^{τ}	outflow from urban storage at time τ (m/hr)
Q_s	surface flowrate (m^3/s)
Q_{To}	initial predicted baseflow (m^3/hr)
Qu^t	total vertical unsaturated flow at time t (m/hr or m^3/hr)
Qu_i^t	vertical unsaturated flow at column i at time t (m/hr or m^3/hr)
Qu^0	total vertical unsaturated flow at time 0 (m/hr or m^3/hr)
$Qurb^t$	urban area flow at time t (m/hr or m^3/hr)
R	surface water through flow (m)
$\bar{R}$	average rainfall across catchment (mm)
R_i	constant volumetric runoff coefficient
R_n	net radiation at crop surface ($MJm^{-2}d^{-1}$)
R(x,y,t)	instantaneous vertical recharge into the unsaturated zone (m/hr)
R^2	variance
RT	return period (yrs)
S	reservoir storage (m^3)
S_{sink}	source/sink term for root extraction and soil evaporation (m)
S_k	calibration parameter in API method
S_d^t	saturation deficit when water table is at depth Z_d^t (m)
S_{fx}	friction slope in x-direction
S_{fy}	friction slope in y-direction
S_i^t	saturation zone deficit in column i at time t (m)
$S_.^t$	loss parameter at time t (mm)
$S_.(X_p)$	$S_.$ corresponding to exceedence probability X_p (mm)
S_{max}	maximum of $S_.^t$ (mm)
S_{min}	minimum of $S_.^t$ (mm)
S_{uQ}^{τ}	water held in urban storage at time τ (m)
Sr_{max}	maximum size of root zone for catchment (m)
Sr_i^t	root zone deficit in column i at time t (m)
Sr^t	catchment root zone deficit at time t (m)

Sr^0	catchment root zone deficit at time 0 (m)
Su_i^t	saturated zone storage in column i at time t (m)
S_o	ground slope
S_{ox}	ground slope in x-direction
S_{oy}	ground slope in y-direction
S_s	sorptivity parameter of the soil (cm $hr^{1/2}$)
S_r	maximum catchment retention (inches)
$\bar{S}^t$	average catchment soil moisture deficit at time t (m)
S(x,y)	specific yield
T	average temperature (°C)
T_d	time constant (hr/m)
To	catchment transmissivity of saturated soil at the surface (m^2/hr)
To_i	transmissivity of saturated soil at the surface for column i (m^2/hr)
T_{RV}	time it takes for runoff to reach basin outlet (hr)
$T(S_i^t)$	transmissivity of the soil in column i at time t (m^2/hr)
U_2	wind-speed measured at 2 metres height (m/s)
V	total hydrograph volume (m^3)
V_{bo}	initial value of groundwater storage depth (mm)
V_b^t	depth of water in groundwater reservoir at time t (mm)
V_i^t	cumulative depth of runoff at time t from impervious areas (mm)
V_p^t	cumulative depth of runoff at time t from pervious areas (mm)
X	wedge storage
X_d	distance downslope (m)
X_p	exceedence probability
Z_d^t	low depth of water table at time t (m)
a	interception constant
a_i	up-slope area draining through column i per unit width (m)
a_i'	treated up-slope area draining through column i per unit width (m)
b	interception constant
c	flow velocity (m/s)
c_x	flow velocity in x-direction (m/s)
c_y	flow velocity in y-direction (m/s)
d_r	relative earth-sun distance (km)
e_a	saturation vapour pressure at T (kPa)
e_d	actual vapour pressure at T (kPa)
f(t)	infiltration rate into soil (cm/hr)
f_c	asymptotic constant rate of infiltration (cm/hr)

f_o	initial value of infiltration (cm/hr)
f_{UA}	urban area fraction
h_d	surface water depth (m)
h(x,y,t)	phreatic surface level (m)
i	column index
j	rain gauge index
k	flow path segment index
k_2	baseflow constant
k_b	baseflow recession constant (mm/(mm*sec))
k_H	Horton's infiltration recession constant (hr)
k_N	Nash recession constant (hr)
k_W	Williams and Hahn recession constant (hr)
k_{lr}	linear reservoir recession constant (s)
lc_i	cross-sectional length of volume flow (m)
l_{id}	distance between center of cell i and downslope cell centre d (m)
l_k	length of flow path segment (m)
m	recession parameter (m)
n	Manning's n
nac	index of $\ln(a/\tan\beta)_i$ class
n_N	number of Nash reservoirs
n_W	dimensionless parameter in Williams and Hahn Unit Hydrograph method
q	stream flow per unit width (cms)
q_i	lateral saturated flow through column i (m^2/hr)
q_i^t	flow per unit width through column i at time t (m/hr or m^2/hr)
q_s	surface discharge per unit width (m^2/hr or ft^2/hr)
r	downslope cell index
t	time (hr)
t_c	time of concentration (hr)
t_{io}	time to inflection point on hydrograph (hr)
t_l	lag time (hr)
t_o	time zero (hr)
t_p	time to peak (hr)
u	discharge in Williams and Hahn Unit Hydrograph method (cfs)
u_l	discharge at $(t_{io} + k_W)$ (cfs)
u_o	initial discharge in Williams and Hahn Unit Hydrograph method (cfs)
u_p	peak discharge in Williams and Hahn Unit Hydrograph method (cfs)
uacp	urban area calibration parameter

v_a	total volume of water beneath hydrograph (m^3)
v_b	total volume of water beneath baseflow separation line (m^3)
v_j	volume of rainfall falling on element j
v_{RV}	velocity of runoff (m/hr)
w_i	weight assigned to each gauge in RDS method
x	space coordinate orthogonal to y (m)
y	space coordinate orthogonal to x (m)
y_i^p	interpolated elevation at grid cell i (m)
y_i^t	true elevation at grid cell i (m)
y_{sf}	depth of surface flow (inches)
z	vertical space coordinate (m)
z_i^t	elevation difference between ground surface and phreatic surface at time t (m)
zk	TOPURBAN v. 2 recession parameter (hr)

Greek Alphabet (uppercase followed by lowercase letters)

Δ	slope vapour pressure curve ($kPa°C^{-1}$)
$\Delta(A_i')$	total upslope area that is distributed to the downslope neighbouring cell r (m^2)
$\Delta S_{(s+g)}$	net change in storage of water in the surface and subsurface regions of a drainage area (m)
$\Delta\theta$	change in volumetric water content
Δx	reach length (m)
Δt	change in time (hrs)
Σ	sum of squares for peak rain events (m^2)
$\Sigma 1$	sum of absolute difference in peak rain events (m)
Σ^o	initial water balance value for catchment (m)
ψ	soil moisture tension or pressure head (m)
β_i	slope of column i surface
γ	psychometric constant ($kPa°C^{-1}$)
$\bar{\gamma}$	average value of soil topographic index over catchment
η	interception constant
θ	volumetric water content
θs_i^t	saturated zone moisture content of column i at time t
θs_i^t	residual moisture content of column i at time t
λ_i	topographic index at column i
$\bar{\lambda}$	average value of topographic index over catchment

σ^2	variance evaluation statistic (m^2)
ξ_i	elevation of column i (m)
ξ_d	elevation of downslope column d (m)
τ	time in urban component of TOPURBAN v. 2 (hr)

Functions

Γ	Gamma Function
Σ	Summation Sign
tan	Tan trigonometric function
ln	Naperian Logarithm
e	exponential function

Abbreviations

AES	Atmospheric Environment Service
AET	Actual Evapotranspiration
AIRPORT	The Hamilton Airport Meteorological Station
AMC	Antecedent Moisture Condition
API	Antecedent Precipitation Index
BFI	Base Flow Index
BOC	Basis of Comparison
CN	Curve Number
DEM	Digital Elevation Model
FAO	Food and Agricultural Organization
GIS	Geographic Information System
HRCA	Hamilton Region Conservation Authority
PET	Potential Evapotranspiration
RBG	Royal Botanical Gardens Meteorological Station
RDS	Reciprocal Distance Squared Method
REA	Representative Elementary Area
RMSE	Root Mean Square Error
SCS	Soil Conservation Service
UH	Unit Hydrograph
USGS	US Geological Survey

GLOSSARY

This glossary contains a few common terms in hydrology that may not be explicitly defined in the main text. It is only intended to familiarize those members of the examining committee that are not in the field of hydrology.

Baseflow: The flow that sustains streams during dry periods.

Deterministic Hydrologic Modeling: Hydrologic modeling that does not include a random component (as there would be in a stochastic model).

Groundwater Flow: Flow from the aquifer below the overburden.

Hydrograph: The distribution of streamflow in time.

Hyetograph: The distribution of rainfall intensity in time.

Interflow: Subsurface storm flow that contributes to the storm hydrograph.

Precipitation Excess: The resulting precipitation after losses have been subtracted.

Quickflow: The overland flow that contributes to the early and mid stages of the runoff hydrograph.

CHAPTER 1 INTRODUCTION

Engineering Hydrology is a vital part of effective water resources management. Flood mitigation, water supply for irrigation, sediment transport and water quality are all affected by water resources management. The basis of this management often involves the prediction of runoff volumes and streamflow rates from watersheds. Hydrological engineers have a plethora of predictive, deterministic tools at their disposal for this purpose. They range from the most simplistic models with gross assumptions about the system, to very complex and highly parameterized models intended to simulate the system "physically." Regardless of their complexity or the assumptions involved, all of these models endeavor to capture the runoff generating process that might explain measured observations. With regard to runoff and streamflow modeling, Cordova et al. (1983) sum it up well when they state, "the problem is more what to route than how to route." Determining "what to route" requires some understanding of the science of basin response.

Hydrology is a science that has been developing for more than a century with the fundamental goal of understanding the response of watersheds to precipitation. Hornberger et al. (1985) noted that "the development of such quantitative understanding has proved to be elusive because of the complexity of the processes, the difficulty of performing controlled experiments, and the spatial and temporal variability of catchment characteristics and precipitation." In fact, the "complex processes," the "experimental difficulties," and the "spatial and temporal variability" are all inter-related problems in hydrological modeling. The multitude of deterministic models that have been developed is a symptom of this fact. One good way to obtain a deeper understanding of these problems is to examine the approaches that over 100 years of scientific work has taken to develop all of these models. Not surprisingly, the approaches seem to vary in how they model the "complex processes," how they use field and laboratory data, and how they treat the "spatial

and temporal variability" of influencing factors. Before addressing these issues, a brief review of the categories of hydrologic models that are available is appropriate.

1.1 Model Categories

The *black-box* model uses non-physical parameters to modify a given input to some output. Black-box hydrologic models tend to have few parameters making them convenient to use and easy to calibrate. However, Abbott et al. (1986) noted that black-box models need long meteorological and hydrological records for calibration that are not always available; and because of the non-physical nature of the parameters used in the model, it is difficult to assess whether a calibrated parameter is appropriate since it cannot be measured in the field. How can an engineer predict the effects of land-use change using a model that does not physically represent the real system? Regardless of this, the conventional models in engineering hydrology for predicting runoff generation are primarily composed of black-box concepts such as baseflow separation and unit hydrograph techniques (Beven 1987a).

The other extreme is the *physically-based* model. A physically-based model is a type of model that simulates processes using equations derived from the physics governing the system and fundamental physical laws. This tends to make physically-based models naturally more attractive when compared to black-box models. The parameters have physical meaning and can theoretically be measured in the field. The models are generally very complex and involve numerous parameters. However, the use of these models and their appropriateness has recently come into question. Beven (1989b) claims that the theoretical advantages of physically-based models remain unproven in practice and that there is a tendency for users to give rise to "uncritical believe" in their predictions. Beven maintains that these physically-based models are "good descriptors" of processes occurring in well-defined, spatially homogenous, structurally fixed hillslopes in the laboratory. Therefore, like the black-

box model, even the most rigorous mathematical models are simplified representations of reality. They imply an accuracy that may not exist (Grayson et al. 1992).

A *quasi-physically based model*, also known as a *conceptual model*, is the middle-ground between black-box models and physically-based models. They have the convenience of only having to calibrate a few parameters, yet the parameters retain some physical meaning because the model has reduced the real system to a few basic physical principals that are representative of the system.

Another important characteristic of a model is how it treats the spatial and temporal variability in the real system. A *lumped* application assumes a homogeneous distribution of input values or basin characteristics. *Fully-distributed* models however, account for most or all the important heterogeneity that exists in the system by discretizing the system into individual units. Within these units, basin characteristics and inputs are treated in a lumped way. An example of such a discretization would be subbasins within the basin. Due to their nature, black-box models often involve lumped applications. Predictions resulting from lumped applications may compromise model accuracy because the averaging process may ignore important heterogeneity in the system. An example of a lumped parameter model is the Unit Hydrograph method in which the 'lumped parameter' is the time of concentration, which is held constant for all storms (Viessman et al. 1989).

Many physically-based models employ a fully-distributed approach which means that a great deal of data is required to run the model. Fully-distributed, physically-based models have benefitted from the increase in computer technology and the invention of Geographic Information Systems (GIS). GIS are sophisticated database management tools intended for large-amounts of spatial data and can assist in the otherwise difficult task of managing the data in fully-distributed modeling. However,

it is often likely that the data necessary for the application is not available, and this renders the complexity of the physically-based model profitless (Freeze 1974). The calibration and verification of the model will be affected by any errors that exist in the input data. All input data will have some degree of error and as the amount of data required by a model increases, the greater the effect of compounded errors. *Semi-distributed* applications represent a trade-off between the lumped and fully-distributed approaches. It hopes to capture the important influences contributing to runoff and provide "reasonable" accuracy.

1.2 Complex Processes - Runoff Generation and Soil Moisture Accounting

According to Islam (1996) the space-time distribution of soil moisture is a fundamental variable in rainfall-runoff models. Roughly 0.0001% of Earth's water is stored as soil moisture. "Yet this minuscule amount of water exerts significant control over various hydrological, ecological, and meteorological processes ranging from boundary layer dynamics to the global water cycle. The 1993 Mississippi River Flood illustrated the power of 0.0001% of Earth's water to dictate the fate and evolution of regional weather and climate" (Islam 1996). Therefore, some examination of how soil collects and retains moisture is required.

Figure 1.1 shows a block-diagram representation of the global hydrologic cycle. The movement of water occurs in various physical forms, through different mediums and at different relative speeds. Therefore, every block in the diagram has its own special modeling considerations. The hydrologic cycle is considered a closed loop and the amount of water within the loop is finite. Hydrologic models are often calibrated by measurements at gauges placed at the streamflow block. This produces an integrated measurement resulting from three very important processes within the hydrologic cycle: precipitation, evaporation/evapotranspiration and runoff (Becker et al. 1987).

A flowrate gauge (possibly measuring a stage that is converted to a runoff through a stage-discharge curve) will produce hydrographs of discharge versus time. A stream's runoff hydrograph produced by a rain event is often divided up into a baseflow component and a quickflow component. The quickflow, which is considered to be that portion contributing to the rising limb of the hydrograph, has traditionally been felt to be comprised of the surface water blocks in Figure 1.1 and is therefore, influenced by surface and soil characteristics. Baseflow was considered the subsurface moisture that sustained river flow in the inter-event period. Subsurface and groundwater flow were often lumped into baseflow. The separation of runoff into these categories has always been rather arbitrary (Dunne 1978), but the quantity of runoff contribution from either surface or subsurface flow does depend on the basin's characteristics. To determine where, how and when runoff from a rain event reaches the stream gauge, closer inspection of runoff generating mechanisms is required. One must begin at the hillslope scale.

One of the earliest models of runoff generation was Horton's model (Horton 1933). Horton viewed the soil as a separating surface between overland flow and all other components in the cycle. Generally, in Horton's model, if the intensity of the rain exceeds the soil's ability to absorb it, then the water is prevented from further entering the soil, collects on the surface, and flows downhill to become runoff. Any water that does infiltrate into the soil may enter the water table and show up as baseflow. Horton's model when first introduced was considered the dominant runoff generating mechanism that occurred over the entire basin. But *Hortonian overland flow* (also known as *infiltration excess overland flow*) was discovered to be only one of several types of runoff generating mechanisms and new models were being theorized from observations of basin response. Other runoff generating mechanisms are shown in Figure 1.2.

Eventually, the classic Horton model of overland flow has been questioned in areas

where infiltration capacities were high and where storm intensities were low (Carson et al. 1971). The causes of linear errors in estimates of excess runoff were hypothesized to be due to a partial contribution of catchment area to the hydrograph's peak and not the entire basin. The "part" of the catchment contributing to the hydrograph's peak was considered to be fixed and was termed the *partial-area concept* (Betson et al. 1969). Later, it was determined that these areas would swell and contract in size during the rain event and this was referred to as the *variable-source area concept* (Dunne et al. 1975; Freeze 1972; Gregory et al. 1973; O'Loughlin 1986; Troendle 1985). The variable-source area's position and rate of expansion was related to topography, soil type and rainfall characteristics (Dunne et al. 1970a). This is shown in Figure 1.3.

These source areas are saturated areas and any rainfall falling on these areas immediately becomes overland flow. *Saturation excess overland flow* occurs when the soil becomes saturated because the water table reaches the surface by rising up from below. *Return flow* occurs when any subsurface flow returns to the surface because of changes in topographic conditions (Dunne et al. 1970b). But overland flow is not necessarily the only contribution to quickflow. *Throughflow, interflow,* or *subsurface flow* all refer to flow that is completely sub-terrainian and flows laterally through the soil (Weyman 1970). For subsurface stormflow to occur, several conditions must exist: 1) sloping land; 2) a surface permeable soil; 3) a lower soil layer with a low permeability; and 4) saturated soil (Whipkey 1965). A phenomenon described as *saturation wedge flow* can occur if the soil is comprised of three soil horizons where there are two distinct changes in permeability. The drop in vertical permeability of the lowest horizon causes a saturated wedge of soil in the second horizon that contributes to flow (Weyman 1970). The effects of burrowing animals and decaying roots can result in the formation of large pores (macropores) or cracks that cause preferential pathways to cause stormflow contribution known as *piping*. Piping flow velocities greatly exceed the flow through the soil matrix (Beven

et al. 1982). Piping differs from macropore driven flow as it is considered to have larger connectivity and larger dimensions (Anderson et al. 1985). Regardless of this, piping and macropore flow are extremely difficult to model (Beven 1989a). Sklash et al. (1979) noticed that in catchments with low relief and high hydraulic conductivities, groundwater close to the surface was displaced by incoming rainfall causing groundwater to contribute to stormflow. This is sometimes called *piston-like displacement* (Quinn et al. 1993).

Two important factors influencing the formation of these runoff phenomena are observed to be soil characteristics and topography. Field studies have revealed that subsurface flow plays a very important role in the redistribution of soil moisture and for areas of relatively shallow soil, a dominant control on these subsurface flows, and the production of variable-source areas, was the local topography (Dunne 1978; Wood et al. 1990; Beven et al. 1983). Burt et al. (1985) describe a topographic control on soil moisture as points where convergence of soil water flowing into a hollow leads to the accumulation of soil water. When soil water storage is exceeded, the result is saturation excess. Low gradient slopes encourage soil saturation because of the low hydraulic gradient. O'Loughlin (1981) showed that "wet zones" that generate runoff are more likely to be generated in places where subsurface flow converges. Example calculations showed that both runoff and flood frequency predictions may be very sensitive to assumptions about the nature of the contributing source area (Beven 1986a). From this, it was concluded that a physically-based hydrologic model should have an adequate representation of the soil medium and its heterogeneity; adequate representation of land cover and its use; and incorporate changes in topography. Beven et al. (1983) suggested that contributing area dynamics may play an important role in the production of flood peaks. Furthermore, source area dynamics has been used to improve water quality economics by "liming" source areas instead of the entire catchment (Waters et al. 1991).

This section began with a general block-diagram of the hydrologic cycle and later downscaled to a hillslope scale representation of runoff generation. Cordova et al. (1983) state that "what remains as a crucial and unsolved problem, [in hydrological modeling] is the description of the infiltration process at a basin scale."

1.3 Spatial and Temporal Variability - The Scale Issue

It is worthwhile to clarify differences in the definition of scale between various disciplines. A 'large-scale' map in cartography implies that a map will depict fine features over a small area such as would be true in a large-scale map of 1:1,000. Conversely, a 'small-scale' map might have a scale of 1:100,000 in which large areas are shown but with little detail. Notice that the ratio of 1/100,000 is much smaller than the ratio of 1/1,000, hence the naming convention. In hydrology, however, 'large-scale' refers to large areas or the application of laws over large lengths. A small-scale application would be exemplified by the "laboratory scale".

A *catchment*, a *watershed* and a *basin* are each parcels of land that drain to a certain point. While not explicitly stated in the literature, generally, the terms are reserved for systems of various sizes with a catchment being smaller than a watershed, and a watershed being smaller than a basin. While there seems to be no established convention, a small catchment may be less than 10 km^2. A medium-sized watershed may be one between 10 and 1,000 km^2 and large basins are those in excess of 1,000 km^2. A *hillslope* is somewhat different than a catchment, but a catchment of zero-order is solely composed of hillslopes draining to a stream head (that is, there is no main channel). The hillslope is generally considered the smallest field unit for runoff generation. Song et al. (1992) show that different types of modeling occur at different scales. In the *laboratory scale* (which is smaller than the hillslope scale), models use only vertical dimensions while at the basin scale, models will use more sophisticated storage and translation techniques. The *continental scale* focuses on

the effect of atmospheric processes.

What exactly is the scale issue? Suppose we wanted to apply a hydrological model in a lumped manner to a small catchment and determine its runoff in which all parameters of basin response are averaged over the catchment. We then consider a larger catchment that encompasses the smaller one. What effect does an increase in application size have on the runoff generated? We might assume that the runoff would increase since a greater basin area is contributing to the predicted flow. But how would the input of areal precipitation has changed? If the areal precipitation for the event during modeling is an intense but small local thunderstorm, than the increase in catchment size would result in a change in the mean average precipitation over the catchment. Therefore, the change in scale of the application was affected by the spatial heterogeneity of the precipitation field. Suppose we applied the same hydrological model to a medium sized watershed but in a fully distributed way so that a great deal of the heterogeneity was captured for all the factors influencing runoff (precipitation, soil type, land-use type, etc). If we increase the watershed size again, will the model accurately predicted the runoff produced by the change in scale? That depends on the processes that were used by the model to generate the runoff. If these processes were empirically derived in a soil column from the laboratory, then the calibrated model may not predict well if there is an increase in application size, because the processes in the field are operating at a larger scale, i.e., over larger lengths. What was measured in the laboratory was a small section of the entire catchment and cannot capture all the complexity and variation in the physical movement of the moisture through the catchment. In terms of runoff generation, an increase in catchment spatial scale tends to "attenuate the complex, local patterns of runoff generation and water fluxes" (Wood et al. 1988).

Temporal scales deal with the time step of the application. How does modeling over an hourly time step differ from modeling over a monthly time step? If we were to

model a hydrograph from a storm that lasted half of a day at an hourly time step we might capture the moment of the true peak of the flood wave. If we were only interested in a monthly flowrate, then all the flow that occurred over the month would be lumped into one average value and we would never "see" the peak or a typical bell-shaped curve that we might imagine a hydrograph to have. Temporal scales of modeling can be as fine as a few minutes to as large as days or months, as well as involve the overall length of time the modeling takes place. It is this kind of modeling which will ignore certain seemingly important processes of runoff generation depending on what scale the modeler decides to model the catchment.

The importance of scale cannot be under-emphasized since it is recognized that the mathematical relationships describing physical phenomena in hydrology and other geophysical sciences are mostly scale dependent (Gupta et al. 1986). While the principle of mass conservation should apply, descriptions of flow processes will often depend on the specification of empirical parameters (such as hydraulic conductivities and roughness coefficients). These will depend on the structure and geometry of the flow pathways that are difficult to define. Watt (1989) notes that "little is known usually about the details of runoff generation and routing on a basin scale. Most discussion in the hydrological literature refers to laboratory scale plots. Because the basin wide process is not well understood, the magnitude of this source of uncertainty cannot generally be evaluated." In 1982, most of the available models of runoff production were lumped models of soil moisture accounting and were not amenable to addressing the problem of scale effects in catchment response in anything other than an empirical way (Islam 1996). This reiterates the fact that heterogeneity is at the heart of the scale issue. "There is a growing consensus that a unified approach is necessary to monitor, characterize and model soil moisture over a range of scales, but such an approach has yet to be defined" (Islam 1996). According to Beven (1991a), scale affects modeling and analysis of channel routing, hydrologic similarity, and storm runoff production.

One of the ways of dealing with scale issues is to determine what scales of application are suitable for what processes. Wood et al. (1988) presented the concept of a Representative Elementary Area (REA) to investigate how statistical behavior in runoff generation changes with increases in catchment scale. If the heterogeneity of properties in a catchment can be characterized by a statistical distribution, then a small hillslope area will only carry a small sample of the distribution. Neighbouring hillslopes will draw their characteristics from the same distribution but may respond differently due to differing characteristics. If the hillslope area increases, then the sample size increases and new larger neighbouring areas from the same distribution obtain similar characteristics. Eventually, above a certain scale, the sample size will be sufficient that it is no longer necessary to consider differences due to the pattern of characteristics within each area. The simple equations for runoff generation can be used instead of differential equations formulated at the laboratory scale. Famiglietti et al. (1994a, 1994b, 1995) investigated the REA concept and other issues of scale in a series of papers. A multiscale energy and water balance model was developed (1994a) and applied to a tall grass prairie (1994b). The model was then aggregated to determine the effects on water and energy balance. The authors concluded that an REA for evapotranspiration processes was approximately to 1-2 km^2.

One can see that there may be dangers in regional studies which assume hydrological similarity across scales. Similarity in this case is often based on "physioclimatic characterizations without explicit recognition of the environmental controls of runoff generation" (Wood et al. 1990). Developments into scaled models of runoff response have been examined along with parameterization of processes across a range of scales (Wood et al. 1990; Sivapalan et al. 1987). But Beven (1995) notes that the search for scale invariance may be futile especially if hydrologic response depends on a history that is subject to climate change, and this limits the potential for scale-invariant behaviour. Researchers may have to acknowledge the possibility that

scale-dependent model structures may be a necessity.

The sensitivity of physical models to the variation that exists within the modeling unit requires further study (Song et al. 1992). The problems that can result from the application of equations at inappropriate scales often involve parameter calibration (Beven 1989b).

1.4 Experimental Difficulties - Calibration

There is always some degree of misrepresentation in hydrologic models and verification is required to provide user confidence. Verification is usually preceded by calibrating certain parameters so that predicted flowrates match observable flowrates, and it is this calibration that essentially defines the model. Usually, calibrations are performed on one time period and the verification is performed on another. The parameters that are calibrated are usually those that influence the results the most. According to Beven's (1991b) experience, while a particular model may give poor results on one period, it may over a longer period of time provide better results. Calibrating over different time periods will result in changes to the calibration parameters. This leads to the question of which parameter set is correct. This illustrates the inherent flaw in the calibration process. To suddenly change a parameter's value without regard to the model's theoretical structure removes the physical meaning of the parameter and therefore, of the model (Beven 1987a).

Physically-based models are highly over-parameterized and when calibration is necessary it is not always obvious which ones should be adjusted. Parameter interaction "is inherent in the physics of hydrological systems and given the number of parameter values available in physically-based models, any optimization of parameters must be subject to far greater problems of interaction than simpler lumped models" (Beven, 1989b). Normally, the parameters that are calibrated are those that

have the highest influence on the results, while other less influential ones can be estimated from field values. Blackie and Eeles (1985) noted that "in all but the very simplest conceptual models some degree of interdependence is present between parameters. Thus in the optimization process, the parameter values achieved are not necessarily the best estimate of the physical values they normally represent but simply a set of numbers which gives the best fit to the data within the constraints imposed." Beven (1989b) believes that 3 to 5 parameters should be sufficient to reproduce most of the information in a hydrological record.

1.5 Urban Hydrology

Urban hydrology focuses on catchments with some degree of urbanization. Urbanization is characterized by an increase in impervious surface area caused by rooftops, roadways, sidewalks and other paved surfaces. The increase in impervious area causes a change in the natural drainage of the system where a greater proportion of rainfall becomes runoff, peak flows will normally increase and the timing of the runoff hydrograph is affected by an increase in flow velocities. The amount of soil moisture recharge is reduced, and as percolation to subsurface storage decreases, dry weather flow supported by this storage will decrease (Hall 1984). Obviously, modeling the flow over urban areas is radically different than modeling a soil matrix and even a small degree of urbanization can drastically affect a runoff hydrograph. Loague (1990) found that roads and trails that cut a catchment in his application were found to have a tremendous impact on the routing and short-circuiting of runoff. Hortonian flow was observed to occur on a compacted gravel road.

O'Loughlin et al. (1996) examined the state of rainfall-runoff modeling in urban hydrology. They outlined the theory of urban rainfall-runoff processes, modeling practices and the current use of computer models. The main points of their paper include:

- Climate, topography, geology, soils and vegetation have an important influence on the hydrological impacts of urban development.

- Urban impacts are greatest for low intensity storms because in rural areas, losses in small storms are relatively large but impervious areas will always produce runoff.

- The response from an impervious surface should be more predictable than that from a pervious surface, and in theory, the reliability of rainfall-runoff model results should increase with the percentage of impervious area.

- Urban rainfall-runoff models are primarily composed of a loss part and a routing part.

- Current limitations to urban rainfall-runoff models include inaccurate data and insufficient quantities of data.

- Different models are developed independently at different scales, but are often combined into one large unit. This creates model incompatibility problems.

The following research directions were recommended by O'Loughlin et al.:

- When combining models for urban areas and rural areas, research should study the appropriate levels of detail and the relationships between models of various scales.

- Model a catchment with some degree of urbanization at many scales.

- Include the spatial variability of rainfall in urban modeling.

- Use a continuous mode for modeling in urban areas.

- Integrate Geographic Information Systems with urban models.

O'Loughlin et al. (1996) raise some excellent points concerning urban modeling. Several of their recommendations for urban modeling will be encompassed in the objectives of this research.

1.6 Dissertation Objectives

Section 1.2 of this dissertation revealed a need for hydrological models to incorporate the important mechanisms of hillslope hydrology. These mechanisms are primarily influenced by topography and soil type, which may not be captured well in lumped, black-box approaches. There are in fact, few hydrological models that consider the variability of catchment topography. Freeze et al. (1969) used partial differential equations describing surface and subsurface flow processes. Simplifications were introduced by Bathurst (1986) and Beven et al. (1987). However, these physically-based models are very computationally intensive and their physical basis is derived from laboratory studies with well defined boundary conditions that would not necessarily exist in a real catchment (Sections 1.1 and 1.3). Furthermore, large data requirements and the problems involved in calibrating or estimating the multitude of parameters necessary to run the model often ends in their preclusion (Section 1.4). A new generation of models has recently emerged that considers the importance of soil type and topography in a conceptual framework with a minimum number of parameters. O'Loughlin's TAPES (1981) and Beven and Kirkby's TOPMODEL (1979) both incorporate the topographic influence on runoff. The latter model is a quasi-physically-based model and is becoming more and more popular. It is

computationally efficient and also captures the essence of runoff production at the basin scale. Quinn et al. (1993) report that TOPMODEL will trace the position and evolution of variable source areas; provide for "piston-like displacement"; account for macropore flow and piping; and simulate the possibility of high subsurface contributions to runoff by allowing subsurface stormflow.

One of the general purposes of this thesis is to study such a model and determine its suitability in flood and water resources management. The model should account for soil heterogeneity and topography, generate variable source areas, be quasi-physically based, semi-distributed, and have only a few parameters. TOPMODEL, as Chapter 2 and 3 will show, is an ideal model for such a study. But TOPMODEL is primarily intended for rural areas where the primary mode of moisture movement is through the soil medium. How can TOPMODEL concepts be integrated with the urban component that is often present in even very small catchments? Modeling the urban component of catchments in continuous hydrologic models often means sectioning off the urban component and modeling it as a completely decoupled entity from the rest of the catchment. But if hillslope hydrology is so dependent on the spatial variation in topography that permits or inhibits the transmission of subsurface flow, then is not this type of urban modeling an incompatible approach? Does the soil beneath the impervious surface play no role in the small scale hydrology of hillslopes?

O'Loughlin et al.'s (1996) concise and helpful review of the status of urban hydrology brought forth several important recommendations for furthering research in this area. These included the integration of urban models with continuous models intended for rural areas on a variety of scales. Therefore, how does an urban area fit into a continous variable source area model? This dissertation will attempt to answer some of the questions posed above and has the following general objectives:

- Theoretically integrate urban land use in a hillslope hydrology framework.
- Keep the number of parameters low.
- Apply this integration at a variety of scales.
- Apply this integration on a continuous time series.
- Use a geographic information system in the integration.
- Draw conclusions on this integration for both continuous and flood event modeling.

Chapter 2 will provide a review of hydrologic modeling and the hydrologic models available. The purpose of this review is to justify the selection of TOPMODEL in this research. This chapter will also provide a definitive list of research objectives. Chapter 3 reviews TOPMODEL theory, the numerous applications cited in the literature, and provides various criticisms. Chapter 4 introduces the reader to the catchment study area: Ancaster Creek in the Region of Hamilton-Wentworth. Climate and geology are discussed to show the suitability of this catchment for this research. Also, the Geographic Information System ARC/INFO is introduced to create Digital Elevation Models of terrain that will allow us to apply the model at a variety of scales. The catchment and subcatchment boundaries are delineated using ARC/INFO. Chapter 5 details how urban areas are incorporated into the model in one of the most important TOPMODEL parameters: the topographic index. This index is directly responsible for the formation of the variable source areas. Chapter 6 details the application of the revised model on three continuous time periods at 10 different application scales. An application scale is recommended and is passed on to Chapter 7 which describes some further model revisions and the application on

three more continuous data series and on single events. The revised TOPMODEL is also compared to a conventional Hortonian flow model to provide a benchmark for its performance. Chapter 8 is the concluding chapter of this work and includes recommendations for future research.

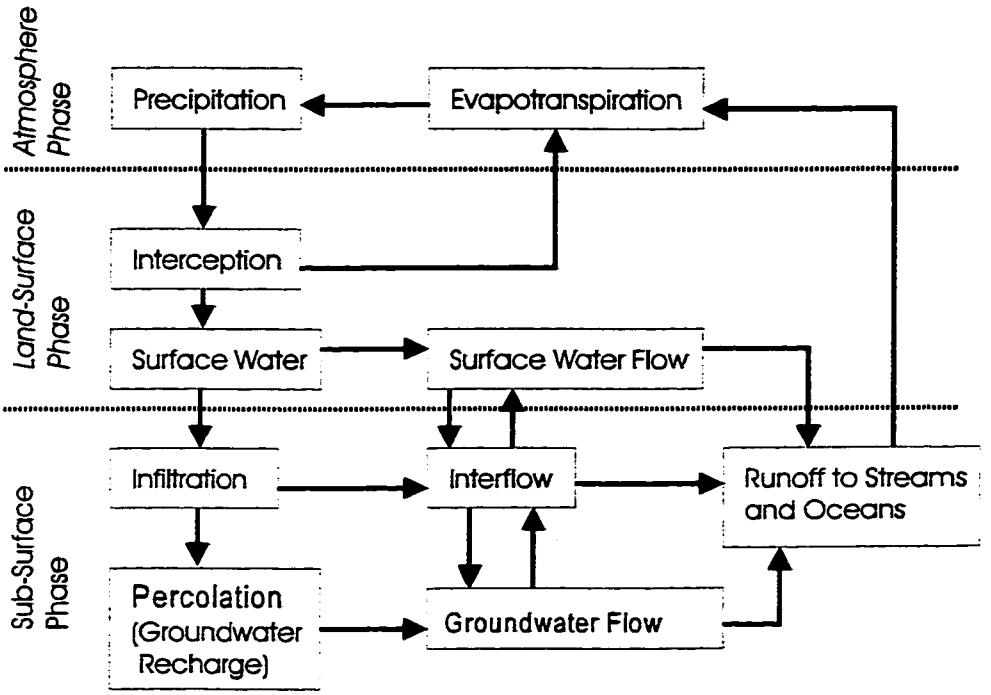

Figure 1.1: Block-diagram representation of the global hydrologic cycle (adapted from Chow et al. 1988).

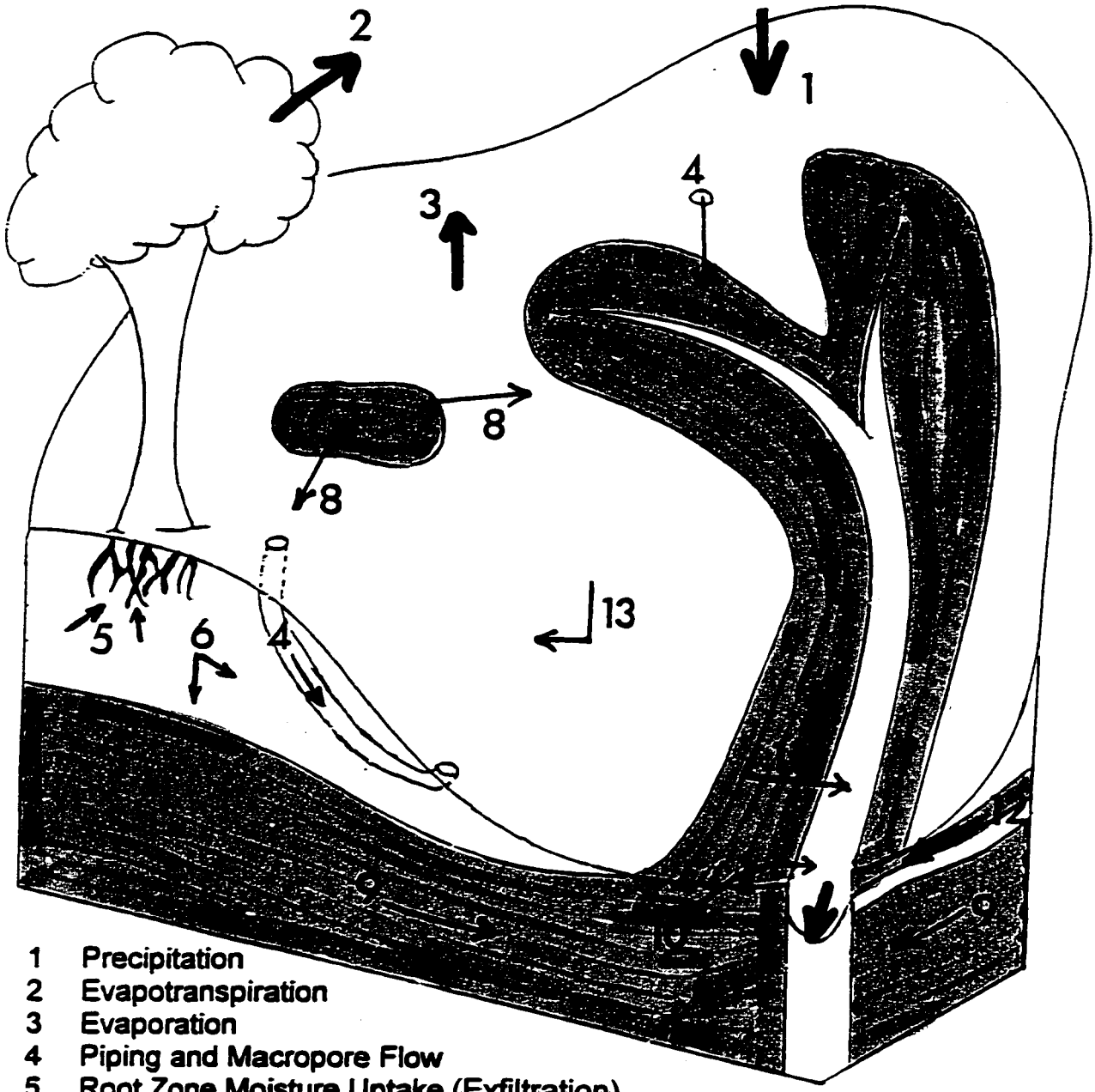

1 Precipitation
2 Evapotranspiration
3 Evaporation
4 Piping and Macropore Flow
5 Root Zone Moisture Uptake (Exfiltration)
6 Lateral and Vertical Unsaturated Zone Flow
7 Infiltration Excess Overland Flow
8 Run-on
9 Subsurface Flow (Throughflow, Interflow)
10 Return Flow
11 Saturation Excess Overland Flow
12 Saturation Wedge Flow
13 Interception

Figure 1.2: Components of the hillslope hydrologic cycle (adapted from Quinn 1991).

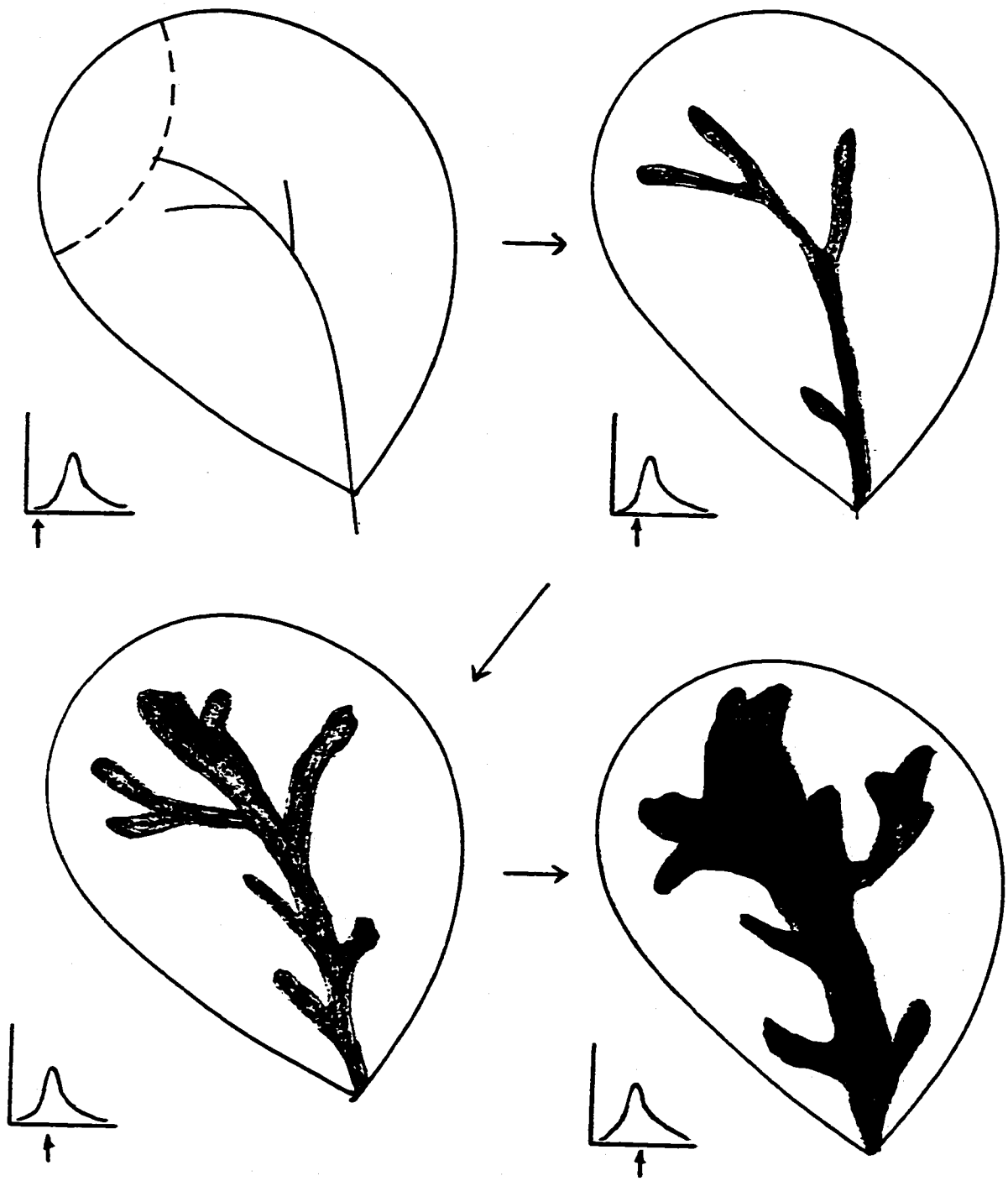

Figure 1.3: A time-lapse view of a basin showing the variable-source area concept (adapted from Chorley 1978).

CHAPTER 2 LITERATURE REVIEW OF HYDROLOGICAL MODELS

2.1 Introduction

There are a myriad of deterministic hydrologic models available to engineers but some type of evaluation of these models should be made in order to determine where problems exist, and how solutions should approached. In this chapter, a *mathematical model* is expressed through a single equation, while a *computer model* is the integration of these separate mathematical models to make up an overall model of the hydrologic cycle or a combination of sub-components. Before embarking on a review of computer models, an examination of some of the established mathematical models for hillslope hydrology will be made. It is not the author's objective to detail every fact and concept dealing with the hydrologic cycle. Many voluminous texts do this very well. The mathematical model review will simply point out important facts and present the reader with examples of black-box and physically-based models of elements in hillslope hydrology; such as infiltration, for example. After the mathematical model review, Section 2.3 will present a review of the various computer models available to engineers. The review will focus on how the model generates runoff, how it considers spatial heterogeneity and the number of parameters that should be calibrated.

2.2 Mathematical Models in Hydrology

Figure 1.1 in Chapter 1 showed a block-diagram representation of the global hydrologic cycle. The system is represented by the basic hydrologic equation,

$$P - R - G - ET = \Delta S_{(s+g)} \tag{2.1}$$

where P is the total precipitation to the surface (m), ET is a loss of moisture from the

surface due to evapotranspiration (m), G is the net water subsurface through flow (m), R is the net water surface through flow (m), and $\Delta S_{(s-g)}$ is the net change in storage in the surface and subsurface regions (m). The flow measured at a gauge is some function of the total precipitation input, evapotranspiration, and the manner in which the land phase stores and releases this moisture. The mathematical model review will focus on precipitation input, losses, and moisture movement in the land phase. In the first two sections on precipitation and losses, the author will only pinpoint important modeling considerations. In the two subsections after that, the author will present some mathematical models for generating runoff, and overland flow routing. Black-box and physically-based models will be presented and the issues of scale, number of parameters required, and the difficulty in applying the model will be noted. A section on modeling in urban areas is also presented. Again, the author would like to reiterate the fact that this is not intended as a formal review of all mathematical models, but only to provide the reader with an understanding of why models are black-box, conceptual or physically-based. This will provide a framework for how models are evaluated in Section 2.3.

2.2.1 Precipitation

The primary input to hydrologic models is precipitation. It comes down in various forms such as rain or snow and each is modeled differently. Precipitation is highly variable both spatially and temporally, and it is this variability that can present major obstacles to accurate model calibration and verification.

The properties of a rainstorm that need to be captured by a hydrologic model are the total depth of rainfall, the temporal distribution, and the spatial distribution. Precipitation is often measured in point form using rain gauges and these must then be used to infer some aerial distribution. High intensity, local storms can produce rainfall over part of the catchment where no rain gauge is located. Subsequently,

there is no rainfall reading but a measurable rise in streamflow. This illustrates the importance of two things: 1) a spatially distributed rainfall field may be more appropriate than a catchment average rainfall depth in certain applications; and 2) the spatially distributed rainfall field is only as good as the rain gauge network that is used to compute it. There are numerous methods available for estimating the spatial distribution of rainfall throughout a catchment. The suitability of each method will depend on topography, gauge density, gauge configuration and computing ability (Singh 1989b). But ultimately, the smallest modeling unit in the catchment, whether it is a subcatchment or a fine grid cell, will require some lumped value of precipitation. And this average value must be computed from the assumed or estimated spatial distribution.

Obled et al. (1994) examined the sensitivity of a hydrologic model to synthetically generated spatially varying rainfall patterns. Spatially lumped values of precipitation were computed from five rain gauges and 21 rain gauges scattered throughout the basin. The estimation of average depth from the five gauges in comparison to that computed from the 21 gauges produced just slightly lower runoff volumes (3%) and slightly lower peaks of rainfall intensity. However, the small differences that did exist were found to be important to the final optimizations. Their results suggested that improving the accuracy of the average rainfall depth significantly improves simulated discharges. The authors remarked that their conclusions are partly functions of catchment scale and rainfall field variability. Obled et al.'s exercise was an important one. Often, rain gauge networks are thin, or configured poorly, and an average depth is really the only suitable measure of rainfall. Various methods exist to determine average rainfall depth from a rain gauge network. Singh et al. (1986) reviewed 13 different methods for determining areal mean precipitation using such common methods as the Thiessen Polygon Method and the Isohyet Method. While some methods used in the study were much more complex than others, all gave very comparable results.

The research in this dissertation will be using an existing rain gauge network in the area of the study catchment. Based on the above information, and given the topography, climate and available rain gauge network in the study area, this research will endeavor to provide the most accurate estimate of average rainfall depth for the smallest modeling unit. The estimate will be determined using one of the methods in Singh (1989b) and will be presented in Chapter 4.

2.2.2 Abstractions

2.2.2.1 Interception and Depression Storage

A reduction in the amount of precipitation that reaches the ground is known as a loss or abstraction, and can occur by interception or depression storage. Interception of rainwater by vegetation and man-made structures becomes a loss if it is allowed to evaporate. Depression storage occurs when rainwater is captured in small local ground depressions. This moisture either percolates into the ground or evaporates. Depression storage is a function of ground conditions and land slope. Interception losses vary with land-coverage and can be very high in forested catchments, for example. Obviously, both types of losses will vary spatially depending on the land-coverage or conditions. There is also a temporal variability as interception and depression storage are assumed to decrease with time, and this may be an important quality that should be captured by the model.

There are both black-box and physically-based models of interception and depression storage. Modeling interception loss for example, may simply involve a lumped term subtracted from the total rainfall prior to infiltration. This is the black-box model approach in which the lumped loss term must be calibrated or estimated from field data. A slightly more sophisticated example but still a black-box, is the empirically derived relationship of the form, $I = a + bP^{\eta}$ where I is the interception (mm), a, b

and η are constants that depend on vegetation cover, and P is the total precipitation (mm), (Singh 1989b). Estimates of these three parameters can be obtained from tables, estimated from field data or calibrated. One of the best examples of a physically-based model of interception is Rutter's model (Rutter et al. 1975). This model considers canopy capacity, free throughfall, trunk water capacity and, stemflow. It involves six separate parameters that must be estimated from field data or calibrated. This model requires a number of estimates and experienced judgement. It would only be used if canopy interception was a significant component of the hydrological processes in a catchment.

2.2.2.2 Evaporation and Evapotranspiration

Nearly 75% of the total annual precipitation on land surfaces is returned to the atmosphere by evaporation and transpiration (Singh 1989b). Hence, this is an important component of hydrological modeling and particularly in setting up antecedent moisture conditions that may influence runoff generation.

The net exchange of water molecules from the water surface to the atmosphere is the net rate of evaporation and is a function of meteorological variables such as solar radiation, temperature, wind, and atmospheric pressure. Evaporation from bare soil is modeled differently because soil exerts some resistance to evaporation and this is governed by such factors as relative humidity and hydraulic conductivity. The process of transpiration is the vapour transfer of water to the atmosphere through pores in the leaves of plants and is governed by the same types of variables that govern evaporation from a water surface (Singh 1989b). If the catchment is primarily composed of land (i.e. there are no large internal lakes or marshes), then evaporation and transpiration can be lumped into one term. *Potential evapotranspiration* is the total evapotranspiration that would occur if the soil always has enough moisture for use by the vegetation. *Actual evapotranspiration* occurs when the supply of soil

water is limiting. This is governed by climatic factors and soil characteristics. Vegetation extracts moisture from the soil in the amount between what is called a *field capacity* and a *wilting point*. The wilting point is the low level of soil moisture at which plants begin to wither and die. If the soil is wetted to increase moisture levels, then the field capacity is that point at which soil moisture movement is dominated by capillary flow. The maximum amount of moisture available to plants is the difference between the field capacity and the wilting point. Moisture between these two limits is available to evapotranspiration, but at the same time, this moisture is not subject to gravity drainage. This means that field capacity represents a deficit that must be satisfied before drainage to the saturated zone can begin.

Various methods exist for modeling evapotranspiration. The methods can be divided into radiation methods, temperature methods and combination methods. Radiation methods consider the sun to be the primary source of energy for evapotranspiration. Temperature methods use temperature as the primary variable and these methods are often used when other data is unavailable. Combination methods combine radiation or energy balance methods with the effects of wind. Burman et al. (1994) provide a thorough review of the methods available for estimating evaporation and evapotranspiration. The choice of model will depend on several factors including whether or not the area is primarily made up of man-made structures, low-lying shrubs or tall vegetation. Singh (1989b) provides several reviews of methods to estimate evapotranspiration. While methods either over- or under-estimated evapotranspiration in various climates, generally combination methods produced the best results all around, while temperature methods produced the worst results.

The Food and Agriculture Organization of the UN (FAO) provides and promotes the use of methodologies for determining evapotranspiration in an effort to sustain and increase agricultural production. Their report on a revision of FAO methodologies for crop-water requirements (Smith 1990) lists a comparison of 20 evapotranspiration

methods and their rank in both humid and arid environments. The Penman-Monteith method ranked first in both environments. Smith (1990) maintains that the theoretically most sound method should be used when all meteorological variables are available. The FAO makes a strong recommendation in their report for the Penman-Monteith method.

2.2.3 The Land Phase - Post Losses

After losses and abstractions are taken into account, the water comes in contact with the soil. Infiltration is the penetration of this water into the surface of the soil. Numerous models exist for infiltration and it is one of the most important elements of runoff generation. The mechanisms of saturation excess and infiltration excess are directly affected by infiltration.

2.2.3.1 Black-Box Models of Infiltration

An empirical, non-physical method of infiltration was developed by the Soil Conservation Service (1972). This method effectively determines storm excess rainfall volumes depending on soil type and land-use. The excess precipitation P_e is simply,

$$P_e = \frac{(P - 0.2S_r)^2}{(P + 0.8S_r)} \tag{2.2}$$

where P is the total precipitation (mm), and S_r is the maximum amount of moisture that the catchment can retain (mm). The storage parameter S_r is related to a Curve Number (CN) by the following relationship,

$$S_r = \frac{25400}{CN} - 254 \tag{2.3}$$

The method assumes that P_e is the total depth of runoff. The curve numbers can be preselected from tables based on soil type and land-use. This black-box model is essentially defined by the Curve Number, which ultimately becomes a calibration parameter. It is applicable anywhere the Curve Number is constant, therefore the land should be subdivided into homogeneous units of land use and soil type. It is simple to use because only one parameter is calibrated and only land use and soil data are needed.

2.2.3.2 Physically-Based Models of Infiltration

In a physically-based model, runoff generation would integrate infiltration with percolation (moisture movement beneath the surface) by modeling unsaturated and saturated zone flow. Unsaturated zone flow can be modeled using Richards' equation which is one of the fundamental equations of flow through porous media. The following one dimensional equation of vertical flow is solved with numerical methods,

$$C\frac{\partial \psi}{\partial t} = \frac{\partial}{\partial z}(K(\theta,z)\frac{\partial \psi}{\partial z}) + \frac{\partial K(\theta,z)}{\partial z} - S_{sink} \tag{2.4}$$

where ψ = soil moisture tension or pressure head (m); t = time (hr); z = vertical space coordinate (m) (positive upwards); $C = \partial\theta/\partial\psi$ = specific water capacity (m^{-1}); θ = volumetric water content; $K(\theta,z)$ = unsaturated hydraulic conductivity (m/hr); S_{sink} = source/sink term for root extraction and soil evaporation (m). Two other relationships are needed to solve the equation: the relationship between $K(\theta,z)$ and the volumetric moisture content θ; and the relationship between soil tension and the

volumetric moisture content. The equation is then solved by an implicit finite difference scheme. This equation was derived by combining Darcy's law with the equation of continuity. One can see instantly that the use of such a model would depend on having a homogenous soil where the relationships between $K(\theta,z)$ and C, on θ and ψ, are known from point to point. The estimation of the term S_{sink} would likely vary with vegetation type.

Saturated zone flow in a physically-based model would be defined by the change in phreatic level of the unsaturated zone and can be modeled by the nonlinear Boussinesq equation,

$$S(x,y)\frac{\partial h(x,y,t)}{\partial t} = \frac{\partial}{\partial x}[K_x(x,y)H(x,y,t)\frac{\partial h(x,y,t)}{\partial x}] + \frac{\partial}{\partial y}[K_y(x,y)H(x,y,t)\frac{\partial h(x,y,t)}{\partial y}] + R(x,y,t) \quad (2.5)$$

where $S(x,y)$ is the specific yield; $h(x,y,t)$ is the phreatic surface level (m); $K_x(x,y)$ and $K_y(x,y)$ are the saturated hydraulic conductivities in the x and y directions, respectively (m/hr); $H(x,y,t)$ is the saturated thickness (m); and $R(x,y,t)$ is the instantaneous vertical recharge into the saturated zone (m/hr). This equation is solved by a finite difference approximation using an implicit scheme. The parameters that must be calibrated or specified in this equation are the saturated hydraulic conductivities in both directions and the specific yield. Thus, to use both the unsaturated and the saturated zone equations, requires roughly five parameters. Again, the hydraulic conductivities at each point would have to be known and modified accordingly from point to point.

2.2.3.3 Conceptual Models of Infiltration

Several conceptual models of infiltration exist that are essentially approximations to Richard's equation. Philip (Chow et al. 1988) solved Richards' equation in the form

of an infinite series where due to rapid convergence, only the first two terms are considered. The infiltration rate into the soil $f(t)$ (cm/hr) becomes,

$$f(t) = \frac{1}{2} S_s t^{-1/2} + K \tag{2.6}$$

where K is the hydraulic conductivity (cm/hr), S_S is the sorptivity parameter which is a function of the soil suction potential (cm $hr^{1/2}$). Therefore, this method involves estimating the sorptivity parameter and the hydraulic conductivity. Other models that are conceptual in that they present simplified pictures of infiltration include the Green-Ampt (Chow et al. 1988) model,

$$F(t) - \psi \Delta\theta \, ln\left(\frac{F(t)}{\psi \Delta\theta} + 1\right) = Kt \tag{2.7}$$

where $F(t)$ is the cumulative rate of infiltration (cm), ln is the Naperian Logarithm and $\Delta\theta$ is the change in moisture content due to the infiltrating moisture. This equation is solved through a method of successive substitution and requires estimates of K, ψ, and the soil porosity. Similarly, Horton viewed the soil surface as a separating medium between surface runoff and subsurface percolation. Horton's equation (Chow et al. 1988) of infiltration is,

$$f(t) = f_c + (f_o - f_c) e^{-k_H t} \tag{2.8}$$

f_c is an asymptotic constant rate of infiltration (cm/hr), f_o is some initial value (cm/hr) and k_H is a recession constant (hr^{-1}). Again, three parameters exist that must be estimated or calibrated.

Because of the nature in which many of these conceptual models have been developed, many do not require such detailed knowledge of the variation in the hydraulic conductivity with moisture content. An effective hydraulic conductivity is assumed that therefore, must be calibrated. In Horton's model, hydraulic conductivity is effectively replaced with a term containing a recession constant.

2.2.4 Surface Flow

Surface or overland flow is that runoff that remains on the surface with no further abstractions occurring until it reaches the stream. Several of the infiltration equations above are used to estimate the volume of surface runoff simply based on the infiltration rate and the rate of incoming precipitation. After the surface runoff volume is computed, a routing method is used to distribute the volume through time. Therefore, overland flow routing methods are an essential part of surface runoff computation.

2.2.4.1 Black-Box Models

Some of the more popular and traditional methods of transforming surface runoff volume to surface runoff flowrates are based on *Sherman's Unit Hydrograph* concept (Sherman 1932). The unit hydrograph is defined as the direct runoff hydrograph produced by a pulse of 1 cm of excess rain falling uniformly over the catchment at a constant rate for a certain duration (Chow et al. 1988). Sherman's method implies that for a given duration of rainfall, the hydrograph time base should remain the same. Complete hydrographs were then computed for a storm of greater than one cm by simply summing individual unit hydrographs. By definition, the runoff rates generated are presumed to be generated by the entire basin and there is the assumption that rainfall is distributed in the same spatial pattern for all storms. *Synthetic unit hydrographs* can be created for ungauged catchments and produce

hydrograph characteristics from an assumed set of rules, that are usually related to basin characteristics. There are many synthetic methods available and each has been developed for a specific type of area (Veissman et al. 1989).

The SCS Unit Hydrograph method is a classic example of a synthetic unit hydrograph method. The method requires determining the time to peak (t_p) and the peak discharge (Q_p),

$$t_p = \frac{D}{2} + t_l \tag{2.9}$$

$$Q_p = \frac{484A}{t_p} \tag{2.10}$$

where t_P is the time from the beginning of rainfall to peak discharge (hr), D is the duration of rainfall (hr) and is equal to $0.133t_c$ where t_c is the time of concentration, t_l is the lag time from the centroid of rainfall to the peak discharge (hr), Q_P is the peak discharge (cfs) and A is the drainage area (mi^2). The parameter t_l can be related to the size of the watershed. The primary calibration parameter in this model is t_p.

2.2.4.2 Physically-Based Models

An example of a physically-based model of overland flow routing is using the diffusion wave approximation of the Saint-Venant Equations for continuity and momentum. The two dimensional model is,

$$\frac{\partial h_d}{\partial t} + \frac{\partial (c_x h_d)}{\partial x} + \frac{\partial (c_y h_d)}{\partial y} = P_e \tag{2.11a}$$

$$\frac{\partial h_d}{\partial x} = S_{ox} - S_{fx} \qquad x \text{ direction} \tag{2.11b}$$

$$\frac{\partial h_d}{\partial y} = S_{oy} - S_{fy} \qquad y \text{ direction} \tag{2.11c}$$

where h_d is the surface water depth (m); c_x and c_y are flow velocities (m/s) in the x and y directions, respectively; P_e is rate of surface flow generation (m/s) or the effective precipitation; S_{ox} and S_{oy} are ground slopes in the x and y directions, respectively; and S_{fx} and S_{fy} are friction slopes in the x and y directions, respectively. A formula to compute flow resistance is used in conjunction with Equation (2.11) which is solved with an explicit finite difference approximation. The kinematic approximation to the Saint Venant Equations is,

$$\frac{\partial q_s}{\partial t} + c\frac{\partial q_s}{\partial X_d} = cP_e \tag{2.12a}$$

$$c = \frac{\partial Q_s}{\partial A_s} \tag{2.12b}$$

where q_s is the discharge per unit width (m^2/s), c is the speed of the flow (m/s), X_d is the distance down the slope (m), P_e is the effective precipitation (m/s), A_s is the cross-sectional area of the flow (m^2) and Q_s is the discharge (m^3/s). In the system of equations above, the bed slope is assumed equal to the friction slope. In order to solve (2.12), the initial value of q_s must be known as well as some relationship between q_s and A_s, which may involve a roughness parameter. This involves the knowledge of at least two variables to apply this method.

2.2.4.3 Conceptual Models

A conceptual model could be exemplified by Manning's model for overland flow,

$$y_{sf} = \left(\frac{nq_s}{S_o^{1/2}}\right)^{3/5} \tag{2.13}$$

where y_{sf} is the depth of the surface flow (m), n is Manning's Coefficient of Roughness and q_s and S_o are as before. Here, the primary calibration parameter is Manning's 'n'. The equation applies when the flow is turbulent and therefore, some knowledge of this condition should exist.

2.2.5 Urban Area Modeling

The steps to transforming rainfall to runoff in an urban area involve (1) proportioning off the total volume that appears as surface runoff; and (2) distributing this runoff volume through time (Hall 1984). Surface area, length, slope and roughness all impact this transformation (Fleming 1975); but generally, impervious surfaces are expected to route the majority of precipitation to the stream, after some minor abstractions from interception and detention storage. Urban drainage areas are highly variable in shape, size, roughness and degree of imperviousness so Viessman (1966) claims that knowledge of the entire hydrograph not just the peak flow is essential if various inlet flows are to be routed and combined in determining a peak flow. Continuous urban flow models have been formulated and all tend to use some variation of the linear reservoir scheme.

In a linear reservoir scheme,

$$-O = \frac{dS}{dt} \tag{2.14a}$$

$$S = k_{lr} O \tag{2.14b}$$

$$O = \frac{I}{k_{lr}} e^{-t/k_{lr}} \tag{2.14c}$$

where O is the outflow from the reservoir (m^3/s), S is the storage in the reservoir (m^3), and k_{lr} is the recession constant (s) that linearly relates outflow to storage. Equation (2.14c) is the final equation for outflow in terms of time t (s). The Nash model (1957) uses a number of linear reservoirs in succession to obtain the following function for translated surface flow,

$$O_{n_N} = \frac{I}{k_N \Gamma(n_N)} \left[\frac{t}{k_N}\right]^{n_N - 1} e^{-t/k_N} \tag{2.15}$$

where the left hand term is the outflow from the last reservoir, n_N is the number of reservoirs and $\Gamma(n_N)$ is the gamma function of n_N. Notice now that this model requires estimates of two parameters: k_N (the recession constant) and n_N.

Cruise and Contractor (1980) applied a variation of this model to several urban areas but they found that their regression model had no generality. The data set had to be divided according to geographical location. Rao et al. (1972) applied this model and the simpler single linear reservoir to urbanizing catchments. Rao et al. found that the model parameters varied from storm to storm. For areas less than 13 km^2, a single linear reservoir model was found to provide an adequate description of catchment behaviour. Synthetic unit hydrograph methods have been used for impervious areas (Hall 1984) and these require information on overland flow length, slope and percent imperviousness. However, Viessman (1966) claims that a linear reservoir seems to support the accurate simulation of the actual storm hydrographs in urban areas.

The linear reservoir models above are generally conceptual models in that they begin with the fundamental equation of continuity but provide an assumption that simplifies the system and reduces it to one that can be simulated with one to two parameters. The issue of scale in this matter is difficult to assess; however, Heeps et al. (1974) and Marsalek et al. (1975) both compared three different urban runoff models: the Road Research Laboratory Model, the Storm Water Management Model and the University of Cincinnati Urban Runoff Model. In both studies the SWMM model provided the best performance but most importantly, predicted peak discharge was greatly influenced by the degree of subdivision of the catchment for all models.

2.2.6 Discussion

By now the reader should have some understanding of the differences between a black-box model, a conceptual model and a physically-based model in the area of runoff generation. If we were to use only black-box models in the four sections just above, the overall computer model of runoff generation would involve three parameters. If only physically-based mathematical models were used, the number of parameters would jump to a minimum of six. This does not include the effects of field capacity that must be overcome before saturation excess flow can occur. While other models could have been included in the previous section, the illustration has been sufficiently made. The mathematical models shown in the preceding sections were selected because they are classical models and are frequently used in the computer models of the next section.

2.3 Computer Models of Watershed Hydrology

2.3.1 Introduction

Models can also be categorized by the time scale of the application and two classifications include *event* models and *continuous* models. Event models simulate runoff rates and volumes produced over the period of a single storm, and often do not take into account such water balance components as evaporation. Usually used for flood predictions, these models treat antecedent moisture conditions in terms of initial soilwater, detention storage, and channel flows, or some index representing these variables (Watt 1989). Continuous hydrological modeling involves water balance approaches that operate for as long as input data are available. In these models, the water is tracked as direct runoff, infiltration, evapotranspiration, interflow, deep percolation, baseflow and finally streamflow. Between storms, the models track the storage of water and its depletion by evaporation, deep percolation and baseflow (Viessman et al. 1989). This thesis will focus on continuous simulation models; however, the model chosen in this research will also be used on single events.

Linsley (1967) provided a review paper on the relationships been rainfall and runoff at the beginning of the computer era. He noted the advantages that high speed computers could offer but maintained that these advantages could only be realized if the proper and adequate amounts of hydrologic data could be obtained. Several reviews of computer models exist that assess the applicability of models for various catchments. Fleming's (1975, 1979) work on deterministic models attempted to bring together the many aspects of deterministic models including terminology, hardware and data requirements, mathematical processes that are modeled, a full description of the parameters involved, and several case studies of several models. This was one of the first attempts to combine all the deterministic models into one

text. Singh (1989a and 1989b) provide reviews of numerous mathematical models and computer models of watershed hydrology. Both Fleming and Singh do an excellent job of introducing the models available and the applications in which they are appropriate. Franchini et al. (1991) provides an excellent comparison of some of the most well-known conceptual rainfall-runoff models. A review is given of the verifying ability of the various models and the ease of calibration and estimation of the parameters as well as their physical interpretation. These general reviews examine model structure and ease of implementation but they do not always provide an easy way to choose when a model should be applied based solely on number of parameters requiring calibration, ability to model hillslope processes and the issue of scale independence. Therefore the following review will attempt to answer these questions.

This section examines a handful of computer models that were selected based on their generality, popularity and origin. The original text on which the review is based is from Singh's Computer Models of Watershed Hydrology (1995) which provides model descriptions by the authors of these models. In this section, a description of how each model generates runoff is given first. Then, Table 2.1 lists how these models treat spatial heterogeneity and the number of parameters required for calibration. In this way, a model can be selected using the three criteria of 1) ability to simulate most, if not all, of the hill-slope runoff generating mechanisms; 2) a model whose number of parameters requiring calibration is no more than five; and 3) the model should be conceptual and semi-distributed. A self-imposed restriction of roughly 15 lines of text has been made for the description of runoff generation. There are key words in the following review that the reader should look for. If the writing indicates that "this is some function of that", than this implies that some empirical relationship has been developed that may not have a physical basis. If a mathematical relationship mentioned in the previous section was used, then it will be noted without a full description.

1. Tank Model (Sugawara 1995)

The land phase is represented by a series of four water storage tanks laid vertically. Precipitation is received as input into the top tank and moisture is lost to evaporation from this tank. If there is no moisture in the first tank, then evaporative losses are incurred by the second tank or any tank that contains water when a tank above it does not. Each tank is given a storage constant that determines the rate of discharge from outlets placed at the sides. If the outlet is placed at the bottom of the tank, then the tank becomes a simple linear storage-discharge system. By giving a tank several outlets at various positions, and assigning a different storage constant to each outlet, the tank can take on a non-linear quality. The discharge from the top tank is considered surface runoff, discharge from the second tank is intermediate runoff, discharge from the third tank is described as sub-base runoff and output from the fourth tank is baseflow. The tank's allocation to generate a certain type of flow (i.e. surface runoff, baseflow, etc.) is determined by the rate of discharge from the tank. The first two tanks can be emptied completely with the first tank discharging at a faster rate than the second tank. The third tank drains very slowly while the bottom tank will produce nearly constant discharge.

2. Stanford Watershed Model (Crawford et al. 1966)

The soil is divided into an interception zone, and upper storage zone and a lower storage zone. Precipitation is intercepted by the interception zone at a rate which is function of land use, and must be filled before water can enter the upper zone. Evapotranspiration (ET) depletes moisture in the interception and upper zones at the potential rate. Once they are emptied, moisture in the lower zone is depleted by ET at a rate determined by the land use and the lower zone *ratio*. The upper and lower storage zones have associated nominal values of moisture storage, and the *ratio* is the ratio of actual moisture level to this nominal value. These ratios also determine infiltration rates through the soil. The amount of moisture entering the upper zone storage is some function of this ratio. That portion of upper zone storage that is not

depleted by ET is proportioned to either overland flow, interflow or percolation to the lower zone. The percolation to the lower zone is a function of the both the upper zone and lower zone ratios. The overland flow discharge rate is some function of precipitation rate, slope and overland flow length. Interflow is placed in a temporary storage where it is discharged to the stream with an exponential recession. A proportion of lower zone moisture is diverted to groundwater storage and enters the stream with an exponential recession.

3. Xinanjiang Model (Zhao et al. 1995)

Runoff is generated as a function of both soil moisture deficit and precipitation. The soil is divided into three layers: upper, lower and deep. Evapotranspiration (ET) increases the soil moisture deficit in each layer at a certain rate until the moisture is depleted. Soil moisture deficit is spatially distributed throughout the basin using a water-capacity curve and the total soil moisture deficit of the basin is represented by a point on this curve. It provides a relationship between the total soil moisture deficit in the basin and the amount of basin area that contributes to runoff. When rainfall exceeds ET at that point in time, the state of the basin moves up on the curve and runoff is generated from a larger area. In this way, the runoff generated is proportional to the area of points where rainfall exceeds evaporative losses. The runoff is then subdivided into overland flow, subsurface flow and groundwater flow through a series of user specified parameters. The overland flow is not routed but is assumed to immediately reach the stream, while the other two flow types are routed through linear reservoirs.

4. Precipitation Runoff Modeling System (Leavesley et al. 1995)

The basin is divided into units based on Hydrologic Response Units (HRU) which in turn are based on soil type, interception, precipitation and evapotranspiration (ET). The soil is divided into three reservoirs: soil zone (divided into a recharge zone and a lower zone), subsurface, and groundwater. The recharge zone has a maximum

water holding capacity and incurs losses from ET, while the lower zone loses moisture through transpiration. The amount of surface runoff is computed as some function of the moisture in the soil recharge zone and a user specified maximum and minimum contributing area of HRU. It is routed using a kinematic wave approximation. Excess moisture moves from the soil zone to the subsurface and groundwater reservoirs once the soil zone capacity has been reached and surface runoff has been computed. The proportion of flow to the two lower reservoirs is a function of a user specified groundwater recharge parameter. Infiltration rates between zones are computed using a variation of the Green-Ampt equation which is in turn related to moisture levels. Subsurface outflow from the subsurface reservoir is computed by a non-linear relationship. Inflow to the groundwater reservoir can be from both soil zone excess and one or more subsurface reservoirs. The ground-water reservoir is a linear reservoir and is the source of all baseflow.

5. Sacramento Catchment Model (Burnash 1995)

The soil is divided into an upper zone and a lower zone. Each zone in turn has a tension water storage (does not contribute to flow), and a free water storage (can contribute to flow). Within any zone, the tension water storage must be filled before any moisture can move into the free water storage. Each storage of each zone has a maximum capacity and losses are incurred through evapotranspiration from the tension water storage. If the tension water storage are filled then vertical percolation and lateral drainage (interflow) can occur. Percolation rates are controlled by the contents of the upper free water storage zone and the deficit of lower zone moisture volumes. Interflow occurs when the rate of precipitation exceeds the rate at which percolation can occur from the upper free water storage zone. When the precipitation rate exceeds both the percolation rate and the maximum interflow drainage rate, then the upper zone free water capacity is completely filled and the excess precipitation results in surface runoff. The lower free water storage contributes to lateral drainage as some fraction of moisture content per day. This is essentially the base flow.

Maximum storage sizes are all specified by some parameter. Impervious surface are classified as lakes, streams, rocks and pavement and consistently contribute to runoff.

6. Streamflow Synthesis and Reservoir Regulation (SSARR) (Speers 1995)

The runoff is generated through the continuous accounting of the Soil Moisture Index (SMI) resulting from a simple mass balance relationship between moisture input (precipitation) and a weighted loss term due to evapotranspiration. The amount of runoff is some empirical function of the SMI and the precipitation rate. The division of this runoff into surface flow, subsurface flow and base flow, is a function of the Baseflow Infiltration Index (BII). The BII value determines the appropriate proportioning by some empirically derived function involving the precipitation rate. A higher precipitation rate decreases the subsurface component, reaches a limiting value and a greater proportion of runoff becomes surface runoff. The runoff rates are determined by routing through a cascade of linear reservoirs and increasing time delays and higher degrees of attenuation are attributed to the successively lower zones of runoff.

7. **HBV** (Bergstrom 1995).

The basin is subdivided into units of similar climatological input and response characteristics. The runoff response in each unit is governed by a maximum soil moisture storage capacity, a potential evapotranspiration (PET) reduction factor, and a parameter that determines the relative contribution to runoff from a millimeter of rain or snow-melt at a given unit soil moisture content. The soil receives precipitation input and moisture losses are incurred from the soil at an actual evapotranspiration (AET) rate. The AET is an empirical function of the PET, the PET reduction factor and the soil moisture level. At soil moisture levels below the reduction factor, actual evapotranspiration occurs. At soil moisture levels above the reduction factor, a reduced AET loss occurs. Interception is assumed to be integrated into the PET reduction factor. The fraction of runoff to rainfall is some

function of the soil moisture content in the basin, and the first and third parameters mentioned above. The effect of this function determining runoff generation is that runoff is gradually increasing with increasing wetness. The excess water from the soil moisture routine is routed through a two reservoir system with three recession constants, a threshold parameter and a constant percolation rate. These two reservoirs effectively determine the distribution of excess runoff.

8. Simple Lumped Reservoir Parametric Model (Kite 1995)

Designed to use satellite data for land cover information it can also operate without remotely sensed data. Developed primarily to consider snow-melt, the watershed is divided into Grouped Response Units which are similar in concept to the HRUs of the Precipitation Runoff Modeling System. Runoff is generated by computing a vertical water balance of three non-linear reservoirs. The first represents the snow-pack, the second represents the rapid hydrograph response (may be considered top soil layer storage), and the third represents the slow response in hydrograph flow (may be considered as groundwater). Areal evapotranspiration deficits must be satisfied (if possible) first from the snow-pack tank, then from the rapid tank, and then from the slow tank. Above a certain temperature, moisture from the snow-pack tank percolates into the second tank. The second tank has an associated maximum depression storage. If moisture in rapid storage exceeds the maximum depression storage than rapid runoff occurs. The rapid runoff rate is a function of land slope, roughness and area. Moisture percolates from the second tank to the third tank via Philip's infiltration equation. Lateral flow from the third tank is a function of the maximum field capacity of that tank, the contents of the tank, the temperature, and the hydraulic conductivity assigned to the slow store.

9. TOPMODEL (Beven et al. 1995)

TOPMODEL is short for Topographic Model and runoff is generated as a function of topography and soil type. The soil is divided into three zones: a root zone, an

unsaturated zone in the middle and a saturated zone at the bottom. TOPMODEL adopts a non-linear saturated zone but a linear representation of the other stores. Losses due to interception and actual evapotranspiration (AET) are made from the root zone. The root zone must be completely filled before moisture can proceed to the unsaturated zone. The overall catchment storage deficit and local levels of the water table are continually updated with input of precipitation, losses from AET and depletion from lateral subsurface flow. The lateral subsurface flow at a point is a direct function of the local topography and the amount of upslope area that drains through that point. This function defines a topographic index at that point. If the lateral subsurface flow is low, the water table rises with effective precipitation. When the local water table is above the surface, then saturated overland flow is predicted to occur. The spatial distribution of these saturated areas constitute the variable saturated source areas and are direct functions of the topographic index. Hortonian overland flow is possible, and overland flow generated at each time step is routed using a time-area approach.

10. THALES/TAPES-C (Grayson et al. 1995)

The soil is essentially divided into an unsaturated zone and a saturated zone and water percolates vertically from the unsaturated zone to the saturated zone. Subsurface flow is generated by infiltrated water that flows downslope in a saturated layer overlying an impermeable base. If the subsurface flow rate exceeds the capacity of the soil profile to transmit the water, surface saturation occurs and rain falling on the saturated areas becomes direct runoff (saturation excess flow). The soil profile's ability to transmit water is based on the topography of the land. The unsaturated zone contributes no lateral flow. Runoff can also be generated by infiltration excess overland flow. The method allows complex terrain to be represented by a series of one-dimensional equations. THALES can simulate runoff generation from infiltration excess using one of various equations including Green-Ampt or Philip's equation. Overland flow is routed using the kinematic wave assumption. The model is able to

consider run-on infiltration.

11. CREAMS (Knisel et al. 1995)

Developed to assess non-point source pollutant loadings from large areas, the region is divided into areas of similar soil, crop cover and precipitation. Runoff volume is estimated by using a modification of the SCS curve number technique for daily time steps. In this model, the soil medium is conceptualized by a root zone with seven layers. Plant transpiration and soil evaporation are computed separately and deplete the root zone as a function of root zone depth and soil water availability. In the SCS technique, the maximum moisture retention parameter is used to determine the amount of runoff. In CREAMS, this parameter is assumed to vary with depth. Each of the seven layers has an associated weighting for the retention parameter - with the lowest layer having the lowest value. Infiltration volume is computed as the difference between precipitation and runoff and this excess is allowed to infiltrate through the root zone once a field capacity has been reached. The percolation rate is a function of the soil moisture level, the saturated conductivity and the field capacity value.

12. SHE/SHESED (Bathurst et al. 1995)

The system consists of sub-components continuously accounting for interception, evapotranspiration, unsaturated zone flow, saturated zone flow and overland flow routing. Interception is used to calculate the net rainfall reaching the ground through the canopy, water stored on the canopy and evaporation from the canopy. Actual evapo-transpiration is calculated using the Penman-Monteith equation and this becomes a loss term for the unsaturated zone. The unsaturated zone assumes vertical flow only and uses a one-dimensional version of Richards' equation. This equation determines infiltration at the ground surface and the exchange with the saturated zone which is allowed to eventually rise up and eliminate the unsaturated zone. Saturated zone flow is modeled by the non-linear Boussinesq equation. Overland flow is

generated by Hortonian flow or saturation excess overland flow and is routed using the diffusion wave approximation of the Saint Venant Equations.

The following table details the way each model treats spatial variability, temporal variability and the number of calibration parameters. In this table, the following codes are used:

Type	B: Black-box	C: Conceptual	P: Physically-Based
Spatial	L: Lumped	S: Semi-distributed	D: Fully-Distributed
Time	H: Hourly	D: Daily	Any

Note that abbreviations have been used for some of the model names.

Table 2.1: Model qualities.

Model	Type	Spatial	Time	No. of Calibrated Parameters
1. Tank	B	L	D	7: 3 outlets in 1st tank; 2 outlets in 2nd tank; 1 in last two tanks
2. SWM	C	S: lumped in soil, veg., precip.	Any	6: interflow, [illegible]
3. Xinanjiang	C	S: water moisture deficit L: all others	Any	6: ET adjust.; 3 runoff separation; 2 runoff concentration
4. PRMS	C	S: lumped in soil, precip. (HRU)	D	6: ET adjust.; 2 [illegible]
5. Sacramento	C	L: perv. surface vs. imperv. surface	H	14: 2 imperv. surf.; ET; tension storage sizes; interflow discharge rate; 3 percolation rate; 5 lower zone; baseflow
6. SSARR	B	L	Any	4: 3 [illegible]
7. HBV	B	S: lumped in land use, precip.	Any	4: 2 ET; maximum soil storage; runoff
8. SLURP	C	D: satellite pixel size	D	5: rapid tank; [illegible]
9. TOPMODEL	C	S or D: soil, topog., precip.	H	4: ET; 2 soil transmissivity; routing
10. THALES	C	S or D: soil, topog., precip.	Any	5: field capacity; 3 [illegible]
11. CREAMS	B	S: lumped in crop type, soil	D	4: curve number;2 root zone;1 routing
12. SHE/SHESED	P	D	Any	5-26: If 5: 3 soil properties, 2 others such as routing and ET depending on [illegible]

2.3.2 Other Models

Many other continuous models exist but they all use similar mathematical models or concepts to generate flow. KINEROS (Smith et al. 1995) models runoff generation by the Hortonian method. Similarly, EPIC (Williams 1995), was developed to assess the effect of soil erosion on soil productivity. Runoff surface volume is predicted for daily rainfall by using the SCS curve number equation. The Hydrological Simulation Program - Fortran or HSPF (Donigian et al. 1995) is a comprehensive watershed model that integrates hydrologic models with hydraulic and water quality process models. Water budgeting is the same as that used in the Stanford Watershed Model. The Institute of Hydrology Distributed Model (IHDM) (Calver et al. 1995) is a completely physically-based model that uses the finite element method for the spatial discretization in the subsurface flow and finite differences for the time-stepping. The basic equation of subsurface flow is Richards equation and the set up is very similar to that of SHE/SHESED. SWMM (Huber 1995) is a Stormwater Management Model intended for urban areas. Runoff is generated from rainfall by a non-linear reservoir technique that couples the spatially lumped continuity equation with Manning's equation for overland flow. Infiltrated losses are computed using either the Green-Ampt or integrated Horton equation. Event based models include the popular HEC-1 developed by the US Army Corp of Engineers Hydrologic Engineering Center (Feldman 1995). The model is versatile in that it allows the user a variety of mathematical models of the kind mentioned in Section 2.2 for computing infiltration, surface flow routing, etc. The model assumes however, that flow is generated over the entire basin.

2.4 Discussion of Computer Models

From the 15 line descriptions of how each model generates runoff, there is a clear distinction between how physically-based models such as SHE/SHESED and the

IHDM model simulate surface flow production versus the conceptual models and the black-box models. But, the line between conceptual models and black-box models is often blurred as conceptual models will often employ black-box approaches in sub-components of the overall computer model.

Physically-based models revolve around the use of Richards equation, the Boussinesq equation and the Saint-Venant Equations. These models are certainly capable of generating saturation excess overland flow and infiltration overland flow. They should also be capable of generating return flow, saturation wedge flow and macropore flow. Table 2.1 reveals that the SHE/SHESED model requires approximately 26 parameters that must be estimated or calibrated. The SHE/SHESED authors suggest that perhaps only five truly need to be calibrated. However, the 21 other parameters that need to be estimated can make these models rather inconvenient to use.

The conceptual models such as the Stanford Watershed Model divide the land-phase into different zones and each zone has some capacity to store and move moisture depending on the moisture levels in adjacent layers. Field capacity is often considered in losses to evapotranspiration and infiltration may take the form of Philip's equation or the Green-Ampt equation. Of all the conceptual models, with the exception of TOPMODEL and THALES/TAPES-C, the infiltration equation ultimately determines how much surface runoff is produced. After that division has been made, moisture which infiltrated the soil enters various stores by percolation. These stores essentially govern the movement of subsurface lateral flow to produce interflow and baseflow. The equations governing the filling and depletion of these stores are generally not physically-based and will rely on some parameter that must ultimately be calibrated to account for the timing of the arrival of interflow and baseflow in the hydrograph. The number of parameters required for calibration of these models ranges from five to 14. With the exception of TOPMODEL and

THALES/TAPES-C, the conceptual models can only generate infiltration excess overland flow and presumably this occurs over the entire basin at one time. The models divide up the catchment generally by soil-type and land-use as these data provide the two most important factors for generating runoff in these models: abstractions and hydraulic conductivity. TOPMODEL and THALES/TAPES-C distinguish themselves from the other models in that these are two conceptual models which can generate saturation excess overland flow. They consider soil type, land-use and topography, and can be applied in a distributed or semi-distributed manner. Surprisingly, these two models do not depend on the calibration of many more parameters than the black-box models in Table 2.1. Xinanjiang is similar to TOPMODEL and THALES/TAPES-C because it allows for a statistical distribution of the parameter affecting abstractions and therefore, soil moisture deficit. It does however, model only infiltration excess overland flow.

The black-box models SSARR, HBV and CREAMS have only four parameters requiring calibration, yet the Tank model uses seven parameters in the calibration process. Tank requires this many parameters for the simple reason, that it is so unrepresentative of many real systems. Tank's author had to place three additional outlets in two of the tanks in order to simulate the observed flow in a variety of situations. SSARR, HBV and CREAMS all have slightly more sophisticated, albeit black-box approaches to runoff generation and therefore, only use four calibration parameters.

It is evident from this list, that TOPMODEL and THALES/TAPES-C satisfy the requirements in selecting a model for this research. The author has selected TOPMODEL for this research because it requires one less calibration parameter than THALES/TAPES-C and it is growing in popularity and use.

2.5 Study Objectives

The information in Chapters 1 and 2 reveal a need to incorporate a physically meaningful representation of urbanization, into a model that includes all the major components of hillslope hydrology. This dissertation has the following objectives:

1. Revise TOPMODEL to incorporate urban areas in the calculation in the topographic index and in the generation of surface flows.

2. Apply TOPMODEL to an area in Southern Ontario and prove that the use of urban areas can effectively be incorporated with a minimum number of parameters.

3. Compare the revised TOPMODEL to a conventional hydrologic model used for continuous modeling in the southern Ontario Region.

4. Draw conclusions on the use of revised TOPMODEL for flood estimations and continuous modeling.

TOPMODEL uses terrain slope to determine the value of a topographic index at a point. Digital Elevation Models (DEMs) are raster models of terrain that are often used to derive information such as slope. The resolution of these digital representations of terrain may therefore affect the calibration process. Therefore, the research objectives have been expanded to include,

5. Draw conclusions on the effect of aggregation and DEM grid cell size on the modeling process.

Objective 1 will be achieved in Chapter 5 of this dissertation while objectives 2 and 5 will be achieved in Chapter 6. Objectives 3 and 4 will be achieved in Chapter 7.

2.6 Summary

Section 2.2 of this chapter provided the reader with an understanding for the differences in black-box, physically-based and conceptual models. Various mathematical models that are often used in computer models of hydrology were presented and differences in what makes them black-box or physically-based were brought to the reader's attention. Surface runoff generation involves determining a surface runoff volume and a routing scheme to translate the flow. The surface runoff volume can be determined through a black-box method like the SCS technique, or a conceptual model of infiltration. Physically-based models will use equations of continuity and momentum to simulate flow at the surface and beneath the surface. These models require highly detailed knowledge of the physical system.

The second section provided the more formal review of several well-established computer models of hydrology. The models were reviewed based on their technique for generating runoff, their treatment of heterogeneity and the number of parameters requiring calibration. This section reiterated the advantages and disadvantages that were noted in Chapter 1. The physically-based model, and the two conceptual models are able to generate variable source areas of saturation but the other models could not. Therefore, this dissertation will use TOPMODEL as the computer model in this research.

Chapter 3 will continue the literature review by focusing solely on TOPMODEL. Where and how TOPMODEL has been used and its performance in the literature will be reviewed. Its application in urban areas, if any exist, will also be investigated.

CHAPTER 3 TOPMODEL THEORY

3.1 Introduction

The purpose of this chapter is to present TOPMODEL's conceptual representation of hillslope hydrological processes, the underlying theory, and its performance reported in the literature. This chapter has four sub-sections outside of the introduction and the summary. The first sub-section discusses TOPMODEL's representation of the land-phase, the model's mathematical development, the sequence of calculations and initial conditions. The second section discusses the physical meaning of TOPMODEL's parameters. This is followed by a review of TOPMODEL's performance in real-world applications. The model will be critiqued and weaknesses and strengths will be identified. Finally, how TOPMODEL will be used to achieve the dissertation objectives will be described in the last section before the summary.

3.2 Mathematical Development and the Modeling Process

TOPMODEL is a conceptual hydrologic model that aims to capture the essential runoff generating processes in the catchment at the hillslope scale by considering soil type and varying topography to simulate the dynamic response of the catchment. The model uses simple mathematical representations and can be used in a semi-distributed way. The runoff generating processes that are captured include infiltration excess overland flow, saturation excess overland flow, vertical unsaturated flow, throughflow and baseflow. TOPMODEL's concept of the soil column is shown in Figure 3.1. The soil column i has surface slope $tan\beta_i$ and the column is not completely saturated.

3.2.1 Precipitation and Losses

Precipitation is provided as rainfall (as no snow-melt component is involved) in units of m/hr and received by the first zone, the root zone. The root zone is actually part of the unsaturated zone and has a definite maximum size, Sr_{max}, (m) and an associated water deficit, Sr^t, (m) at any time t. This zone represents that part of the unsaturated zone that holds 'inactive moisture'. The moisture is termed 'inactive' because it is available for evapotranspiration losses but is not allowed to drain into the saturated portion of the soil. The potential evapotranspiration values provided in the input file are converted to actual evapotranspiration and are added to the root zone deficit. If the actual evapotranspiration exceeds the amount of water left in the root zone (Sr_{max} - Sr^t) then the actual evapotranspiration is simply set to this remaining value and any further evapotranspiration is ignored. When there is no rainfall, the evaporation continues to increase the storage deficit until all the moisture is depleted. If the root zone fills completely due to precipitation (i.e. $Sr^t = Sr_{max}$), then the excess travels vertically to the next section of the unsaturated zone - the 'active moisture' section. The parameter Sr_{max} essentially converts the precipitation to effective precipitation and therefore, represents all possible losses due evapotranspiration and interception. It is essentially the field capacity and this is why the root zone is the 'inactive' portion of the unsaturated zone.

TOPMODEL's first assumption is that the transient response of a catchment over time can be approximated as a sequence of steady states. Under steady-state conditions and an assumed spatially uniform recharge rate P to the surface of each column i, we have,

$$q_i^t = a_i P^t \tag{3.1}$$

where a_i is the area draining through column i per unit width (m), P^t is the rainfall

at time t which is uniform across the catchment (m/hr), and q_i^t is the lateral subsurface discharge from the saturated zone (m^2/hr).

The model computes actual evaporation from the potential evapotranspiration input data by the following expression,

$$Ea_i^t = Ep^t(1 - Sr_i^t/Sr_{max}) \tag{3.2}$$

Where Ea_i^t is the actual evapotranspiration (m/hr) at time t for column i, Ep^t is the potential evapotranspiration averaged across the catchment at time t (m/hr), and Sr_i^t is the size of the root zone deficit in column i at time t (m). Quinn and Beven (1993) claim that this is a useful and popular form of soil moisture driven representation of actual evapotranspiration. Evaporation is continued into the root zone and a deficit will build up during inter-storm periods.

3.2.2 Subsurface and Surface Flows

3.2.2.1 Unsaturated Flow

The active moisture in the unsaturated zone is any water outside of the root zone that is able to contribute to the saturated zone. This storage receives any fluid in excess of the root zone maximum storage. Note that in Equation (3.2), Sr_i^t is a deficit, therefore,

$$Su_i^t = Su_i^{t-1} - Sr_i^t \qquad \text{if } Sr_i^t < 0 \tag{3.3}$$

In Equation (3.3), Su_i^t is the active unsaturated zone storage (m) of column i at time t, and not a deficit. The active unsaturated storage essentially controls the vertical movement of water from the layer of soil above the saturated zone to the saturated

zone. The speed at which this vertical flow takes place is affected by a time delay function. This model refinement was implemented since it was noted that during a drought, the evapotranspiration losses were being underestimated and there wasn't an adequate consideration given to the delay that may exist when the vertical unsaturated zone flow reaches the saturated zone flow. Further to this, the delay is also a function of the degree of saturation. That is,

$$Qu_i^t = \frac{Su_i^t}{S_i^t T_d} A_i \tag{3.4}$$

where Qu_i^t is the vertical drainage flowrate (m^3/hr) from the unsaturated zone to the saturated zone for column i at time t, Su_i^t is the storage in the active part of the unsaturated zone for column i at time t, S_i^t is the saturation deficit in column i at time t (m), T_d is a constant that effectively delays the water in traveling from the unsaturated zone to the saturated zone (hr/m) and A_i is the area of the column (m^2). Therefore, if initially the entire unsaturated zone is dry then Su_i^t is zero and during rainfall, Su_i^t continues to be zero until field capacity is reached. Once rainfall begins to spill into the unsaturated storage zone, Su_i^t will begin to increase. The maximum value that Su_i^t can reach is the initial saturation deficit of the column.

3.2.2.2 Saturated Zone Flow

As precipitation to the catchment continues, the soil column's saturation deficit S_i^t decreases. The root zone fills up, excess contributes to the unsaturated zone where moisture flows vertically to the saturated zone until the saturation zone deficit decreases to zero. When S_i^t is zero, then the column is entirely saturated and becomes a source area contributing to saturation excess overland flow. Water "effectively" travels "upward". The storage deficit of this column is affected by the slope of the column's surface and the amount of water draining through the column.

The lower the slope and the greater the area draining through the soil column, the less the hydraulic head difference and this causes the build up of water in the vertical direction. Hence the transmissivity of the soil, i.e. its ability to transport water laterally, influences the ability for a column to saturate. The "effective" transmissivity is allowed to vary with depth whereby the transmissivity decreases with decreasing moisture content. Each column is classified by a soil-topographic index and the model assumes that all columns with the same index will behave in the same manner thus, lending itself to a semi-distributed approach. The model predicts the amount of water in the catchment and how it is distributed through time by integrating over all the soil columns. Several assumptions are involved in the mathematical development.

The second assumption is that the saturated hydraulic conductivity within the soil profile exhibits an exponential decline with depth. At some time t,

$$K(S_i^t) = Ko_i e^{(-S_i^t/m)} \tag{3.5}$$

where $K(S_i^t)$ is the saturated hydraulic conductivity of the soil in column i at time t (m/hr), Ko_i is the saturated hydraulic conductivity at the surface, m is the decay rate of the conductivity with depth (m), S_i^t, is the local storage deficit of column i at time t. The moisture deficit S_i^t is related to the depth to the water table z_i^t through the equation,

$$S_i^t = (\theta s_i^t - \theta r_i^t) z_i^t \tag{3.6}$$

where θs_i^t is the moisture content in the saturated soil and θr_i^t is the residual moisture content in the rest of the column that is not saturated (for details of this derivation, please see Appendix A1).

The third assumption is that the water table is parallel to the soil surface. It then follows from Darcy's Law that the down-slope saturated subsurface flow rate q_i^t can be expressed as,

$$q_i^t = T(S_i^t)\tan\beta_i \tag{3.7}$$

where β_i is the local slope angle of the surface of column i, $T(S_i^t)$ is the transmissivity of the soil in column i (m^2/hr) and q_i^t is the discharge per unit width (m^2/hr). The transmissivity through column i is obtained by integrating Equation (3.5) from S_i^t, which is the storage deficit when the water table is at depth z_i^t, to S_d^t which is the storage deficit when the water table is at a depth Z_d^t (depth to the impermeable surface).

$$T(S_i^t) = \int_{S_i^t}^{S_d^t} K(S_i^t)\,dS_i^t = mKo_i[e^{-S_i^t/m} - e^{-S_d^t/m}] \tag{3.8}$$

We can assume that the last term in Equation (3.8) is small; therefore,

$$q_i^t = To_i e^{-S_i^t/m}\tan\beta_i \tag{3.9}$$

where,

$$To_i = mKo_i \tag{3.10}$$

in which To_i is the transmissivity of the soil.

The baseflow, Qb^t (m^3/hr), is computed by integrating Equation (3.9) over both sides of the stream channel. Equation (3.9) is the general equation for subsurface flow from the saturated zone from column i. Therefore, by integrating this equation over

twice the length of the stream channels, we can determine the subsurface flow rate, or the baseflow. Therefore,

$$Qb^t = \int_{L_s} q_i^t dL_s = \int_{L_s} To_i e^{-S_i^t/m} tan\beta_i dL_s \tag{3.11}$$

where L_s is twice the length of all stream channels.

Note that,

$$A = \int_{L_s} a_i dL_s \tag{3.12a}$$

$$A = \int_A di \tag{3.12b}$$

and A is in units of metres. Now, the areal average of S_i^t is $\bar{S}^t$ (which is conceptually the catchment average value of saturated deficit at time t) and is equal to,

$$\bar{S}^t = \frac{I}{A} \int_A S_i^t di \tag{3.13}$$

Combine Equations (3.9) and (3.1) to get,

$$a_i P^t = To_i e^{-S_i^t/m} tan\beta_i \tag{3.14}$$

From Equation (3.14) we can solve for the local deficit in column i as,

$$S_i^t = -m ln\left(\frac{aP^t}{To\, tan\beta}\right)_i \tag{3.15}$$

Therefore,

$$\bar{S}^t = \frac{1}{A}\int_A S_i^t di = \frac{1}{A}\int_A [-m\ln(\frac{aP^t}{To\tan\beta})_i] di \tag{3.16a}$$

$$\bar{S}^t = \frac{m}{A}\int_A [-\ln(\frac{a}{To\tan\beta})_i - \ln P^t] di \tag{3.16b}$$

$$= -m\{\frac{1}{A}\int_A [\ln(\frac{a}{To\tan\beta})_i] di - \frac{S_i^t}{m} - \ln(\frac{a}{To\tan\beta})_i\}$$

$$\bar{S}^t = S_i^t + m\ln(\frac{a}{To\tan\beta})_i - m\bar{\gamma} \tag{3.17}$$

where,

$$\bar{\gamma} = \frac{1}{A}\int_A \ln(\frac{a}{To\tan\beta})_i di \tag{3.18}$$

If To_i is constant over the area A (i.e., $To_i = To$) then,

$$\bar{\gamma} = \frac{1}{A}\int_A \ln(\frac{a}{\tan\beta})_i di - \ln To = \bar{\lambda} - \ln To \tag{3.19}$$

$$\bar{\lambda} = \frac{1}{A}\int_A \ln(\frac{a}{\tan\beta})_i di \tag{3.20}$$

The value $\ln(a/To_i \tan\beta)$ is known as the *soil-topographic index,* while $\ln(a/\tan\beta)$ is known simply as the *topographic index.* Re-arranging Equation (3.17) produces,

$$S_i^t = \bar{S}^t - m[ln(\frac{a}{To\tan\beta})_i - \bar{\gamma}] \tag{3.21}$$

and if To_i is constant then,

$$S_i^t = \bar{S}^t - m ln(\frac{a}{\tan\beta})_i + m\bar{\lambda} - lnTo \tag{3.22}$$

Therefore, the topographic index is a measure of the column's propensity to saturate.

Continuing with the computation of baseflow, let's assume that To_i is constant with i in any further mathematical development. Substituting Equation (3.22) in Equation (3.11) gives,

$$Qb^t = To \int_{L_s} exp(-[\bar{S}^t + m\bar{\lambda} - mlnTo - m ln(\frac{a}{To\tan\beta})_i]/m) \tan\beta_i dL_s \tag{3.23}$$

$$Qb^t = To \int_{L_s} e^{-\bar{S}^t/m} e^{-\bar{\lambda}} exp[ln(\frac{a}{\tan\beta})_i] \tan\beta_i dL_s = To e^{-\bar{S}^t/m} e^{-\bar{\lambda}} \int_{L_s} a_i dL_s \tag{3.24}$$

$$Qb^t = A To e^{-\bar{S}^t/m} e^{-\bar{\lambda}} \tag{3.25}$$

This equation relates baseflow at any time t to the catchment average of soil moisture deficit.

3.2.2.3 Overland Flow

Infiltration excess runoff is modeled using the Green-Ampt Equation and is assumed to occur over the entire basin (or subbasin) if the conditions are right for this type of runoff mechanism. The mathematical development in the preceding pages has shown how the computer model models saturation excess runoff. When any rainfall comes in contact with a saturated area, it immediately becomes runoff. The total overland flow due to saturation excess is therefore,

$$Qov^t = P^t A_c \tag{3.26}$$

where Qov^t is in units of m/hr and A_c is the fraction of contributing area. This is the area that is saturated to the surface (i.e. all columns i that have $S_i^t \leq 0$).

The topographic indices which play a major role in determining the contributing area A_c, are the distributed parameter in this analysis. If computational demands are too great to use a fully-distributed approach, then a semi-distributed approach may be used in which a distribution of topographic index class versus area is obtained. The modeler would select a range of classes (values of topographic indices) and determine the catchment area that falls within that class range. This way, when a certain class of topographic index becomes saturated, then all areas within that class and higher, contribute to saturation excess overland flow.

3.2.4 TOPMODEL Computation Sequence

3.2.4.1 Initial Conditions (t = 0)

From Equation (3.25), we can obtain an initial condition for $\bar{S}$ by starting the simulation after an extended dry period so that the unsaturated zone is assumed

empty and saturated zone flow is not being recharged by flow from the unsaturated zone. Therefore,

$$\bar{S}^0 = -m\ln\left(\frac{Qb^0}{ATo\,e^{-\bar{\lambda}}}\right) \tag{3.27}$$

By the start of the simulation, this implies that,

$$\begin{aligned} Qb^0 &= Q_o \\ Qu^0 &= 0 \end{aligned} \tag{3.28}$$

where Q_o is the given initial catchment or subcatchment discharge (m^3/hr). The catchment water balance is initialized as,

$$\Sigma^0 = -\bar{S}^0 - Sr^0 \tag{3.29}$$

where Σ^0 is the initial water balance of the catchment (m) and the value Sr^0 is the initial value of the root zone deficit all over the catchment. Since the simulation begins after the extended dry period, the value of Sr^0 should be equal to the value of Sr_{max}.

The influence of initial conditions is weakened with the occurrence of the first large storm. This occurs because storage zones and deficits have been altered sufficiently by large rain events (mostly filled). The initial discharge (which is essentially the only initial condition) and thus, the initial moisture content of the catchment, has little bearing on the moisture conditions and catchment discharges thereafter. The authors of the model recommend that a period of about half a month is required for stability to be achieved (Beven et al. 1984) but this may vary with climatic and catchment conditions.

3.2.4.2 Sequence of Calculations (t > 0)

The local storage deficit for each column (or class of columns) is computed using Equation (3.22). Then, root zone calculations are made in which,

$$Sr_i^t = Sr_i^{t-1} - P^t \tag{3.30}$$

and actual evapotranspiration is calculated and added to the root zone deficit. Unsaturated zone calculations are made using Equation (3.3), and the drainage from the unsaturated zone is computed using Equation (3.4). The vertical unsaturated zone flow for the entire catchment is computed as,

$$Qu^t = \sum_{nac=1}^{N_{nac}} Qu_i^t \tag{3.31}$$

where *nac* is the index of each column class and N_{nac} is the total number of classes of topographic index. The total saturation excess overland flow is computed using Equation (3.26), and finally the baseflow is computed using Equation (3.25). The average catchment deficit is then computed for the next time step using the following equation,

$$\bar{S}^{t+1} = \bar{S}^t - \frac{(Qu^t - Qb^t)}{A}\Delta t \tag{3.32}$$

The model can distribute the soil type and topography, but any other type of variation in the catchment that influences runoff should be discretized into subcatchments.

3.2.5 Overland Flow Routing

The model in its original form uses a Time-Area method to route overland flow. This is a very common method involving a number of steps and it is detailed in Appendix A2. The most important parameter in this method of overland flow routing is the speed of the flow which is specified by the user; and therefore, this parameter may require calibration. Kirkby (1978) notes that "except in very large catchments, the form and peak of flood hydrographs will be primarily controlled by rate of runoff production on hillslopes, rather than overland or channel flow routing." This implies that the speed of the overland flow may not be a very influential variable in the calibration process.

3.3 Discussion of TOPMODEL Parameters

TOPMODEL simulates the formation of variable sources areas in a catchment through a distributed or semi-distributed method of soil moisture accounting. Saturation excess overland flow is predicted along with infiltration excess overland flow and return flow. Pipe flow is taken into account through the hydraulic conductivity which is essentially an "effective" hydraulic conductivity. The parameter m governs the release rate of soil moisture in the catchment and is a function of the transmissivity. Sklash and Farvolden's (1979) movement of old water is effectively included as water enters to recharge the system.

On examining the TOPMODEL assumptions, there are certain constraints that come to light for these assumptions to hold. The first assumption which is manifested in Equations (3.1) and (3.14) involves the continuity equation, and implies that steady state is reached within each time step. In this way, the transient response of the catchment over time can be approximated by a sequence of steady states. This simplifies the relationship between the recharge and the flow. For the flow to equal

the recharge, enough time must pass for steady state to occur. For this to be true, the time step would have to have some minimum value, perhaps depending on the catchment in question. The authors of TOPMODEL recommend that a time step of no less than one hour should be used.

The second assumption implies that the soil's saturated hydraulic conductivity exhibits an exponential decline with depth. This is shown in Equation (3.5). Beven (1984) claims that where rainfall or irrigation rates cause the soil surface to be close to, or at saturation, then moisture movement will be governed primarily by the largest continuous pores, which may be in the macropore size range. It is further assumed that the condition creating these large pores or channels would decrease with depth in some regular way. This assumption is born of observations that tilling and other agricultural activities near the surface can create greater pathways in the soil through which water can flow, thus causing transmissivity to decline exponentially with depth. This was considered a reasonable assumption by Beven (1982) for many soils. However, Ambroise et al. (1996) discovered that in two particular catchments, in order to properly describe catchment response, a relationship between hydraulic conductivity and depth that was not exponential had to be formulated.

The third assumption presumes that the water table is essentially parallel to the soil surface, so that the hydraulic gradient is determined by the surface slope. This assumption is only true if the slopes are not too mild. Otherwise, gravitational forces may not be the dominate mechanism of moisture movement.

The topographic index $ln(a/tan\beta)_i$ has been stated previously as a measure of the propensity of a column to contribute to saturation excess overland flow for a specific rain event. How well does soil moisture content correlate with this index? The literature seems to imply that the correlation is quite high. Nyberg (1996) studied a 6,300 m^2 catchment with a central valley and steep side-slopes where there was a

drop of 20 m between the catchment boundary and the outlet. Using a 5 m grid and maps of soil moisture distribution in the catchment, they found that there was a good correlation between $ln(a/tan\beta)_i$ and the observed water content. Furthermore, the soil depth was found to be shallow on side-slopes with low topographic indices but deeper in the valley where the topographic index was high. The relationship between mean soil depth and mean $ln(a/tan\beta)_i$ tended to be linear. "This indicates that macro-topography is a major contributor to the variability in water content" (Nyberg 1996). Wolock et al. (1989) showed that there was a positive correlation between the index of soil contact time and the alkalinity in surface waters. The longer the subsurface water came in contact with the soil, the more its alkalinity increased. The index of soil contact time was directly related to TOPMODEL's topographic index whereby the index of soil contact increased with increasing topographic index (the less the ability of the soil to move moisture, the greater the time the water was in contact with the soil).

3.4 TOPMODEL Review and Performance

TOPMODEL has grown in popularity since its introduction to the literature. It has been applied to various catchments worldwide and the following review describes some of the research that has been conducted using this model. These reviews will point out model deficiencies as well as accomplishments and they have been grouped by application type.

3.4.1 Flood Frequency Applications

Beven et al. (1983) applied TOPMODEL to four catchments in sizes ranging from 5 to 45 km^2. The research was conducted to show that runoff predictions and flood frequency predictions may be sensitive to assumptions about the overland flow contributing area. The model performed well but the authors noted that there was

parameter interaction in the calibration process, so that the final fitted values did not necessarily reflect the true balance of surface and subsurface flow processes. It was recommended that there be a greater inclusion of timing in the model (i.e., a parameter that affected the arrival time of certain types of flow) which might prevent problems in the calibration process. This model actually preceded the use of a field capacity in the root zone.

Beven et al. (1984) used TOPMODEL as a flood forecasting model on three catchments in the U.K of sizes 8 km^2, 10.5 km^2 and 36 km^2, during winter and summer months. There was generally good agreement between observed and predicted hydrographs, but there was a tendency to over-predict discharge during the summer. These discrepancies were attributed to evapotranspiration estimates that were based on open-pan estimates. The parameter m was found to be the most important parameter since it not only influences the predicted contributing area, but also the contribution to discharge from the subsurface store. The authors then introduced the concept of a field capacity and this improved the model's predictions during dry periods. It also improved the timing of subsurface store response It was concluded that the model would be useful for un-gauged, un-forested catchments of up to 500 km^2 in humid-temperate climates. A test was conducted to plot peak flow versus contributing area and it was discovered that large increases in storm size are achieved by a small increases in saturated area. The model was observed to perform best under wet conditions and the parameter m was found to exhibit a seasonal variation. Sr_{max} also appeared to exhibit some seasonal changes when calibrated. This would imply that a better prediction of losses during the summer months was required.

Beven (1986b) used TOPMODEL on three catchments in the UK of sizes 11.1 km^2, 14.3 km^2 and 4.3 km^2. In a sensitivity analysis of hydraulic conductivity, lower conductivities resulted in increases in saturated areas with the lowest conductivities

providing areas close to 100% of the catchment. The study noticed the "remarkable similarities" in the flood response of the three catchments over a wide range of hydraulic conductivities. Saturation excess overland flow dominated the mean annual flood response.

Beven (1987b) conducted further testing using TOPMODEL for the purposes of flood frequency predictions under varying climatic conditions. Beven used a 10.5 km^2 catchment in the UK and a model of rainfall processes for varying climatic conditions. Initial conditions were randomly drawn from probability distributions and two sets of spatially variable soil conditions were used. Rainfall intensity and duration were derived from exponential distributions and the soil hydraulic conductivities were derived from log-normal distributions. The results indicated that the simulated distributions of mean annual floods were of Extreme Value Type 1 or of the Gumbel Type, and in most cases, the bulk of the simulated discharges resulted from subsurface flow.

TOPMODEL was also used to model runoff generation in the North Appalachian Valley (Troch et al. 1994). Twelve flood events were selected from 13 years of stream flow observations. The initial catchment wetness before each storm event, crucial to the correct simulation of runoff production, was estimated from observed baseflow. Soil moisture in the catchment generally varied in only the first 100 cm depth and below this depth, soil moisture content remained nearly constant. The authors concluded that the flood frequency distribution seems to be very sensitive to the initial storage capacity. Simulated hydrograph characteristics, such as peak discharge, are very sensitive to the overland flow velocity parameters in the routing model.

3.4.2 Environmental Applications

Waters et al. (1991) used TOPMODEL topographic indices to estimate the area of a catchment that would likely become saturated under a variety of conditions. They chose a value of $ln(a/tan\beta)$ equal to nine, above which the area would likely become a source area according to ground observations. To improve the water quality in local streams, engineers will often apply lime over a catchment in order to raise the pH levels in the stream. In this paper, the researchers chose to apply the lime on source areas instead of the entire catchment (blanketing) in an effort to save money. In comparing one catchment that was blanketed to another which had the lime applied only to the source areas, the authors found water quality was actually better in the stream with source area liming, than in the stream whose catchment was blanketed. The source-area liming was also done at a fraction of the cost of blanketing.

Wolock et al. (1991) investigated the effects of CO_2 change on the hydrological response of catchments in the Eastern U.S. A time-series of precipitation and temperature that would account for the effects of the CO_2 increase were used as input to TOPMODEL. In their sensitivity analysis, they found that increasing values of average storm intensity were associated with higher average daily flow, peak flow and total volume. Increases in annual average daily temperature were associated with lower average daily flow and yield but not peak flow.

3.4.3 Effects of Land-Use

Durand et al. (1992) applied TOPMODEL to two adjacent catchments in the south of France: an 0.81 km^2 grassland catchment and a 0.57 km^2 forested catchment, during a period of study which was particularly dry and only three major storms were observed. Potential evaporation was estimated roughly as a function of temperature

and duration of sunshine. To account for interception loss from the forest and to mitigate the rough estimates of potential evaporation, a rainfall correction factor was introduced and optimized for each run along with *m* and *To*. The calibrated maximum transmissivity was high and did not seem realistic when considering the nature of the soils. Good fits were obtained but not so in 1987 in which floods were underestimated after a long drought in both catchments. The authors were able to hypothetically explain the poor fit by examining the circumstance surrounding each storm which included the existence of forest litter composed of leaves.

Robson et al. (1993) applied TOPMODEL to two catchments in the UK to compare the differences in the flow generation mechanisms occurring in the catchment, and to study the effects of land-use change. Using a daily time step, the parameters *1/m*, *Ko* and *To* were optimized on a calibration period in 1984-1985 and verified using a period in 1987-1988. The authors felt the model gave a satisfactory fit for both catchments in the calibration period but performed poorly during the winter of 1987-1988 because of heavy snow falls. With the first catchment, the authors felt that the model was insensitive to *Ko* which gave similar results over a wide range of values. Also, *Ko* was calibrated at a value higher than field measurements and the authors felt that the parameter may not be physically realistic. When the second catchment was re-calibrated using the validation period to improve the model fit, there was a noticeable difference in the optimized parameters. In particular, the *Ko* value jumped from ~80 to ~400 m/hr. This may have been due to a small percentage of land being ploughed in strategic areas. The authors noted that the assumption of quasi-steady conditions in the unsaturated zone may not hold: "where soil moisture content varies rapidly with depth, this may be a problem when water tables are shallow."

Quinn and Beven, (1993) applied TOPMODEL to grassy catchment of 10.5 km^2, and a coniferous forested catchment of 8.7 km^2. Hourly flow and rainfall data were used as well as daily estimates of Penman-Monteith potential evapotranspiration. Using

a predetermined parameter set, the model was applied to the grassy catchment for two nine-month periods and one nine month period on the forested catchment. The model was found to over-predict (estimated from graphs as approximately 2-50%) storm peaks in the forested catchment and this is believed to be due to the model not having an explicit accounting of interception storage. The authors noted that TOPMODEL predicted flow very well from a wet period to a dry period, but the converse is not true. To check this, the model was tested on a dry period followed by a wet period. The values of Sr_{max} changed dramatically after optimization and became unrealistically low implying the parameter may not be very meaningful. They concluded that the calculation to determine efficiency may not be an accurate criterion for goodness of fit because of the observed sensitivity to the chosen data period. Also, the efficiency measure used may not be sensitive enough to define a single unique modeling parameter set. They also concluded that there was a weakness in the root zone conceptualization and that the model needs to be made more complex to reflect the range of processes operating in the field.

3.4.4 General Applications

Jordan (1994) applied TOPMODEL to a catchment in Switzerland of 12.5 km^2 to determine the types of stormflow mechanisms present. For this catchment, saturation excess overland flow appeared to be a dominant mechanism for most of the events. However, the contributing areas varied significantly with the return period of the floods. The types of stormflow mechanisms present were determined with hydrometric measurements, groundwater depths and isotopic tracing. Jordan noted that saturation excess overland flow was the process occurring most frequently in this catchment however, this portion of the catchment could explain the hydrological behaviour only for small frequent events.

Iorgulescu et al. (1994), found in applying TOPMODEL that simulations with field-

estimated parameters gave poor results and although it was possible to verify some of the underlying concepts of TOPMODEL for a small Swiss catchment, the model could not be fully validated with respect to field measurements and knowledge of the physical processes involved in catchment response.

Merot et al. (1995) compared maps of potentially waterlogged soils as simulated by the topographic index, to those derived from soil survey maps of wetness distribution for two catchments. Both catchments are in France where one is 54 km^2 and the other is 77 km^2. A cell by cell comparison found that 84% of the well draining soils and 56% of the poorly draining soils are "correctly identified" by the index for the smaller catchment. The authors felt that the correspondence between the soil water regime maps and the topographic index maps were satisfactory for poorly draining soils, and the best results were for the smaller catchment where well draining soil covered the majority of the catchment. Comparative results for the larger catchment were not as good but the authors attributed this to errors in the relief map used to create the topographic index.

An excellent evaluation of TOPMODEL was conducted by Franchini et al. (1996). The authors made several good insights into the model's physical basis and discovered that the average topographic index was found to be sensitive to the resolution of the Digital Elevation Model and that the calibrated hydraulic conductivities became meaningless for large grid cell sizes. However, the model did perform well in comparison to 7 popular watershed models, including the Stanford Watershed Model (version IV), the Sacramento Model, the Tank model, the APIC model, Streamflow Synthesis and Reservoir Regulation model, Xinanjiang model and the ARNO model. These models were applied to an area approximately 840 km^2 in size. TOPMODEL produced slightly better results in terms of both calibration and validation. But the authors observed high values of optimized hydraulic conductivity and that these values may pertain to an effective hydraulic conductivity that

incorporates a truly physical property as well as the scale effect connected with the size of the grid.

3.4.5 Revising TOPMODEL

Various modifications have been made to TOPMODEL to improve its accuracy in certain applications and conditions. TOPMODEL concepts were generalized by Ambroise et al. (1996) for use in a variety of watersheds. TOPMODEL was applied to a small forested catchment in Virginia (Hornberger et al. 1985) but the author's attempts to calibrate a more complex revised model to account for interception in the forested catchment failed as the objective functions used were insensitive to many of the model parameters. The authors eventually concluded that the original model was just as good as the more complex one. Chairat (1993) modified TOPMODEL to account for the storage in an agricultural catchment with subsurface tiles for drainage. The modification resulted in a dramatic increase in the model's efficiency for four rain events where it was obvious that the tile storage dominated the flow curve. Lamb (1996) proposed a compound model of recession to improve TOPMODEL's predictions, because one value of m could not simulate the recession observed in his catchment. He noted that in the upper part of receding limb of the hydrograph, the curve was steeper, perhaps indicating the recession of a rapid surface storm flow rather than from a saturated zone storage.

3.5 Conclusions

The literature review shows that TOPMODEL has been widely tested in a variety of catchments and has performed reasonably well under a variety of conditions. It has been used for both continuous flow modeling and flood frequency analysis. Also, the relationship between soil moisture content and topographic index has been verified in a number of cases. But there is also the consistent appearance of a number of

inadequacies including: 1) the effect of elevation grid cell size on optimized parameters; 2) the poor performance in times of drought indicating an inadequate representation of the root zone; 3) seasonal variation in parameters; and 4) the unrealistically high values of optimized *Ko*. Obviously, TOPMODEL requires further testing in order to resolve some of these problems.

The elevation grids mentioned in this chapter, are known as Digital Elevation Models (DEMs). These are regular grids with an elevation value in each cell. The model depends on the topographic index which is derived from the DEM, and several studies have proven that the distributions of topographic indices derived from DEMs depend on grid size. None of these studies, however, systematically analyzed the effect of grid size on either the statistical characterization of the land surface, or the effect on hydrologic response (Zhang et al. 1994). The study done by Franchini et al. (1996) is one example of research aimed at conducting such tests and they showed that the final optimized values of the hydraulic conductivity depended on grid cell size. The values of hydraulic conductivity in most applications are found to be unrealistically high in comparison to laboratory values. This research will attempt to address some of the issues dealing with the effect of grid cell size on calibration parameters, as well as provide an optimum grid cell size for use with TOPMODEL in the Region of Hamilton-Wentworth. Field estimates of the primary parameters will be used, but the author realizes that the final optimized values may differ greatly in order to account for heterogeneity in the field.

To date, there has been no example of an application of TOPMODEL on a small catchment with a small degree of urbanization. The parameter interaction observed in the literature indicates that the number of parameters in the model should be kept to a minimum. Therefore, any modification to the model to incorporate urbanization effects will need to keep the number of parameters low.

3.6 Summary

This chapter presented the mathematical theory and concepts underlying TOPMODEL. The model can simulate saturation excess overland flow, macropore flow, subsurface storm flow, piston-like displacement as well as infiltration excess overland flow. TOPMODEL's processes are modeled by only a handful of important parameters including hydraulic conductivity, catchment recession and losses due to evapotranspiration. The model was reviewed in the literature and it has earned a reputation for accurately modeling the soil contribution to flow in several cases. In one study, it fared better than several other popular models. General problems include non-physical calibration of some parameters and an apparent dependence on grid cell size when calibrating; in particular for the hydraulic conductivity.

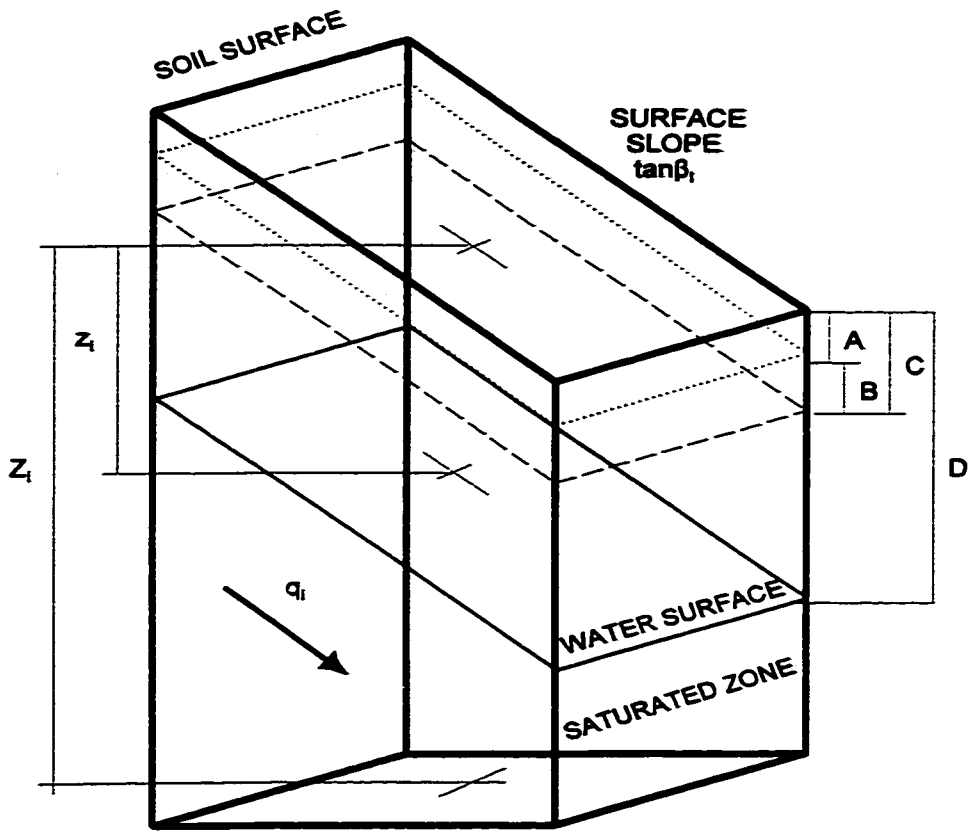

A: Sr_i
B: Inactive Part of Unsaturated Zone
C: Root Zone (Sr_{max})
D: Unsaturated Zone

Figure 3.1: TOPMODEL concept of the soil column.

CHAPTER 4 STUDY BOUNDARIES AND DATA MANAGEMENT

4.1 Introduction

The minimum data requirements for a TOPMODEL application are precipitation, estimates of potential evapotranspiration, and some form of topographic data. Streamflow data are necessary if model calibration and verification are to be conducted, and soil information should be consulted to determine the variability in soil types across the catchment. Therefore, the criteria for choosing a study area should incorporate these data requirements. The purpose of this chapter is to present the study catchment and provide details of the minimum data collection and processing.

Section 4.2 describes the climate and geology of the Hamilton-Wentworth Region. After assessing the available data, a catchment draining through Ancaster Creek in Ancaster, Ontario is determined as a suitable study region. Following this, precipitation data and discharge data are plotted and manipulated to indicate possible choices for wet, dry and median climatic periods that will be used in the TOPMODEL applications.

Distributions of the topographic index will be derived from Digital Elevation Models (DEMs) in Chapter 5. Section 4.3 describes the construction of these DEMs using the Geographic Information System (GIS) ARC/INFO. The aggregation phase (Chapter 6) of this dissertation will compare results obtained using a variety of DEM sizes. Section 4.3 describes how and why those DEM sizes were chosen. ARC/INFO is used again in Section 4.4 to delineate Ancaster Creek's catchment and subcatchment boundaries.

Following the basin delineation, Section 4.5 describes how spatial averages of

rainfall are determined over the catchment given the rain gauges that are available. Estimating potential evapotranspiration is detailed in Section 4.6. And finally, the routing schemes used in this dissertation are presented in Sections 4.7 and 4.8 for overland flow and main channel flow, respectively.

Continuous deterministic modeling tends to use large amounts of data from a wide variety of sources. The existence of errors in this data is inevitable and has traditionally been accepted as an inescapable element of every continuous application. Recently, the effects of input data errors on predicted streamflow have been treated more seriously, particularly when it involves rainfall data (Obled et al. 1994). Eliminating all sources of error in input data is impossible, but efforts will be made to eliminate as many as possible in this research. Therefore, each section involving the collection and manipulation of input data will have a sub-section on data quality assurance. These sections discuss how errors are detected and eliminated.

4.2 Criteria for Case Study Selection

TOPMODEL is a physically-based conceptual model that does have limitations. The theory in Chapter 3 implies several model restrictions:

1. The climate in the region should not be too dry as the evapotranspiration component of TOPMODEL is not sophisticated enough to incorporate long extended periods of dry weather.

2. TOPMODEL should not be applied in conditions where the exponential decay law may not apply. Problems may arise if the soil is too thick giving rise to permanent pools of subsurface water.

3. Soil types should not be dominated by impervious soils such as clay because that may result in Hortonian flow as the major contributor to storm runoff.

4. When assuming that water table slopes are parallel to ground slopes, the ground slopes should not be too small such that soil moisture movement is not topographically controlled.

5. The catchment should not be greatly regulated or have large man-made reservoirs that alter the flow radically from a natural state.

6. As the degree of urbanization is also important, the catchment should have some urbanization but not be so extensive that there is little contribution from the soil to the storm hydrograph.

7. Input data for the study area should be readily accesible and ideally, the area should be close by for visual inspection.

In view of reason number seven above, a study drainage area was chosen in the Region of Hamilton-Wentworth. Therefore, the existing hydrometric network provided by Environment Canada for the Hamilton-Wentworth Region was used to help find a suitable study area that will satisfy all of the above criteria.

4.2.1 Geology and Climate of the Hamilton-Wentworth Region

The Niagara Escarpment is the edge of an ancient lake and runs through the Hamilton-Wentworth Region. The Escarpment is approximately 100 metres higher in elevation than the Plain (a term used for the area below the escarpment). This increase in elevation causes differences in average temperatures between the Escarpment and the Plain (Royal Botanical Gardens 1995). Areas above the

Escarpment do experience greater snowfall. Climate in the Hamilton-Wentworth Region is considered continental but is affected by the close proximity to Hamilton Harbour and Lake Ontario. Precipitation is fairly consistent from year to year but there is some variation in the distribution of precipitation during the year. Normal yearly precipitation is estimated as 866.8 mm, consisting of 740.1 mm of rain and 126.7 cm of snow (Royal Botanical Gardens 1995). Summer rainfall comes in relatively brief showery periods but heavy thunderstorms do sometimes occur. Temporary local flooding of small streams may occur in March when snow-melt is rapid. The average date for last frost is May 3 and the first autumn frost occurs on about the 15th of October (Royal Botanical Gardens 1995). Dry or wet spells usually end before they produce any serious effects on agriculture, but irrigation is used in the area. Therefore, the first in the list of criteria for choosing a study catchment has been satisfied.

The Escarpment has exposed bedrock indicating fractured layers of Limestone and Ordovician Shale (Karrow 1963). The depth of overburden above the bedrock is easily known at the edge of the Escarpment and grows with distance from the edge. The overburden at the Escarpment edge in the vicinity of the Town of Dundas can be as little as one metre and grows to as much as 20 metres just 10 km south of the Escarpment (Ontario Department of Mines 1969). Quinn (1991) discovered that in one study area in which the soil thickness was almost 30 m, TOPMODEL was rendered unsuitable because the model was having difficulty modeling water table movement at that depth. Therefore, a drainage area relatively close to the Escarpment edge is suitable for a TOPMODEL application.

From examining a map of the hydrometric network monitored by Environment Canada (Environment Canada 1993a), gauge 02HB021 "Ancaster Creek at Ancaster" was chosen. According to Environment Canada, the gauge is less than one km away from the Escarpment edge and drains an area of approximately 9.0 km^2. The Creek

and the gauge are shown in Figure 4.1. The Drift Thickness Map (Ontario Department of Mines 1969) indicates that the overburden thickness in this area is anywhere from 7.0 to 14.0 metres. This is believed to be a suitable thickness.

A map indicating drainage characteristics of soils in the vicinity of the Creek is shown in Figure 4.2. Presant et al. (1965) indicate that the soil in this area is mostly comprised of a sandy loam that drains well. There are small regions that drain poorly but they are not extensive.

The degree of slope in the Ancaster Creek area is wide ranging with values averaging roughly 15% in the vicinity of the stream and as low as 0.5 % close to the divide. A preliminary investigation of the area draining into Ancaster Creek at the gauge reveals an average slope across the area of roughly 3-5 %. The mild slopes occur primarily in the headwater areas near the divide. These slopes are considered within the range acceptable by TOPMODEL.

MacLaren (1990) conducted an extensive watershed study of Spencer Creek that included Ancaster Creek. The land-use maps used in their study indicate that the percentage of urbanization in the area draining to gauge 02HB021 is approximately 20%. Other land use types in the area include farmland, parks, golf courses, and forest. Therefore, all seven criteria have been satisfied and Ancaster Creek near Ancaster, Ontario is the focus of this study.

4.2.2 Meteorological and Hydrometric Data

Ancaster Creek eventually drains into Hamilton Harbour which is approximately 10 km downstream of the gauge. The Harbour, the Lake and the Niagara Escarpment alter climate in the area. Various meteorological data are available at two of the closest Environment Canada stations: Atmospheric Environment Service (AES)

station 6153300 at the Royal Botanical Gardens (RBG) in Burlington, and AES station 6153194 at the Hamilton International Airport (which will henceforth be referred to as AIRPORT). Hourly temperature and wind data are available at the RBG; however, rain data is only available at daily time-steps along with the number of hours of sunshine and pan evaporation levels at daily time steps. Monthly values of soil moisture are also recorded. The AIRPORT station collects similar data at similar resolutions. More than a decade's worth of digital meteorological data were obtained from Environment Canada for these two stations. Any required data that were not available in the digital format were entered manually from hardcopy formats available for both stations. These include relative humidity, the number of hours of sunshine per day, wind speed and direction, soil moisture levels and daily pan evaporation values. The temperature, humidity, hours of sunshine and wind speeds will be used to estimate daily potential evapotranspiration in Section 4.7.

The hydrometric gauge that defines the Ancaster Creek catchment collects cumulative rainfall and discharge data (hydrometric data) in 15 minute increments. The hydrometric data were made available by Environment Canada and the rainfall collected were made available by the Hamilton Region Conservation Authority (HRCA). Additional hourly rainfall data were provided by the Regional Municipality of Hamilton-Wentworth from five other tipping bucket rain gauges that surround the Creek in this area. The locations of these gauges are shown in Figure 4.3.

The rainfall data provided by the HRCA was available from 1982 onwards. However, the rainfall data made available by the Municipality ly between 1989 and 1993. The HRCA data were provided in a format that required a great deal of processing before it could be used by the model. Furthermore, only one gauge was available from the HRCA. To assess whether the HRCA gauge data contain errors, its data should be compared to the data of other gauges nearby. For this reason, it was decided that using test periods before 1989 was impractical. However, since

1988 is generally known to be a very dry year, it was decided that 1988 would be included in the testing. Therefore, the simulation periods for this dissertation will take place between, and including, 1988 and 1993, making a total of six years.

4.2.3 Choosing the Wet, Dry and Average Test Periods

A continuous hydrologic model should be able to model a wide range of meteorological conditions. It is impractical however, to model very long periods that extend for decades. Instead, hydrologists often select periods of wet, dry and average levels of precipitation on which to conduct tests. How a year is determined as "wet" must be resolved.

4.2.3.1 Using Meteorological Data

Canadian climatic normals (Environment Canada 1993b) were referenced for information on precipitation values observed over extended periods of time. "Normals" are climatic elements averaged over a fixed, standard period of 30 years and the publication cited above computes normals for the period of 1961-1990 for sites in Ontario. Several sites near Ancaster Creek were selected and they show the following precipitation normals for the entire year and in the snow-free period.

Table 4.1: Climatic Normals for Meteorological Stations in the Vicinity of Ancaster Creek.

Station	Annual Normal Precipitation (mm)	May - Oct. Normal Rain (mm)
Hamilton Airport 43°10'N79°56'W Elev. 237 m 1959-1990	890.4	455.7
Hamilton Municipal Lab 43°15'N79°46'W Elev. 76 m 1967-1990	847.8	437.2
Hamilton Psych. Hospital 43°14'N79°54'W Elev. 198 m 1960-1990	904.0	473.6
Hamilton RBG 43°17'N79°53'W Elev. 102 m 1950-1990	866.8	455.1

How a year is determined as dry or wet is important. The author maintains that if the precipitation is less than or greater than the climatic normal by a certain number of standard deviations, than it can be considered dry or wet. Unfortunately, standard deviations are not published with the climatic normals. Instead, standard deviations were computed using data over the 12 year period between 1983 and 1994 at the RBG and AIRPORT stations. Figures 4.4 and 4.5 show total precipitation for the AIRPORT and the RBG, respectively. Values for two different periods are indicated: the entire year in Figures 4.4 a) and 4.5 a); and the period between May and October in Figures 4.4 b) and 4.5 b). Climatic normal values are provided along with the computed standard deviations. The precipitation totals for the period between May and October are shown because the version of TOPMODEL that will be used in this dissertation does not include a snow-melt component. Therefore, TOPMODEL applications will occur during the snow-free period of any year.

The AIRPORT lies above the Escarpment while the RBG resides in the Plain. As the Ancaster Creek catchment lies entirely above the Escarpment, one may feel that using just the AIRPORT for a decision regarding meteorological conditions would suffice. But the lines of ±1 and ±2 standard deviations shown in Figure 4.4 indicate that the computed 12 year average is higher than the climatic normal. This indicates that the 12 year period experienced greater than climatic normal precipitation levels. If the standard deviation lines are used to select the wet, dry and average test periods, then some years would be deemed dry in comparison to their neighbours, but they are in actuality average when compared to the climatic normal. Thus a bias to label years as dry exists. For this reason, an analysis of RBG data was also included in this discussion.

From examining the figures, it was determined that any year extending between one and two standard deviations would be either wet or dry, depending on whether they were greater or less than the mean, respectively; and any year extending between the normal and one standard deviation would be an average year, with some indication of being either on the slightly wet or slightly dry. The RBG observations fluctuate around the climatic normal with no noticeable upward or downward trend while the AIRPORT data show a general downward trend. From Figure 4.4 a), one may conclude that 1988 and 1991 are dry; 1989 and 1993 are average with 1993 being slightly dry; and 1990 and 1992 are wet. Figure 4.4 b) implies that the snow-free period of 1988 was average to slightly dry; 1989 and 1990 were average but slightly wet; 1991 was dry; 1992 was wet; and 1993 was average but just slightly wet. Figure 4.5 a) shows 1988 and 1989 as dry; 1990 and 1992 as wet; and 1991 and 1993 as average but just slightly dry. Figure 4.5 b) shows 1988, 1989, 1991 and 1993 as average but on the dry side; 1992 as wet; and 1990 as average but slightly wet. There does exist in the discussion above, a few cases where the same year is consistently wet or dry but there is also a fair amount of crossover. From these observations, the author considers the years of 1988 and 1991 to be dry, 1990 and 1992 to be wet, and

1989 and 1993 to be average.

4.2.3.2 Using Baseflow Data

An important parameter indicating the retention characteristics of a catchment is the Base Flow Index (BFI). This parameter is an indicator of the hydrological effects of the catchment's geology and soil, as well as the retention characteristics of the catchment (Moin et al. 1986). Developed at the Institute of Hydrology in the UK (Institute of Hydrology 1980), it is considered the most significant independent variable in low flow analysis. The procedure for computing BFI involves calculating the total volume of baseflow v_b, (m^3) over the total volume of runoff v_a (m^3). The volume v_b is determined through a baseflow separation technique. The BFI provides a quantitative measure of the ability of a drainage area to sustain low flows. For this reason, it is not expected to vary greatly from year to year, yet the BFI when calculated on an annual basis does show some variability depending on the climatic conditions of that year. Consider the following analysis.

BFI estimates from flow data can be calculated using the following steps (Moin et al. 1986):

1. Using daily discharge data over a period of one year, break the year into successive five day periods.

2. Identify the minimum flow in each of the five day periods.

3. Consider in turn the minima (Q_1, Q_2, Q_3), (Q_2, Q_3, Q_4), .. (Q_{n-1}, Q_n, Q_{n+1}). For each group of 3, if (0.9 x the central value) is less than both the outer values, then the central value is identified as a turning point on the baseflow separation line. Continue this process until the penultimate five day minimum is found.

4. Construct the baseflow separation line by joining all the turning points.

5. The volume v_b is computed from the trapezoidal rule as the volume of water below the baseflow separation line.

6. The volume v_a is the sum of the mean daily flows between the first and last turning points inclusive (volume beneath the hydrograph).

7. Compute BFI equal to v_b/v_a.

A short FORTRAN program was written to compute the BFI for daily discharge data (free of ice and when a continuous series was available) for the years between 1988 and 1993. The following BFI were obtained,

Table 4.2: BFI values for the period between 1988 and 1993.

Year	BFI
1988	0.683
1989	0.689
1990	0.598
1991	0.684
1992	0.630
1993	0.647

The higher a BFI value is, then the greater the volume of baseflow to total hydrograph flow. This could indicate conditions in which precipitation levels were low during that year, and the soil was able to absorb large amounts of moisture. This would be indicative of a dry year. Table 4.2 above indicates that 1993 is the median year in the table, and 1993 was considered an average year in Section 4.2.3.1. The

years 1992 and 1990 have lower BFI's than 1993, thus indicating they are wetter years. The remaining years have BFI's higher than that of 1993 which indicate they are all drier than 1993. This coincides well with the results of Section 4.2.3.1. Therefore, the labels indicating which years were wet, dry or average that were given in Section 4.2.3.1 will be used as a guide in the calibration and verification of TOPMODEL.

4.2.4 Topographic Data

Topographic data in the form of contours and spot data were taken from Ontario Base Maps in digitized format received from the Ontario Ministry of Natural Resources. The contour interval is 5 m in most areas and 2.5 m in urban areas. The scale of the original map is 1:10,000. Other digitized information taken from the Ontario Base Maps include road networks, home and building locations, quarries, vegetation, land-forms and lakes.

4.3 Digital Elevation Models for Ancaster Creek

4.3.1 Using GIS Technology with TOPMODEL

A Geographic Information System (GIS) can be defined as "an organized collection of computer hardware, software, geographic data, and personnel, designed to efficiently capture, store, update, manipulate, analyze and display all forms of geographically referenced information" (ESRI 1990). The last decade has seen a rapid development in GIS technology and its use is found in a wide variety of applications including land use planning, natural resources management, ecological research, and water resources management (ESRI 1990). The use of GIS in hydrology is becoming more and more common; primarily because of its powerful ability to manage large amounts of spatial data. GIS are highly specialized spatial

database management tools intended to provide the user with the ability to access and manipulate large amounts of the data with relative ease.

The literature contains various TOPMODEL applications in conjunction with GIS. Chairat (1993) used GRASS, a US Army Corps of Engineers GIS, to compute various TOPMODEL parameters. Quinn (1991) used a GIS-like software to construct Digital Elevation Models (DEMs) for the catchment study area. Wollock et al. (1995) used the GIS ARC/INFO to construct DEMs as well as compute some of the topographic indices used in their research. A more sophisticated integration of TOPMODEL with a GIS is described by Romanowicz et al. (1993) who implemented TOPMODEL as one of a number of application modules within the Water Information System (WIS) - a "four-dimensional" database and GIS. The integration of TOPMODEL into WIS allows a user access to catchment characteristics; conduct sensitivity analysis; predict flow and soil moisture distribution, as well as display maps for visual inspection. This last application is the best integration between TOPMODEL and GIS seen in the literature thus far. But, it is not the author's objective to integrate TOPMODEL with a GIS to this extent; but only to use the GIS to perform some otherwise tedious tasks quickly and easily.

The GIS ARC/INFO version 7.0.4 is used in this research. ARC/INFO is a very sophisticated and powerful GIS and has the capability to construct DEMS, delineate watershed boundaries and a host of other useful tools in watershed analysis. In this dissertation, any ARC/INFO commands that are given to the reader will be shown in `courier font` in both the main text and in the Appendix.

Digital Elevation Models are representations of terrain elevation in the form of grids with internal cells of equal dimension. Each cell is associated with a value of elevation, whereby that value is the average elevation of the terrain within the area of that grid cell. The source data used in the construction of the DEMs were obtained

from Ontario Base Maps provided in digital format by the Ontario Ministry of Natural Resources. The minimum requirements to construct a DEM are contours of elevation or spot elevation data. Both can be used together if they exist. Furthermore, positional information on the stream network should also be used in the DEM construction. Spot elevation data, contour line data and stream position data, were provided at a scale of 1:10,000 by the digitized Ontario Base Maps, and were placed into an ARC/INFO database.

4.3.2 DEM Sizes

The first question of importance in constructing the DEMs is the cell resolution. The DEM's resolution provides the smallest modeling unit within which all values are averaged. In an effort to investigate cell resolution effects on modeling hillslope processes, several test sizes are required. A cell size that is too large can't represent subtle but possibly important features. Cell sizes that are too small, mean sacrificing computation time and may lead to interpolation errors. Practically speaking, what is the finest resolution that can be used in this type of hydrological application?

There are several issues involved in choosing the finest resolution, or the coarsest, in an aggregation study. The US Geological Survey (USGS) (1993) contend that the accuracy of a DEM will depend on the level of detail of the original source map and not surprisingly, the cell size chosen for the DEM. The most significant limiting factor for the level of detail in the source map is the scale of the source. Furthermore, if there is little detail in a section of the map, then there is little reason to have a small DEM cell size for that region. Hence, the amount of topographic relief is also a factor. According to Aronoff (1991), the selection of map resolution is a judgement call in which both the representation of the information and any lack of information should be addressed.

The literature review on studying the effects of DEM aggregation seems to show a point of contention between what the smallest DEM cell size should be to accurately capture hillslope processes. Wolock at al. (1994) concluded that TOPMODEL is highly sensitive to the mean of the topographic index and this is in turn greatly affected by DEM scale and resolution. Zhang et al. (1994) found that decreasing grid size shifted the distribution of topographic index towards lower values. Consequently, predicted saturated areas and the computed peak discharge increased with increasing grid cell size. They found that a 10 m DEM provided significant improvement over coarser grids for modeling discharge in moderate to steep topography. The authors suggest that the length scale of the primary landscape features of interest in the field should provide a natural guide to an appropriate grid size and that it is unreasonable to use a 30 or 90 m grid size to model hillslope or runoff generation processes in moderately to steep gradient topography without some calibration of the process model. Quinn et al. (1995) found that grid sizes of around 100 m were considered too large to depict the topographical form of individual hillslopes and that large grid cell sizes tend to ignore the existence of lower order channels. They found that using a DEM with cell size of 50 m is adequate for simply predicting hydrographs, but smaller sizes would be necessary for any internal validation. This was re-iterated by Bruneau et al. (1995) who found that DEMs of cell sizes of 30 m to 50 m provided the best results when predicting hydrographs.

Therefore, the minimum cell resolution for the aggregation phase of this research is chosen as 10 m. With regard to the discussion in the paragraph above, is a 10 m cell size inappropriate? An examination of the contours near the creek shows that there is a high concentration of contours which are very closely spaced and at times, less than 10 m apart. The rural areas near the catchment divide have few contour lines and spot data indicating low relief. However, there are numerous and closely spaced contour lines in the urban areas and in the region close to the gauge, thus indicating high relief. By considering the fair amount of relief that exists in the area the author

believes that a 10 m cell size is appropriate. Other cell sizes that were chosen were 15 m, 20 m, 25 m, 30 m, 40 m, 50 m, 60 m, 80 m, and 100 m. The cell size of 100 m was chosen as an upper limit for various reasons: 1) to keep down the number of tests that would have to be conducted for each DEM size (at least 3 calibrations for each DEM size); and 2) Quinn et al. (1995) warned that 100 m DEMs were unable to capture topographic form at the hillslope scale. Note, that the catchment is only 9 km^2 and it was felt that any further increase in grid cell size would certainly obscure features important to hillslope processes in a catchment of this size. Finer differences in DEM sizes were chosen at the lower end of the range because the literature review indicated that the smallest DEM cell size should be somewhere between 10 m and 50 m.

4.3.3 Quality Assurance: DEM Accuracy

"Error is introduced at every step in the process of generating and using GIS. The objective in dealing with it is to manage it, not eliminate it" Aronoff (1991). As a starting point to managing DEM errors, we begin with the USGS which provides DEM products for engineering and scientific use. The USGS has developed a set of accuracy standards for their DEM products depending on the final intended use. DEMs can have two types of error: vertical accuracy dealing with the predicted elevation vs. the actual elevation, and horizontal accuracy that deals with differences in actual and predicted positions (Aronoff 1991). The latter is caused by the fact that any terrain feature within a cell is reduced to a value at the centre of the cell and now its spacing from any other terrain feature is some function of the regular spacing of grid cells. This creates problems if attempting to recover positions of terrain features that may be less than the cell spacing. The USGS (1992) define three types of errors: blunders, systematic errors and random errors. Blunders are easily identified and often caused by misreading contours, transposing values and other carelessness. Systematic errors are those that follow some fixed pattern or rule, such as a constant

magnitude or sign and are introduced by procedures and cause bias. Random errors "result from accidental and unknown combinations of causes beyond the control of the observer".

Since the DEMs in this dissertation are constructed from contour lines, blunders can be identified by constructing another contour map from the constructed DEM (use LATTICECONTOUR command in ARC/INFO). Any blunders due to an incorrect input of contour elevation will result in the creation of concentric circles of contour lines around the erroneous contour line. When the new contour map is overlain on top of the original, the blunders become obvious and can easily be corrected. Root Mean Square Error (RMSE) is a statistic used to encompass both random and systematic errors. The RMSE of each DEM will be used to assess the degree to which the constructed DEMs contain these two types of errors.

The USGS has three quality levels for a DEM. Level 2 DEMS are derived from hypsographic (contour lines and spot elevations) and hydrographic (streams and lakes) data from existing maps and are similar to the type of DEMs constructed in this research. The RMSE should be less than or equal to one-half of the contour interval and no errors should be greater than one contour interval in magnitude. The program used in this thesis to construct the DEMS is a special function called TOPOGRID in ARC/INFO. TOPOGRID uses contour lines, spot elevations and streams to construct DEMs according to the method of Hutchinson (1989). The DEM accuracy was tested against known benchmarks and a minimum number of 28 test points per DEM is required. Test points should be well distributed and representative of the terrain (USGS 1992). The following equation for RMSE was used as a measure of systematic and random error,

$$RMSE = \sqrt{\frac{\sum_{i}^{N_P}(y_i^P - y_i^t)^2}{N_p - 1}} \quad (4.1)$$

where N_P is the number of test points, y_i^P is the interpolated elevation of the point i (m), and y_i^t is the true elevation of the point (m).

The input file for the TOPOGRID module and other commands used for processing DEMs with ARC/INFO is shown in Appendix A3. The tolerances shown are preselected based on such things as contour interval (ESRI 1995). Geodetic bench marks were obtained and are based on the mean sea level. The DEM was sampled at the locations of these bench marks and the elevations at these points were then compared to the bench marks using ARC/INFO commands. There were only 25 geodetic benchmarks in the area of the catchment and five of these had to be removed from the test because their description placed them at elevations other than ground level. There were some benchmarks in the set of 20 that were suspicious in that the elevations differed significantly from nearby contour lines or spot elevations. However, the description that accompanied these benchmarks did not provide enough information to warrant their elimination from the test. Because of the lack of benchmarks, the RMSE test was also conducted using the original point coverage of spot elevation data. The geodetic bench marks were provided in the form of a point coverage. Both this coverage and the coverage of spot elevation data were converted to grids using GRIDPOINT. A series of simple commands were used to compute the RMSE. The following table lists the DEMS and the resulting RMSEs that were computed.

Table 4.3: RMSE for each DEM

DEM	RMSE - Geodetic Benchmarks (m)	RMSE - Spot Data (m)
10	1.9	0.8
15	2.3	0.6
20	2.0	0.4
25	2.2	0.5
30	2.2	0.6
40	2.1	0.6
50	2.3	0.8
60	2.7	0.6
80	2.7	1.5
100	3.3	1.9

The RMSE values computed using the spots coverage indicate that the DEM is comparable in accuracy to a USGS level 2 DEM. The RMSE computed using the Geodetic Benchmarks for the DEMs up to 50 m in cell size is less than 1/2 the contour interval but for the coarser DEMs the RMSE is between 1/2 and 1/3 of the contour interval. Because, the number of geodetic benchmarks is low, this RMSE cannot be used to classify the accuracy of these DEMs according to USGS standards. But considering the low number of benchmarks available, and the possibility of the inclusion of some ineligible benchmarks, the RMSE values are still quite low. In no case was there an RMSE value that was greater than the contour interval. The author concludes therefore, that the DEMs are comparable to level 2 USGS DEMs in accuracy.

It is interesting to note the variations in benchmark RMSE and spot data RMSE, with DEM cell size. In the benchmark RMSEs, the lowest error is seen in the 10 m DEM and the RMSE remains relatively constant up to 50 m. But the RMSE jumps in value at the 60 m DEM and increases to a value of 3.3 for the 100 m DEM. This would

imply that the DEM cell size in excess of 50 m created by TOPOGRID is too coarse to accurately model terrain elevation as well as the finer DEMs. But in the spot data RMSE values, the 10 m DEM has one of the higher errors and the 20 m one of the lowest. The errors are relatively constant up to 60 m and more than double at 80 m and above. This is an indication that the DEMs above 60 m are markedly different in the portrayal of terrain elevation when compared to the DEMs from 10 m to 60 m. It is evident that the average elevations found in DEMs with cell sizes higher than 50 m or 60 m are not as accurate in modeling the relief that exists in the Ancaster Creek catchment, as well as DEMs of finer cell size.

4.4 Catchment and Subcatchment Delineation

4.4.1 Catchment Delineation

Basins are delineated in ARC/INFO using the WATERSHED command and a user specified *pour point*. A pour point is the grid cell that defines the location of the catchment outlet. Therefore, the pour point in this research is the hydrometric gauge. The WATERSHED function determines all those cells that drain into the pour point cell by using an input grid of drainage direction with the following command line,

```
ancaster_boundary = WATERSHED(ancaster_direction, pour_point)
```

where ancaster_boundary is the grid indicating the cells that reside within Ancaster Creek catchment, pour_point is the point coverage indicating the location of the hydrometric gauge, and ancaster_direction was created using the FLOWDIRECTION command,

```
ancaster_direction = FLOWDIRECTION(ancaster_dem)
```

where ancaster_dem is the DEM created in the previous section. The

FLOWDIRECTION command will determine the direction of steepest descent from one cell to another. By knowing the direction in which all cells flow, the WATERSHED command is able to determine which cells drain into the pour point.

The catchments delineated for each DEM are shown in Figures 4.6 through to 4.8. With the exception of Figure 4.6 a), the catchment delineated using the 10 m DEM is shown in all the figures as a lightly dotted line. The table below lists the resulting catchment areas that resulted for each DEM size.

Table 4.4: Catchment area versus DEM grid cell size.

DEM Grid Cell Size	Area (km^2)	% Difference from 10 m DEM
10	7.84	
15	8.02	2.3
20	7.79	-0.6
25	8.17	4.2
30	7.82	-0.2
40	7.86	0.3
50	7.94	1.2
60	7.43	-5.2
80	7.69	-1.9
100	7.33	-6.5

The table above seems to imply a slight downward trend of catchment size with increasing grid cell size. From Figures 4.6 to 4.8, notice that there is not a great deal of variation between catchment shapes and the location of the boundary remains relatively unchanged. However, there are marked differences in boundary location in sections of catchment outline produced with the 30 m DEM and the 60 to 100 m DEMs. The 30 m DEM boundary has what seems to be a large section "missing" from the lower left section of the boundary when compared to the 10 m DEM

boundary. Similar differences are seen with the 60 m, 80 m and 100 m DEM boundaries which have sections differing from the 10 m boundary in the upper right.

Differences in watershed divide location and catchment size are explained by the simple fact that as cell sizes increases, the area represented by a given cell elevation increases, and the cell's boundaries will change position with each new DEM size. As a catchment boundary can only be constructed from the boundaries of grid cells, cells close to the catchment divide will begin to average areas that skirt both sides of the boundary as the cell size increases. Consider the situation where cells outside the boundary have a much steeper slope than those cells inside the boundary. Depending on the location of the cells and the amount of area they average, it is likely that the elevations near the divide will start to lower in favour of elevations on the outside of the boundary simply because the slopes are much steeper there. This may lead to a gradual loss of catchment area near the boundaries, and the catchment divide gets drawn further inward from the divide of the finer DEMs. The two areas in the figures where coarse DEM boundaries differ from the 10 m boundary, happen to occur in relatively flat areas. Therefore, it is not surprising that these flat areas are sometimes excluded and sometimes included in the catchment boundary.

A watershed study was conducted of the Spencer Creek Watershed which includes Ancaster Creek (MacLaren 1990). The catchment delineated manually by MacLaren Plansearch, Inc. from contour lines and spot elevation data had an area of 8.36 km^2. This is greater than any of the areas shown in Table 4.3, but only 2.3% greater than the 20 m DEM catchment, which is the largest, and 14.1% greater than the smallest catchment delineated using the 100 m DEM.

4.4.2 Subcatchment Delineation

Ancaster Creek experiences a fair amount of varying slope within the catchment boundary; thus, with regard to main channel routing, the catchment will be subdivided in subareas of constant channel slope. Slopes along the stream course were determined using the SLOPE function. These slopes indicate that there are four distinct sections within which the slopes do not vary greatly, but between sections the slopes vary by a fair amount. Hence, three pour points in addition to the pour point defined by the gauge were used to delineate four subbasins. The subcatchments are shown in Figures 4.9 through to 4.11. Table 4.4 lists the subcatchment areas. Each subcatchment has been given a name which the author will use in future sections dealing with the subcatchments. These names are shown in Figure 4.9 (a) and were chosen based on the location of the pour point.

Table 4.5: Subcatchment areas in km^2 for each DEM.

	10	15	20	25	30	40	50	60	80	100
Hwy 403	3.34	3.44	3.55	3.69	3.48	3.39	3.77	3.44	3.29	3.54
Maple Lane	1.47	1.47	1.22	1.37	1.15	1.66	1.03	1.37	1.79	1.17
Golf Links	1.20	1.32	1.22	1.27	1.35	1.04	1.32	0.92	1.06	0.94
Wilson St.	1.82	1.79	1.81	1.83	1.83	1.77	1.81	1.70	1.55	1.68

There is some variation in subcatchment boundary position between DEM sizes, and there is some variation in the size of each subcatchment with regard to DEM size. This would be caused by the same reasons that were noted in Section 4.4.1. Boundaries dividing subcatchments are likely to change position with DEM size as

the number of rows and columns in each grid changes and area is exchanged between neighbouring subcatchments.

4.5 Spatial and Temporal Distribution of Rainfall

The precipitation data provided by the HRCA is in 15 minute increments, but the data provided by the Municipality are all at hourly time steps. The literature review in Chapter 3 indicated that in order for the TOPMODEL assumption of quasi-steady state to hold true, a time step of one hour or greater is preferred and a time step less than one hour may violate this assumption. Therefore, the HRCA data will be aggregated to hourly time steps.

While the Ancaster Creek catchment is one of the smaller catchments to be monitored by Environment Canada in this region, there may be some variation in the spatial distribution of rainfall. In order to determine if any spatial variation in rainfall existed across the catchment, the rain data from all the gauges were compared to one another. A slight variation was observed in the values but the shape of the hyetographs were nearly identical amoung gauges (i.e. rises, falls and peaks each occurred at the same time for every gauge). For this reason, it is practical to model with an areal average of rainfall over the entire catchment.

Singh (1989b) gives an excellent review of 15 different methods to determine areal average rainfall over a catchment from multiple gauges. The Reciprocal Distance Squared Method (RDS) has been chosen to determine the areal average for the catchment. From examining the 15 methods in Singh's review, the RDS method revealed itself to be one of the most amenable to computation by a GIS. The method is sound, rigorous and robust and not often used because of the intensity of the computations. The equation provided by Singh (1989b) was modified to consider a grid of equal cell sizes. The derivation of Equation (4.2) below is shown in

Appendix A4.

$$\bar{R} = \sum_{i=1}^{N_R} w_i P_i \tag{4.2}$$

$$w_i = \frac{1}{N_E} \sum_{j=1}^{N_E} \frac{\frac{1}{D_{ji}^2}}{\sum_{i=1}^{N_R} \frac{1}{D_{ji}^2}} \tag{4.3}$$

where N_R is the number of rain gauges, N_E is the number of cells within the catchment, w_i is the weight assigned to each gauge, D_{ji} is the distance between the cell j and the gauge i (m), $\bar{R}$ is the average rainfall across the catchment (mm) and P_i is the rainfall observed at that gauge (mm). The commands used in ARC/INFO to compute the weights w_i are shown in Appendix A5. The computed weights are shown in Table 4.6.

Table 4.6: RDS rain gauge weights for the Ancaster Area.

Gauge	1988	1989	1990	1991	1992	1993
02HB021	1.0		0.245[1]	0.245[1]	0.245[1]	0.307
					0.292[2]	
					0.307[3]	
Ancaster Reservoir 18		0.089	0.064[1]	0.064[1]	0.064[1]	
			0.089[2]	0.089[2]		
Daffodil Crescent PS		0.062	0.036[1]	0.036[1]	0.036[1]	
			0.062[2]	0.062[2]	0.045[2]	
Harmony Hall PS		0.689	0.564[1]	0.564[1]	0.564[1]	0.693
			0.689[2]	0.689[2]	0.663[2]	
					0.693[3]	
Lee Smith PS		0.160	0.092[1]	0.092[1]	0.092[1]	
			0.160[2]	0.160[2]		

[1,2,3]A common superscript indicates a single series of weights used for a certain period of time. Often, the rain data provided by a gauge for a given year would contain gaps. When a gap occurred, that gauge was rendered unavailable. If weights have the same superscript for a certain time period of a given year, then all those gauges were available.

The rain gauge values measured at the Ancaster Industrial Park were only available in 1993 and for that year, very little rainfall was measured at that gauge. The data at the gauge was considered suspect when compared to rainfall from the other gauges, so its input was excluded.

4.5.1 Quality Assurance of Rain Data

The precipitation data had to be checked for anomalies such as measured rainfall that did not coincide with observed rises in hydrometric flow and vice versa. The gauges did suffer from such problems as lightening strikes that cause sudden high peaks or

unlikely changes in observed values. For this reason, the following steps were taken to ensure that the rain data were reliable:

1. If the hyetograph showed sudden sharp jumps in value, then those values were compared against data from the other available gauges. If the other gauges indicated that no rainfall had occurred, then the suspect value was set to 0.0. If no other gauges were available, then AIRPORT daily rain data were used to assess the likelihood of the sudden change in values.

2. If the rain data showed a rise from 0 but no increase in streamflow was observed, then again that rain data were compared to other gauges, or Airport daily rain data and necessary adjustments were made.

3. If the flow data showed a rise where no rise in rain data existed, then that section of the series (both flow and rain) was removed.

When these three steps were taken, the hyetographs between rain gauges were very comparable. Temporal variations were identical with regard to time to peak, and variations in peak rain intensity varied by less than 20%.

4.6 Evapotranspiration

The Ancaster Creek catchment defined by gauge 02HB021 drains land that is urban (low and high density), recreational (golf courses) and agricultural (corn and short crops). Thus, estimates of potential evapotranspiration will vary across these types of landscapes. Meteorological data is available for estimating evapotranspiration at the AIRPORT but modeling with a spatial variation in potential evapotranspiration is simply impractical. As stated in Section 2.3, the Penman-Monteith method will be used to calculate daily potential evapotranspiration. A FORTRAN program was

created from the equations given in the Food and Agricultural Organization document by Smith (1990). Daily values were converted to hourly values by assuming a sinusoidal fluctuation in radiation intensity from 6 a.m. to 6 p.m., with the maximum intensity at 12 noon. This relationship assumes that net radiation is the main driving force of the evaporation regime (Quinn 1991). Values of relative humidity, wind speed, hours of sunshine, and other meteorological data were obtained from the AIRPORT for the years in question. The equations used in the FORTRAN program are shown in Appendix A6 where daily evapotranspiration is computed as,

$$ET_o = \frac{0.408\Delta(R_n - G_f) + \gamma(\frac{900}{T+273})U_2(e_a - e_d)}{\Delta + \gamma(1 + 0.34U_2)} \quad (4.4)$$

ET_o is the reference crop evapotranspiration (mm/day), R_n is the net radiation at the crop surface ($MJm^{-2}d^{-1}$), G_f is the soil heat flux ($MJm^{-2}d^{-1}$), T is the average temperature (°C), U_2 is the windspeed measured at 2 m height (m/s), γ is the psychometric constant (KPa $°C^{-1}$), Δ is the slope vapour pressure curve (KPa $°C^{-1}$), e_a is the saturation vapour pressure at temperature T (KPa) and e_d is the actual vapour pressure (KPa).

4.6.1 Quality Assurance of Evapotranspiration Estimates

The only way to verify the estimates of potential evapotranspiration was to compare them to pan evaporation data collected at the RBG. The AIRPORT does not collect evaporation data. When estimates of potential evapotranspiration computed using Equation (4.4) were compared informally to the RBG pan data, the RBG values were marginally higher. Potential evapotranspiration should be less than pan evaporation and therefore, this was considered an acceptable measure of quality assurance for the

potential evapotranspiration estimates in this thesis.

4.7 Internal Catchment Routing

The process by which overland flow reaches a subcatchment outlet is difficult to describe. But if the time that runoff takes to reach a channel is longer than one time step, then an overland flow routing scheme should be employed. The overland flow routing scheme used in this research is similar to that used by Quinn (1991) which is easily implemented in the TOPMODEL structure. Each subcatchment is divided into N_{RV} segments of flow path and the fraction of subcatchment area that is drained by that segment is also computed. The time it takes for the total subcatchment runoff to reach the subcatchment outlet is,

$$T_{RV} = \sum_{k=1}^{N_{RV}} \frac{l_k}{v_{RV}} \tag{4.5}$$

where T_{RV} is the time it takes for the runoff to reach the basin outlet (hr), l_k is the length of the flow path segment k (m) and v_{RV} is the velocity of the runoff (m/hr).

The estimated overland flow path was subdivided into roughly 500 m segments, and the fraction of area that drained through each segment was determined with ARC/INFO using the FLOWACCUMULATION command. This command provides the number of upslope cells draining into a cell:

```
ancaster_accum = FLOWACCUMULATION(ancaster_direction)
```

where ancaster_direction was created using the FLOWDIRECTION command. By knowing the number of upslope cells draining to the head of a segment k, then the fraction of area draining to that point is easily known.

The equation above is used to compute a time delay histogram and thus, the overland flow routing method employed here is essentially the time-area routing method of Clark (1945). The method for computing the time-area-histogram is shown in Appendix A2 (as mentioned in Chapter 3). The velocity of the runoff is assumed constant across the catchment. While it is uncertain what effect runoff will have in this application at this time, a calibration parameter is introduced called F_{RV} which will factor the constant runoff velocity v_{RV}.

4.8 River Routing

As the catchment has been subdivided into subcatchments, a main channel river routing scheme must be employed to route flow from one subcatchment to another. Numerous schemes for river routing exist, but because backwater effects are negligible in Ancaster Creek, and the slopes are believed to be sufficiently steep, a kinematic method is appropriate. MacLaren (1990) indicated that the Muskingum-Cunge routing scheme is one of the more suitable routing methods for watersheds in Southern Ontario. Muskingum-Cunge routing is a variation of kinematic wave routing and is based on the Muskingum method which has traditionally been applied to linear hydrologic storage routing (Chow et al. 1988). This method has been adopted in this research. The full set of equations used to implement the Muskingum-Cunge Routing method are shown in Appendix A7. The degree of attenuation exhibited by an output hydrograph is a measure of a dimensionless constant X, representing the wedge storage in the routing reach,

$$X = \frac{1}{2}\left(1 - \frac{q}{S_o c \Delta x}\right) \tag{4.6}$$

where Δx is the reach length through which the flow is routed (m), S_o is the bed slope, c is the wave celerity (m/s) and q is the stream flow per unit width of water surface (m^2/s), i.e., $q = Q/B$ where B is the water surface width (m) and Q is the

discharge (m^3/s). The bed slope S_o would be determined from ARC/INFO using the SLOPE function which computes the slope across each cell. The values of topographic parameters that were obtained using ARC/INFO are also shown in Appendix A7.

The parameter that is specified by the user in this method is the speed of the flood wave through the channel c. The flood wave celerity is considered constant but a calibration factor F_{CHV} has been introduced in this application of TOPMODEL which will be multiplied by the channel routing velocity in the computation process.

4.9 Application Periods

A calibration period and verification periods for the aggregation phase of this research should be selected. The calibration period was selected as May 23 to Oct. 31, 1991. This period was selected for two reasons: 1) of the six time series available it was the second longest (with 1993 being the longest time period), (2) although it is considered a dry year in terms of the total rainfall that fell in that period, it contained more incidents of rain events than any other series and showed a greater variety in events. The verification periods for the aggregation phase are May 30 to Aug. 12, 1988 (dry year) and May 16 to Oct. 15, 1992 (wet year). Three other time series: May 19 to Oct. 31, 1989; May 27 to Oct. 31, 1990; and May 13 to Oct. 31, 1993 will be used in addition to the first three series, for every other phase of this research.

4.10 Summary

This chapter described how existing meteorological, hydrometric, topographic and soil information were assessed to select the application study area of Ancaster Creek. Precipitation totals and climatic normals from the AIRPORT and RBG

meteorological stations were used to determine the precipitation status (i.e. is a year wetter, drier or average when compared to the climatic normal) of six application periods that will be used in the various phases of this research: 1988 (dry), 1989 (average), 1990 (wet), 1991 (dry), 1992 (wet), and 1993 (average). Base Flow Index values were used to confirm the precipitation status of each year.

Data from six rainfall gauges were used to construct precipitation input series for TOPMODEL. Rainfall was processed in hourly time increments and areal average values for the Ancaster Creek catchment were determined using the Reciprocal Distance Squared method. The six application periods were constructed in the snow-free period between May and October. Evapotranspiration values were computed using the Penman-Monteith method and hydrometric gauge data necessary for calibration and verification were extracted for the application periods. A time-area routing method was suggested for overland flow routing and the Muskingum-Cunge method will be used for channel routing.

Ten DEM sizes were chosen and constructed using `TOPOGRID` for analysis in the aggregation phase of this research. These DEMS have grid cell sizes of 10 m, 15 m, 20 m, 25 m, 30 m, 40 m, 50 m, 60 m, 80 m, and 100 m. Catchment boundaries were delineated using the `WATERSHED` command in ARC/INFO for each DEM size. The overall catchment area was discovered to decrease with increasing grid cell size. Four subcatchments, Hwy 403, Maple Lane, Golf Links and Wilson St. were delineated for each catchment using the `WATERSHED` command.

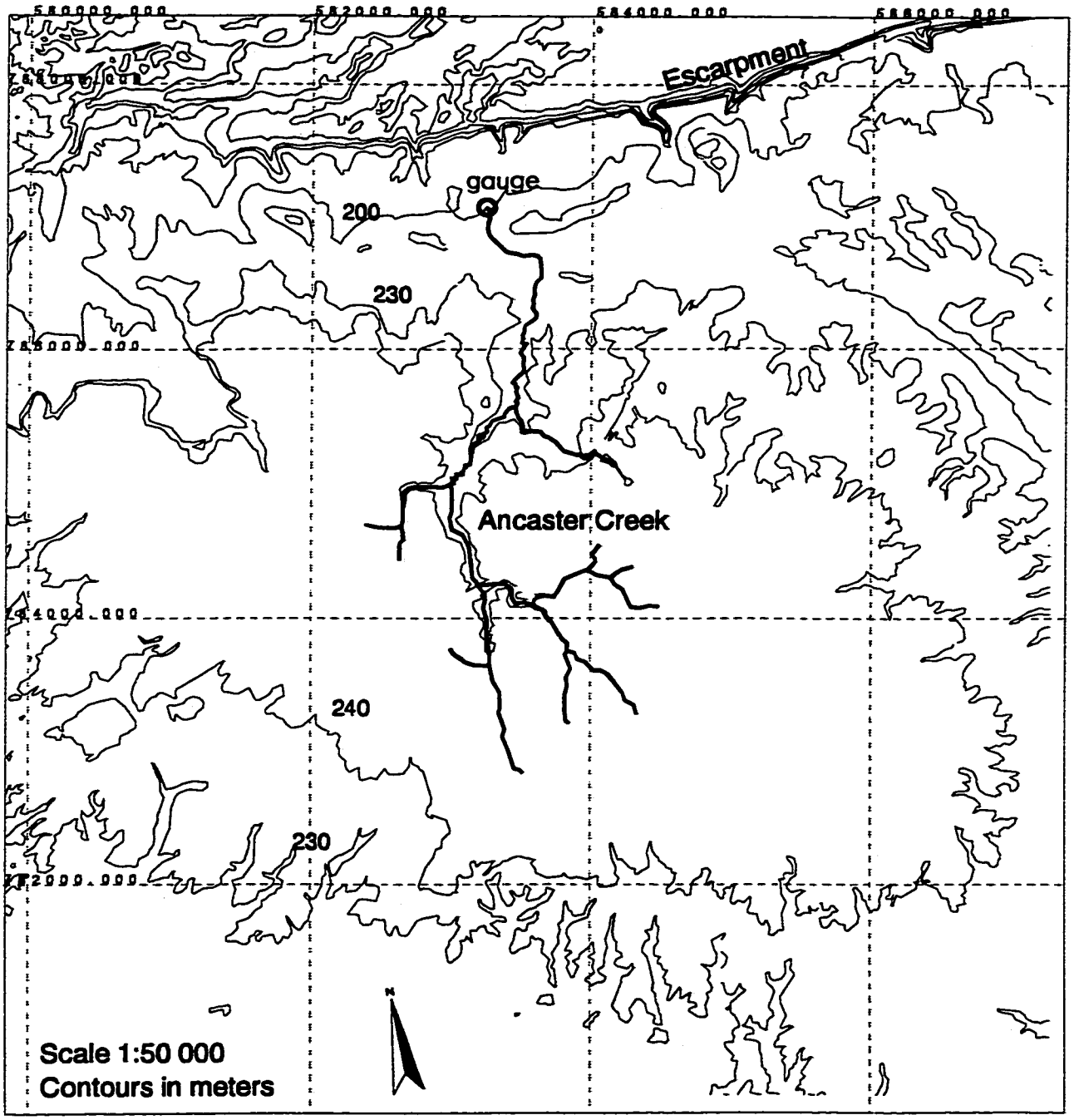

Figure 4.1: Ancaster Creek above the Niagara Escarpment.

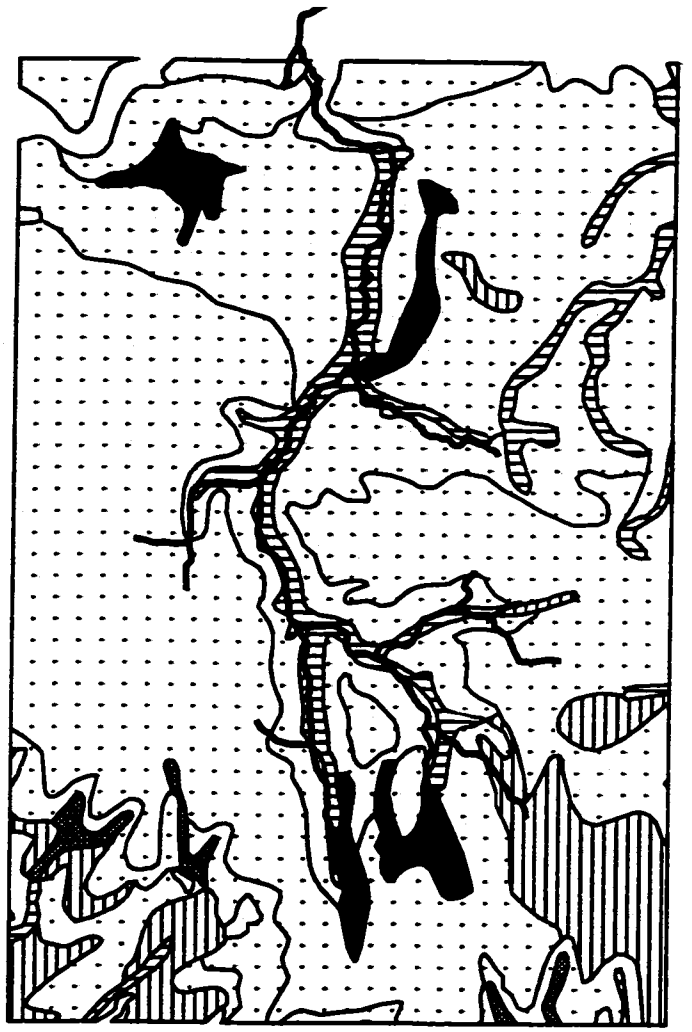

Source: Presant, E.W., Wicklund, R.E. and Mathews, B.C. (1965). "The Soils of Wentworth County", Report No. 32 of the Ontario Soil Survey, Canada Department of Agriculture and Ontario Department of Agriculture, Ottawa, Ontario.

Scale: 1:9,000

Ancaster Creek

Imperfectly Draining
Poorly Draining
Variable Drainage
Very Poorly Draining
Well Draining

Figure 4.2: Soils in the Ancaster Area.

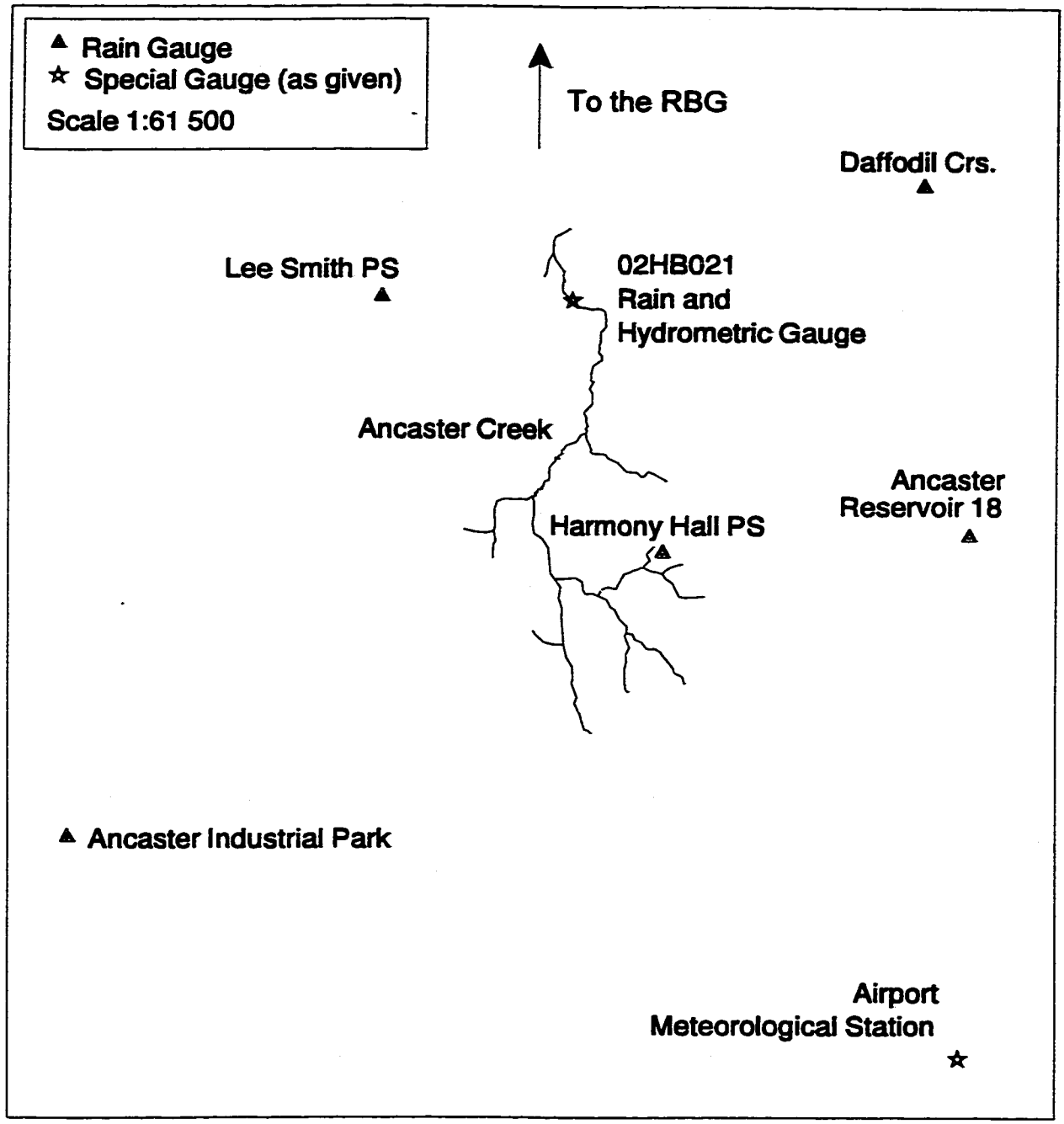

Figure 4.3: Various gauges available in the Ancaster Area.

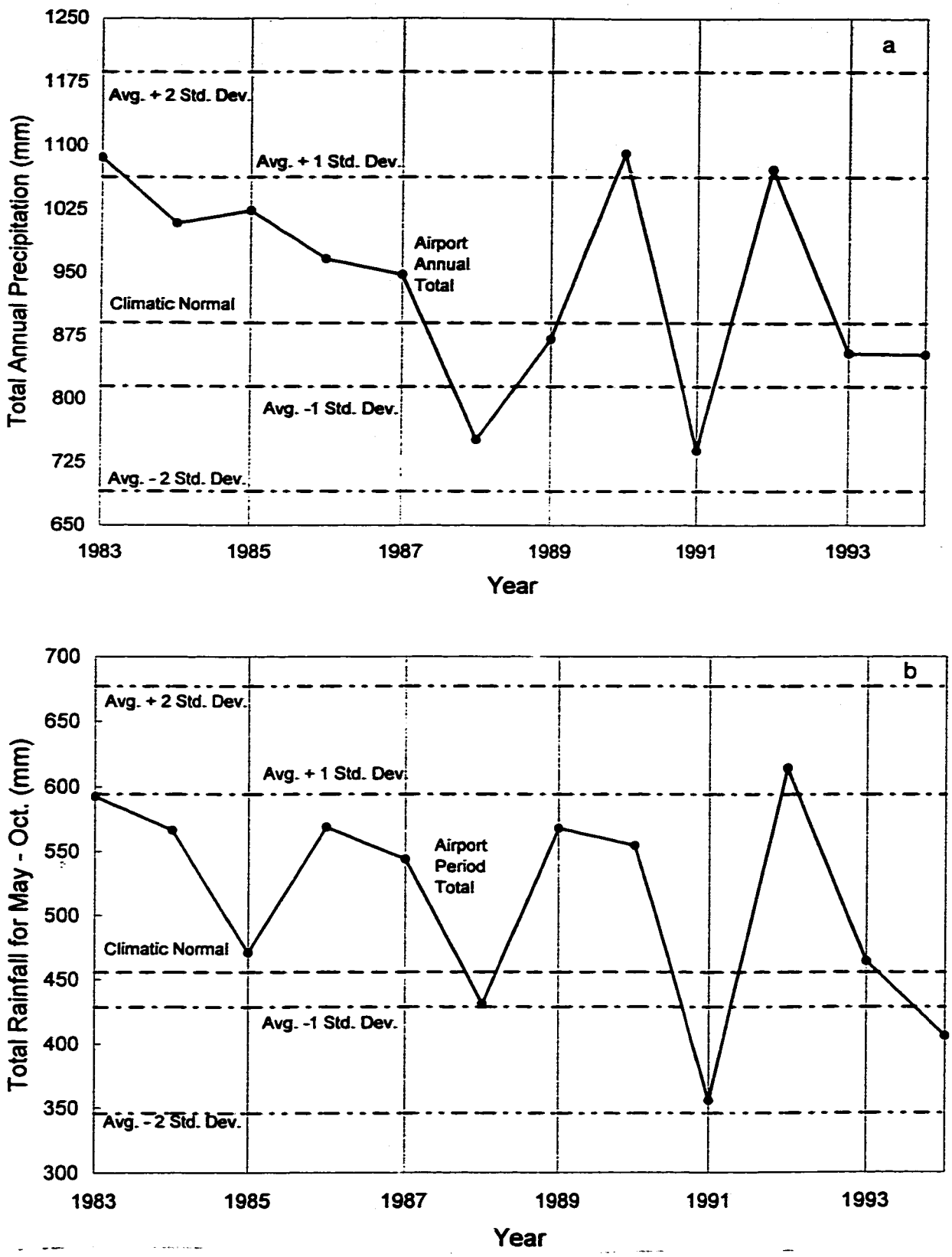

Figure 4.4: Total precipitation measured at the AIRPORT for a) the entire year; b) snow-free period between May and October.

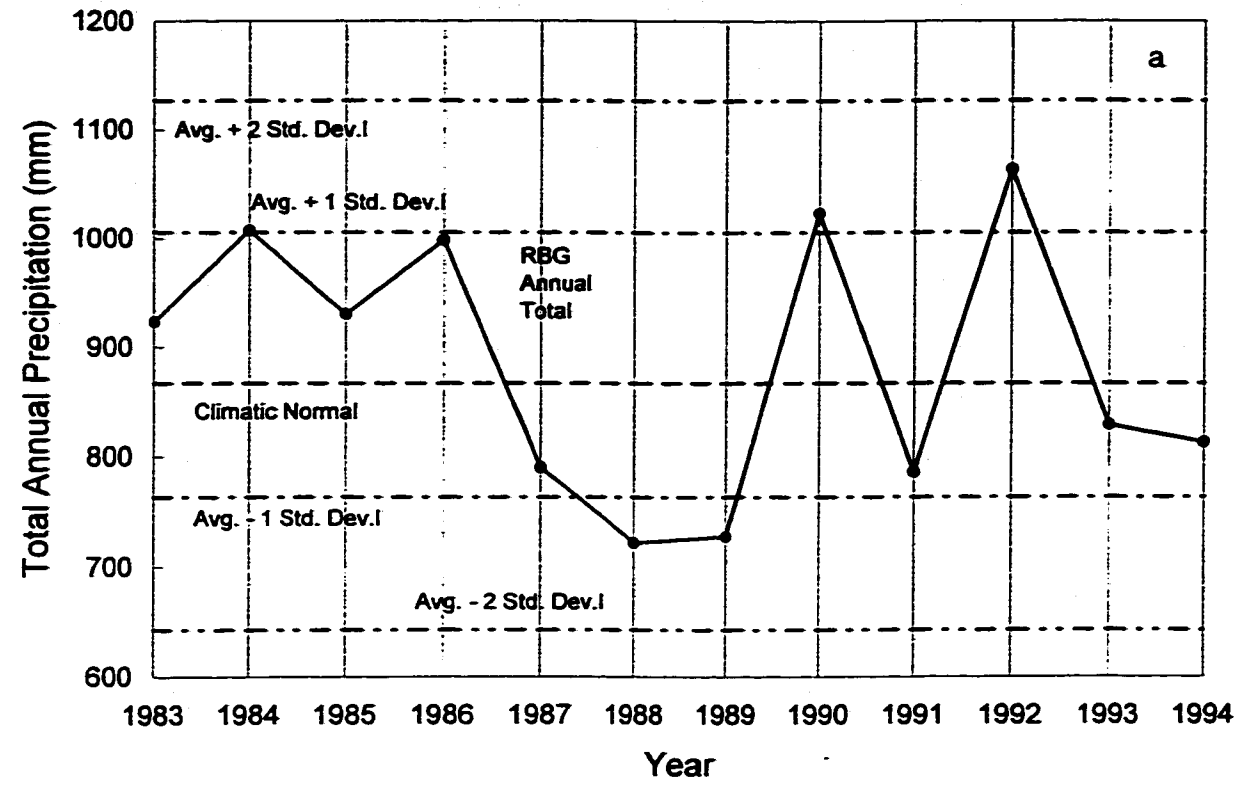

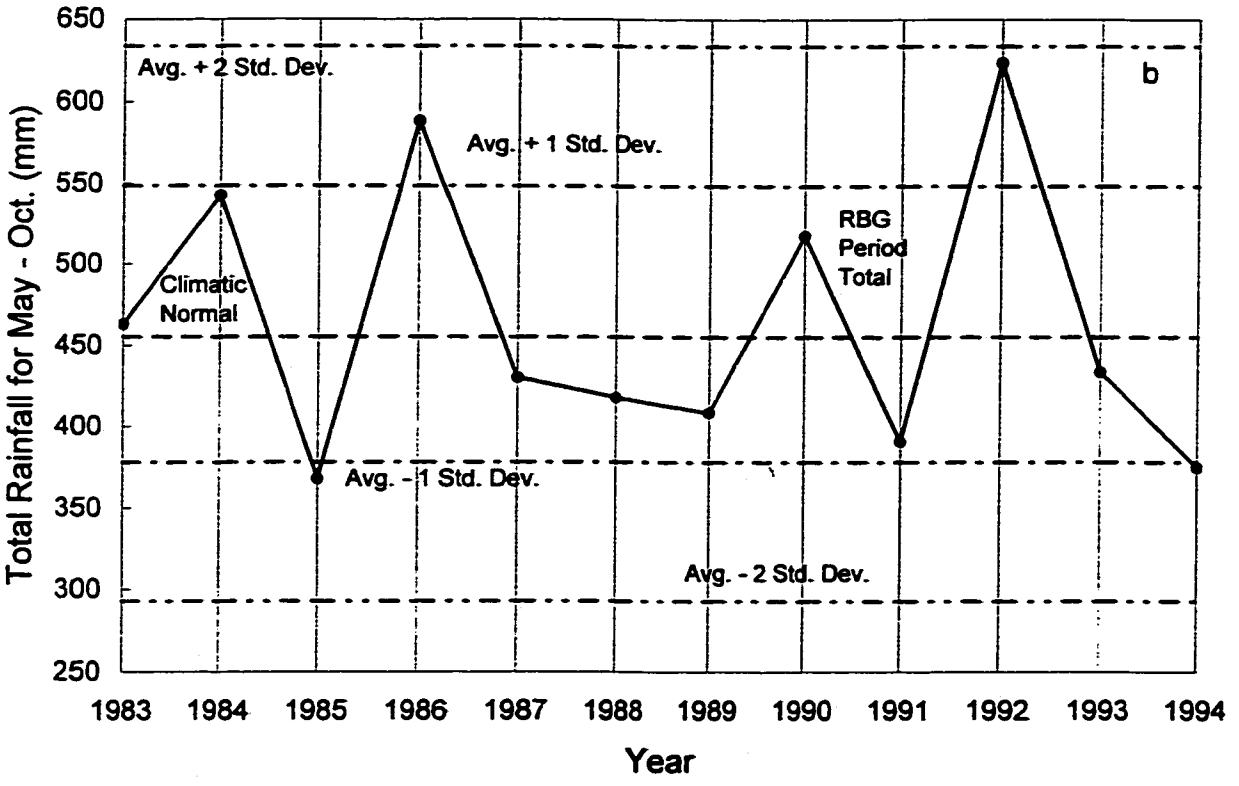

Figure 4.5: Total precipitation measured at the RBG for a) the entire year; b) snow-free period between May and October.

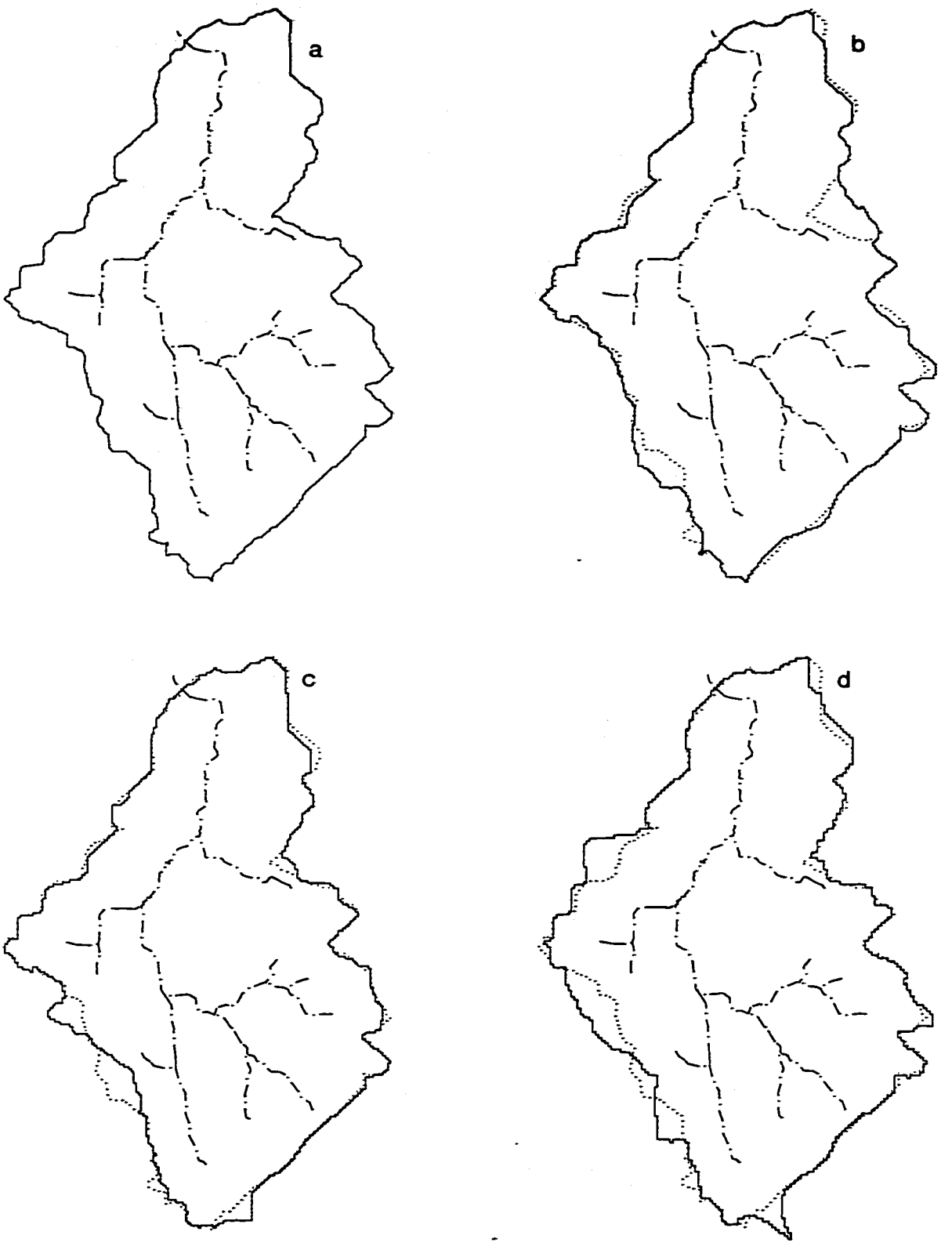

Figure 4.6: Catchment delineated for a) 10m; b) 15m; c) 20m and d) 25m DEMs (dotted line shows 10 m catchment boundary).

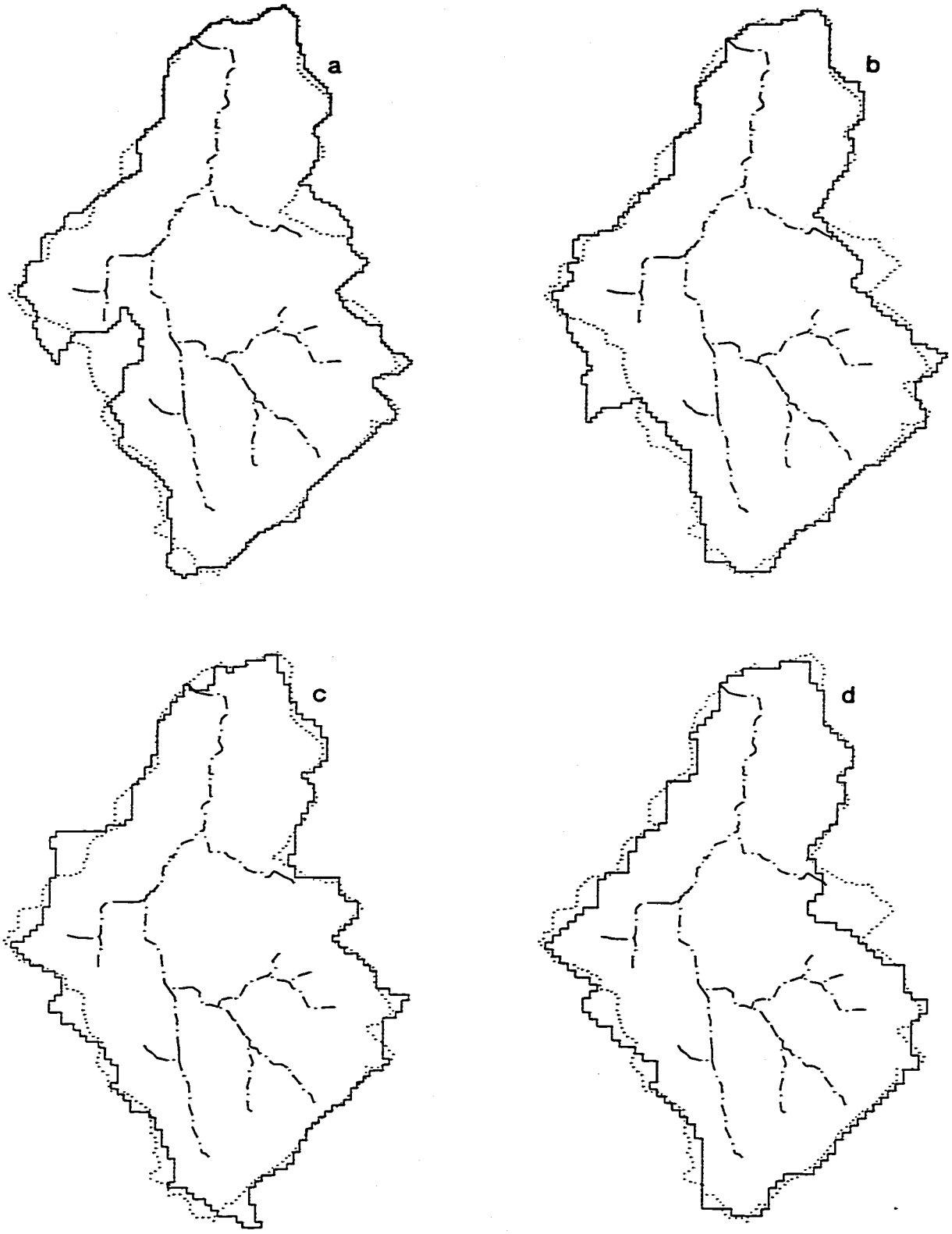

Figure 4.7: Catchment delineated for a) 30m; b) 40m; c) 50m and d) 60m DEMs (dotted line shows 10 m catchment boundary).

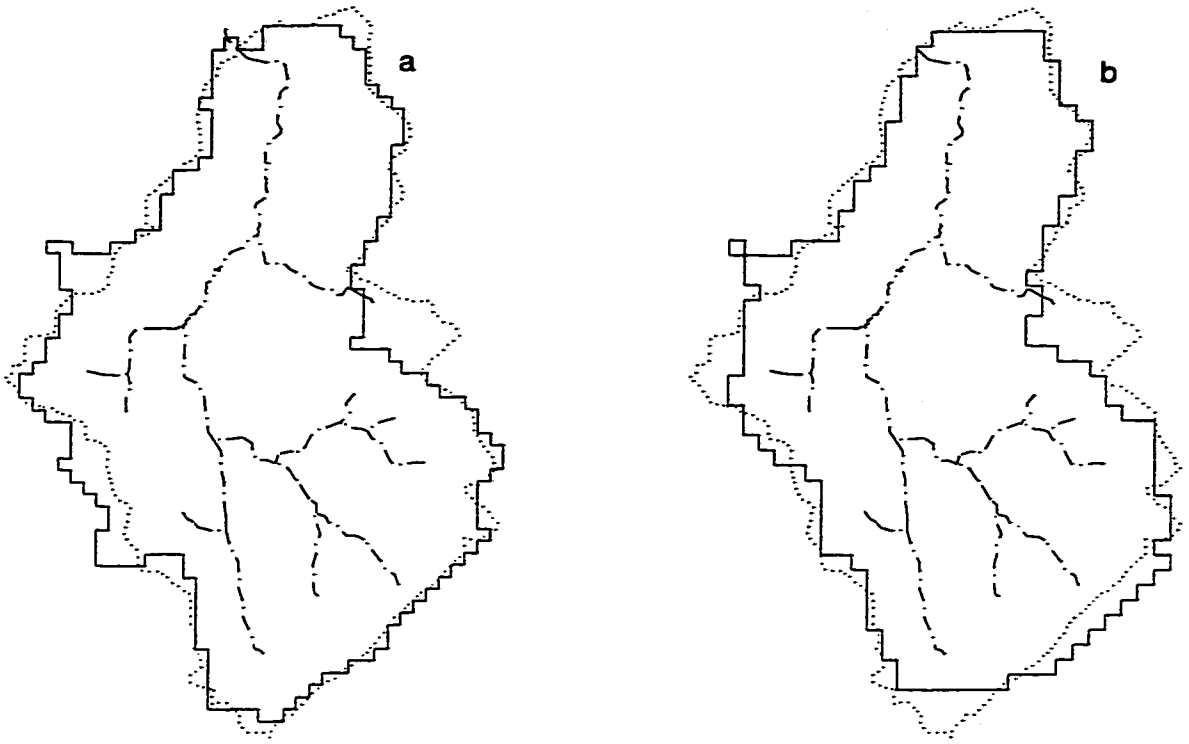

Figure 4.8: Catchment delineated for a) 80m and b) 100m DEMs (dotted line shows 10 m catchment boundary).

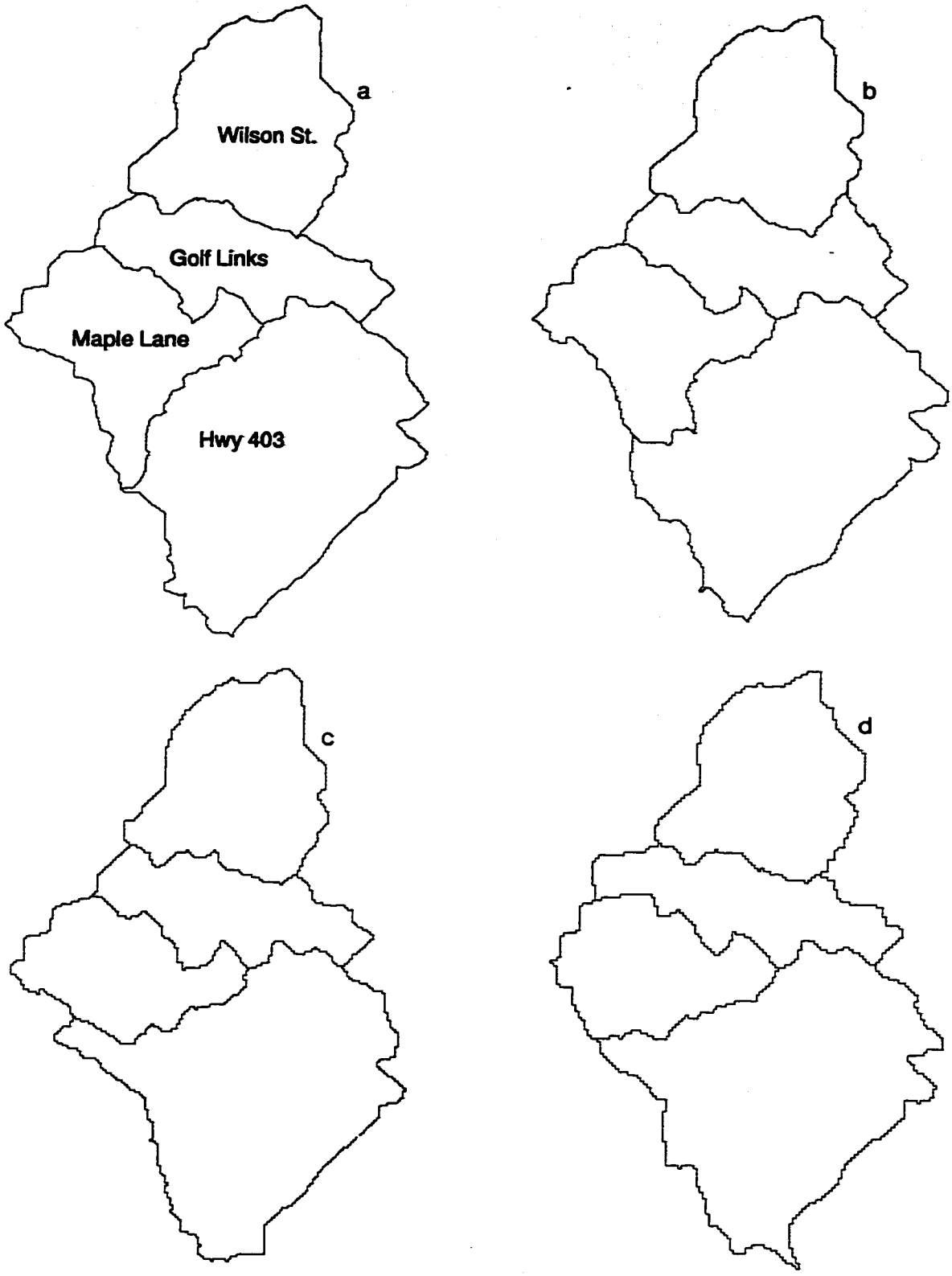

Figure 4.9: Subcatchments delineated for a) 10m; b) 15m; c) 20m and d) 25m DEMs.

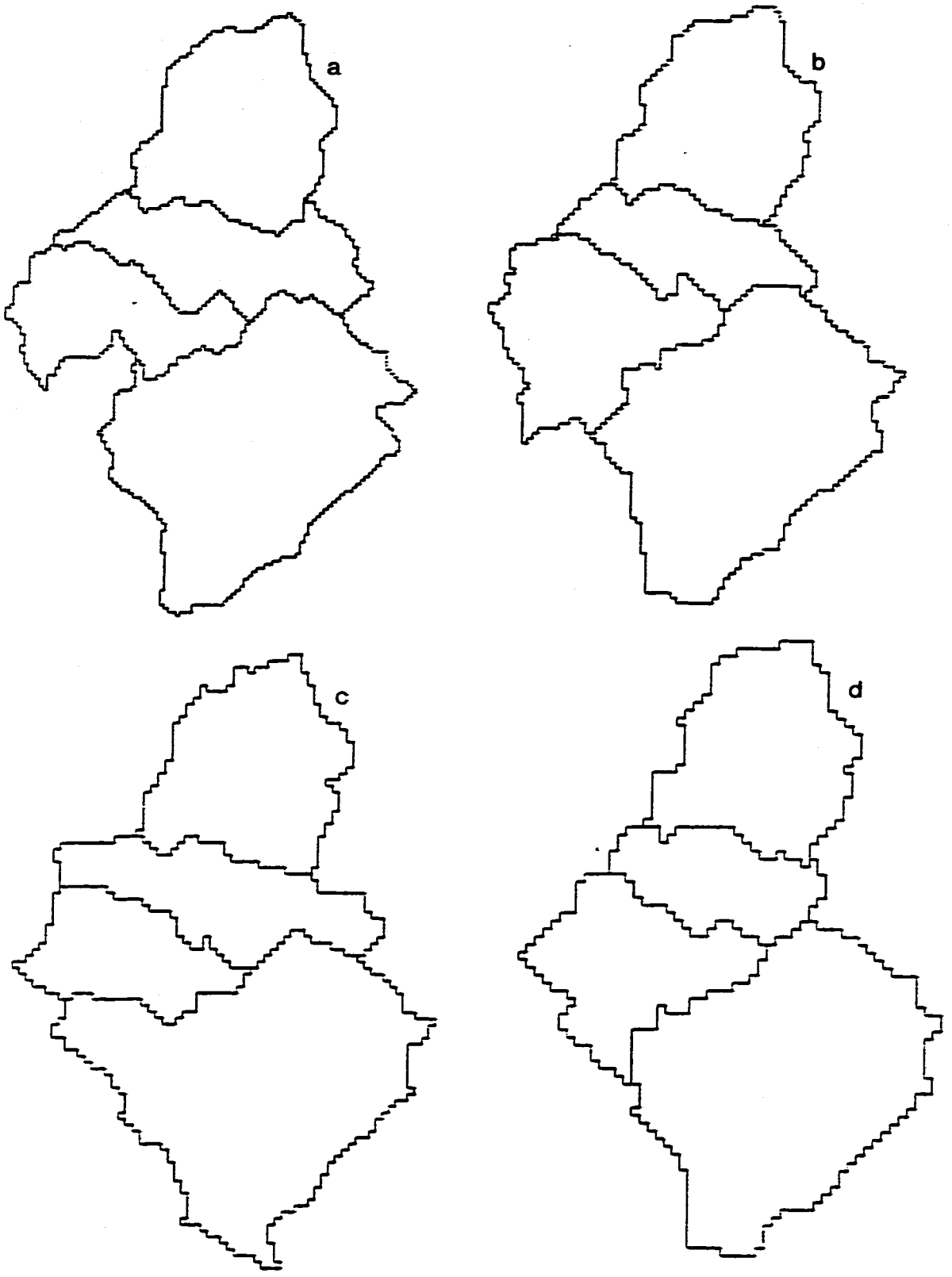

Figure 4.10: Subcatchments delineated for a) 30m; b) 40m; c) 50m and d) 60m DEMs.

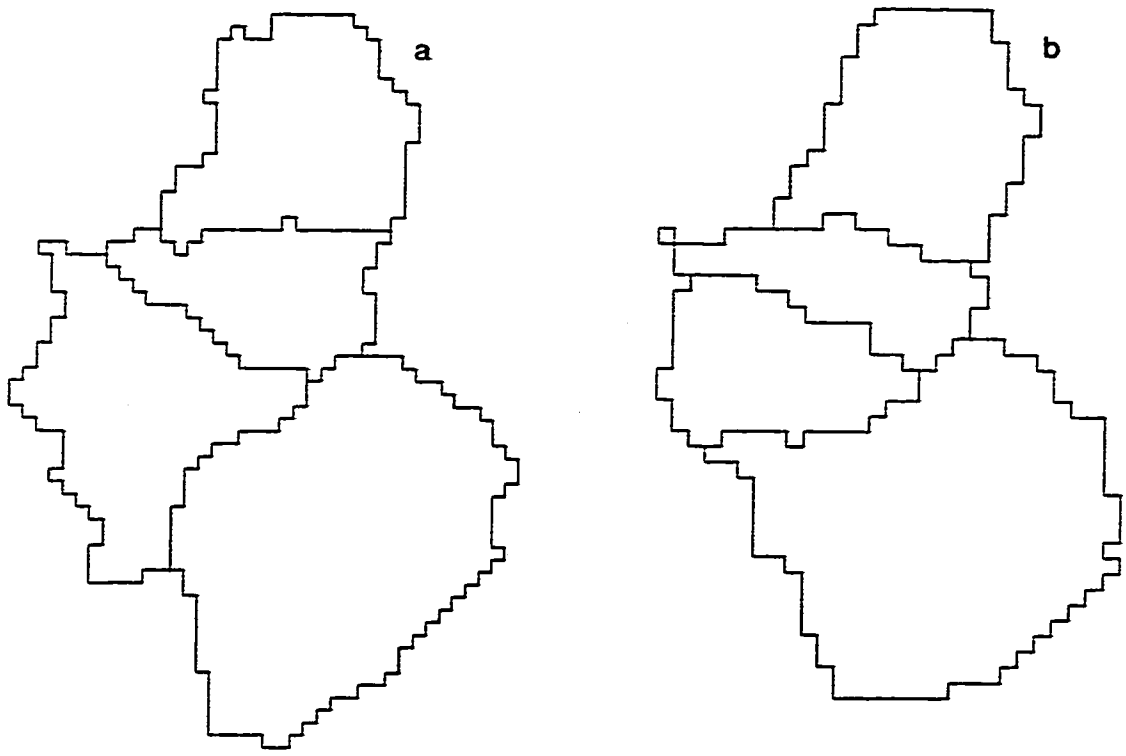

Figure 4.11: Subcatchments delineated for a) 80m and b) 100m DEMs.

CHAPTER 5 IMPLEMENTING URBAN LAND FORMS IN TOPMODEL

5.1 Introduction

This chapter opens with a discussion of the range of physical values possible for some of the most important model parameters. These parameters include *Ko*, *m* and Sr_{max}, and are examined this way in order to provide some insight into how to set up an initial input file and sensitivity analysis. This is followed by the most important section of the chapter: Section 5.3. This section presents the author's concept of how urbanization and other anthropogenic components of the catchment are simulated by the model. Section 5.4 details the procedure for calculating the topographic indices in the presence of a stream network for each DEM size. Topographic index calculations are made for two cases: 1) when the type of surface that exists in the catchment is simply ignored and all surface types are lumped together; and 2) when urban areas are explicitly considered. A discussion of the results is included. Sections 5.5 presents the revised version of TOPMODEL that explicitly accounts for impervious surfaces. Also, the results of a sensitivity analysis is presented to determine the parameters that will be calibrated in Chapters 6 and 7. The last section presents the optimization scheme that will be used to calibrate the parameters.

5.2 Field Estimates of TOPMODEL Parameters

The literature review has shown that TOPMODEL predictions on a continuous series are highly sensitive to the values of three parameters: *Ko*, *m* and Sr_{max}. If TOPMODEL is applied to a single event for flood prediction purposes, for example, then the parameters Q_o and Sr^0 should also be added to the above three. A discussion of the possible range of values of these parameters may shed some light into initial estimates and future results in the calibration and verification process.

5.2.1 Hydraulic Conductivity *Ko*

Initial estimates of hydraulic conductivity can be obtained with the help of the soils map shown in Chapter 4. A thorough description of the various classes of soil shown in Figure 4.2 are provided by Presant et al. (1965). Within the general catchment boundaries delineated by ARC/INFO, there are 10 different soil series in the area. Each series is comprised of either completely one type of soil or a mix of soil types. Of those series that contain a mix of soil types, one soil type will dominate the composition over the other types of soils in the mix. These soils range in texture, being either a sandy loam, a silt loam or a clay loam. The majority are of the sandy loam variety and these types exhibit good drainage. Those soil types that include silt or clay drain poorly, but as Figure 4.2 indicates, these soils are only present in a small percentage of the overall catchment. The majority of Ancaster Creek catchment is fairly well draining and therefore, using a single hydraulic conductivity estimate for the entire catchment is not appropriate.

There have been a handful of studies that have attempted to determine the hydraulic conductivity of topsoil in the region. A table was developed at Agriculture Canada that combined data from topsoil all over Southwestern Ontario (Hohner 1996). These estimates are shown below.

Table 5.1: Estimated ranges of saturated hydraulic conductivity for the topsoil in Southwestern Ontario (average value shown in brackets).

Texture	Surface Layer (m/hr)	Subsurface Layer (m/hr)
Sandy Loam	0.002 - 0.5 (0.11)	0.00009 - 0.1 (0.03)
Silt Loam	0.0002 - 0.6 (0.06)	0.00001 - 0.3 (0.02)
Clay Loam	0.00004 - 0.4 (0.05)	0.00009 - 0.6 (0.04)

The surface layer conductivities are estimates in the top 15 cm of the soil and

subsurface estimates are from the next 15 cm in the layer. The subsurface layers will have less dominant soil if the soil is a mix (Presant et al. 1965). Hohner (1996) notes that hydraulic conductivity increases after construction, and depends on the season of sampling and the degree of soil tillage. Soils are sampled in late summer where surfaces are least permeable due to the compacting effects of harvesting machinery, and crusting from rainfall and water erosion. Soils sampled in spring tend to be looser and more permeable than in late summer because of fall plowing, spring tillage, and winter frost action. Additional estimates of the clay loam series soils in the Regional Municipality of Haldimand-Norfolk that is near the Hamilton-Wentworth Region, showed similar conductivities in the range of 0.07 - 0.003 m/hr (McBride 1996). It is not certain what types of the hydraulic conductivities will be produced from the calibration output, but the literature has shown that the hydraulic conductivities obtained from calibrating TOPMODEL are several orders of magnitude higher than those shown in the table.

5.2.2 Recession Parameter *m*

By manipulating the equations in Chapter 3, it is possible to derive an expression for the recession parameter *m* as a function of observed discharge. Consider Equation (3.25).

$$Qb^{t} = ATo\, e^{-\bar{\lambda}} e^{-\bar{S}^{t}/m} \tag{5.1}$$

Let $Q_{To} = AT_o e^{-\bar{\lambda}}$ and assume that unsaturated zone flows area negligible ($Qu^{t} = 0$). When precipitation input is equal to zero, the general equation of continuity becomes,

$$\frac{d\bar{S}^{t}}{dt} = Qb^{t} \tag{5.2}$$

If we differentiate Qb^t with respect to $\bar{S}$, then

$$\frac{d(Qb^t)}{d\bar{S}^t} = -\frac{1}{m} Q_{To} e^{-\bar{S}^t/m} \tag{5.3}$$

Furthermore,

$$\frac{d(Qb^t)}{d\bar{S}^t}\frac{d\bar{S}^t}{dt} = \frac{d(Qb^t)}{dt} \tag{5.4}$$

Inserting (5.3) and (5.2) into (5.4) gives,

$$-\frac{1}{m} Q_{To} e^{-\bar{S}^t/m} Qb^t = \frac{d(Qb^t)}{dt} \tag{5.5a}$$

$$-\frac{1}{m} dt = \frac{d(Qb^t)}{(Qb^t)^2} \tag{5.5b}$$

$$-\frac{1}{m}\int_{t_o}^{t} dt = \int_{Qb^{t_o}}^{Qb^t} \frac{d(Qb^t)}{(Qb^t)^2} \tag{5.5c}$$

$$-\frac{1}{m}(t - t_o) = -\left(\frac{1}{Qb^t} - \frac{1}{Qb^{t_o}}\right) \tag{5.5d}$$

$$\frac{1}{m} = \frac{(Qb^t)^{-1} - (Qb^{t_o})^{-1}}{t - t_o} \tag{5.6}$$

Therefore, the slope of the line of $1/Qb^t$ versus time should provide a reasonable estimate of the parameter $1/m$. Note that in this derivation, Qb^t is in units of m/hr.

In determining m from Equation (5.6), it is preferable to do so when the effects of

evapotranspiration are minimal (Beven et al. 1983) as evapotranspiration may alter catchment flow recession. Furthermore, the values should be computed at least 3 days after the rain event to ensure that there is no activity in the unsaturated zone. Several rain events were selected from the application periods to compute recession. It was not always easy to isolate events that were followed by more than a three day absence of rain, simply due to the frequency of rain in the Ancaster area. Ironically, the recession parameter should not be estimated during very long dry periods, but it was usually these kinds of conditions that led to periods where the recession parameter could be calculated. Events were isolated in the spring and fall and in the summer, if necessary. Since only a general estimate of m was desired, only three of the six years available were examined. Table 5.2 provides these estimates as well as the variance (R^2) in the slope computed by least squares regression.

Table 5.2: Recession *m* for several time periods.

Event	m (metres)	No. of Values	R^2
April 1988	0.0412	421	0.35
May 1988	0.0082	194	0.87
June 1988	0.0103	591	0.78
September 1988	0.0086	240	0.66
November 1988	0.0321	610	0.79
March 1990	0.0280	245	0.73
April 1990	0.0254	260	0.84
June 1990	0.0211	269	0.72
August 1990	0.0105	177	0.79
May 1992	0.0163	307	0.87
June 1992	0.0071	199	0.76
September 1992	0.0226	388	0.67
October 1992	0.0285	194	0.83

A general glance at this table seems to indicate that in the hot drier summer months, the recession parameter is lower than in the spring or late fall. A lower value of m means that runoff recedes much more rapidly than it would for a higher recession parameter. This may be due to the effects of evapotranspiration in the summer. Table 5.2 indicates that the range of m lies between 0.04 and 0.007. An initial value of $m = 0.02$ was selected for the calibration and sensitivity analysis. Note that this value is the average of all the values of m in Table 5.2.

Figure 5.1 shows plots of some of the events in Table 5.2 and the corresponding regression lines. The reader should immediately notice the jagged appearance and oscillatory behaviour in these graphs. Abrahamse (1997) suggests that the spikes and dips can be attributed to several factors including the natural stream flow; the introduction of rocks and other obstructions into the stream; and withdrawal by local residents. Lamb (1996) also noticed similar observations of a periodic oscillation in discharge during periods of low flow. Lamb attributed these oscillations to diurnal variations in evaporation. This may also be the cause of the oscillations observed in Figure 5.1. However, they do not affect the computation of m.

5.2.3 Root Zone Sr_{max}

The root zone in TOPMODEL encompasses moisture storage for both interception and evapotranspiration losses. Traditionally, the root zone has been defined as that layer of soil through which the roots extract moisture. An initial estimate of the root zone for the entire catchment is senseless because the catchment has a mix of land-uses ranging from urban to recreational to farmland. Hence, interception losses will vary as well as the amount of evapotranspiration. The initial value of Sr_{max} will be set to the arbitrary value of 0.2 m and will be optimized in all phases of this research. By the very nature of the optimization scheme, the initial value selected for this parameter will not affect the final optimization results.

5.2.4 Initial Conditions Q_o and Sr^0

The initial value of Sr^0 can be set to Sr_{max} if the application period begins when the root zone is completely depleted. The six application periods that were devised were started at a time when there were at least three dry days from the last rain event. Therefore, Sr^0 will initially be set to the value of Sr_{max} in all the calibration and verification periods. This parameter will not be calibrated explicitly but variations in Sr^0 will be investigated to ensure high modeling efficiency.

Q_o is the initial catchment discharge and can be taken from the hydrograph. However, Q_o will be used in the initial estimate of $\bar{S}^0$ therefore, an initial discharge for each subcatchment is necessary as $\bar{S}^0$ will be estimated for each subcatchment. However, to estimate Q_o for each subcatchment would be difficult considering there is little knowledge of how each subcatchment contributes to the flow. Therefore, Q_o for each subcatchment is simply set as the initial value of Q_o for the entire catchment. The author understands that is an overestimation and will have certain ramifications in the calibration process. Because Q_o has been set so high, the initial value of root zone deficit should be filled, i.e., Sr^0 should equal zero. The initial conditions will be left this way and Sr^0 will be adjusted to account for the value of Q_o. This implies however, that to obtain an accurate synthesis of hydrograph values, the hydrograph must have at least one large rain event to dampen out the initial conditions.

5.3 Urbanization in the Catchment

TOPMODEL concepts involve the medium of soil. No application of TOPMODEL has ever considered the inclusion of impervious areas in either the formation of the topographic index or in the generation of flow. The traditional way to treat mixed land use that included impervious and pervious surfaces is to completely separate the two surface types and model them separately. Thus effectively removing the

pervious soil beneath the impervious surface as a medium for subsurface flow. The impervious watershed was essentially decoupled from the pervious watershed. The primary objective of this thesis is to incorporate urban areas in a more physically realistic way using TOPMODEL's topographic indices.

5.3.1 Conceptual Treatment of Urbanization

Urbanized areas will be incorporated in the formation of the topographic index as well as in the formation of overland flow. Recall from Chapter 3 that if P^t is the recharge to column i, and a_i is the area per unit width of upstream soil that drains through column i, then

$$q_i^t = a_i P^t \tag{5.7}$$

If the column is covered with an impervious layer that is relatively thin in comparison to the total depth of the soil, then this column will receive no recharge. However, the soil beneath the impervious layer still provides a through path for subsurface flow. Figure 5.2 shows a bird's eye view of a hypothetical catchment boundary and the internal discretization of the catchment into columns. The general direction of flow is from the upper left to the lower right. Impervious areas are marked with an **x**. If we were to compute the topographic index of the column marked i, then we would expect from Equation (5.7), that any upstream area that collects recharge, contributes to the lateral flow q_i^t through column i. Therefore, in the following equation for the topographic index,

$$\lambda_i = ln(\frac{a_i'}{tan\beta_i}) \tag{5.8}$$

a_i' is the upstream area per unit width (m), and does not include areas marked with

an **X**. If we were computing the topographic index for a column with an impervious cover, then one would still use Equation (5.8) but again upstream areas marked **X** would not be included in the calculation and nor would the surface area of the impervious column. All other equations in TOPMODEL that include subcatchment area in their calculations will include impervious surface area if it exists in the subcatchment area.

While impervious columns do not allow recharge to the soil matrix below, they do produce overland flow. Hence, a revision to TOPMODEL that includes more than just modifying the topographic index is necessary. To keep the number of parameters to a minimum, the author proposes that precipitation onto impervious surfaces will immediately become overland flow. Therefore, $Qurb^t$ is the flow generated by urban areas within a subcatchment, and,

$$Qurb^t = P^t A f_{UA} uacp \tag{5.9}$$

and $Qurb^t$ is the contribution at each time step (m^3/hr), P^t is the rainfall (m/hr), A is the subcatchment area (m^2), f_{UA} is the fraction of urban area in the subcatchment and *uacp* is the urban area calibration parameter. This calibration parameter was included in order to study the effects of aggregation on the urban area estimates, as well as account for any errors in the assumptions regarding f_{UA}. The runoff will be routed along with the other contributions to flow.

The author realizes that a more sophisticated model of urban flow can, and probably should be implemented, but for the aggregation portion of this research, the author will endeavor to keep TOPMODEL as close to the original version as possible without compromising the efficiency too greatly. The version of TOPMODEL that includes the modifications to computing the topographic index within urban areas, and the inclusion of Equation (5.9) for impervious areas, will henceforth be referred

to as TOPURBAN.

5.3.1.1 Determining Urban Areas with ARC/INFO

The urban areas in the Ancaster Creek catchment were defined by buffering all the roads in the residential areas by 25 m on either side using ARC/INFO's BUFFER command. This distance of 25 m was the average distance from a road centerline to the adjacent homes depicted on the Ontario Base Map. In this way, the urban areas are defined as that area residing in the buffer. Note that the surface in a residential area is not entirely impervious. An assumption could have been made as to the degree of imperviousness in the urban areas, but instead, the calibration parameter was introduced to determine this value. Other roads, such as Southcote road, were not included as part of the urban area and this was done for two reasons. First, these roads are major transportation routes and were generally not bordered by urban land use. Second, the actual width of these roads would be less than a cell size once the DEM cell size exceeded 10 m and their contribution would be immediately overestimated by the fact that their surface area would be overestimated. Any contribution from these roads will manifest themselves in the calibration parameter *uacp*. The urban areas are shown in Figure 5.3 b) and the road network is shown in Figure 5.3 a). The following table lists the urban area fraction determined using ARC/INFO.

Table 5.3: Urban area fraction (f_{UA}) for each subcatchment and each DEM size.

DEM	Hwy 403	Maple Lane	Golf Links	Wilson St.	Total Urban Area (km^2)
10	0.028	0.339	0.096	0.313	1.28
15	0.024	0.352	0.076	0.318	1.27
20	0.045	0.346	0.088	0.311	1.25
25	0.043	0.307	0.114	0.317	1.30
30	0.040	0.288	0.080	0.327	1.18
40	0.031	0.283	0.079	0.337	1.25
50	0.064	0.291	0.105	0.330	1.28
60	0.038	0.328	0.020	0.359	1.21
80	0.030	0.331	0.091	0.362	1.35
100	0.067	0.284	0.043	0.425	1.32

The variation in values of subcatchment urban area fraction across DEM sizes is in part due to the variation in location of the subcatchment boundary. But there is generally no distinct trend between the total catchment urban area and the DEM cell size. This implies that there should be little variation in the calibration parameter *uacp* with DEM cell size.

5.3.2 Other 'Urban' Elements

Pits and quarries may interfere with subsurface flow of water, and the Ancaster area is known to have a few small quarries in the vicinity of the creek. A quarry which extends down to bedrock, will collect rainfall, surface flow and subsurface flow, that may eventually evaporate, feed deep groundwater stores, or perhaps be pumped out of the quarry and discharged into the stream nearby. In the latter case, the discharge rate into the stream must be included in the streamflow modeling. To account for such an input would be very difficult. For this reason, all quarries within the

Ancaster Creek catchment are regarded as sinks.

Three small quarries reside close to Ancaster Creek near the centre of the catchment. To determine the sink area drained by these quarries, pour points were selected on the quarries' edges, and the quarry drainage area was delineated by ARC/INFO's WATERSHED command. This area was effectively removed from the overall catchment area. Table 5.4. shows the resulting areas. Figure 5.3 b) shows the quarry drainage area in hatched markings.

Table 5.4: Quarry area vs. DEM cell size.

DEM	Quarry Area (km^2)	Final Catchment Area (km^2)
10	0.2543	7.5850
15	0.2401	7.7760
20	0.2320	7.5604
25	0.2763	7.8888
30	0.2295	7.5915
40	0.2736	7.5888
50	0.1950	7.7400
60	0.2520	7.1820
80	0.2496	7.4368
100	0.2500	7.0800

It is difficult to ascertain a trend in quarry drainage area from this analysis. The values in the third column are the effective catchment area and they do decrease with increasing DEM cell size.

5.4 Ancaster Creek Topographic Indices

Equation (5.8) is used to compute the topographic indices for each column *i*. The value $tan\beta_i$ is the surface slope of the column and is defined as,

$$tan\beta_i = \frac{\zeta_i - \zeta_d}{l_{id}} \tag{5.10}$$

where ζ_i is the elevation (m) of column *i*, ζ_d is the elevation (m) of a downslope column receiving flow, and l_{id} is the distance (m) between column *i* and the downslope column *d*. If a_i' is the upslope area per unit width that is distributed downslope, than how is it distributed if a cell slopes down in more than one direction? Several algorithms exist to compute the topographic index. Single flow direction algorithms (SFD) assume that water flows downslope in one direction - the steepest direction. A multiple flow direction algorithm (MFD) assumes that water flows in all down-slope directions from any given point. The differences in these algorithms are illustrated in Figure 5.4. An MFD algorithm allows for flow convergence (several cells draining into one downslope cell) and flow divergence (one cell draining into multiple downslope cells). But, an SFD algorithm only allows flow convergence. When flow convergence occurs the upslope area is concentrated into a downslope neighbouring cell, thereby increasing the value of upslope area per unit contour length for that downslope neighbouring cell. When both convergence and divergence are allowed in an algorithm, the upslope contributing area is more dispersed and evenly distributed (Wolock and McCabe 1995). An MFD algorithm would require a greater number of computations and is considered physically more realistic than an SFD algorithm and a better indicator of soil moisture distribution. An SFD is unrealistic in view of the large amounts of flow that can be generated from a single grid cell as DEM sizes increase (Quinn 1991). In computing a topographic index for the center cell in Figure 5.4, in the single flow direction algorithm, the index is equal to,

$$ln\left(\frac{a_i'}{tan\beta_i}\right) = ln\left(\frac{A_i'}{lc_i tan\beta_i}\right) \tag{5.11}$$

where A_i' is the area draining into the cell (m^2) (includes the surface area of that cell) and lc_i is the cross-sectional length of the surface through which the water flows; in this case, it is the DEM cell size (m). For a multiple direction algorithm, the flow is apportioned amongst the downslope cells according the steepness of the slope. According to Wolock and McCabe (1995), if a cell i, has N_c downslope neighbouring cells, then,

$$lc_i = \sum_{r=1}^{N_c} (lc_r)_i \tag{5.12}$$

$$tan\beta_i = \sum_{r=1}^{N_r} (lc_r\, tan\beta)_i \left(\sum_{r=1}^{N_r} lc_r\right)_i^{-1} \tag{5.13}$$

$$(\Delta A'_r)_i = A'_i (lc_r tan\beta_r)_i \left(\sum_{r=1}^{N_c} lc_r\, tan\beta_r\right)_i^{-1} \tag{5.14}$$

The contour lengths lc_r in the three equations above are equal to 60% of the grid cell length when the downslope cell r is in one of the four cardinal directions; and 40% of the grid cell length for a downslope cell in the diagonal direction. This way, if all of a cell's neighbours are downslope, then lc_i would equal a maximum value of 4 times the grid cell length. The slope $tan\beta_r$ is the slope between the center slope and the downslope cell r, and $(\Delta A'_r)_i$ is the total upslope area (m^2) that is distributed to the downslope neighbouring cell r.

Wolock and McCabe (1995) compared topographic indices computed by the SFD

and MFD algorithms for several catchments in the United States with diverse topography. They compared the mean, variance and skew of the distributions of topographic index for grid resolutions ranging from 3.0 m to 94.2 m. The mean value of topographic index was lower for the SFD algorithm as compared to the MFD algorithm, but the variance and skew were higher. A higher mean increases the likelihood to produce overland flow. But so too does a higher variance, and when the SFD algorithm with the lower mean and higher variance was used in a TOPMODEL application, the net effect was only a very small decrease in the percentage of overland flow to total flow. After calibration, both algorithms produced nearly identical results, but the optimized value of *Ko* was very different between algorithms. This is not surprising as Quinn et al. (1995) noted that the change in shape and position of the distribution of topographic index will affect runoff dynamics in the model, and that these changes would be offset by changes in certain parameters when re-optimized. If accurate spatial patterns of soil moisture are desired, than Wolock and McCabe (1995) recommend the use of the MFD algorithm over the SFD algorithm. An MFD algorithm will be used in this research as opposed to an SFD algorithm. While hydrograph synthesis will be the primary method of evaluating TOPMODEL, an accurate spatial representation of soil moisture is desired and can help validate any field observations that may be taken in the course of this research.

5.4.1 Computing Topographic Indices with ARC/INFO DEMs

In regions where low topographic relief and little contour or spot elevation data are present, flat areas appeared in the DEMs created by ARC/INFO. This problem was also observed by Wolock and McCabe (1995). Not surprisingly, the larger the grid cell size, the fewer the number of flat areas that were observed. The 25 m DEM was the finest resolution DEM that was free of flat areas. These flat areas require special treatment as flow upstream of the flat area is assumed to somehow find its way

through to the lower elevation side. The procedure adopted to handle this problem was taken from Wolock and McCabe (1995). In their method, a flat area was assigned a direction based on the elevations that bordered that area. The following procedure was used to compute the topographic indices used in this research:

1) Sort the cells of elevation from highest to lowest using a Shell Sort.

- The general direction of flow through the flat area was determined and elevation cells in flat areas were ordered manually based on their relative position in this flat area.

2) Beginning with the highest elevation cell, determine the downslope neighbours and compute the contour length with Equation (5.12).

- If the cell is within a flat area, then let lc_i equal one grid cell length.

3) Compute the slope gradient in the downslope direction using Equation (5.13).

- If the cell is within a flat area then $tan\beta_i$ is assigned a value of ½ the vertical resolution divided by the horizontal distance between neighbouring cell centres. In this case, the vertical resolution of the data was assumed to be 0.05 m as the spot elevation data was given to the near decimetre.

4) Compute the topographic index according to Equation (5.11).

5) Distribute the total upslope area to the downslope neighbouring cells using Equation (5.14).

- If the cell is in a flat area, then all of A_i' is distributed to one neighbour in the general direction of the flat area.

This process continues until all the cells are processed. These steps were implemented into a FORTRAN program that was supplied with TOPMODEL v. 95.1

to compute topographic indices. The modifications included the Shell Sort and the method of treating cells in flat areas.

5.4.2 Treatment of Rivers

In computing topographic indices one can see that as flow builds up downstream, larger and larger values of $ln(a'/tan\beta)_i$ appear in cells that actually correspond to the location of the river. Rivers represent the meeting of flow from hillslopes but are not hillslopes and hence represent another object that should be treated accordingly. The treatment of rivers for this work was conducted in the same manner as that of Quinn (1991) in which rivers are "pushed back" into hillslopes cells. Essentially, if a cell is deemed a "river cell" then the value of $tan\beta_i$ is taken as the average of all upslope angles, lc_i is set equal to the sum of both sides of the channel (two grid cell lengths) and A'_i is not apportioned to any downslope cells because the downslope cells are also assumed to be along the main river course. This has the net effect of substantially lowering the $ln(a'/tan\beta)_i$ of a river cell since it now only receives flow from the sides of the river and not upstream of the river. The original program to compute topographic indices that was provided with TOPMODEL included this method of treating river cells but it was modified further to include the use of river networks generated by ARC/INFO. ASCII files showing the locations of river cells was generated by ARCINFO using the `FLOWACCUMULATION` command,

```
ancaster_accum = FLOWACCUMULATION(ancaster_direction)
    stream_300 = CON(ancaster_accum > 300, 1)
```

The `CON` command tests the condition that if a cell in `ancaster_accum` is greater than 300 (i.e. more than 300 cells flow into that cell), then assign the value of 1 to that cell in grid `stream_300`. The program that computes topographic indices tests each cell to see if it is a river cell (i.e. is `stream_300 = 1`) and then modifies it accordingly.

Several river network grids were created in order to determine the most suitable threshold of river cell. The first threshold used was for the 10 m DEM. Figure 5.5 a) shows the spatial distribution of topographic indices with no river cell treatment. Figure 5.5 b) shows the same figure with the actual stream network superimposed on the figure. Figure 5.6 a) is the treated spatial distribution using a threshold of 300. Notice the long linear features located at stream heads. This was not considered a true representation of variable source area formation so it was felt that the threshold should be lowered. Figures 5.6 b), 5.7 a) and 5.7 b) all show the effects of various thresholds on the spatial distribution of topographic index. These three figures correspond to thresholds of 100, 50 and 20, respectively. The long linear features disappear for thresholds of 50 and 20, but notice that in Figure 5.7 b), a great deal of higher topographic index values have been removed in comparison to Figure 5.6 a).

What is the most suitable threshold to use? Quinn et al. (1995) indicate that the use of two plots can help us to determine a minimum threshold to use in treating river cells. A plot of the distribution of topographic index (i.e. Ac/A versus $ln(a'/tan\beta)_i$ where Ac is the variable source area (m^2)) and a plot of the value of Ac/A at the distribution peak versus the cumulative upslope area can provide clues as to the appropriate threshold. According to Quinn et al., wherever these plots show rapid changes in shape, then an optimum threshold for river ending has been reached. Appendices A8 toA12 show plots of Ac/A versus $ln(a'/tan\beta)_i$ for each DEM size and under various thresholds. Appendices A13 and A14 show plots of Ac/A peak value versus cumulative upslope area. In the figures of Appendices A8 to A12, the value shown for each curve corresponds to the cumulative upslope area obtained by multiplying the threshold with the value of DEM cell area. Figure A8 a) shows distributions of topographic index for the 10 m DEM using four thresholds. There seems to be a rapid change in peak between the plots corresponding to 5,000 and 2,000 m^2. Figure A13 a) shows that the value of Ac/A drops rapidly at a value of about 7,000 m^2. Therefore, for the 10 m DEM, a threshold of 50, or a cumulative

upslope area of 5,000, was chosen as the optimum value at which cells would be treated as river cells. In a similar manner, the following values of cumulative upslope area were chosen as the optimum values for each DEM size.

Table 5.5: Cumulative upslope area values indicating river cell treatment for each DEM size.

DEM	Cumulative Upslope Area (m^2)
10	5,000
15	5,000
20	10,000
25	10,000
30	15,000
40	20,000
50	25,000
60	30,000
80	40,000
100	50,000

The area increases with increasing grid cell size because the minimum area that can be contributed to a downslope cell increases. If we divide the second column of Table 5.5 by the DEM cell area to obtain the threshold, then the threshold decreases from 50 for the 10 m DEM, to 5 for the 100 m DEM.

5.4.3 Results

The topographic indices were computed in three ways: 1) for the entire catchment and without giving special treatment to urban land forms; 2) for the entire catchment and giving special treatment to urban land forms as described in Section 5.3.1; and 3) for each subcatchment with special treatment given to urban land forms. Figures

5.8 and 5.9 show the distributions of topographic indices for Case 1 above. The table below lists several statistics. The two figures seem to indicate a gradual change in distribution shape, but Figure 5.9 b) shows the change in peak between the 10 m, 50 m and 100 m DEM. While the value of *Ac/A* does not change greatly between 10 m and 50 m, there is a sharp rise in the value of *Ac/A* for the 100 m DEM.

Table 5.6: Statistics of topographic index for Ancaster Creek -Case 1.

DEM	Mean	Variance	Skew
10	7.73	2.03	0.22
15	7.87	1.96	0.26
20	8.08	2.05	0.26
25	8.23	1.90	0.30
30	8.42	2.11	0.47
40	8.66	1.97	0.38
50	8.80	1.90	0.62
60	8.82	1.72	0.41
80	9.10	1.81	0.72
100	9.23	1.85	0.73

In Table 5.6, the means and skews are shown to increase while the variance decreases. If the mean value of topographic index increases, then the greater the area that should contribute to overland flow since a greater area of the catchment has a higher likelihood of becoming saturated. The variance is a measure of the spread of values around the mean. A lower variance implies that the catchment's topographic indices are concentrated around one value with few lower or higher values. This implies that less of the catchment will contribute to overland flow until values close to the peak are saturated. This in turn implies that less overland flow should be generated. The skewness is a measure of the asymmetry of a distribution. If the skewness coefficient is positive then the distribution is right skewed and has a greater

number of values that are lower than the mean, than are higher than the mean. This again would imply that less of the catchment would contribute to overland flow if the skew increased. It is not certain however, how the increase in skew and decrease in variance will balance the effects of an increase in mean.

In Case 2, where the topographic indices were computed in the manner described in Section 5.3.1 for the entire catchment, statistics were not computed as the same trends shown above were likely. However, Figures 5.10 to 5.14 show the distributions for both Cases 1 and 2. What is noticed immediately is that the value of $ln(a/tan\beta)$ at which the distribution peaks generally remain unchanged for both Case 1 and 2, but the value of Ac/A at which the peak occurs is lower for Case 2. Also, a greater proportion of the catchment has very low values of topographic index for Case 2 when compared to Case 1. This is not surprising considering the manner in which the topographic indices are computed in Case 2 which has the net effect of lowering the average value of topographic index. The average values of topographic index for both Cases 1 and 2 are shown below.

Table 5.7: Average values of topographic index for both Cases 1 and 2.

DEM	Mean Case 1	Mean Case 2
10	7.733	6.95
15	7.867	7.11
20	8.079	7.37
25	8.234	7.50
30	8.424	7.71
40	8.661	7.92
50	8.798	8.09
60	8.819	8.10
80	9.103	8.34
100	9.225	8.53

Notice that as DEM size increases for Case 2, the proportion of area with very low values of topographic index decreases. This is simply a manifestation of the increase in mean that the distribution of topographic index for Case 1 also exhibits. Thus, it is expected that for very high values of grid cell size, the "effect" of urban areas on overland flow generation will decrease and the results of calibrations using topographic distributions from Case 1 and Case 2 will begin to converge.

Appendices A15 to A19 show the distribution of topographic index for Case 3. The table below lists the average values of the index.

Table 5.8: Average topographic index for each subcatchment in case 3.

DEM	Hwy 403	Maple Lane	Golf Links	Wilson
10	7.48	6.67	6.49	6.49
15	7.63	6.97	6.66	6.57
20	7.82	7.08	6.98	6.93
25	7.97	7.37	7.11	6.91
30	8.19	7.39	7.60	7.06
40	8.38	7.97	7.49	7.27
50	8.56	7.67	7.86	7.53
60	8.57	7.96	7.61	7.54
80	8.79	8.41	8.02	7.5
100	9.00	8.13	8.32	7.97

The figures and the table above show that Hwy 403 and Maple Lane have the highest average of topographic index and will produce the greatest amount of overland flow for the entire catchment. Both Hwy 403 and Maple Lane have fairly mild slopes and Hwy 403 in particular drains significant amounts of upslope area. Furthermore, Hwy 403 has very little urbanization. Maple Lane however, is almost 30% urban according to Table 5.3, but the relative flatness compensates for the effect of the

urban land form treatment.

5.5 Sensitivity Analysis

Like TOPMODEL, to run TOPURBAN, three separate input files are required: 1) the meteorologic and hydrometric data input file (INPUT.DAT); 2) the distribution of topographic index (SUBCAT.DAT); and 3) the model parameter values (PARAM.DAT). Examples of these files are shown in A20 for the 10 m DEM. Only a small portion of INPUT.DAT for 1991 was included. Figure 5.15 details the flow chart for TOPURBAN.

A sensitivity analysis is conducted to determine what parameters should be calibrated of the nine that TOPURBAN uses. The literature generally reports that the hydraulic conductivity *Ko*, the recession parameter *m*, and the maximum size of the soil root zone, Sr_{max} are the most influential parameters. The sensitivity of TOPURBAN parameters will be tested on a relatively short series consisting of three rain events with the first being preceded by approximately 72 hours of dry weather. The rain series selected is 272 hours long between June 22 and August 3, 1992. For simplicity and speed, the sensitivity analysis will be conducted using a topographic distribution for the 10 m DEM in which urban land-use received the appropriate treatment. The influence of the eight parameters on model prediction will be assessed using the predicted hydrograph volume divided by the catchment area (V), the time to peak (t_p) and the peak flow (Q_p) for the second and largest rain event. A 'Basis of Comparison' (BOC) was established in order to provide a frame of reference. Parameters were increased or decreased in turn while all others were held constant. The amount of increase or decrease varied by either ±5%, ±25%, or ±50%. The values that were used are shown in Table 5.9. The resulting values are shown in Table 5.10 and plots of the BOC hydrograph versus the test results are shown in Figures 5.16 to 5.19. The BOC provided a time to peak (t_p) of 1.0 hour, a peak flow

(Q_p) of 3.96 m^3/s and a total depth of runoff (V) as 0.016 m.

Table 5.9: TOPURBAN parameters used in sensitivity analysis.

%	*Ko* (m/hr)	*m* (m)	Sr_{max} (m)	Sr^0 (m)	*uacp*	T_d (hr/m)	F_{RV}	F_{CHV}	Q_o (m)
-50	5.0	0.010	0.0250	0.0250	0.10	0.5	0.024	0.121	5.05
-25	7.5	0.015	0.0375	0.0375	0.15	0.75	0.036	0.1815	7.58
- 5	9.5	0.019	0.0475	0.0475	0.19	0.95	0.0456	0.23	9.6
BOC	10.0	0.020	0.0500	0.0500	0.20	1.0	0.048	0.242	10.01
+5	10.5	0.021	0.0525	0.0525	0.21	5.0*	0.0504	0.2541	10.06
25	12.5	0.025	0.0625	0.0625	0.25	12.5*	0.06	0.3025	12.6
+50	15.0	0.030	0.0750	0.0750	0.30	15.0*	0.071	0.363	15.2

* These values do not correspond to the % differences shown in the first column.

Table 5.10 a): Sensitivity of TOPURBAN parameters.

		Ko (m/hr)	*m* (m)	Sr_{max} (m)	Sr^0 (m)
-50%	t_p (hrs)	1	1	1	1
	Q_p (% diff.)	17.25	58.60	16.98	10.26
	V (% diff.)	8.26	46.88	18.72	11.61
-25%	t_p (hrs)	1	1	1	1
	Q_p (% diff.)	6.59	32.86	9.46	5.16
	V (% diff.)	4.46	27.69	10.88	6.12
- 5%	t_p (hrs)	1	1	1	1
	Q_p (% diff.)	0.72	5.84	1.74	1.20
	V (% diff.)	0.85	5.98	2.58	1.29
+5%	t_p (hrs)	1	1	1	1
	Q_p (% diff.)	-2.10	-7.80	-1.19	-0.06
	V (% diff.)	-0.67	-5.35	-1.16	0.00
25%	t_p (hrs)	1	2	1	1
	Q_p (% diff.)	-9.29	-27.95	-5.46	0.25
	V (% diff.)	-3.14	-25.45	-5.04	0.00
+50%	t_p (hrs)	2	2	1	1
	Q_p (% diff.)	-14.73	-43.62	-11.43	-0.02
	V (% diff.)	-6.11	-43.73	-9.47	0.00

Table 5.10 b): Sensitivity of TOPURBAN parameters.

		uacp	T_d (hr/m)	F_{RV}	F_{CHV}	Q_o (m)
-50%	t_p (hrs)	1	1	1	8	2
	Q_p (% diff.)	-3.81	-0.02	-9.40	-35.51	-17.40
	V (% diff.)	-2.38	-0.10	0.15	-12.76	-14.85
-25%	t_p (hrs)	1	1	1	2	1
	Q_p (% diff.)	-1.89	-0.34	-4.39	-8.28	-6.47
	V (% diff.)	-1.18	0.00	-0.04	-4.34	-4.66
- 5%	t_p (hrs)	1	1	1	7	1
	Q_p (% diff.)	-0.34	-0.07	-0.87	-12.76	-1.25
	V (% diff.)	-0.23	0.00	0.027	-1.37	-1.05
5%	t_p (hrs)	1	1	1	1	1
	Q_p (% diff.)	0.25	-0.02	0.778	-0.82	0.99
	V (% diff.)	0.24	0.00	-0.16	0.22	0.99
25%	t_p (hrs)	1	1	1	1	1
	Q_p (% diff.)	2.11	-0.13	5.36	1.311	3.60
	V (% diff.)	1.19	0.04	-0.23	0.98	4.34
50%	t_p (hrs)	1	1	2	1	1
	Q_p (% diff.)	3.98	-0.02	16.13	46.56	6.27
	V (% diff.)	2.38	-0.03	-0.23	2.24	7.61

An additional test was conducted in which T_d was set to 100 hr/m. The results were t_p = 1 hr, Q_p decreased by 2% and V decreased by 1.06%.

From Table 5.10 it can be seen that *Ko* has a significant impact on peak flow but does not influence the volume as greatly. The observed increase in volume is due directly to the increase in peak flow. But as *Ko* decreases, the soil's ability to transmit lateral flow weakens, and the soil is more likely to contribute to overland flow. Figure 5.16 a) shows the significant influence of *Ko* on the peak flow and the marginal effect on hydrograph shape.

The recession parameter *m* is the most influencing parameter of the nine studied. It influences the volume and the peak flow enormously and this is consistent with the literature review. The parameter controls the drainage of the soil. If *m* increases then the decrease in hydraulic conductivity with depth is not very rapid; thus, providing

greater subsurface drainage and a slower rate of filling saturated storage. This creates a delayed catchment response. Figure 5.16 b) shows the change in peak, recession and levels of baseflow that accompany a change in m. If m decreases, peaks increase and recession is quick. The transmissivity $To = mKo$, controls the position of the saturated area (Quinn 1991). An increase in To reduces the size of the saturated area and the surface excess runoff; thus, reducing the size of the peak flow. An increase in To implies an increase in Ko or an increase in m, and both cases imply a greater contribution in subsurface flow.

In Figure 5.17 a), Sr_{max} provides the mechanism by which abstractions are made through evapotranspiration. It has roughly the same degree of influence as Ko on predicted hydrograph flow but with a greater influence on predicted volumes. As it governs the net flow that reaches the unsaturated zone, it is a definite candidate for calibration. Sr^0 is the initial deficit in the root zone and is a measure of the antecedent moisture condition. This is an indication of the initial water available for abstraction. A 50% difference in Sr^0 made a 10% difference in predicted peak and this is illustrated in Figure 5.17 b). A decrease in Sr^0, indicates wetter initial soil conditions and has a large influence on both V and Q_p. Q_o is the other initial condition of interest and its influence is shown in Figure 5.18 b). It provides a measure of the initial average depth to the water table. Since Sr^0 is some indication of the moisture required to raise the water table, these two parameters will have some interaction. If Q_o is very high, indicating that the soil may be saturated, then Sr^0 would have to be close to zero. The influence of Q_o lessens as initial conditions are damped out and this is illustrated in Figure 5.18 b).

The parameter *uacp* does not influence the model simulations greatly and little difference is observed from the BOC hydrograph in Figure 5.18 a). There is some expected parameter interaction however, between *uacp* and Ko, as both govern peak flow rates and hydrograph volume. The time delay parameter has little influence on

predicted flow in these conditions and will not be calibrated or discussed further.

The most influencing parameters on hydrograph shape are F_{RV} and F_{CHV}, illustrated in Figures 5.19 a) and b) respectively. F_{RV} influences the time to peak but has little influence on runoff volumes. It does however influence Q_p slightly. The parameter F_{CHV} has the greatest influence on time to peak and does influence the volume and peak flow almost as much as m. It is believed that an optimum value of this parameter can be quickly determined by simply matching the time to peak of the predicted and observed flow, thus avoiding a rigorous calibration of this parameter.

From Table 5.10, it is evident that the most sensitive parameter is m. The calibration process will involve four parameters, m, Ko, Sr_{max}, and $uacp$. While $uacp$ is not a very influential parameter, a calibration will take place to determine the optimum value of imperviousness in the catchment. Both F_{RV} and F_{CHV} will not be calibrated formally but instead will be adjusted manually. It is suspected that manual manipulations of F_{RV} and F_{CHV} will allow rapid converge to their optimum values.

5.6 Optimization

The objectives of this section are to present the objective function that will help determine TOPURBAN's modeling efficiency, and the optimization scheme that will minimize the objective function. TOPURBAN is a complex model with many computational steps and calibrating four parameters will compound the number of calculations required to determine the optimum parameter set. Therefore, an efficient optimization scheme is highly desirable. The Nelder-Mead Method (Mathews 1987) has been chosen as the optimization scheme in this research. This is a direct search method, also known as the "Simplex Method" and does not compute function derivatives. The minimization function is evaluated at a certain number of initial starting points where one starting point is a set of parameter values in the parameter

space. Depending on the resulting values, the method selects new points in the parameter space in the direction determined by the starting points that provided the lowest function values. This continues until all parameter sets converge to the same point in the parameter space. This method is recommended by Sorooshian et al. (1995) because of its general efficiency and its effectiveness in determining global minimums over other search strategies.

The objective function that will be minimized in this research is the sum of squared errors shown in Equation (5.15). Hornberger et al (1985) noted that this is the criterion most often used for fitting rainfall-runoff models.

$$F = \sum_{t=1}^{N} [Q_{obs}(t) - Q_{pred}(t)]^2 \tag{5.15}$$

Nash et al. (1970) noticed that the above equation is analogous to the residual variance of a regression analysis. Similarily, the intial variance may be defined as,

$$F_o = \sum_{t=t}^{N} [Q_{obs}(t) - \bar{Q}_{obs}]^2 \tag{5.16}$$

where $\bar{Q}_{obs}$ is the average of the observed discharges. This value F_o is defined as the "no model" value of F. Nash et al. (1970) go on to propose that the efficiency of a model can then be defined as the proportion of the initial variance accounted for by that model,

$$E = \frac{\sum_{t=1}^{N} [Q_{obs}(t) - \bar{Q}_{obs}]^2 - \sum_{t=1}^{N} [Q_{pred}(t) - Q_{obs}(t)]^2}{\sum_{t=1}^{N} [Q_{obs}(t) - \bar{Q}_{obs}]^2} \tag{5.17}$$

The value E is sometimes referred to as the "Nash and Sutcliffe Efficiency" or "Nash E" for short. It can be rewritten as,

$$E = 1 - \frac{\sum_{t=1}^{N} [Q_{pred}(t) - Q_{obs}(t)]^2}{\sum_{t=1}^{N} [Q_{obs}(t) - \bar{Q}_{obs}]^2} \qquad (5.18)$$

or,

$$E = 1 - \frac{variance\ of\ the\ residual\ errors}{variance\ of\ the\ observed\ data}$$

The value is close to one if the model perfectly predicts the observed data. If this value was negative, then a data series comprising of the average value of $Q_{obs}(t)$ would be a better predictor of the observed data than the model's predictions. The Nash E has been used to describe the efficiency of models in numerous cases where TOPMODEL has been used (Lamb (1996), Quinn (1991) , Chairat (1993)) and will be adopted for use in this research for comparative purposes.

5.7 Field Survey

A brief field survey of the Ancaster Creek catchment was made during Hurricane Fran, in September of 1996. This field survey was conducted to investigate the possible location of saturation source areas. Hurricane Fran dropped almost 80 mm of rain during a three day period between September 6, and September 8, of 1996 near the area of Ancaster Creek (Horvat 1996). Nothing very significant was observed, however, Figure 5.20 shows a panoramic view of an area looking west while on Southcote Road. The viewpoint is shown with an **X** in Figure 5.3 a) and the pictures were taken in the latter stages of the event. This picture shows a completely saturated field and is considered a saturated excess source area. Notice

that this point corresponds to a region in the headwater areas of the catchment and is actually very close to the catchment boundary. The spatial distribution of topographic index shown in Figure 5.7 a) indicates that this location has relatively high values of topographic index and therefore, has a high propensity to contribute to saturation excess overland flow. An interesting statement made by Horvat (1996) notes that "the period of dry weather prior to the storm promoted the infiltration of a significant amount of initial rainfall and contributed to the minimal rise in creek levels."

5.8 Summary

This Chapter profiled the revisions to TOPMODEL that include urban areas to create the model known as TOPURBAN. TOPURBAN is different than other conventional hydrological models of mixed land-use because it does not decouple the impervious component from the pervious component of the catchment. In this way, the subsurface realm which is important in producing overland flow, is still incorporated in TOPURBAN. A new parameter, *uacp*, represents the degree of imperviousness in the watershed and was introduced into TOPURBAN along with a mechanism for generating surface runoff from impervious surfaces. The mechanism of urban runoff simply assumes that all rainfall on impervious surfaces contributes to surface runoff. ARC/INFO was used to determine the initial estimate of catchment that was urbanized as well as assist in removing sinks within the catchment.

Section 5.4 computed and compared topographic indices for Ancaster Creek under a variety of conditions. A multiple flow direction algorithm showed that the topographic indices that explicitly considered urban areas had a lower average than those topographic indices that did not consider urban areas in any special way. A sensitivity analysis indicated that Ko, m, Sr_{max} and F_{CHV} are the most influencing parameters on predicted time to peak, peak flowrate, and runoff volume. The

parameters that will be calibrated in Chapters 6 and 7 using the Nelder-Mead optimization scheme are Ko, m, Sr_{max} and $uacp$. The objective function that will be minimized is the sum of squared errors.

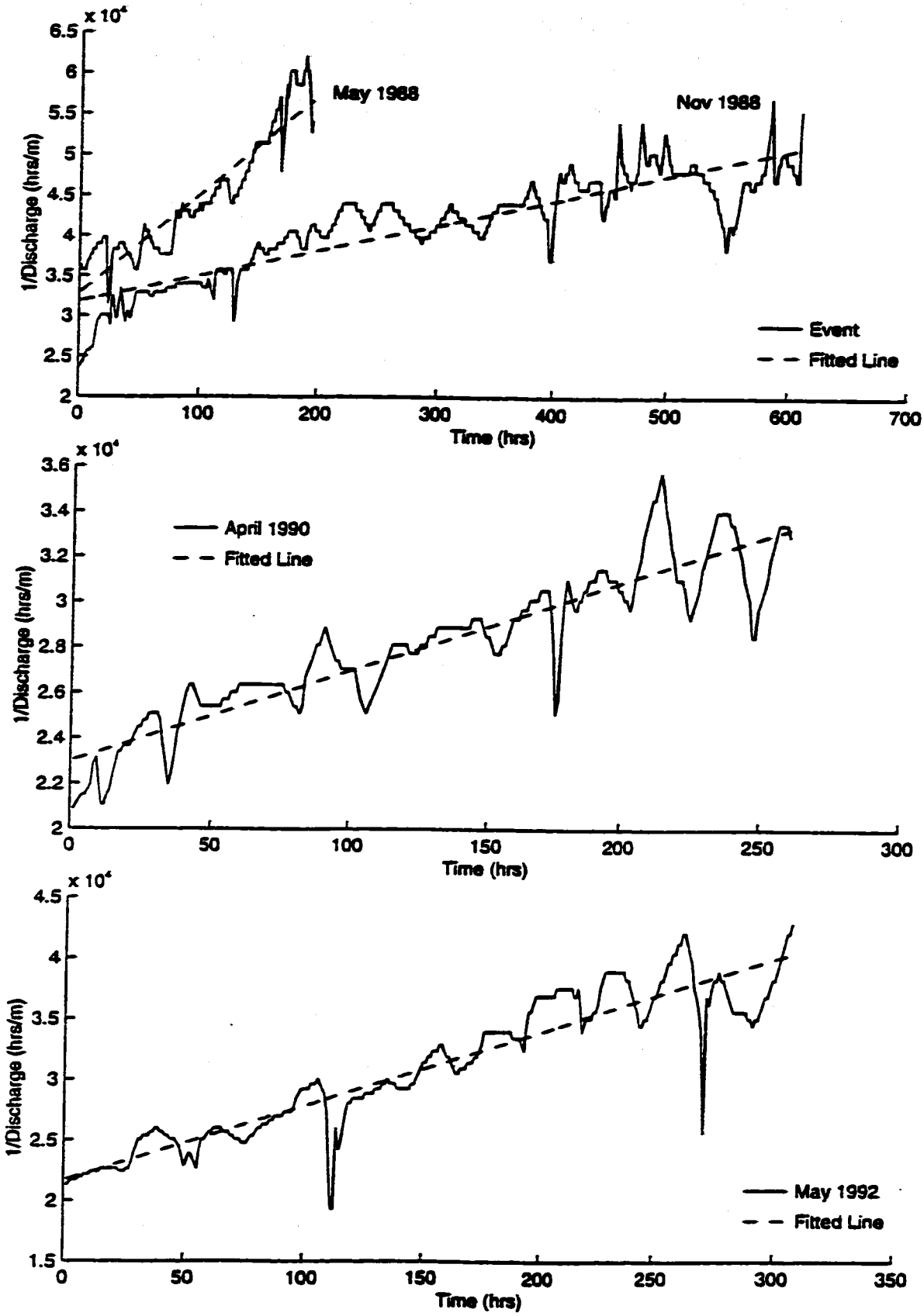

Figure 5.1: Determining the parameter *m* for various dry-weather periods.

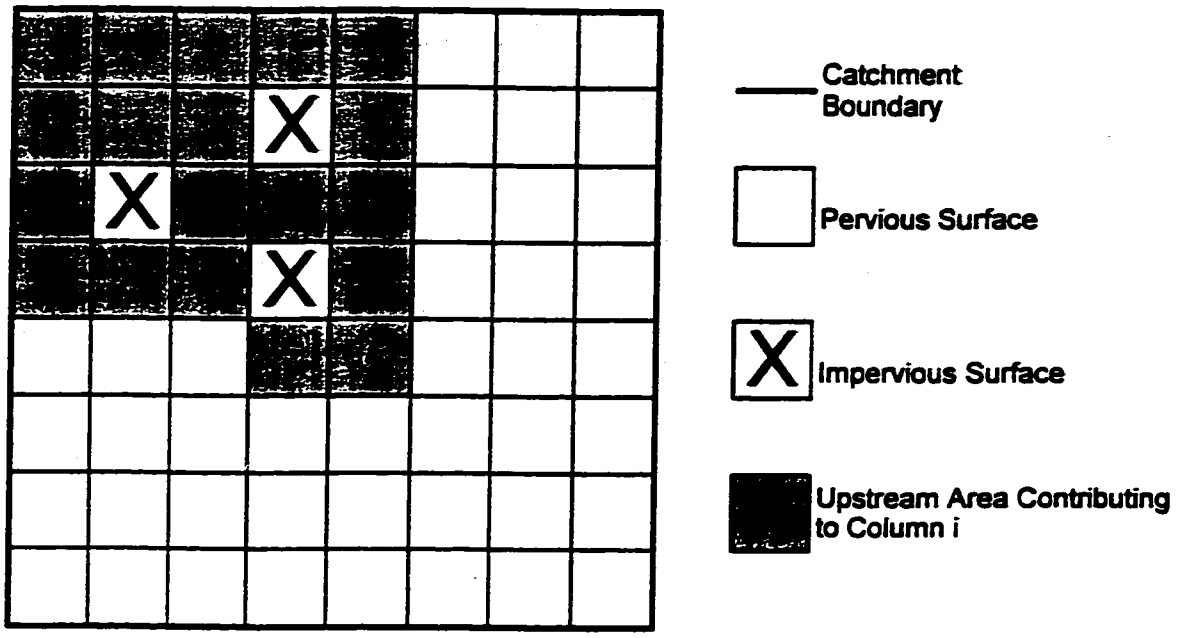

Figure 5.2: Conceptual treatment of urban land forms.

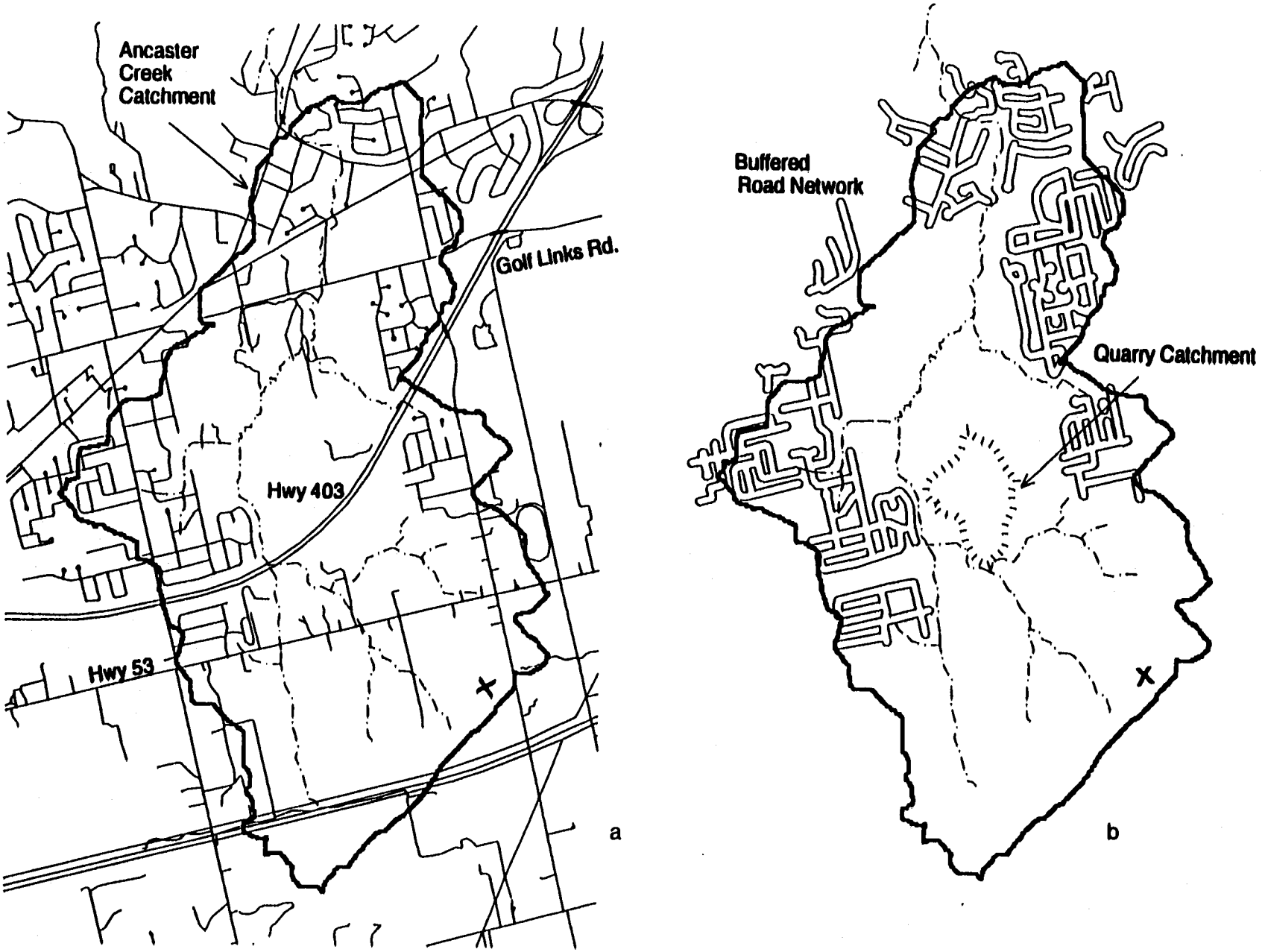

Figure 5.3: a) Transportation network b) buffered residential areas and quarry drainage area for the 10 m DEM.

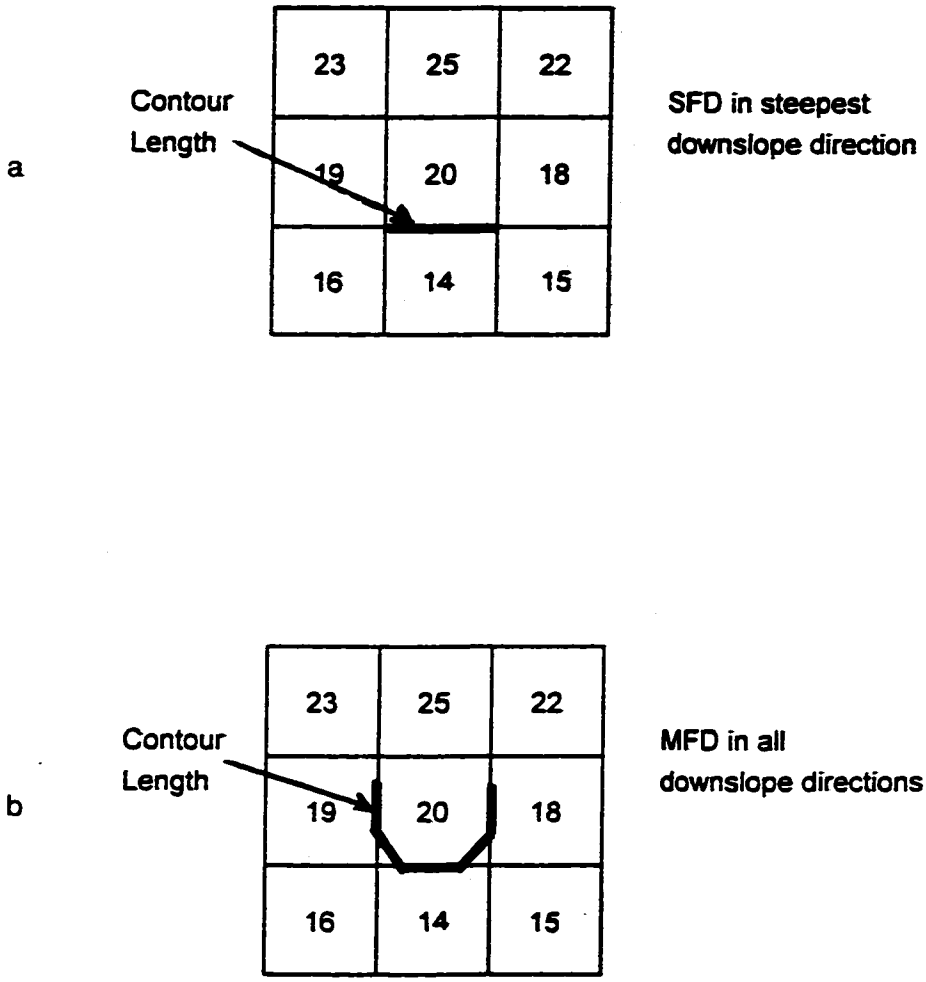

Figure 5.4: Graphical description of flow direction algorithms a) SFD and b) MFD, adopted from Wollock and McCabe (1995).

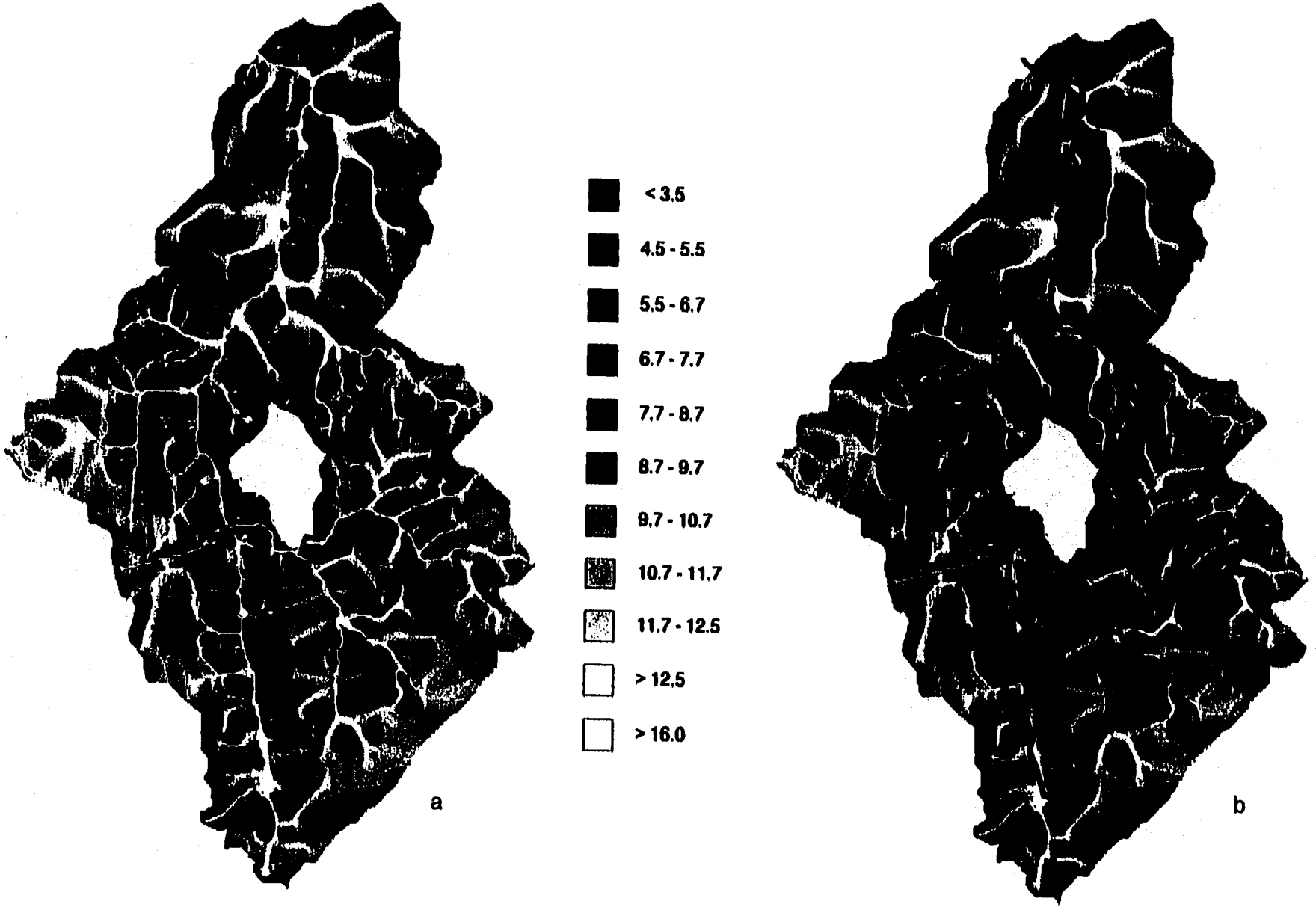

Figure 5.5: Spatial distribution of topographic indices (with no urban land form considerations) a) before river cell treatment and b) before river cell treatment with actual river network superimposed.

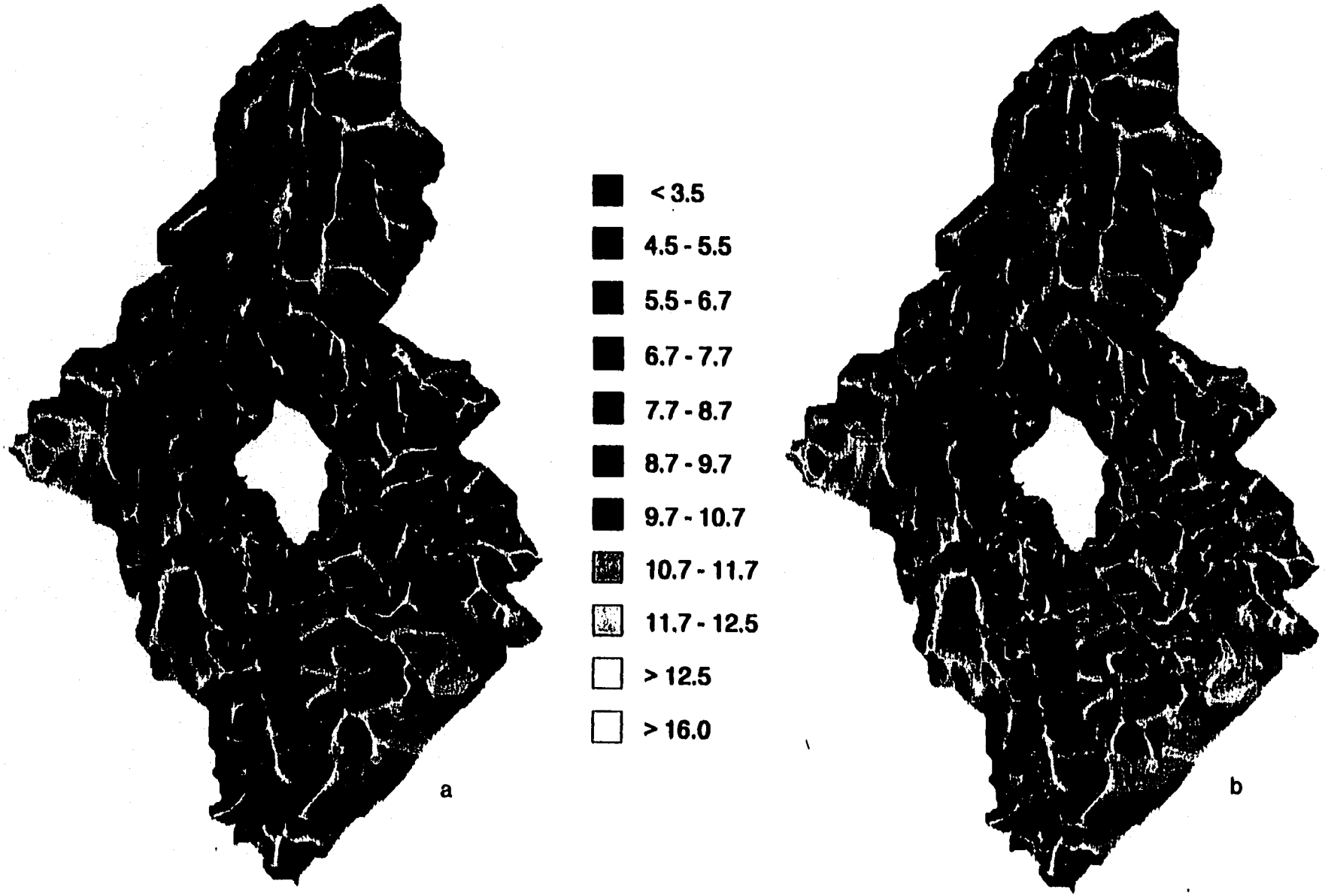

Figure 5.6: Spatial distribution of topographic indices (with no urban land form considerations) a) with river cell treatment at a threshold of 300 and b) with river cell treatment at a threshold of 100.

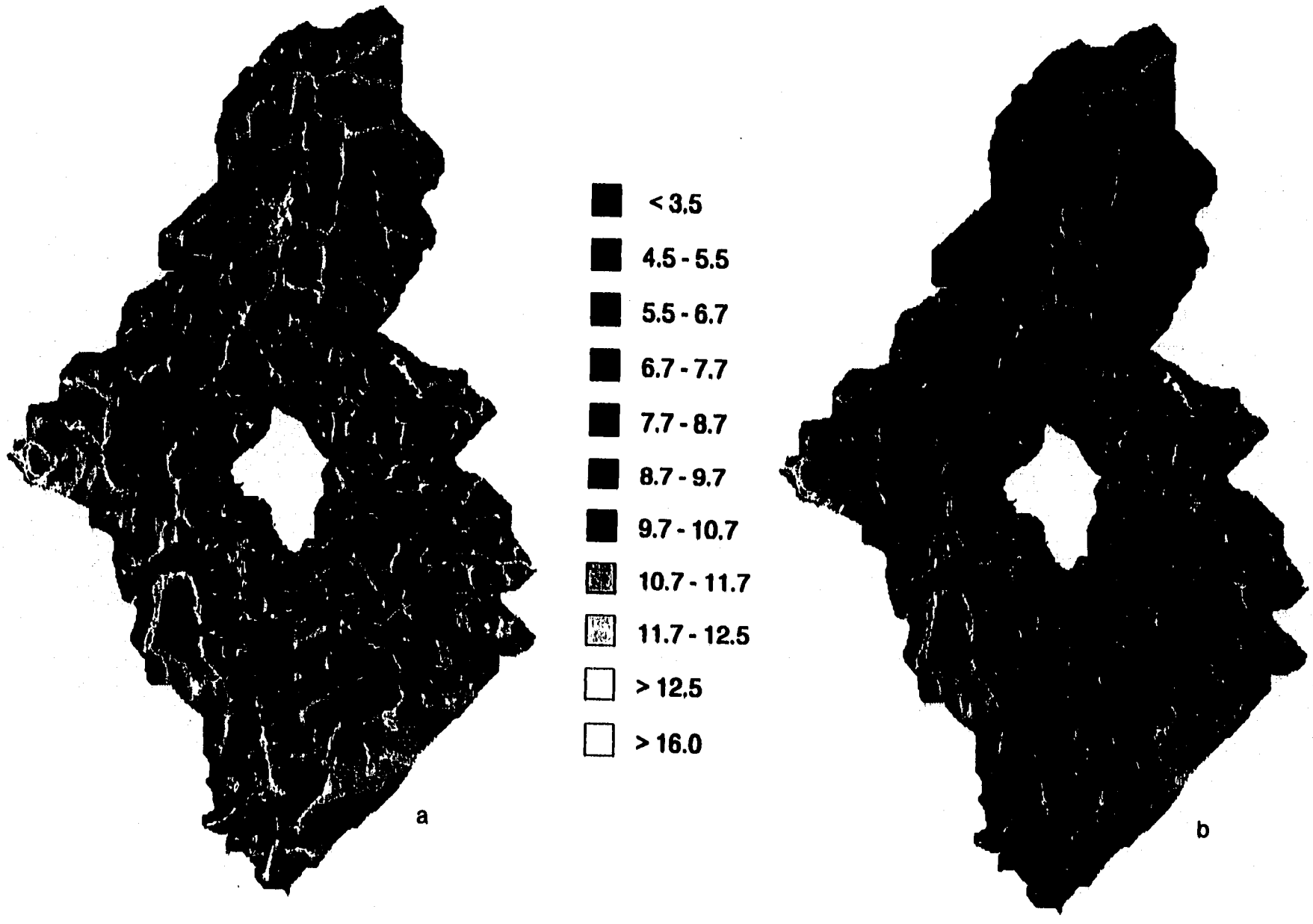

Figure 5.7: Spatial distribution of topographic indices (with no urban land form considerations) a) with river cell treatment at a threshold of 50 and b) with river cell treatment at a threshold of 20.

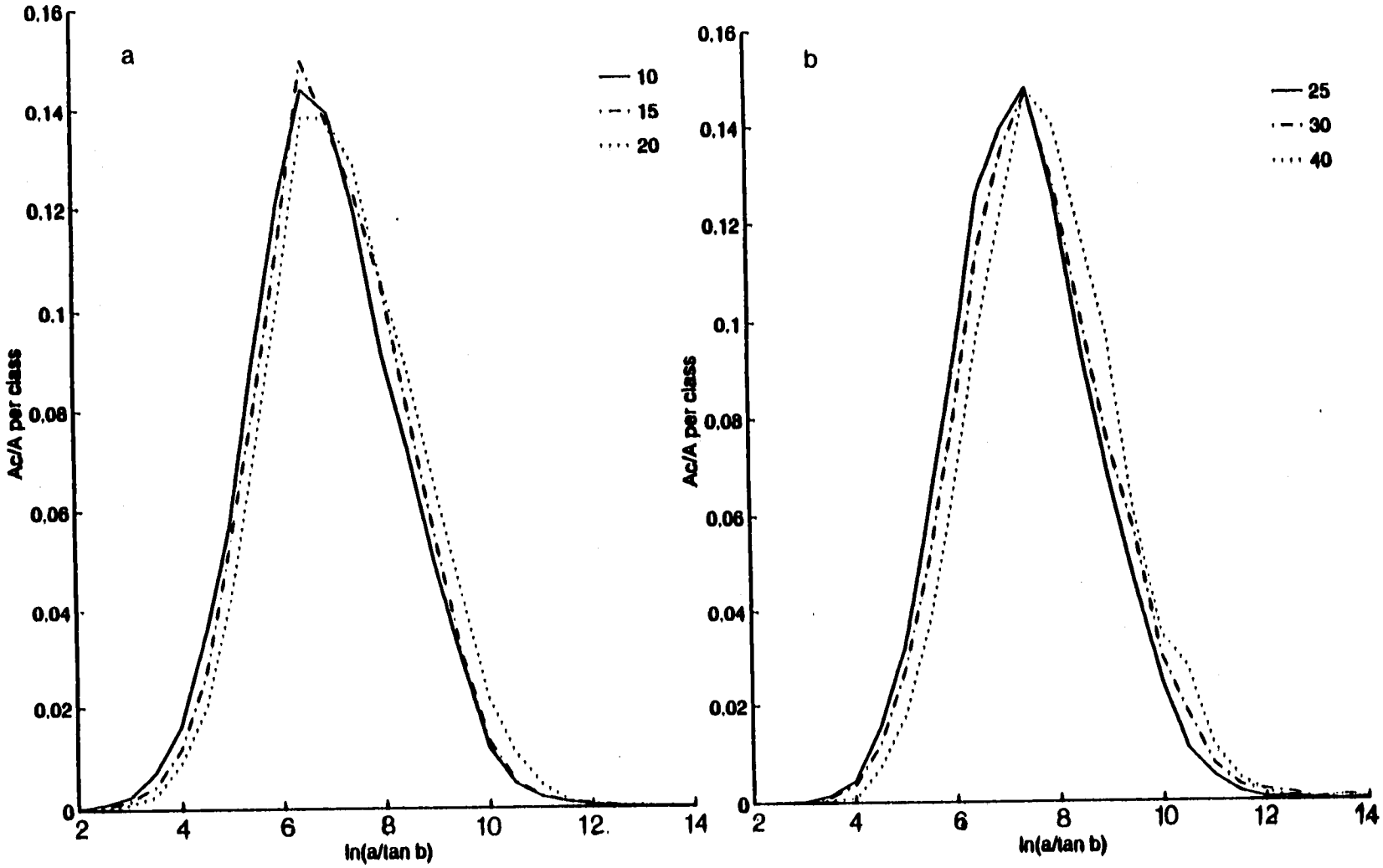

Figure 5.8: Distribution of topographic indices after river cell treatment and with no urban land form treatment for a) 10, 15 and 20 m DEMS and b) for 25, 30 and 40 m DEMS.

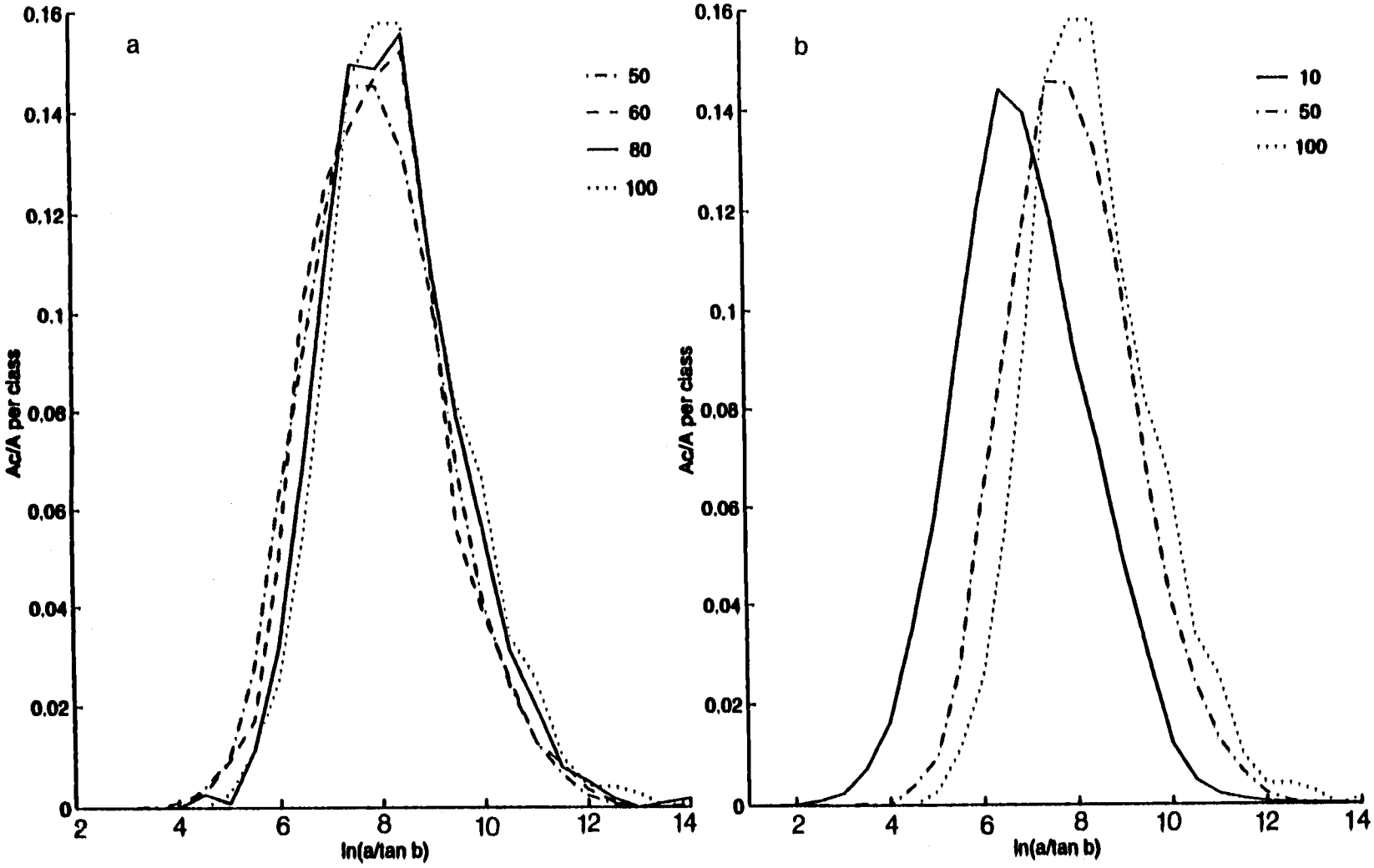

Figure 5.9: Distribution of topographic indices after river cell treatment and with no urban land form treatment for a) 50, 60, 80 and 100 m DEMs and b) for 10, 50 and 100 m DEMs.

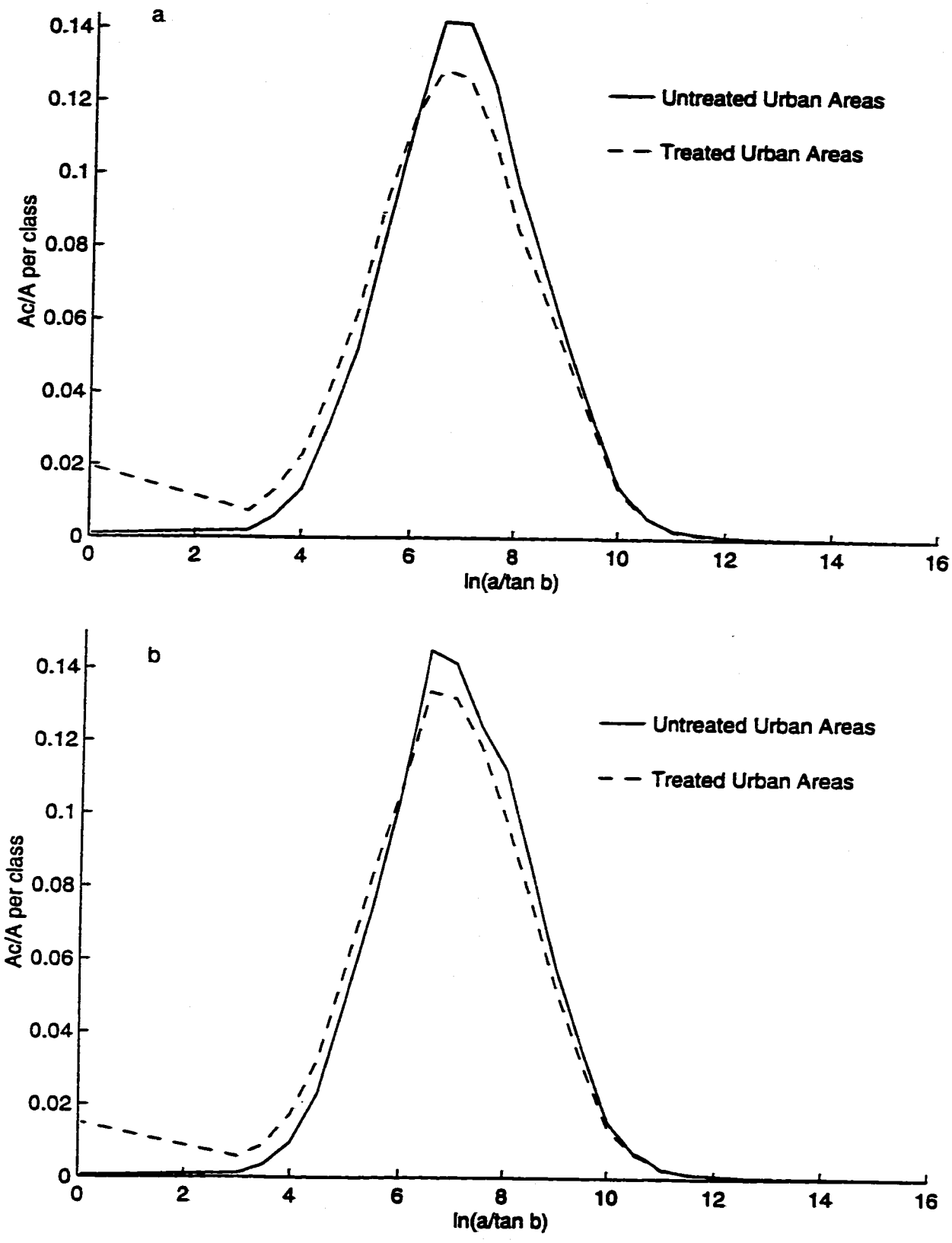

Figure 5.10: Distribution of topographic indices for a) 10 m DEM and b) 15 m DEM, before and after urban land form treatment.

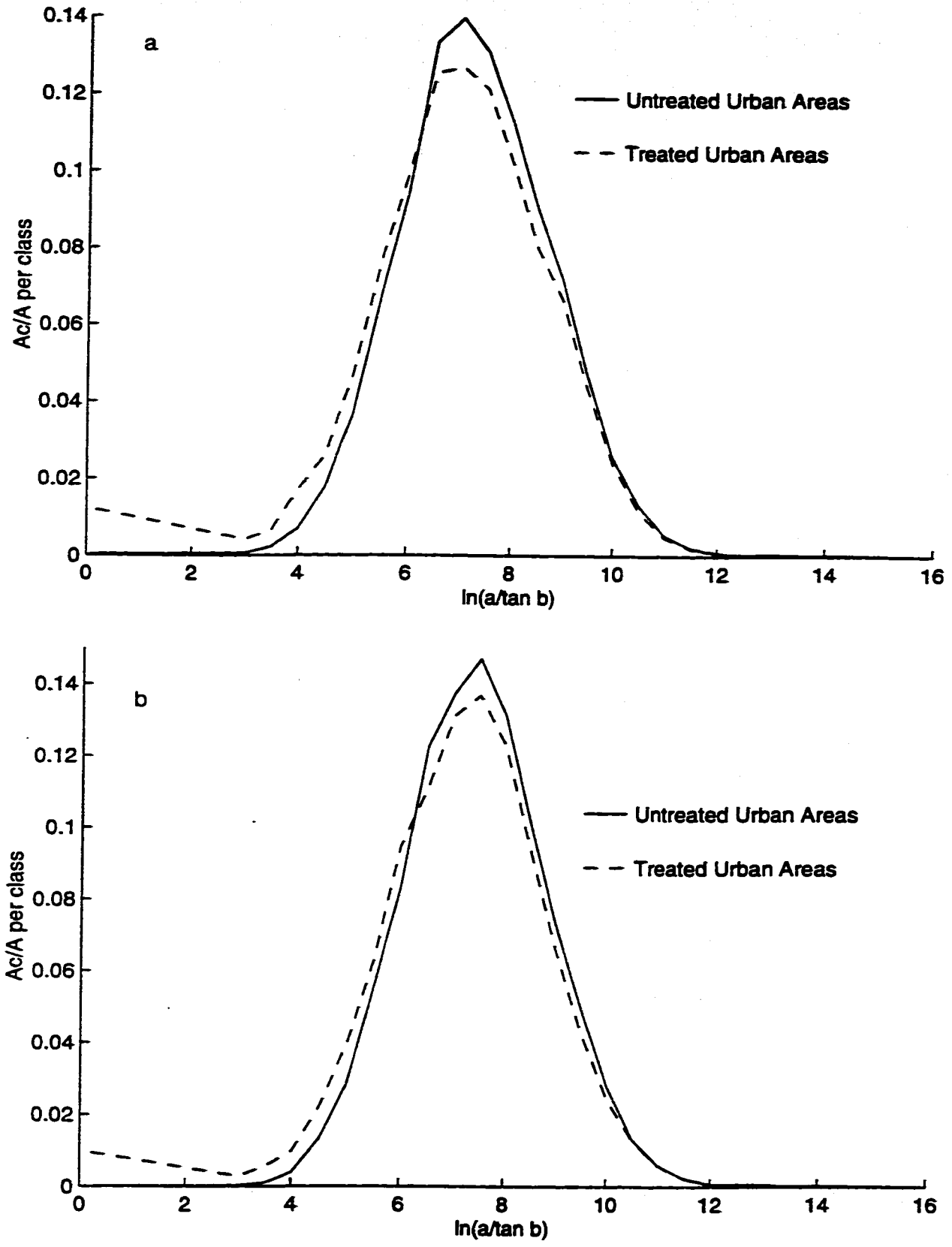

Figure 5.11: Distribution of topographic indices for a) 20 m DEM and b) 25 m DEM, before and after urban land form treatment.

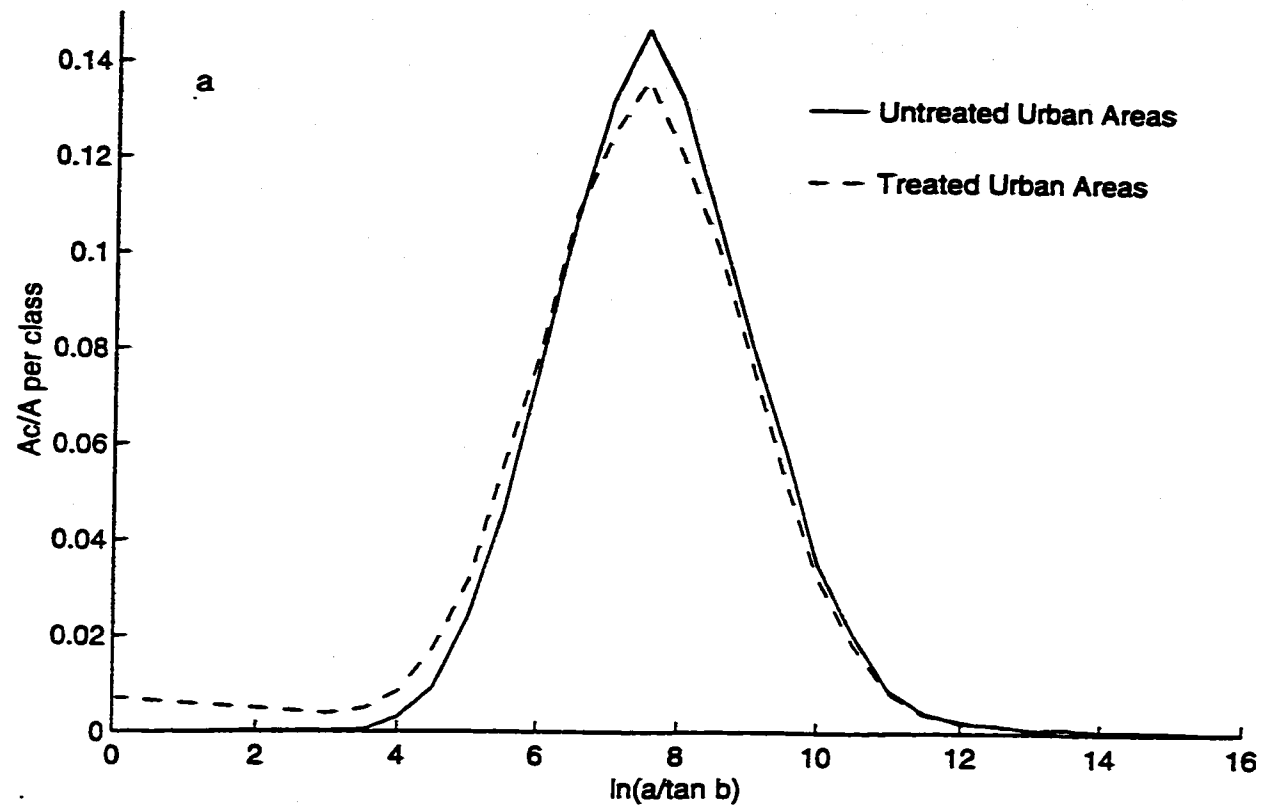

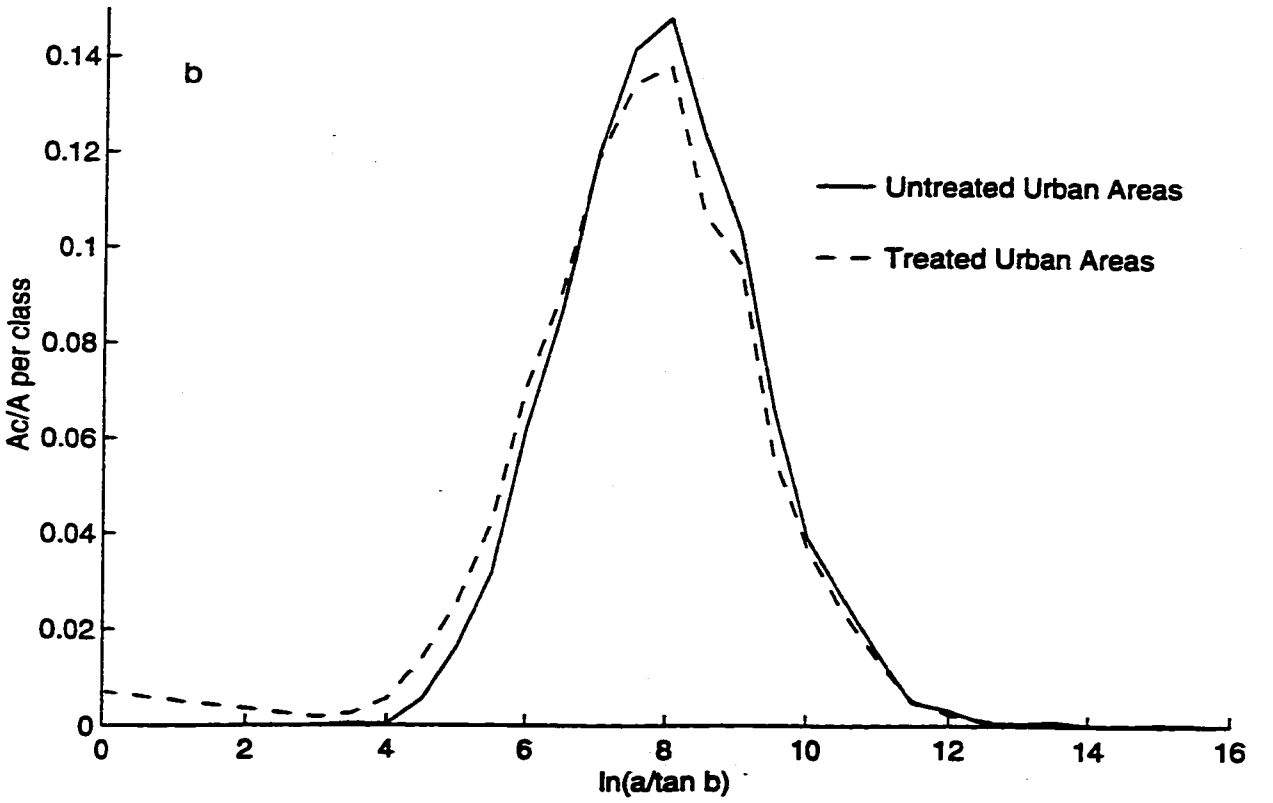

Figure 5.12: Distribution of topographic indices for a) 30 m DEM and b) 40 m DEM, before and after urban land form treatment.

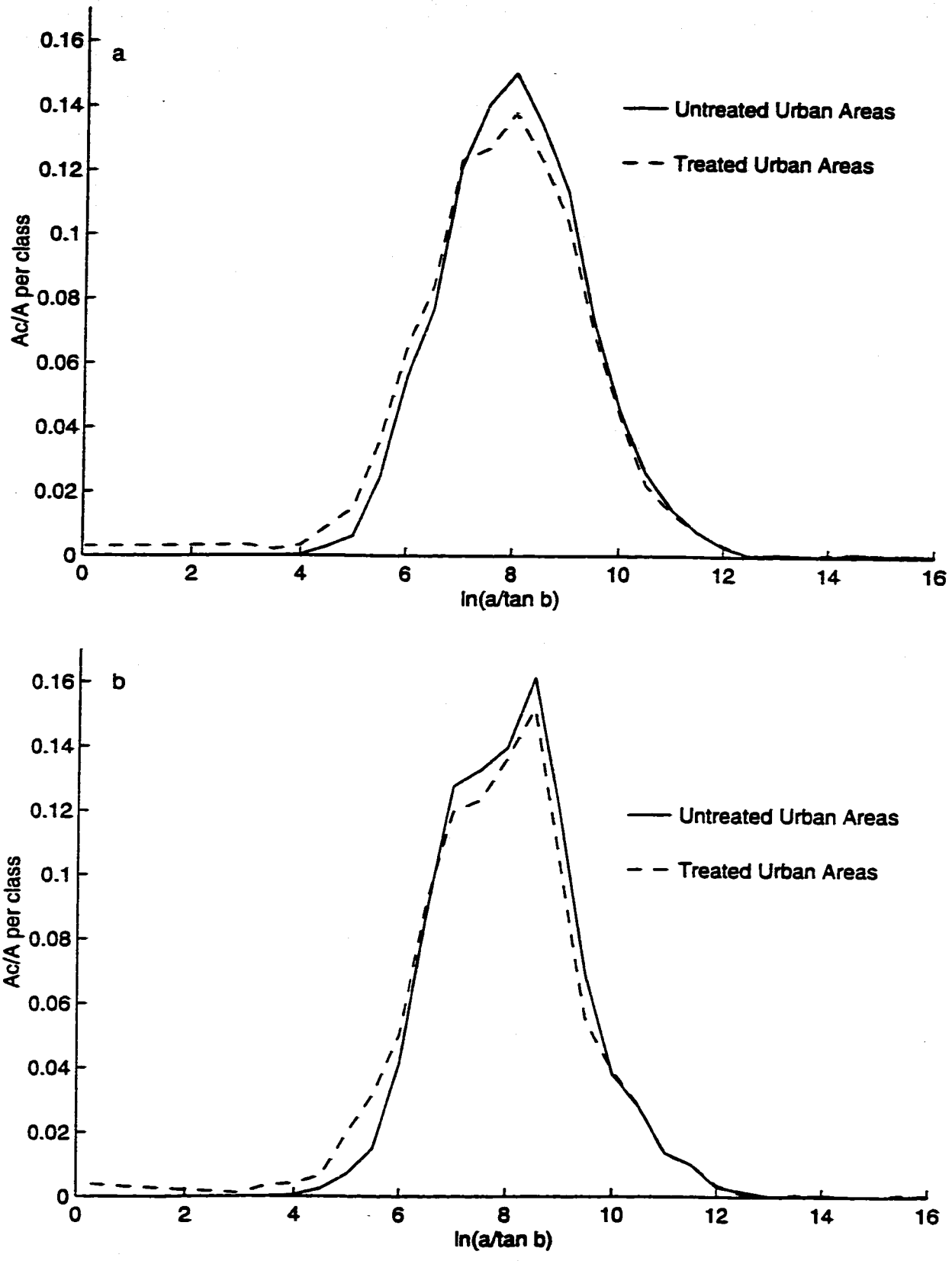

Figure 5.13: Distribution of topographic indices for a) 50 m DEM and b) 60 m DEM, before and after urban land form treatment.

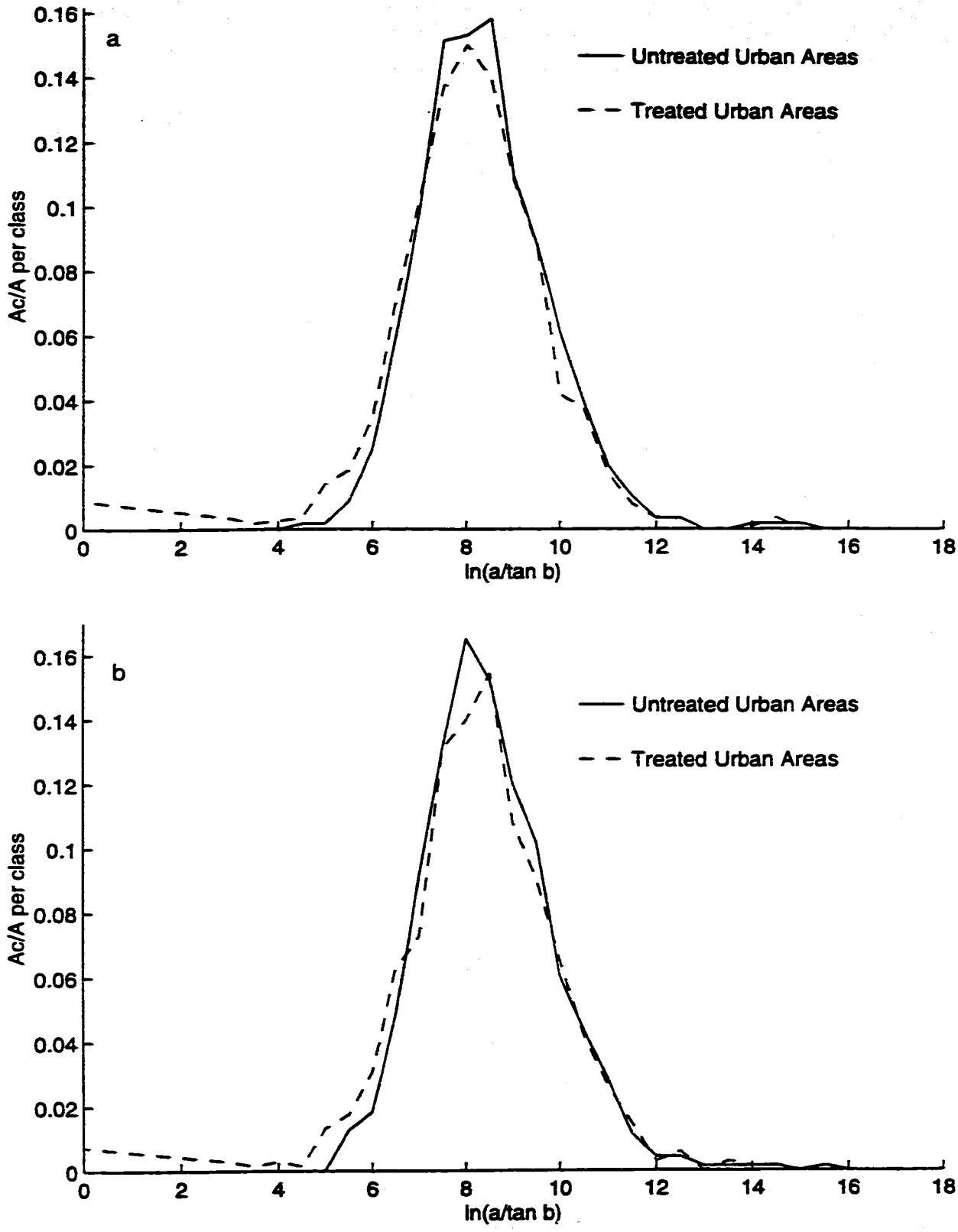

Figure 5.14: Topographic distribution of topographic indices for a) 80 m DEM and b) 100 m DEM, before and after urban land form treatment.

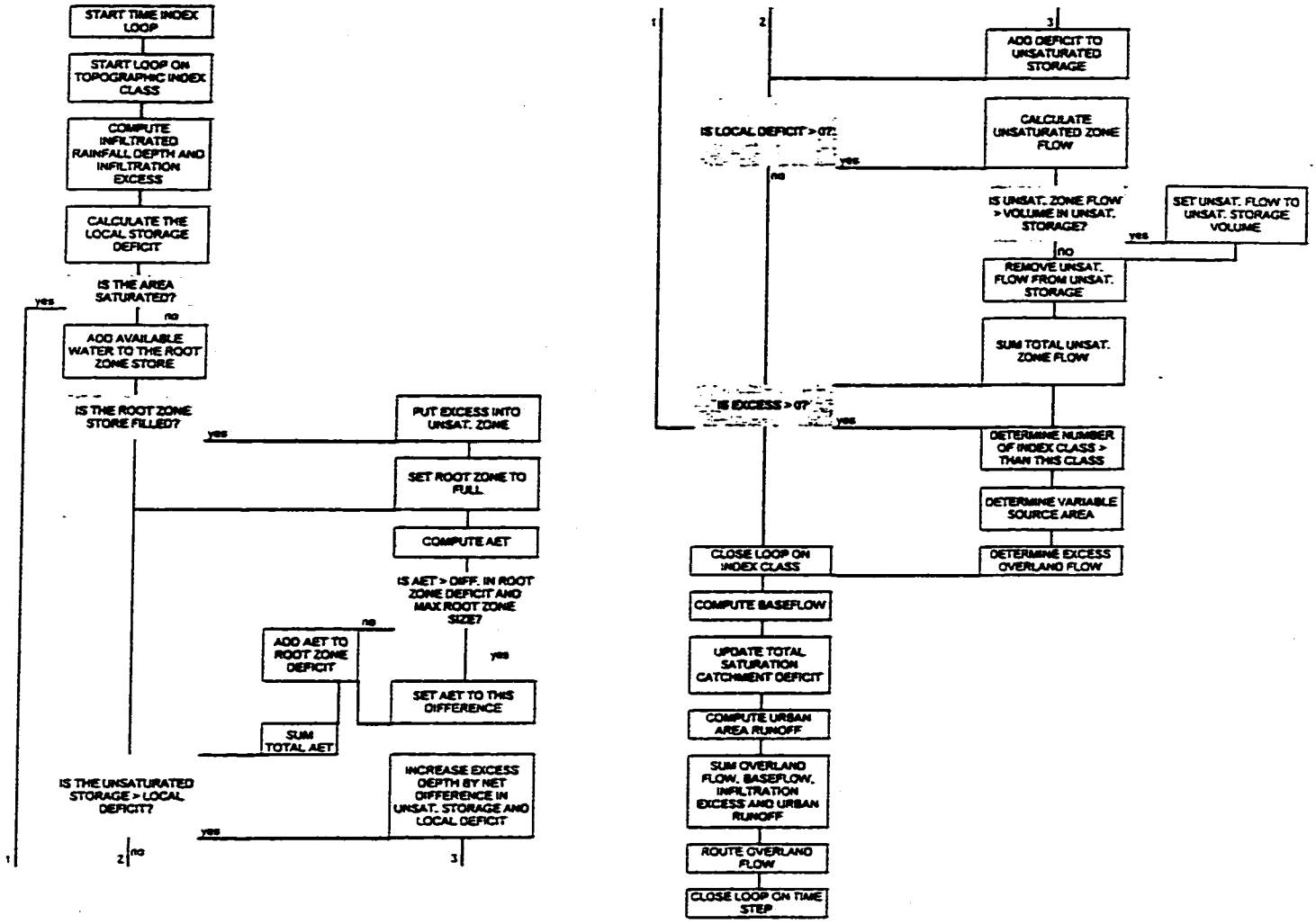

Figure 5.15: TOPURBAN flow structure (modified from Quinn 1991).

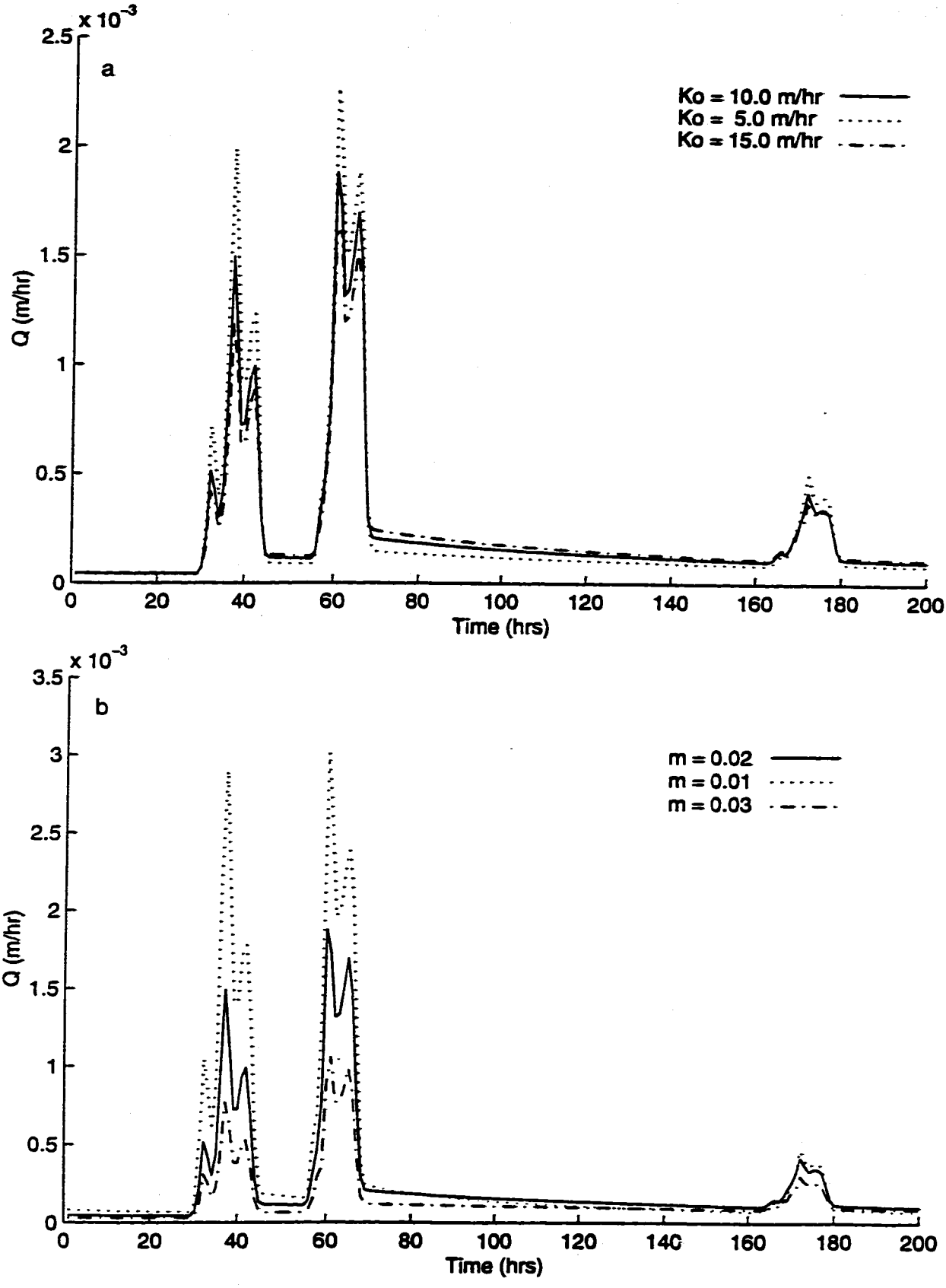

Figure 5.16: Sensitivity of TOPURBAN parameters a) *Ko* and b) *m*.

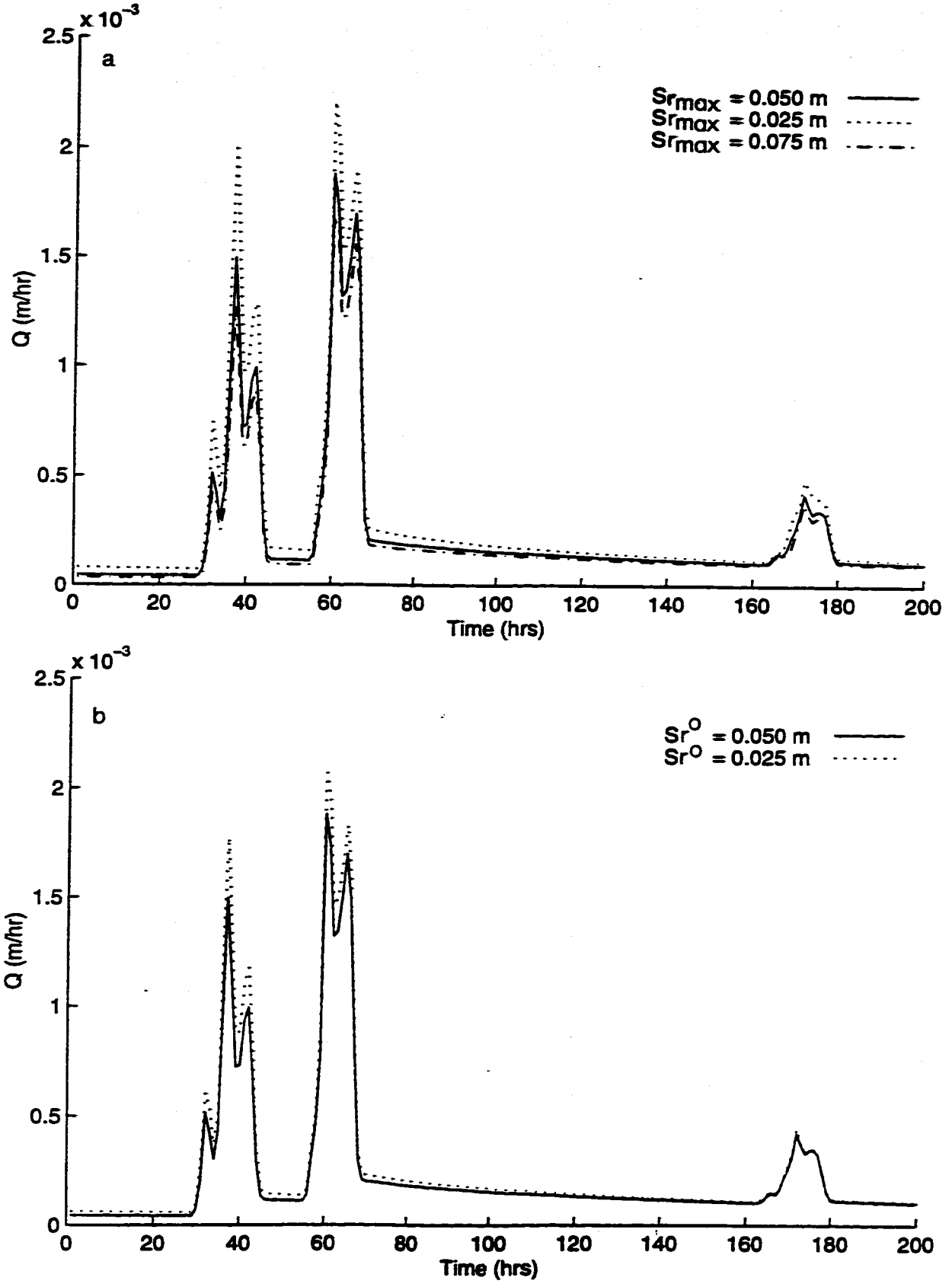

Figure 5.17: Sensitivity of TOPURBAN parameters a) Sr_{max} and b) Sr^{o}

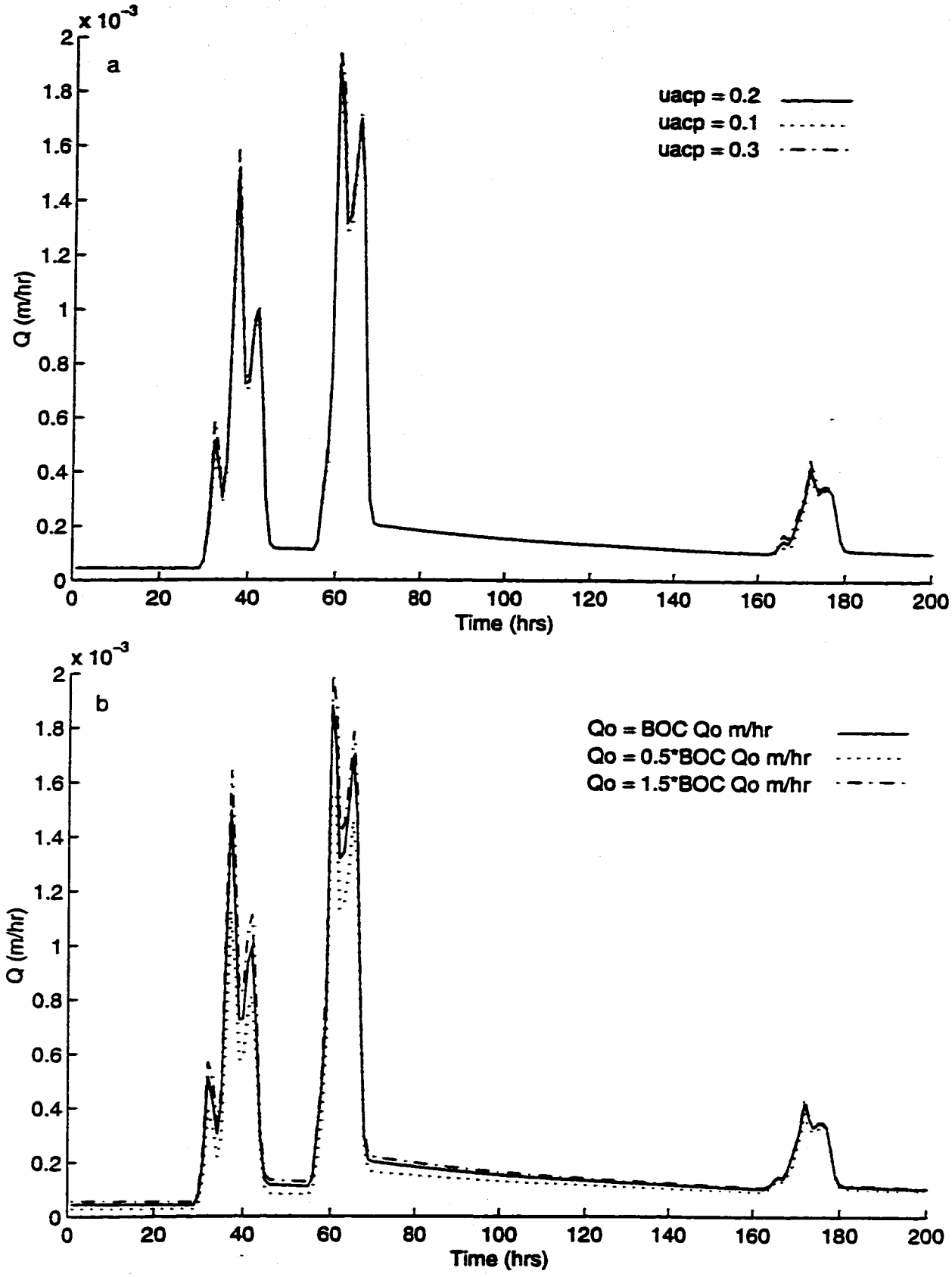

Figure 5.18: Sensitivity of TOPURBAN parameters a) *uacp* and b) Q_o.

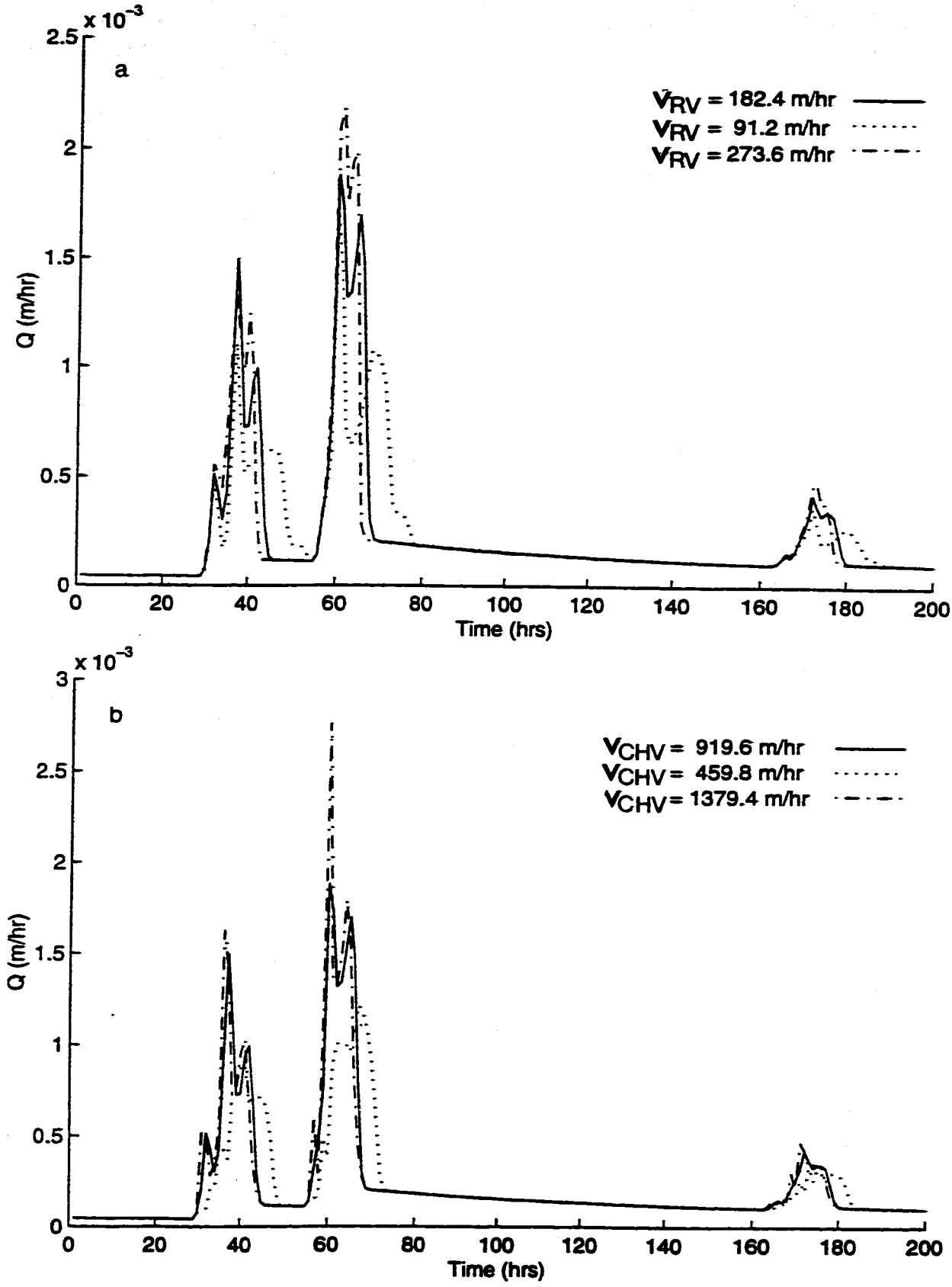

Figure 5.19: Sensitivity of TOPURBAN parameters a) v_{RV} and b) v_{CHV}.

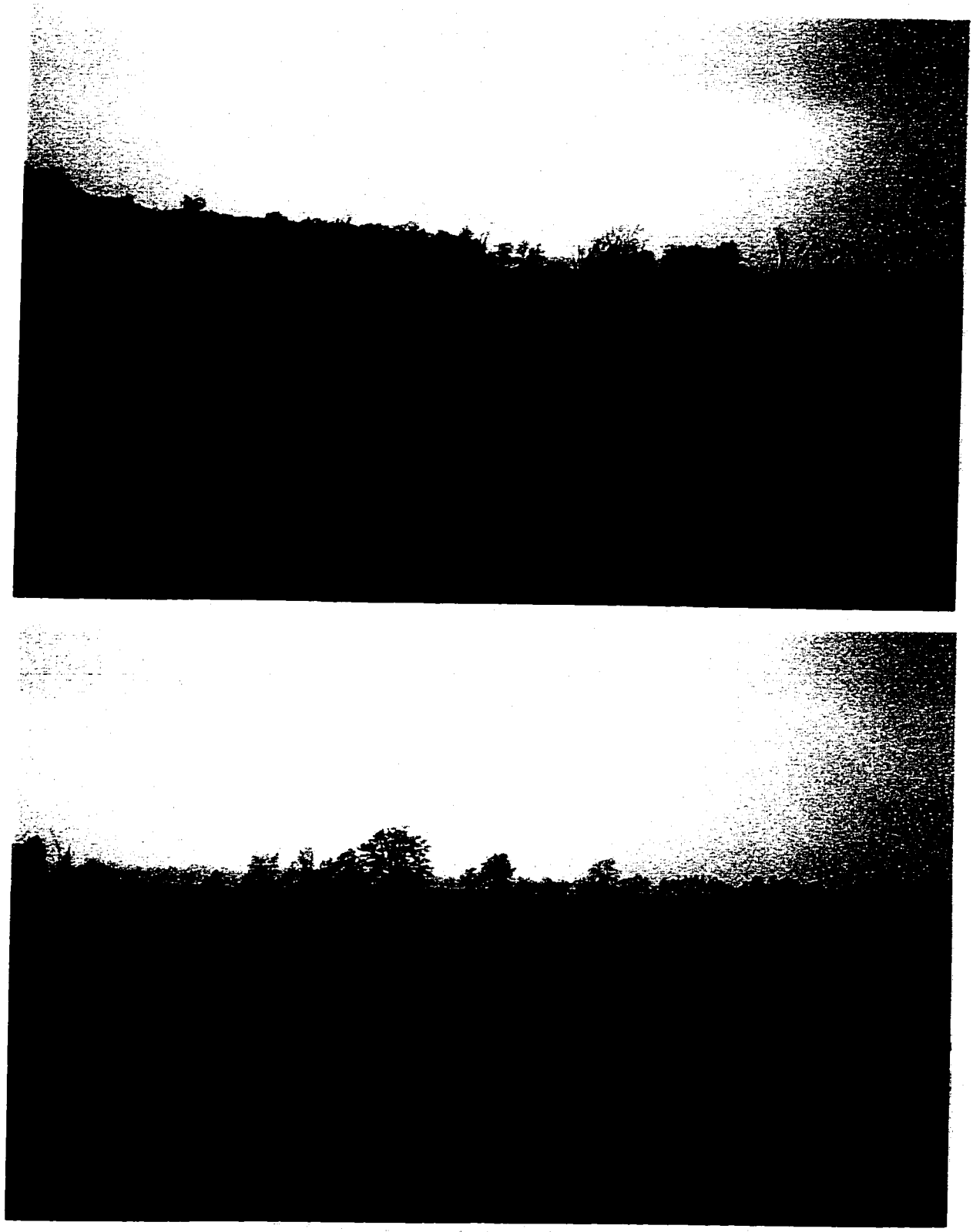

Figure 5.20: Photographs taken during Hurricane Fran in September of 1996.

CHAPTER 6 TOPURBAN APPLICATIONS TO ANCASTER CREEK - AGGREGATION PHASE

6.1 Introduction

This chapter presents the application of TOPURBAN on continuous data in 1988, 1991 and 1992 using data derived from 10 different DEM sizes. This is the aggregation phase of this dissertation research. Initial results using the calibration period in 1991 are presented first. This is then followed with two more experiments on the 1991 data: 1) TOPMODEL is applied but using the distribution of topographic index that does not regard urban areas differently than non-urban areas; 2) TOPURBAN is applied and again using the distribution of topographic index of Case 1 above. This was done to illustrate the effectiveness of the modification to TOPMODEL that created TOPURBAN, as well as the modification to the method of computing the topographic index that explicitly considered urban land forms. Section 6.5 presents the applications of TOPURBAN to data in 1998, a very dry year, and 1992, a very wet year. A DEM size for general use in hydrological modeling in Ancaster Creek and similar catchments is recommended in Section 6.8. This DEM size will be used in Chapter 7.

6.2 Application of TOPURBAN in 1991

6.2.1 Calibration Procedure

The calibrations in this chapter were conducted in two steps: 1) Simple coarse adjustments were made manually to seven TOPURBAN parameters in the following order: *uacp*, F_{RV}, F_{CHV}, Sr^0, Sr_{max}, m and finally Ko. There is a danger in calibrating one component too finely in the early stages of the calibration because of the interdependent nature of some of the parameters (OMOE 1985). The first four

parameters are the least sensitive of the seven and they are believed to have little interdependency. Thus, it was felt that adjusting them first would speed up this initial process. The adjustment made was either an increase or decrease to the parameter depending on the observed change in Nash and Sutcliffe Efficiency (Nash E). The Nash and Sutcliffe Efficiency was considered a suitable measure of model fit in this stage of the calibration. The entire process was repeated until the parameters F_{RV}, F_{CHV}, and Sr^0 had reached their optimum values (reached when no further increase or decrease in parameter value causes an increase in Nash E). This process would cause the Nash E to jump from 0 to as much as 0.6 in only a few repetitions of the process. 2) When the appropriate values of F_{RV}, F_{CHV} and Sr^0 were determined, the Nelder-Mead Optimization routine that was implemented in TOPURBAN was used to automatically optimize the four parameters *Ko*, *m*, *uacp* and Sr_{max}. It should be noted that altering T_d made no increase in Nash E so it was left at 1.0. The following results were achieved for the calibration period in 1991.

6.2.2 Calibration Results

To calibrate TOPURBAN on the 1991 data series, which contained almost 4000 points, required approximately 20 minutes on a Sparc 10. The optimized parameters for each DEM size are shown in Table 6.1 below.

Table 6.1: Optimized parameter values for the calibration period.

DEM	*m* (m)	*Ko* (m/hr)	*uacp*	Sr_{max} (m)
10	0.0487	7.702	0.164	0.0240
15	0.0494	7.484	0.156	0.0238
20	0.0499	12.162	0.195	0.0240
25	0.0477	12.236	0.187	0.0243
30	0.0498	15.652	0.206	0.0244
40	0.0510	19.347	0.170	0.0241
50	0.0416	30.392	0.219	0.0244
60	0.0420	26.789	0.184	0.0217
80	0.0493	32.167	0.157	0.0237
100	0.0447	52.043	0.205	0.0225

$F_{RV} = 0.071$ $F_{CHV} = 0.242$ $T_d = 1.0$ hr/m $Sr^0 = 0.003$ m

	Mean	Standard Deviation
m	0.0474 m	0.0034 m
uacp	0.184	0.022
Sr_{max}	0.0237 m	0.00089 m.

An average value of *Ko* was not computed as there is an obvious increasing trend with grid cell size. Also, there was no contribution to the flow from infiltration excess overland flow.

Figure 6.1 shows the predicted and observed hydrographs for the 10 m DEM. Figures 6.2 to 6.5 show different segments of Figure 6.1 in order to provide a better view of the TOPURBAN predictions next to the observed flows. The plots for all the DEM sizes look very similar; so the plots of the 15 m DEM, through to the 100 m DEM, have been placed in Appendices A21to A29, respectively. Notice from Figures 6.2 to 6.5 that the recession is poorly modeled but there is a fairly good correlation between observed and predicted peak flow values with differences averaging approximately 20%. Table 6.2 provides information on the distribution of flow between flow mechanisms and general hydrologic variables.

Table 6.2: Simulated flow distribution and total AET for the calibration period.

DEM	Total Q_{pred} (m)	% *Qurb*	% *Qb*	% *Qov*	Total AET (m)
10	0.115	7.31	89.02	3.66	0.254
15	0.114	6.75	89.17	4.08	0.254
20	0.117	8.38	88.44	3.18	0.254
25	0.112	8.37	88.31	3.33	0.254
30	0.114	8.19	88.42	3.38	0.255
40	0.115	7.39	89.27	3.34	0.254
50	0.111	10.06	87.37	2.57	0.255
60	0.120	7.68	88.75	3.57	0.247
80	0.115	7.45	89.65	2.91	0.253
100	0.122	9.04	87.93	3.03	0.250

Total P = 0.3208 m Total PET = 0.6367 m

Beginning with the optimized speed factors F_{RV} and F_{CHV}, we notice that an overland flow speed factor of 0.071 implies an overland flow speed of 0.075 m/s or 270 m/hr. It is difficult to determine whether this is a "reasonable" value. The factor F_{CHV} equal to 0.242 implies a channel flow speed of 0.25 m/s or 920 m/hr. Now the distance from the outlet of the Hwy 403 subcatchment to the hydrometric gauge is 3,605 m. At a speed of 0.25 m/s, this implies that a flood wave crest generated by this subcatchment should reach the gauge in less than four hours. This in turn implies that the peak will be observed in the third hour.

From looking at Table 6.1, there is an observed parameter interaction between *m* and *Ko*. These two parameters are related through *To* as *Ko* = *To/m*. In the table, when *m* increased, *Ko* decreased and vice versa. This is observed in the DEM pairs (10,15) and (20,25), where there is little variation between *Ko* in these pairs. Yet *Ko* is observed to increase dramatically with grid cell size. This is consistent with the

literature. The hydraulic conductivity in conjunction with *m* controls the size of the saturated source area. As the average value of topographic index increases, then this implies that more of the catchment is likely to contribute to saturation excess overland flow for a rain event. To compensate, *Ko* increases in order to reduce the increasing size of the source area.

The recession parameter *m* achieves values similar to those seen in Table 5.2, although the average in that table is slightly lower than the average of 0.0474. The urban area calibration parameter, *uacp* fluctuates between approximately 16% and 22% with an average value of 18.4% and a standard deviation of 2.2%. Tables 5.3 and 5.4 together imply that approximately 16% of the catchment is urbanized. The values in Table 6.1 imply that on average, 3% of the catchment is impervious. MacLaren (1990) uses a range of 20-40% to determine the amount of imperviousness in an urban area, depending on the type of urban land use. They too have indicated that roughly 20% of the catchment is urbanized, and therefore, the calibrated value of *uacp* provides a percentage of imperviousness that is just slightly less than that of the MacLaren study. There seems to be some parameter interaction between *uacp* and *m*. As *m* decreases, *uacp* increases and vice versa. This is not surprising as *m* governs the response time - if *m* is low then the response is high, and in-storm response increases resulting in higher peaks. This would tend to decrease *uacp* which responds identically to every rain event (i.e., the same area contributes to overland flow every time). This interaction is also observed in the variation in percentage of urban flow and baseflow to total flow. As *uacp* increases, the percentage of baseflow decreases because of the decrease in *m*. Table 6.2 shows that baseflow comprised almost 90% of the flow from this catchment during this rather dry period. Urban flow is sometimes more than double the saturation excess overland flow contribution. There is no distinct trend of these percentages with grid cell size. Consequently, the type information in Table 6.2 will be only seen again in Chapter 7. Notice that the value of Sr^0 is much lower than the assumed value of

Sr_{max}. This is compensating for the very high initial estimate of baseflow, Q_o, which implies that incoming precipitation is readily available for subsurface flow.

TOPURBAN's special appeal is its ability to compute urban flow and saturation excess overland flow. Tables 6.3 and 6.4 provide information on the maximum size of the variable source area that formed during this series. Table 6.3 shows the lower limit of topographic index when the catchment achieved maximum saturation. Table 6.4 shows the maximum variable source areas that were achieved. These source areas are shown in Figures 6.6 to 6.8 for each DEM size.

Table 6.3: Lower limit of saturated topographic index in the calibration period.

	10	**15**	**20**	**25**	**30**	**40**	**50**	**60**	**80**	**100**
Hwy	9.5	9.5	9.5	10.0	10.0	10.0	10.5	10.5	10.5	11.0
403	(28)	(82)	(82)	(78)	(78)	(82)	(78)	(82)	(82)	(47)
Maple	9.0	9.0	9.5	9.5	10.0	10.0	10.5	10.0	10.5	11.0
Lane	(82)	(82)	(82)	(82)	(78)	(82)	(78)	(82)	(82)	(47)
Golf	9.0	9.0	9.5	9.5	10.0	10.0	10.5	10.0	10.5	11.0
Links	(82)	(82)	(82)	(82)	(78)	(82)	(78)	(82)	(82)	(47)
Wilson	9.0	9.0	9.5	9.5	10.0	10.0	10.5	10.0	10.5	11.0
St.	(82)	(82)	(82)	(82)	(78)	(82)	(78)	(82)	(82)	(47)

Table 6.4: Maximum contributing area fraction in the calibration period.

DEM	Hwy 403	Maple Lane	Golf Links	Wilson St.	Total Fraction	Total (km^2)
10	0.15	0.17	0.07	0.10	0.13	0.97
15	0.17	0.20	0.08	0.10	0.14	1.11
20	0.22	0.16	0.07	0.10	0.16	1.20
25	0.13	0.17	0.06	0.09	0.12	0.91
30	0.18	0.12	0.07	0.06	0.12	0.93
40	0.19	0.19	0.05	0.08	0.15	1.09
50	0.14	0.03	0.06	0.05	0.09	0.72
60	0.14	0.13	0.03	0.10	0.11	0.82
80	0.17	0.15	0.02	0.04	0.12	0.86
100	0.15	0.01	0.09	0.05	0.10	0.69

In Table 6.3, the value in bracket indicates the time step at which the saturation occurred and the upper value is the lowest saturation limit of the topographic index value. This means that every column with a topographic index greater than or equal to the value shown in the table was saturated. Again, it is interesting to note that the lower limit increases with increasing grid cell size. This is not surprising in view of the fact that the higher DEM cell size causes a shift in topographic index to greater values. Notice that in Table 6.4 the actual amount of saturated area decreases with increasing grid cell size. This is a result of the reduced basin area, and not a manifestation of the calibration, as the second column from the right shows. Even though the average value of topographic index increases, overall basin area decreases thus creating a balance against the increase in saturation excess overland flow generated by the higher $\bar{\lambda}$.

6.2.3 TOPURBAN Performance with DEM size in the Calibration Period

The performance of the model with regard to DEM size will be investigated in this section in order to make a recommendation as to the most suitable size. Table 6.5 below lists the differences in observed and predicted hydrograph volumes. The error between the two hydrographs is minimal, and this shows an excellent ability for TOPURBAN to simulate observed runoff volume.

Table 6.5: Predicted and observed total volumes for the calibration period.

DEM	Observed Volume	Predicted Volume	% Difference
10	0.1136	0.1150	-1.23
15	0.1108	0.1145	-3.34
20	0.1139	0.1167	-2.46
25	0.1092	0.1120	-2.56
30	0.1134	0.1147	-1.15
40	0.1135	0.1150	-1.32
50	0.1113	0.1112	0.09
60	0.1200	0.1203	-0.25
80	0.1120	0.1150	-2.68
100	0.1216	0.1227	-0.90

Several other statistics were computed in order to compare TOPURBAN performances using data derived from different DEM sizes. These statistics were devised to test the model's performance during wet weather. This is important considering that the Nash E and the objective function F were computed over a long time series that had a predominance of low flows. The following statistics were computed for the peaks that occurred during each rain event in the series:

1. $\Sigma = \sum [Q_{obs}(t) - Q_{pred}(t)]^2$ for only the peak values during the rain event
2. $\Sigma 1 = \sum |Q_{obs}(t) - Q_{pred}(t)|$ for only the peak values during the rain event

3. D_{max} = maximum of ($\Sigma 1 \div Q_{obs}$ x100%)
4. D_{min} = minimum of ($\Sigma 1 \div Q_{obs}$ x100%)
5. D_{avg} = average of ($\Sigma 1 \div Q_{obs}$ x100%)
6. $\sigma^2 = \Sigma$/(No. of peaks).

Table 6.6 below lists the resulting values for the calibration period. For each element in the table, a smaller value implies a better performance by TOPURBAN. Each piece of information on its own is not extremely useful, but together the information can provide an indication of the best performance by the model.

Table 6.6: Statistics for each DEM size.

DEM	$\Sigma x10^{-8}$	$\Sigma 1 x10^{-3}$	D_{max}	D_{min}	D_{avg}	$\sigma^2 x10^{-9}$
10	5.384	1.116	60.111	5.07E-2	23.655	1.282
15	5.484	1.119	60.346	0.969	24.455	1.306
20	5.509	1.066	59.141	0.520	22.192	1.312
25	5.012	1.003	57.746	0.431	21.746	1.193
30	4.055	0.965	58.952	0.511	21.335	0.965
40	7.583	1.243	61.843	0.218	24.907	1.805
50	4.287	0.970	58.581	1.170	21.186	1.020
60	8.427	1.327	68.438	4.703	26.228	2.007
80	8.656	1.238	66.161	0.243	24.197	2.061
100	5.689	1.163	63.116	1.216	23.738	1.355

In the table above, the DEM with the lowest value in all these columns seems to be the 50 m DEM. The 50 m DEM also provided the best performance of TOPURBAN when predicting total volumes, as shown in Table 6.5. These statistics will be computed for every other calibration in this chapter, but the results will be placed in the Appendix. Table 6.7 below has the objective function and Nash E values.

Table 6.7: Optimization function and Nash E values for the calibration period.

DEM	Objective Function F	Nash E
10	5.0128E-7	0.725
15	4.9049E-7	0.717
20	4.7946E-7	0.739
25	4.4094E-7	0.739
30	4.5522E-7	0.750
40	5.1651E-7	0.717
50	4.3160E-7	0.754
60	5.8719E-7	0.711
80	5.3405E-7	0.699
100	5.3389E-7	0.745

Notice from the table above that when the objective function decreases or increases, the Nash E does not necessarily respond in the same manner. In TOPMODEL, $Q_{obs}(t)$ is converted to metres by dividing by the catchment area. As each catchment area differs, so too will the value of F or Nash E computed using $Q_{obs}(t)$. The 50 m DEM provides the lowest objective function value, and the Nash E indicates an efficiency around 73% overall.

6.3 The Importance of Incorporating the Urban Areas

This section attempts to discuss the effectiveness of the urban component of TOPURBAN. The urban runoff generating component of TOPURBAN was removed in order to produce a model version that was essentially identical to that of the original TOPMODEL except that the Muskingum-Cunge routing scheme and the Nelder-Mead Optimization method were in place. This version of TOPMODEL was used, along with a topographic distribution that does not explicitly account for urban areas. This model was calibrated on the 1991 data and Tables 6.8 and 6.9 show the

optimized parameters and the optimization results, respectively.

Table 6.8: Optimized values for TOPMODEL with no consideration given to urban land forms.

DEM	*m* (m)	*Ko* (m/hr)	Sr_{max} (m)
10	0.0560	6.514	0.0187
15	0.0579	6.266	0.0195
20	0.0614	9.392	0.0190
25	0.0565	10.193	0.0193
30	0.0495	13.305	0.0196
40	0.0557	17.032	0.0184
50	0.0576	16.601	0.0191
60	0.0576	17.548	0.0174
80	0.0537	21.873	0.0195
100	0.0558	26.353	0.0185

$F_{RV} = 0.1$ $F_{CHV} = 0.242$ $T_d = 1.0$ $Sr^0 = 0.0$

All the changes in all the parameters seen above are there to increase flow. The lower values of *Ko* decrease the transmissivity to increase overland flow. Sr_{max} decreases to allow for more runoff so less abstractions occur. The overland flow routing factor F_{RV} increases for less attenuation and Sr^0 decreases to as low a value as possible to lessen initial abstractions.

Table 6.9: Optimization function and Nash E for TOPMODEL simulation with the topographic index that does not incorporate urban areas land forms.

DEM	Objective Function F	Nash E
10	9.3341E-7	0.488
15	8.4317E-7	0.514
20	10.014E-7	0.455
25	9.0650E-7	0.462
30	9.6472E-7	0.470
40	9.6421E-7	0.471
50	10.819E-7	0.382
60	11.184E-7	0.450
80	9.7682E-7	0.450
100	12.655E-7	0.396

The table above shows the resulting Nash and Sutcliffe Efficiency values and are lower than those in Table 6.7 by almost 30% which is significant. Furthermore, the objective function differs by as much as 100%. Therefore, the runoff generating component in which approximately 3% of the catchment is consistently producing runoff for every rain event could not be reproduced by any parameter in the original version of TOPMODEL.

The next simulation uses TOPURBAN with the urban runoff component but again on the distribution that does not explicitly consider urban land forms. The parameter sets obtained in the calibration of Section 6.2 were used to obtain the following values of Nash E.

Table 6.10: Objective function and Nash E values for TOPURBAN simulation with the topographic index that does not incorporate urban areas land forms.

DEM	Objective Function F	Nash E
10	5.1323E-7	0.717
15	5.3111E-7	0.694
20	4.4813E-7	0.738
25	4.5451E-7	0.730
30	4.6537E-7	0.744
40	5.3102E-7	0.709
50	4.2900E-7	0.755
60	5.9656E-7	0.707
80	5.5562E-7	0.687
100	5.3296E-7	0.745

The objective function increases and the Nash E values decrease for every DEM size except the 50 m and 100 m DEMs. Attempting to re-calibrate for the 10 m, 50 m and 100 m DEMs produced no decrease in F and no increase in Nash E. With the exceptions of the 50 m and 100 m DEMs, the model is unable to provide as good a fit for the majority of applications as it would in the case where the distribution did explicitly consider urban areas. These two exceptions actually prove the rule. First of all, the marginal decrease in objective function values is rather insignificant and a 0.001 difference in Nash E is difficult to observe visually in the output. Second, both the 50 m and 100 m DEMs have the two highest ratios of subcatchment Hwy 403 area to total catchment area. This subcatchment has the lowest amount of urbanization and the highest average value of topographic index. This subcatchment generates a great proportion of total flow and since the distribution for this catchment would only change marginally when considering urban areas, there is a marginal change in the performance in the model. The 20 m DEM also has a high Hwy 403 area to catchment total area, and the difference in the model performance for that

DEM is also insignificant.

6.4 Local vs Global Minima

One of the major problems with optimization schemes is that they may lead to one of several possible local minima instead the global minimum. It is important to ensure that a global minimum is found in light of all the parameter interaction which was evident in the calibrations. Therefore, a series of simulations were conducted for each DEM size in which each of the three parameters *m*, *Ko*, and Sr_{max} were in turn increased by marginal amounts and the resulting value of objective function was recorded. The parameter *uacp* was excluded as it was not a very sensitive parameter, and this helped to save computation time. The value of *uacp* was set to that value shown in Table 6.1 for each DEM. The resulting objective function values were then plotted against the parameter values. The parameter space that was tested for the 10 m DEM is shown in Fig. 6.9 a). There is a concentration of values in a certain region because it was suspected to be the location of the global minimum. Figure 6.9 b) and Figure 6.10 a) and b) show various views of the objective function versus the calibration parameters. Note that *Ko* and *m* have in a sense been condensed into *To* for these plots by simply multiplying the two values together. The figures show that there is a definite global minimum in the vicinity of $To = 0.38$ and $Sr_{max} = 0.024$. These values correspond to those values in Table 6.1. Figure 6.11 a) and 6.11 b) show close up views of Figure 6.10 a) in order to pinpoint locations of possible local minima that were bypassed by the optimization scheme. An additional illustration of the tests for global minimum are shown in Figures 6.12 and 6.13. The parameter space tested for the 50 m DEM is shown in Figure 6.12 a) and the resulting objective functions values are plotted against the various parameters in Figures 6.12 b) and Figure 6.13. This DEM size was presented because of the general flatness of the objective function curve in the vicinity of the global minimum. All other DEM sizes produced curves similar to that for the 10 m DEM size, in which the global minimum

was obvious. Therefore, extra care was taken whenever a calibration on the 50 m DEM was being conducted by considering a very wide range of initial starting points for the Nelder-Mead optimization scheme.

6.5 Verification of TOPURBAN

The model was verified on data series constructed in the very dry year of 1988 and another data series in the very wet year of 1992. This section describes the verification results and the new parameters obtained after a recalibration of the model in each data series.

6.5.1 Verification During the Dry Year

The objective function and Nash E values that were obtained for the dry period using the parameters shown in Table 6.1 are presented below in Table 6.11.

Table 6.11: Objective function Nash E values for the dry verification period of 1988.

DEM	Objective Function F	Nash Efficiency
10	3.9586E-7	0.505
15	3.8606E-7	0.493
20	3.8615E-7	0.520
25	3.6548E-7	0.506
30	3.7511E-7	0.530
40	4.1352E-7	0.483
50	3.6975E-7	0.519
60	5.2341E-7	0.414
80	3.9478E-7	0.493
100	4.6201E-7	0.497

The model was recalibrated to obtain the following values.

Table 6.12: Calibrated parameters for the dry period.

DEM	*m* (m)	*Ko* (m/hr)	*uacp*	Sr_{max} (m)
10	0.0558	5.425	0.118	0.0269
15	0.0550	5.388	0.118	0.0290
20	0.0588	8.663	0.141	0.0273
25	0.0495	9.484	0.141	0.0298
30	0.0496	15.850	0.147	0.0261
40	0.053	15.274	0.125	0.0289
50	0.0629	22.072	0.150	0.0256
60	0.0461	28.746	0.163	0.0291
80	0.0524	25.232	0.129	0.0291
100	0.0556	42.294	0.158	0.0280

F_{RV} = 0.22 (836m/hr); F_{CHV} = 0.242 (920 m/hr); Total P = 0.1297 m; Total PET = 0.4427 m

Total	10	15	20	25	30	40	50	60	80	100
AET (m)	0.1039	0.1087	0.1046	0.1074	0.1003	0.1067	0.0993	0.1087	0.108	0.108

The parameter *Ko* has decreased, there is a slight increase in *m* and the size of the root zone Sr_{max} has increased slightly. The increase in Sr_{max} produces a greater abstraction, reducing the net rainfall available to raise the water table. The decrease in *Ko* together with the increase in *m* produce very similar transmissivities to the 1991 calibration period. But the increase in *m* produces a delayed response in the catchment. Furthermore, it was found that T_d had an influence in this case whereas it didn't in the 1991 calibration period. An increase in T_d by as much as 10 hours would increase the Nash E. This is not surprising in view of the fact that this in turn increases the delay in catchment response. The parameter Sr^0 did not seem to influence the results at all in this simulation and thus were left unchanged from their 1991 calibration period values. This series was characterized by a very long dry

period in the first 1100 hours. The series is shown in Figure 6.14 and the last 800 hours are shown in Figure 6.15. The initial long dry period essentially depletes the root zone store regardless of the initial value of Sr^0. The hydraulic conductivity decreases to provide a response that matches that of the actual hydrograph despite the fact that all stores have been expended over the first 1000 hours. The overland flow routing factor F_{RV} has a much higher calibrated value and this reduces attenuation. The following table lists the resulting objective function and Nash E values for the re-calibration on the dry period. This is followed by a table showing the predicted and observed runoff totals.

Table 6.13: Re-calibration objective function and Nash E values for the dry period.

DEM	Objective Function F	Nash E
10	2.6192E-7	0.673
15	2.6272E-7	0.655
20	2.5040E-7	0.689
25	2.4143E-7	0.674
30	2.4694E-7	0.691
40	2.7321E-7	0.658
50	2.3500E-7	0.694
60	3.0479E-7	0.659
80	2.7460E-7	0.648
100	2.7872E-7	0.700

Table 6.14: Dry Period predicted and observed hydrograph runoff volumes.

DEM	Observed Volume (m^3/m^2)	Predicted Volume (m^3/m^2)	% Diff.
10	0.0305	0.0376	-23.3
15	0.0298	0.0363	-21.8
20	0.0306	0.0378	-23.5
25	0.0294	0.0358	-21.8
30	0.0305	0.0374	-22.6
40	0.0305	0.0368	-20.7
50	0.0299	0.0376	-25.8
60	0.0322	0.0381	-18.3
80	0.0301	0.0365	-21.3
100	0.0327	0.0396	-21.1

The Nash E values produced by the calibration on the dry year were poor relative to those obtained during 1991. Furthermore, the observed and predicted hydrograph volumes show significant difference with the predicted volume being overestimated. The over-prediction in volume is primarily due to the poor simulation of the baseflow level. This verification period used rain data constructed from only one rain gauge. While processing this rain data, many errors were detected and this is one reason why the data series is only a little over 1800 hours long. This series will continue to be used in the analysis that follows but it is not considered a reliable data series.

6.5.2 Verification During the Wet Year

TOPURBAN was again verified using the 1991 calibrated parameters on the 1992 period which was one of the wettest years in decades. The following table shows the efficiency that resulted from this verification.

Table 6.15: Objective function and Nash E values for verification on the wet period of 1992.

DEM	Objective Function F	Nash E
10	4.0490E-6	0.466
15	3.9372E-6	0.454
20	3.3985E-6	0.555
25	3.7450E-6	0.466
30	3.2296E-6	0.573
40	3.1873E-6	0.579
50	4.1907E-5	0.424
60	4.9959E-5	0.409
80	3.2315E-5	0.562
100	3.9946E-5	0.541

The Nash E values are lower than those obtained for the calibration in 1991. The model was recalibrated with the following results.

Table 6.16: Calibrated parameters for the wet period of 1992.

DEM	*m* (m)	*Ko* (m/hr)	*uacp*	Sr_{max} (m)
10	0.0484	4.196	0.284	0.224
15	0.0520	3.596	0.259	0.244
20	0.0406	6.875	0.322	0.126
25	0.0436	6.766	0.306	0.265
30	0.0456	6.959	0.292	0.264
40	0.0592	5.294	0.223	0.252
50	0.0532	9.300	0.356	0.266
60	0.0542	6.121	0.256	0.265
80	0.0492	10.644	0.210	0.245
100	0.0510	17.456	0.354	0.317

$F_{RV} = 0.047$ (179 m/hr); $F_{CHV} = 0.242$ (920 m/hr); $Sr^0 = 0.04$ m; $T_d = 1$ hr/m;

Total P = 0.2721 m; Total PET = 0.2075 m .

Total	10	15	20	25	30	40	50	60	80	100
AET (m)	0.173	0.175	0.1874	0.1771	0.1769	0.1759	0.1771	0.1771	0.1752	0.1849

The hydraulic conductivity *Ko* decreases as do the values of *uacp*. This has the net effect of increasing peak flow levels. The recession parameter values are similar to those in the 1991 and 1988 year. The most interesting difference is in the value of Sr_{max} which is almost a full order of magnitude higher than in 1991 and 1988. What the reader should note is that in 1988 and 1991, the total PET exceeded the total precipitation. However, in 1992, the precipitation actually exceeded the total PET. In all three cases, the AET was always computed to some value lower than the PET, as it should be. In the rather short application period of 1992, the difference in PET and AET were much lower than in other years. To induce "similar" levels of abstraction on the precipitation of the 1992 period, the maximum value of the root zone had to be increased by an order of magnitude. When one computes the maximum value of abstraction from precipitation, per hour, for both periods: ([Total Precipitation - Sr_{max}] / Total number of hours in the period) we see that these values essentially work out to be the same (0.026 mm/hr in 1991 and 0.025 mm/hr in 1992). This is neccessary in order to duplicate the similar levels of flow observed in both years (0.03 mm/hr in 1991 and 0.035 mm/hr in 1992); hence the increase in optimized Sr_{max} for the 1992 period. This is an indication that TOPURBAN's root zone concept as a measure of overall abstraction is not the most suitable model for this catchment. The following table lists the resulting model efficiency for each DEM cell size.

Table 6.17: Re-calibrated objective function and Nash E values for the wet year.

DEM	Objective Function F	Nash E
10	1.2856E-6	0.830
15	1.1804E-6	0.836
20	1.2308E-6	0.839
25	1.1309E-6	0.839
30	1.1016E-6	0.854
40	1.3498E-6	0.822
50	1.0626E-6	0.854
60	1.6119E-6	0.809
80	1.4483E-6	0.804
100	1.4323E-6	0.835

The efficiencies shown are of the highest seen so far. The following table shows the observed and predicted volumes for this period.

Table 6.18: Observed and Predicted Hydrograph Volumes for the Wet Period.

DEM	Observed Volumes (m^3/m^2)	Predicted Volumes (m^3/m^2)	% Diff.
10	0.0750	0.0698	6.9
15	0.0731	0.0672	8.1
20	0.0752	0.0699	7.1
25	0.0721	0.0679	5.8
30	0.0749	0.0688	8.1
40	0.0749	0.0676	9.8
50	0.0735	0.0703	4.4
60	0.0792	0.0707	10.7
80	0.0740	0.0667	9.9
100	0.0803	0.0756	5.9

The error between simulated and observed volumes is fairly low. The predicted and observed hydrographs are shown in Figures 6.16 and 6.17, with the latter figure showing the last 800 hours. Although the model efficiency is very high and there is little error between predicted and observed volumes, the plots show that peak values of runoff are modeled poorly, but the baseflow level is modeled very well. The ability of the model to predict the baseflow rates are the primary reason for the model efficiency in this case.

6.5.2.1 Discussion of Sr_{max}

The explanation given for the differences in value of the parameter Sr_{max} in 1992 when compared to the values obtained in 1988 and 1991 is plausible, but it does not remove the difficulty of deciding what value to recommend. Mass balance calculations can reveal a great deal on whether or not a model is considering all the important elements of the hydrologic cycle. Since Sr_{max} represents a loss term in the hydrologic budget, a mass balance can be computed to determine the most suitable value of Sr_{max}. Therefore, seven years of average daily potential evapotranspiration, average daily rainfall and average daily flow were compiled to determine the mass balance of the catchment. The evapotranspiration was computed by TOPURBAN as

$$E_a^t = E_p^t(1 - Sr^t/Sr_{max}) \tag{6.1}$$

where t is the time step in days; Sr^t is the value of the root zone deficit per day for the entire catchment (m) (assumed to be equal to Sr_{max} at the start of the simulation); E_a^t is the actual evapotranspiration (m/day) and E_p^t is the potential evapotranspiration. The sequence of calculations is the same as that shown in Chapter 3 and Chapter 5 and was conducted for the entire catchment. The computed actual evapotranspiration was then subtracted from the daily precipitation to produce a net precipitation. The

observed daily cumulative flow (m) was plotted against the net cumulative precipitation (m) over a seven year period. This plot is shown in Figure 6.18 where Sr_{max} was set to 0.084 m. If the hydrologic budget is being modeled accurately, then the slope of the curve should equal to 1.0. The following results were obtained for various values of Sr_{max} and the values of R^2 for each of these curves is well over 0.9.

Table 6.19: Actual evapotranspiration over a 7 year period.

Sr_{max}	Slope	Total AE over 7 years (m)
0.084	1.09	4.065
0.01	0.67	2.661
0.001	0.45	0.874
0.1	1.16	4.175
0.5	1.92	5.021

The table implies that a value of Sr_{max} between 0.01 to 0.08 m is completely reasonable but a value upwards of 0.2 m does not provide a good long term mass balance. A daily mass balance was performed between April 1, 1992 and November 30, in 1992 using an Sr_{max} of 0.084 m. The reason for this was to check if the same value that provided a good mass balance over a seven year period would do as well over the typical period of application. The resulting slope was 0.646 with an R^2 = 0.93. This implies that the net input into the system exceeds the outflow. This is typical of such slopes in the summer and to simulate a perfect mass balance over just this time period would require an increase in Sr_{max} in order to decrease the effective input. To effectively capture the losses over a long time period, a value of approximately 0.09 m for Sr_{max} would be recommended.

6.6 The Effect of DEM Cell Size on Flow Prediction and Model Efficiency

To facilitate the decision on what DEM cell size should be used in this and other similar areas, several comparisons were made. In order to determine if there is any trend or asymptotic value that was being reached in the DEM sizes, several important parameters were plotted against DEM cell area in order to determine the stability or instability of this relationship. Figure 6.19 a) shows the Nash E values plotted against DEM cell area for all the calibrations and verifications in this chapter. The verifications have low Nash E values but the model can be calibrated to relatively high efficiencies with the dry year (1988) producing the poorest efficiencies, the moderately dry (1991) period providing the second best efficiencies and the very wet year (1992) providing the best efficiencies. Notice the oscillation of values in the first 3,000 m^2 of DEM cell area that eventually levels off to an asymptotic value. This can be seen in the next five plots of *Ko* versus cell area (Figure 6.19 b), *m* versus cell area (Figure 6.20 a); *ln(To)* versus cell area (Figure 6.20 b); *uacp* versus cell area (Figure 6.21 a) and catchment area versus cell area (Figure 6.21 b). There are rapid oscillations to a point and then an upward, downward or horizontal trend. It is possible that the oscillations observed in Figures 6.19 a) to 6.21 a) are direct consequences of the oscillations observed in Figure 6.21 b). These fluctuations were also observed by Bruneau et al. (1995) but they drew no conclusions as to the cause. It is has been shown that there is a direct relationship between the topographic index distribution and catchment area. There has also been shown a correlation between *Ko* and average value of topographic index. Therefore, it is quite likely, that the oscillations seen in Figure 6.19 b) are related to the oscillations in 6.21 b). Because there was observed parameter interaction between *Ko* and *m*, and between *m* and *uacp*, it is possible to infer a relationship between the oscillations in all of the Figures 6.19 a) to 6.21 a) to the oscillations in catchment area up to 2.5 ha or 3.6 ha. Figure 6.20 b) is interesting in that the transmissivities of 1992 are significantly different than in any other calibration. The lower transmissivities were produced from the

calibration in order to account for the large production in runoff. The oscillations in the smaller DEM cell areas shown in these graphs are a direct consequence of the interpolation errors present in the DEMs. From examining all these graphs, the DEM cell size of 50 m seems to be the point in which the oscillations are no longer present implying that this DEM is relatively free of interpolation errors.

Further analysis should be conducted to recommend the most suitable DEM size for use with TOPURBAN and possibly other hydrologic models that rely on DEMs. Statistics similar to the ones in Table 6.6 were computed for 1992 and 1988 and are shown in Appendix A30. By using the values in the last 5 columns of these tables, the value of the final optimized objective function, and the differences in predicted and observed volumes for each data series, 21 different comparisons could be made for each DEM size. The DEMs were then ranked in order of best to worst in each of the 21 values that were examined. The table below shows the total number of times a DEM was sorted at a certain rank.

Table 6.20: Number of statistics observed in a certain rank for each DEM size.

	Rank									
DEM	1	2	3	4	5	6	7	8	9	10
10	0	2	0	3	4	3	3	2	3	1
15	0	1	1	1	4	2	2	3	2	5
20	0	0	3	9	1	2	4	1	1	0
25	1	3	4	3	6	1	0	1	1	1
30	4	5	3	1	1	5	1	1	1	0
40	0	3	2	0	0	1	3	7	3	2
50	10	5	1	1	1	0	0	0	2	1
60	4	1	1	0	1	2	1	1	5	5
80	0	0	1	3	0	1	5	3	4	4
100	2	2	5	0	2	4	2	2	0	2

The table conclusively shows that the 50 m DEM out performs all other DEMs in terms of providing TOPURBAN with the best model fit to the observed data. Notice that the 40 m does poorly in comparison to its neighbours on either side.

6.7 Summary

This chapter applied TOPURBAN to the calibration period in 1991 in which it performed with an overall efficiency of roughly 73%. The parameters produced by this calibration were then verified on the very dry year of 1988 but the resulting Nash and Sutcliffe efficiencies were in the 50% range. The model was re-calibrated on these series to produce parameters that were not too dissimilar to those of 1991 and raised the efficiencies to roughly 65%. The verification of the calibrated 1991 parameters again on the 1992 data resulted in poor efficiencies. When the model was re-calibrated it produced very high efficiencies and the parameters were relatively similar to the 1991 and 1988 parameters with the exception of Sr_{max} in which this parameter was an order of magnitude larger than in the previous two calibrations. This could be attributed to the fact that this year was the one case in which the potential evapotranspiration was exceeded by the precipitation. Hence, the model increased the maximum size of the root zone in order to provide a suitable enough abstraction. In all, the wet year produced the best model efficiencies while the very dry year produced the worst. This is not enough evidence to conclude that TOPURBAN works best in wet conditions as the data in the 1988 period was considered unreliable.

In examining the performance of TOPURBAN with respect to DEM size, the 50 m DEM produced by far the best results in many ways. Statistics such as differences in predicted and observed volumes, objective function values and differences during peak flows proved that this DEM out performed all others. This may be attributed to the fact that it is the smallest resolution at which interpolation errors are suspected

to be non-existent. This DEM size will be passed on to the next section.

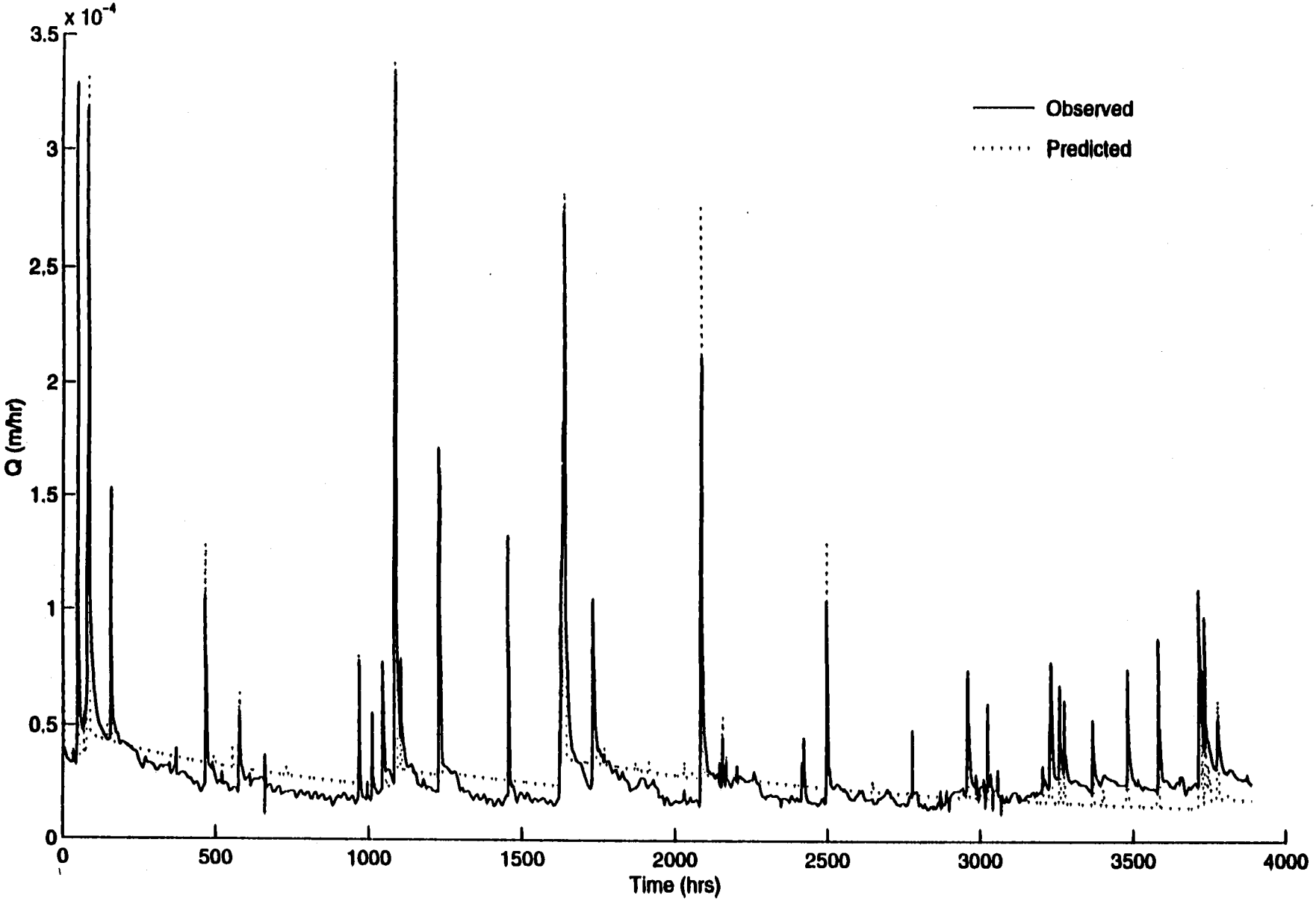

Figure 6.1: Observed vs. calibrated predicted flowrates for the 10 m DEM in 1991.

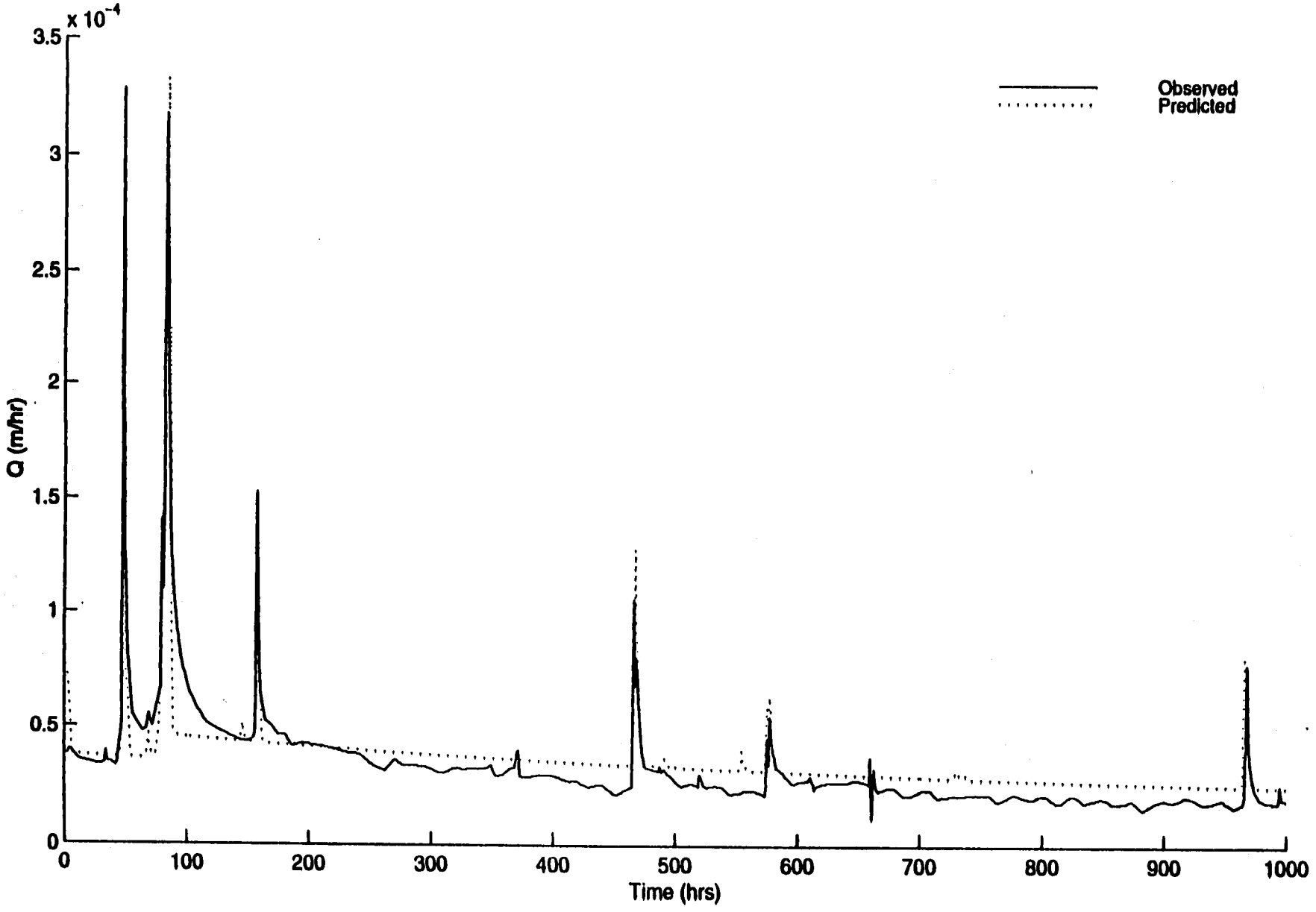

Figure 6.2: First 1000 hours of observed and predicted series for the 10 m DEM in 1991.

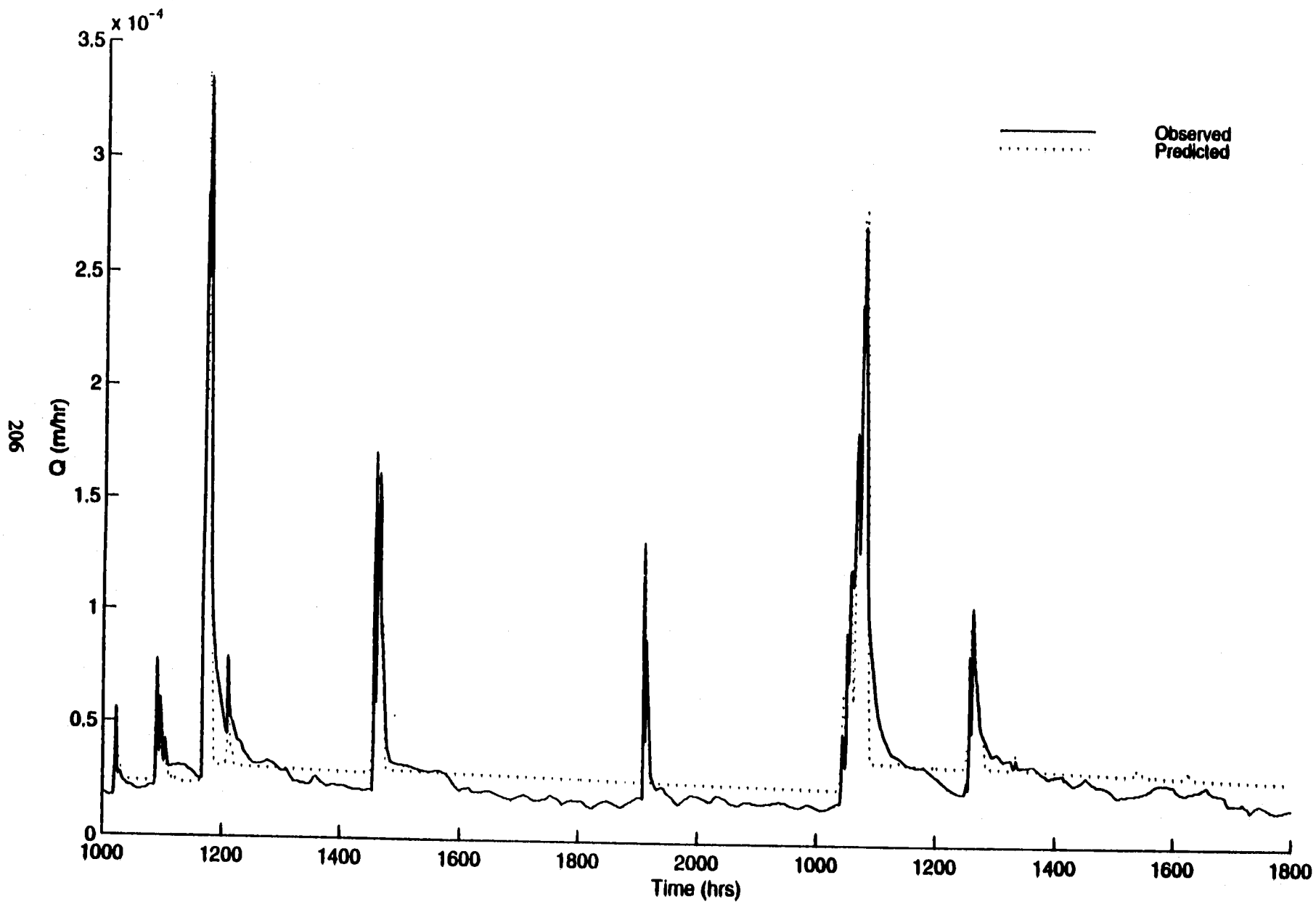

Figure 6.3: Hours 1000 - 1800 of observed and predicted series for the 10 m DEM in 1991.

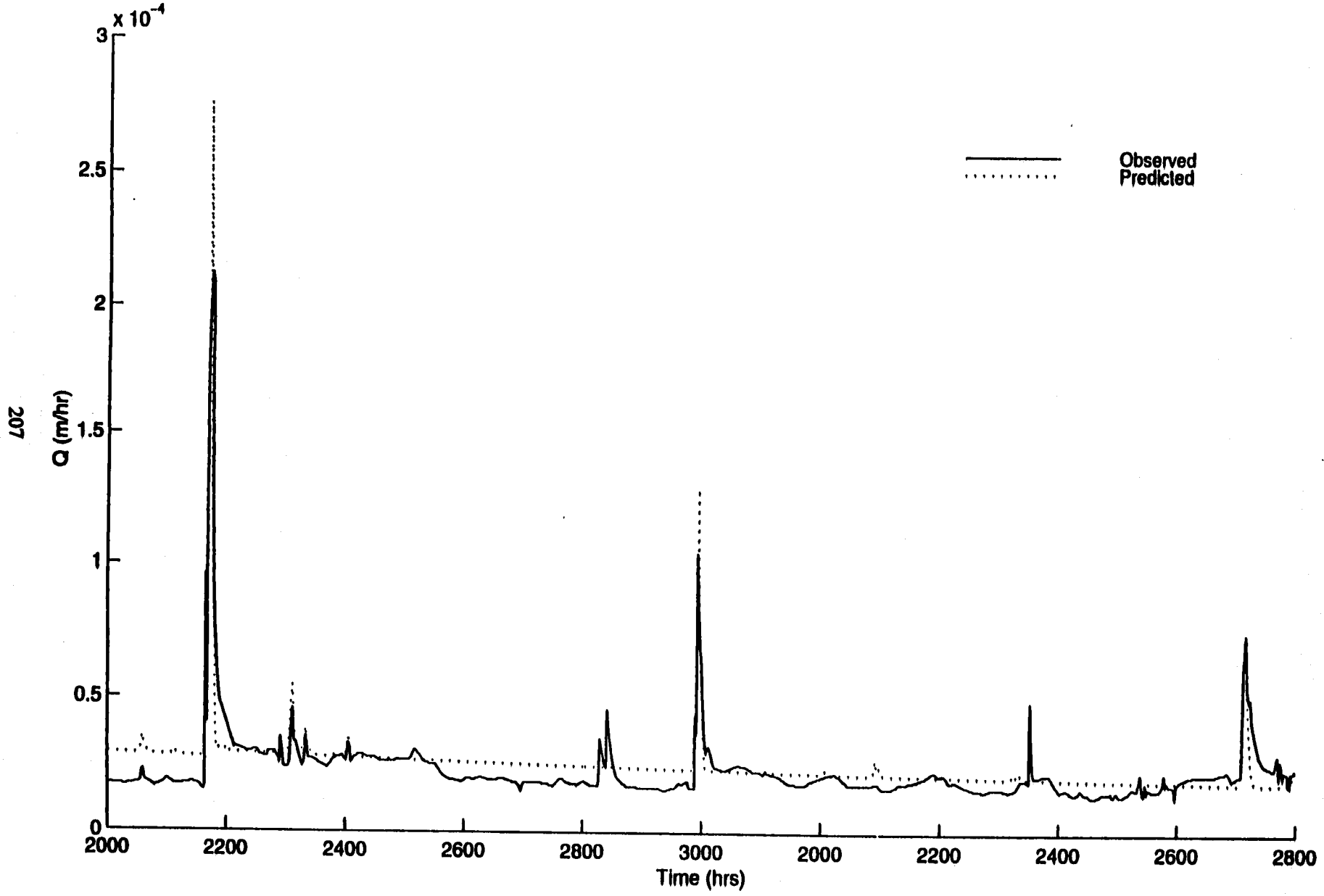

Figure 6.4: Hours 1800 - 2800 of observed and predicted series for the 10 m DEM in 1991.

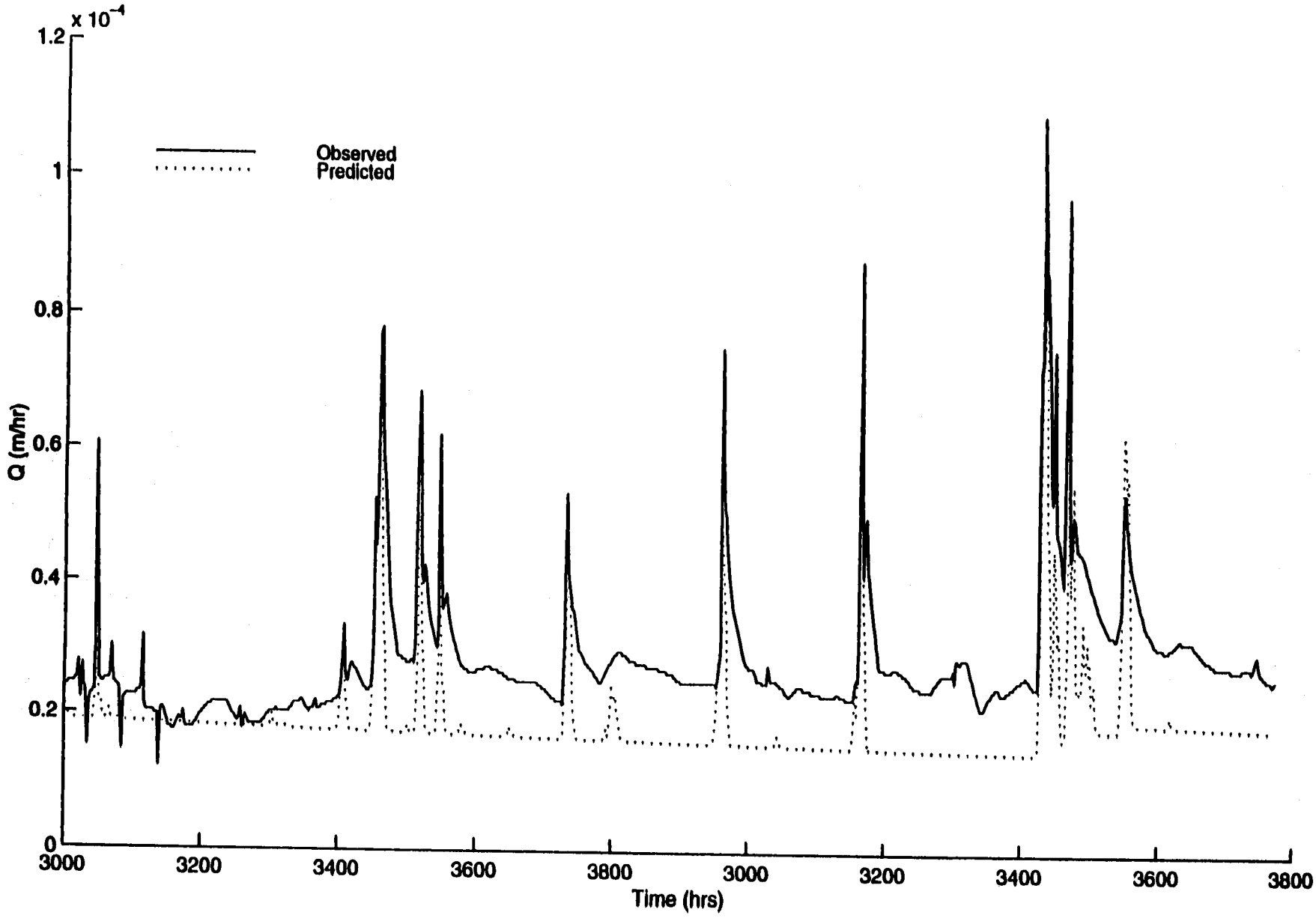

Figure 6.5: Hours 3000 - 3800 of observed and predicted series for the 10 m DEM in 1991.

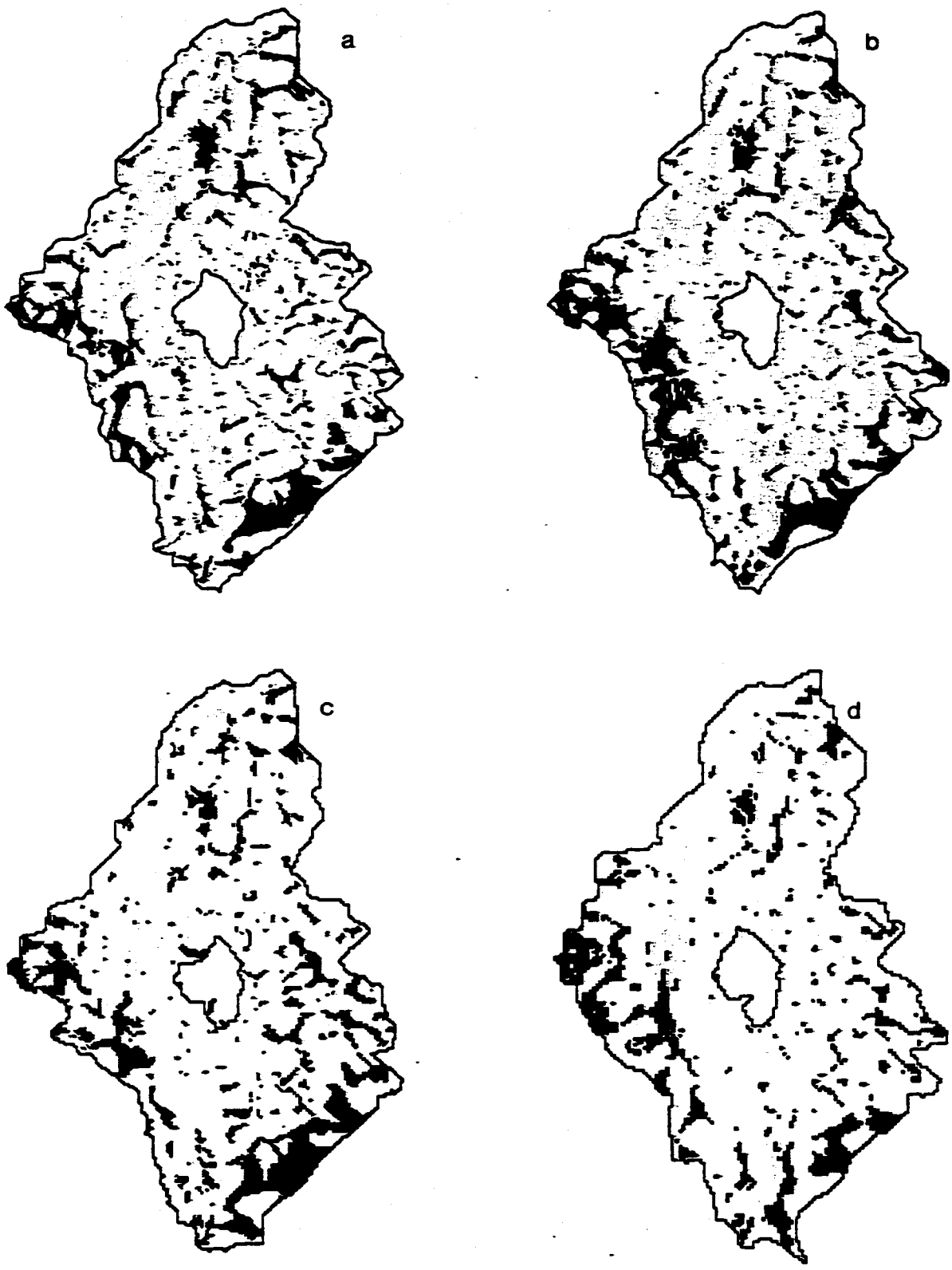

Figure 6.6: Spatial distribution of saturated areas (shown in dark grey) for a) 10 m DEM; b) 15 m DEM; c) 20 m DEM; and d) 25 m DEM.

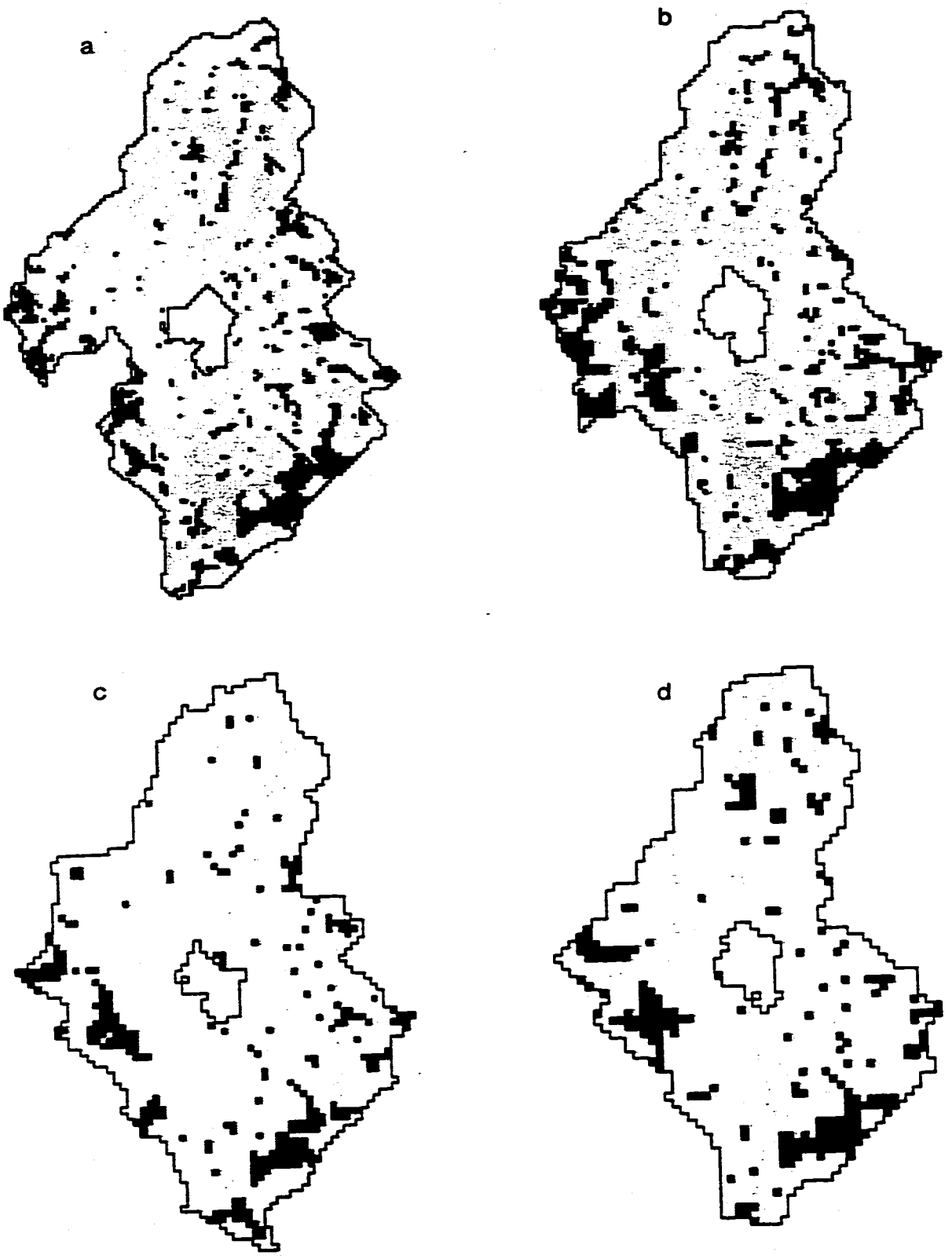

Figure 6.7: Spatial distribution of saturated areas (shown in dark grey) for a) 30 m DEM; b) 40 m DEM; c) 50 m DEM; and d) 60 m DEM.

Figure 6.8: Spatial distribution of saturated areas (shown in dark grey) for a) 80 m DEM; and b) 100 m DEM.

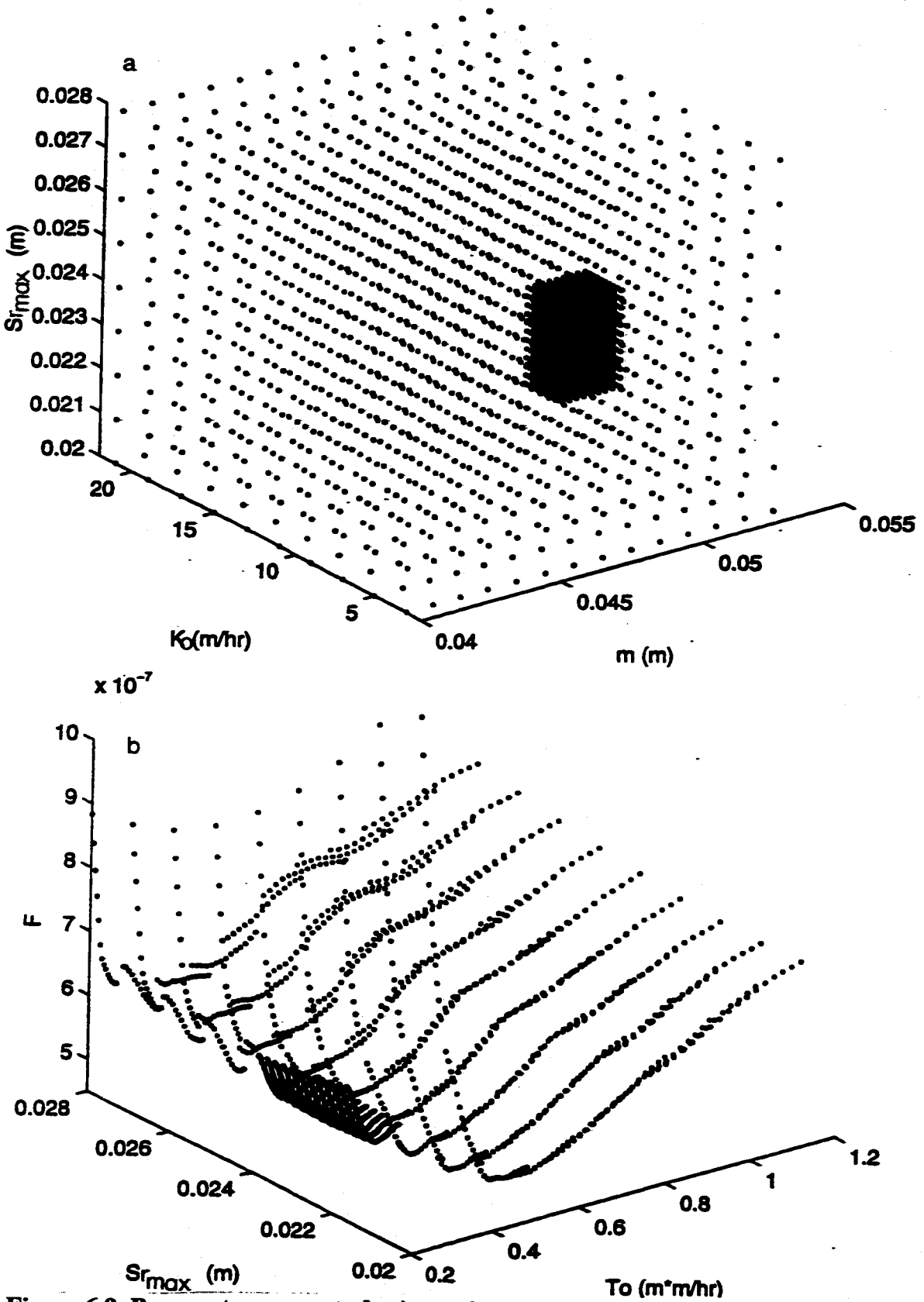

Figure 6.9: Parameter space study a) tested parameter space for 10 m DEM, and b) F vs. Sr_{max} and To .

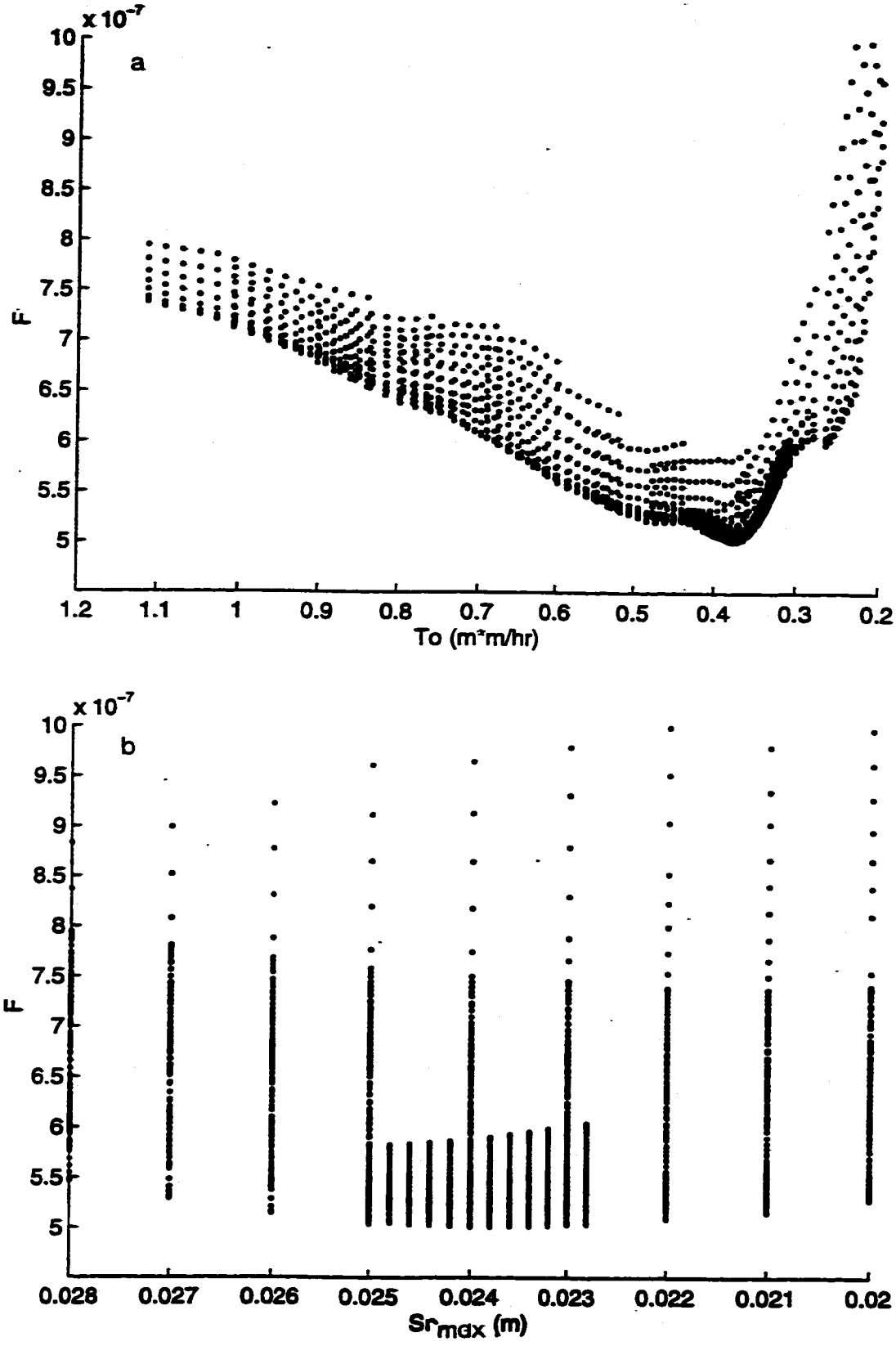

Figure 6.10: Parameter space study of 10 m DEM a) *F* vs. *To*, and b) *F* vs. Sr_{max}.

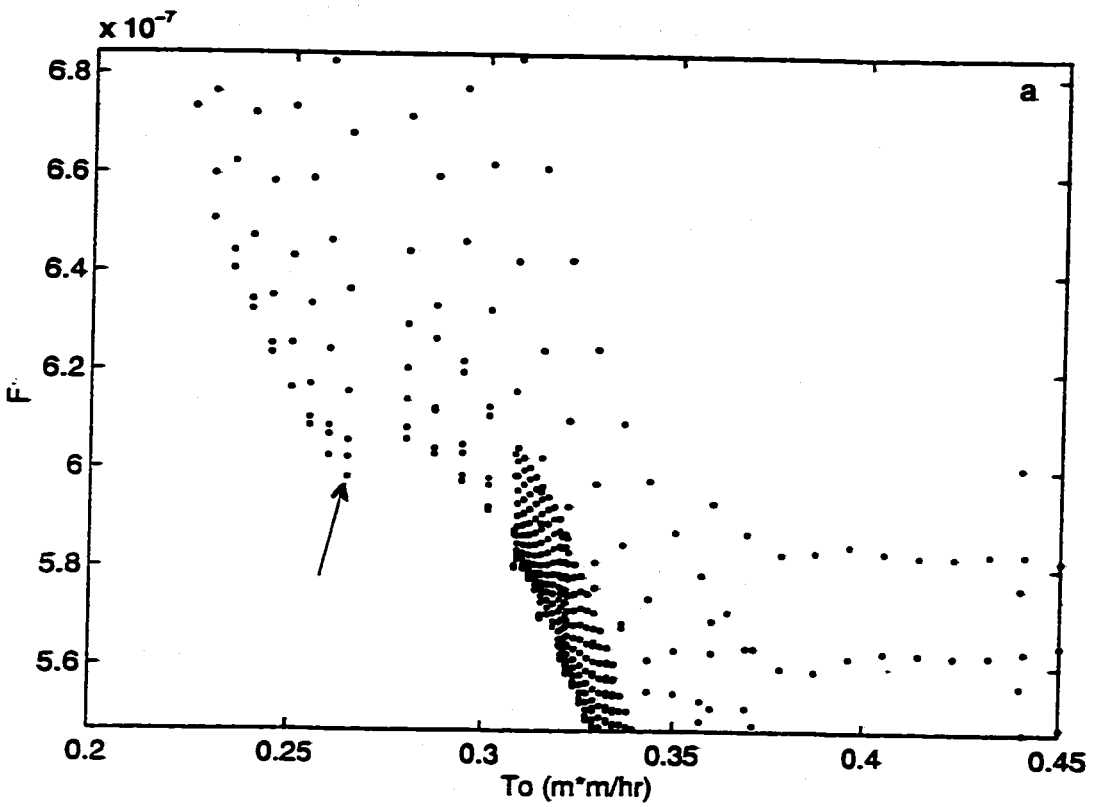

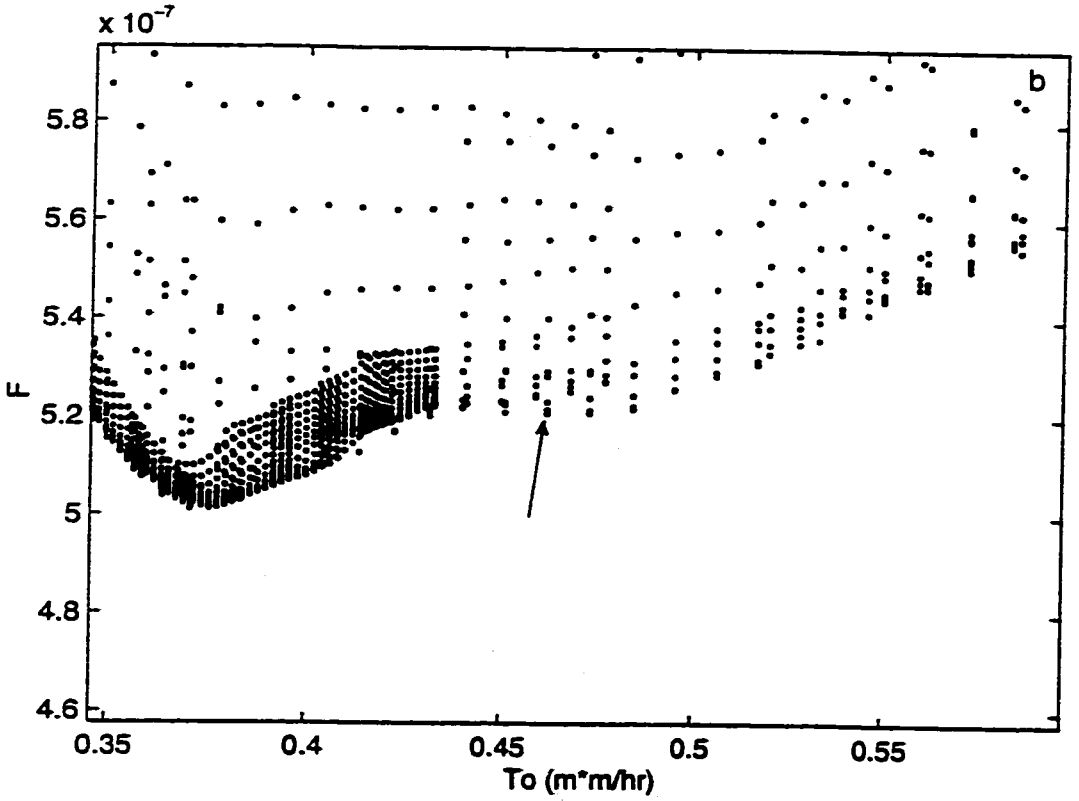

Figure 6.11: Parameter space study of 10 m DEM a) view 1 of *F* vs. *To*; b) view 2 of *F* vs *To*.

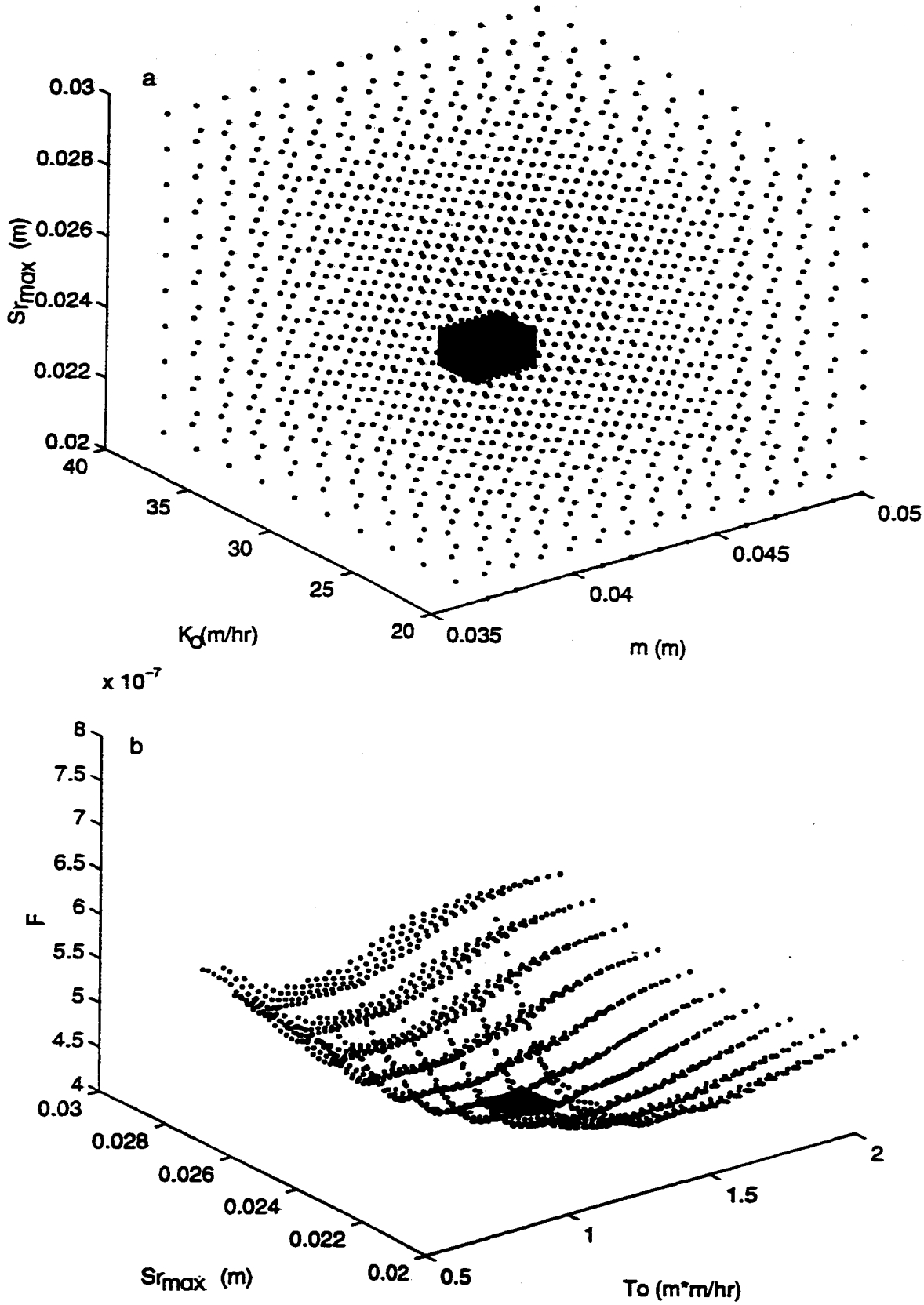

Figure 6.12: Parameter space study for a) tested parameter space for 50 m DEM, and b) *F* vs. Sr_{max} and *To*.

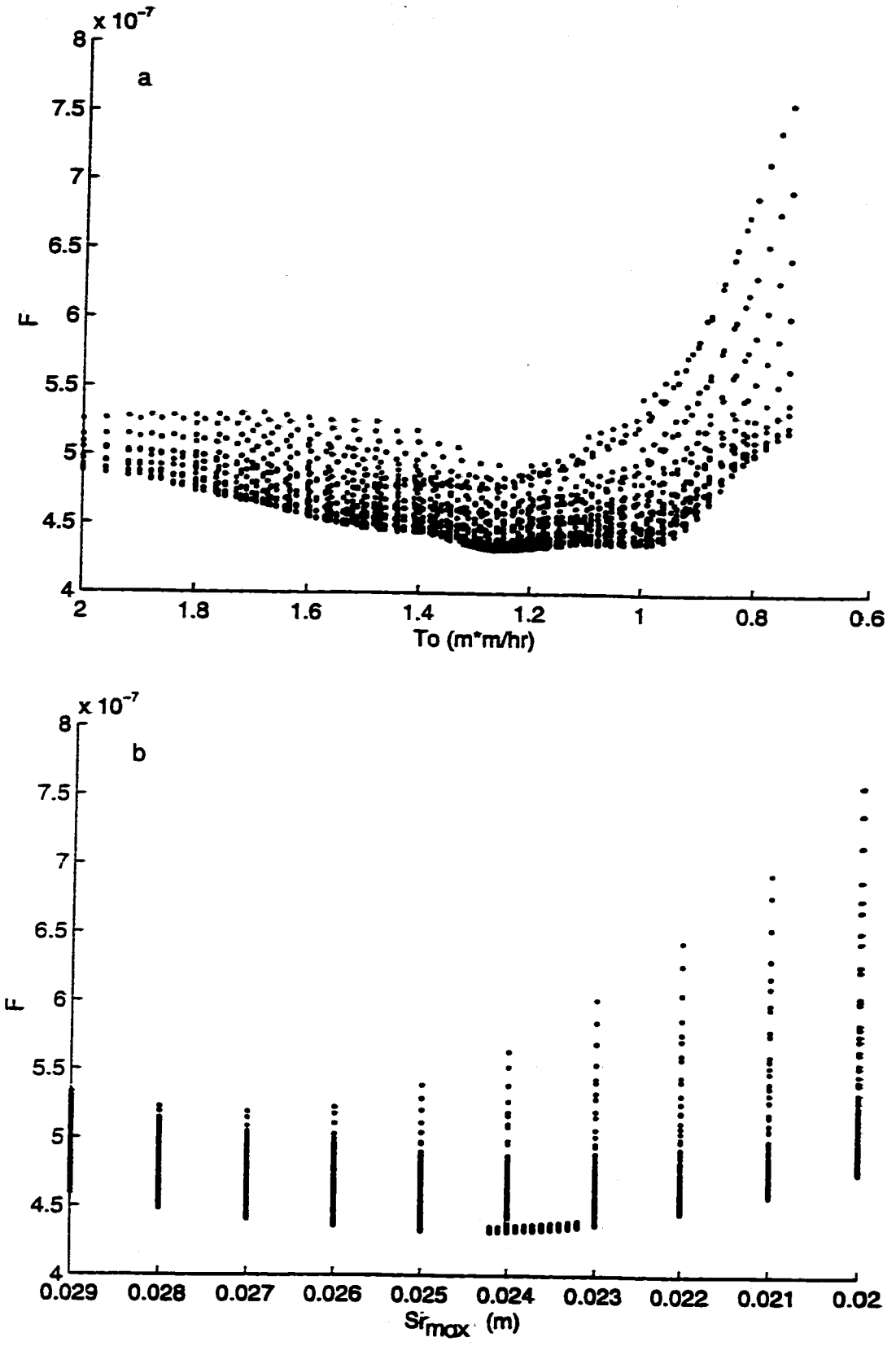

Figure 6.13: Parameter space study for 50 m DEM a) *F* vs. *To* and *F* vs. Sr_{max}.

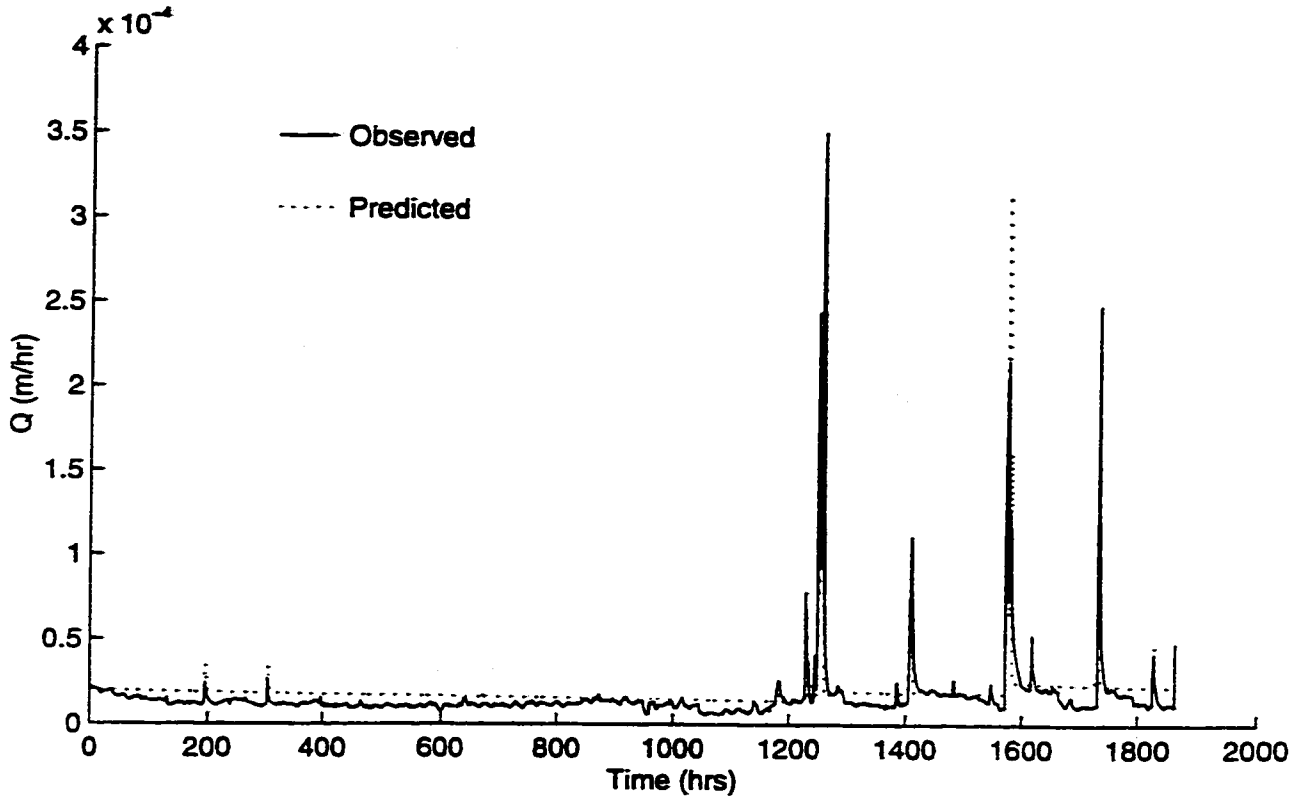

Figure 6.14: Observed vs. calibrated predicted flowrates for the 10 m DEM in 1988.

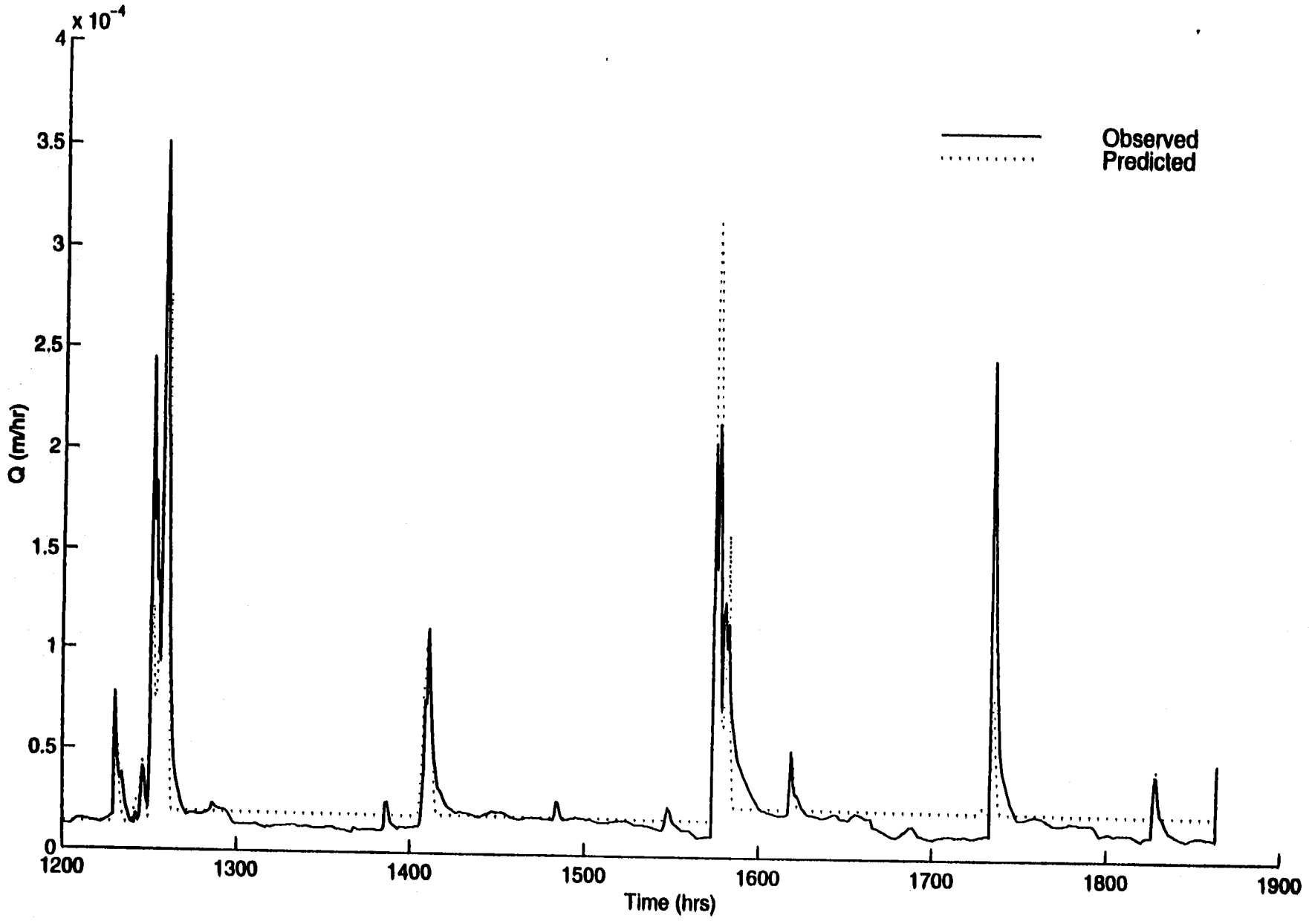

Figure 6.15: Hours 1200 - 1900 of observed and predicted series for the 10 m DEM in 1988.

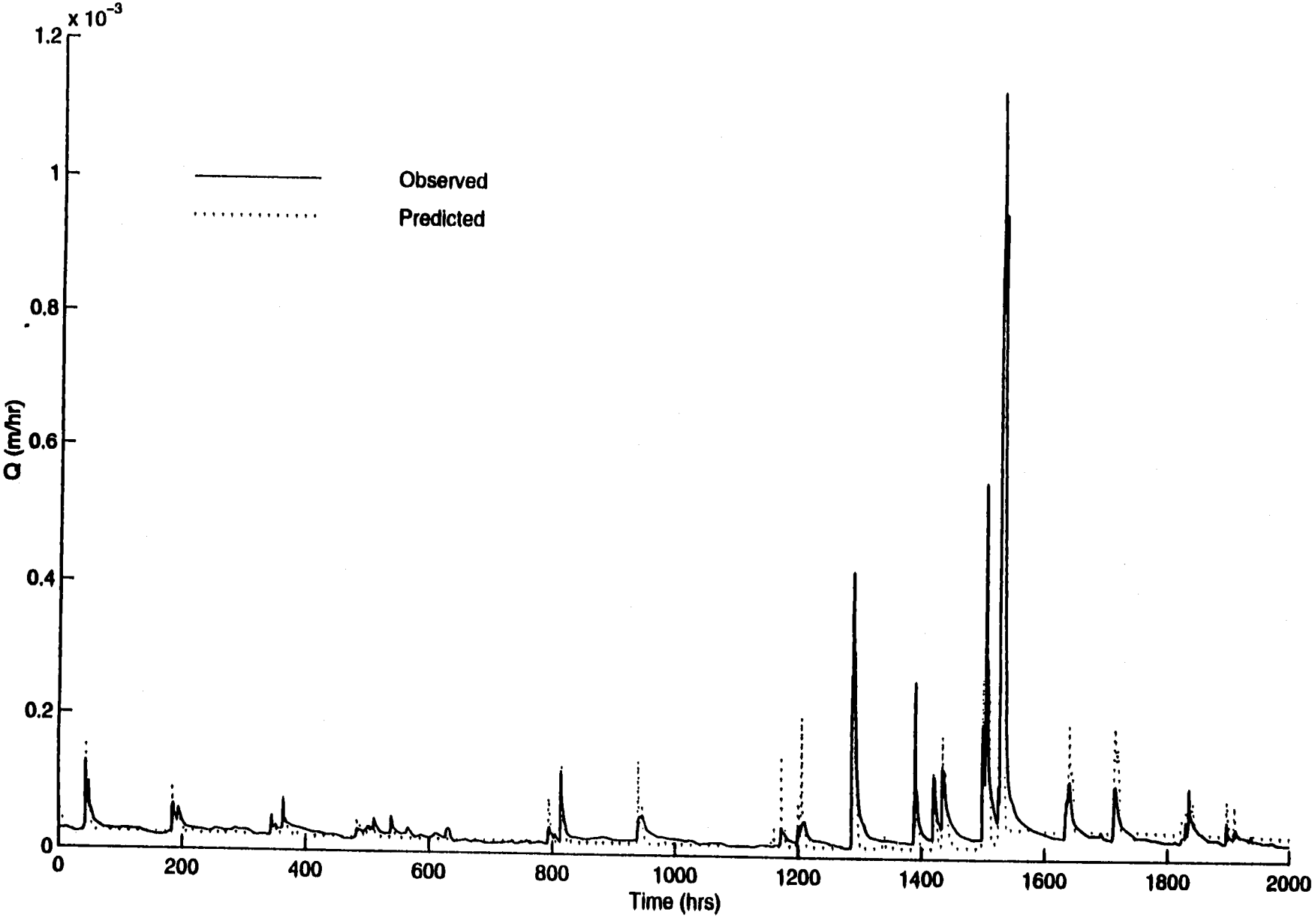

Figure 6.16: Observed vs. calibrated predicted flowrates for the 10 m DEM in 1992.

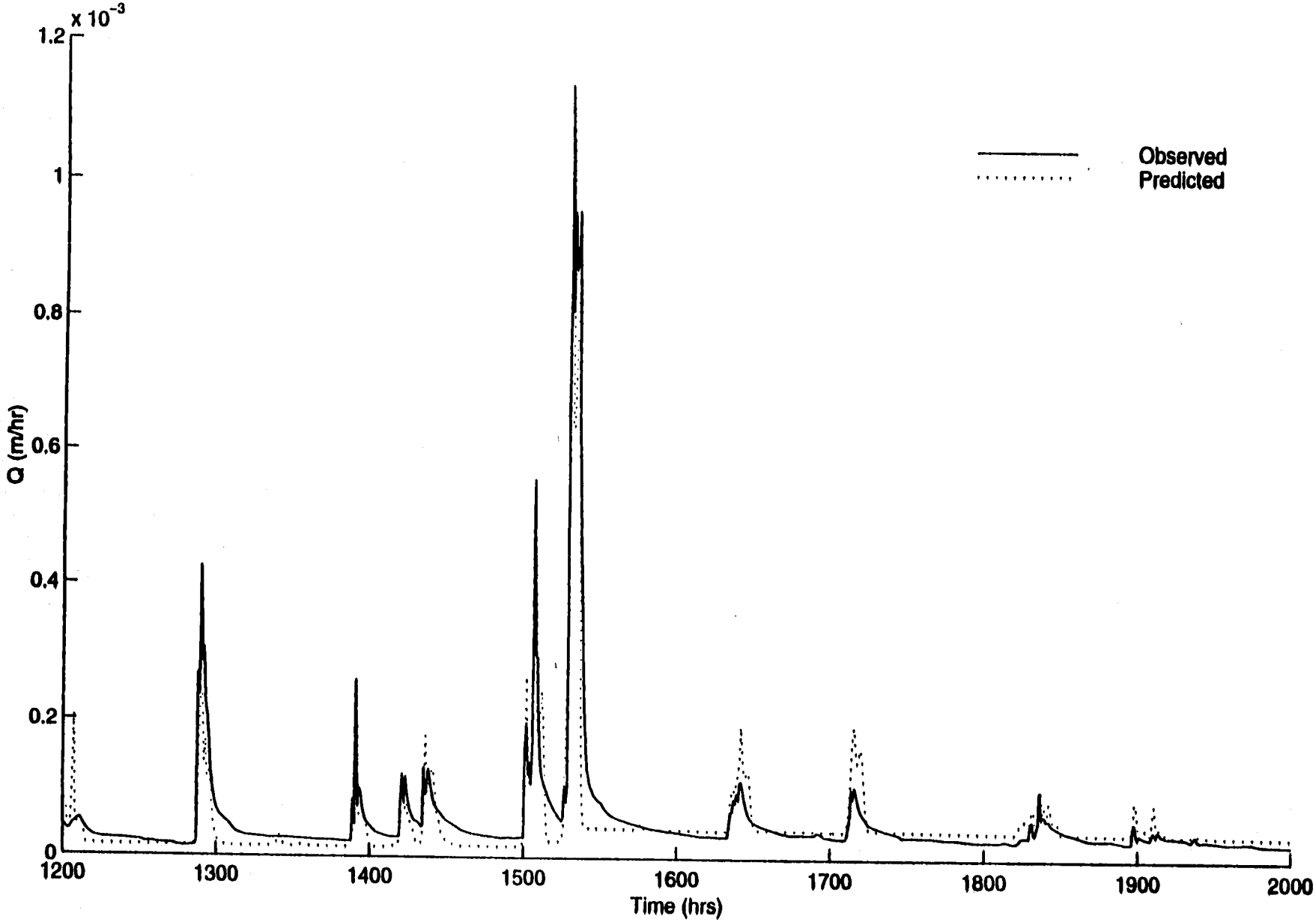

Figure 6.17: Last 800 hours of observed and predicted series for the 10 m DEM in 1992.

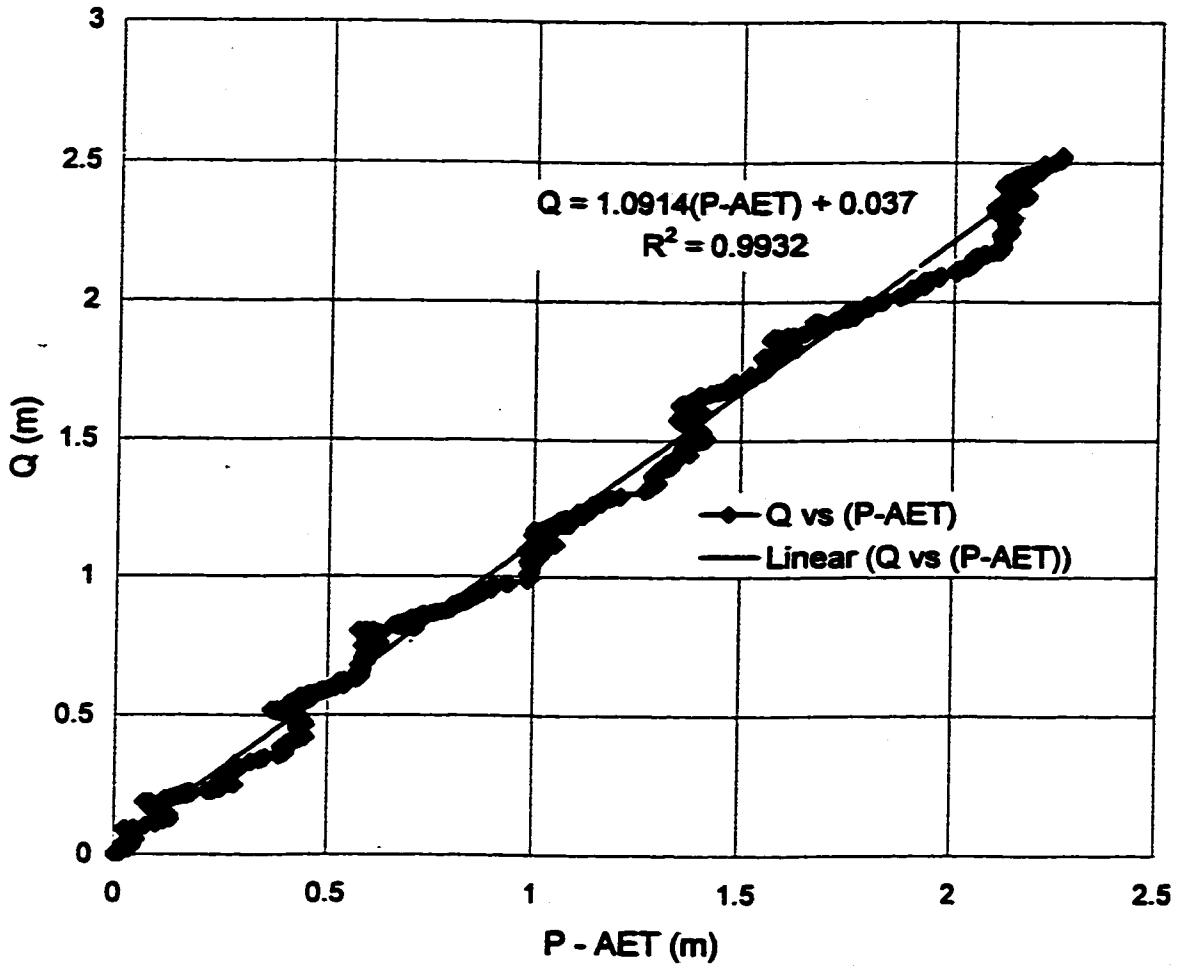

Figure 6.18: Seven year mass balance for Ancaster Creek.

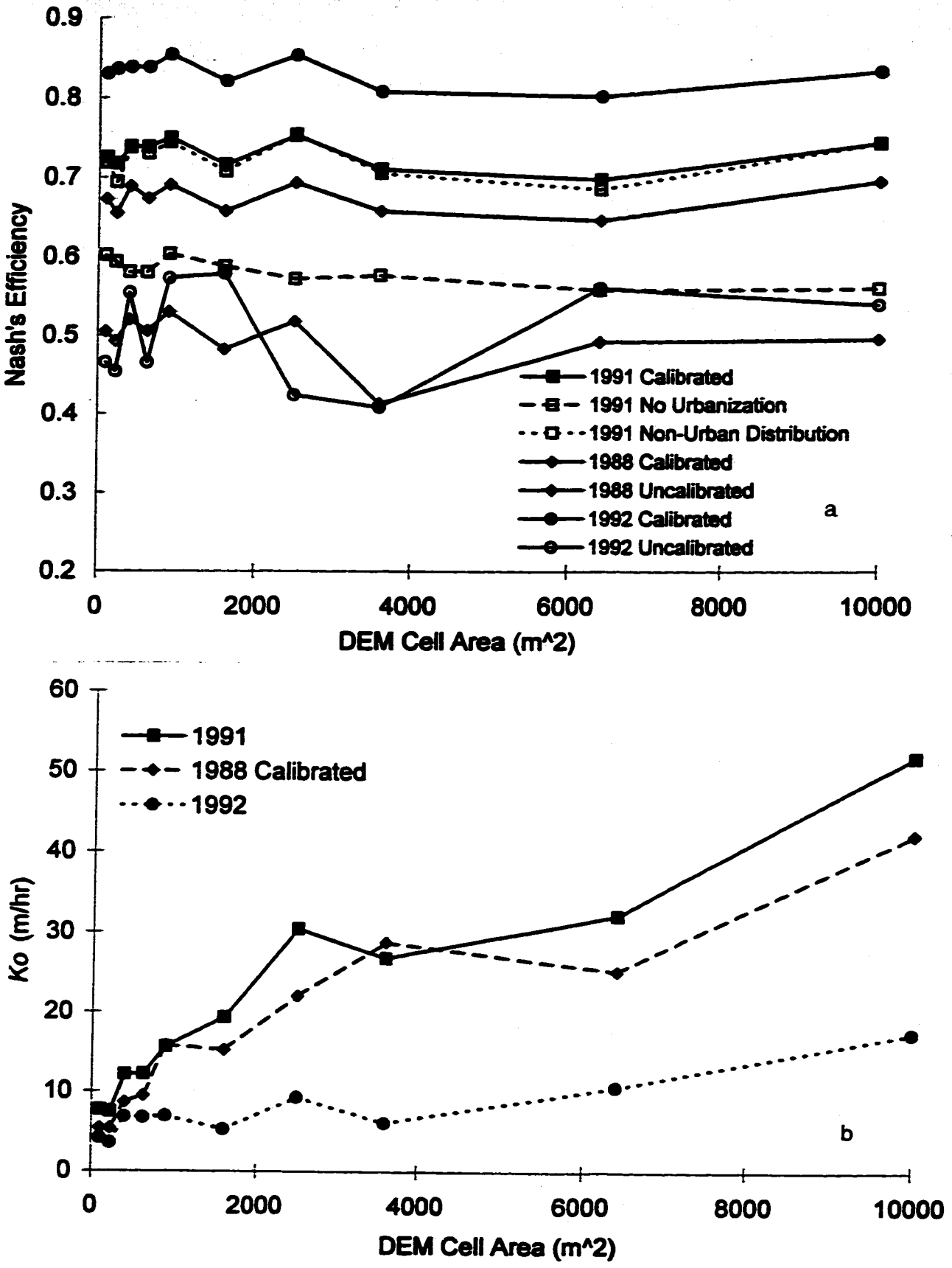

Figure 6.19: a) Nash E vs. DEM cell area and b) *Ko* versus DEM cell area.

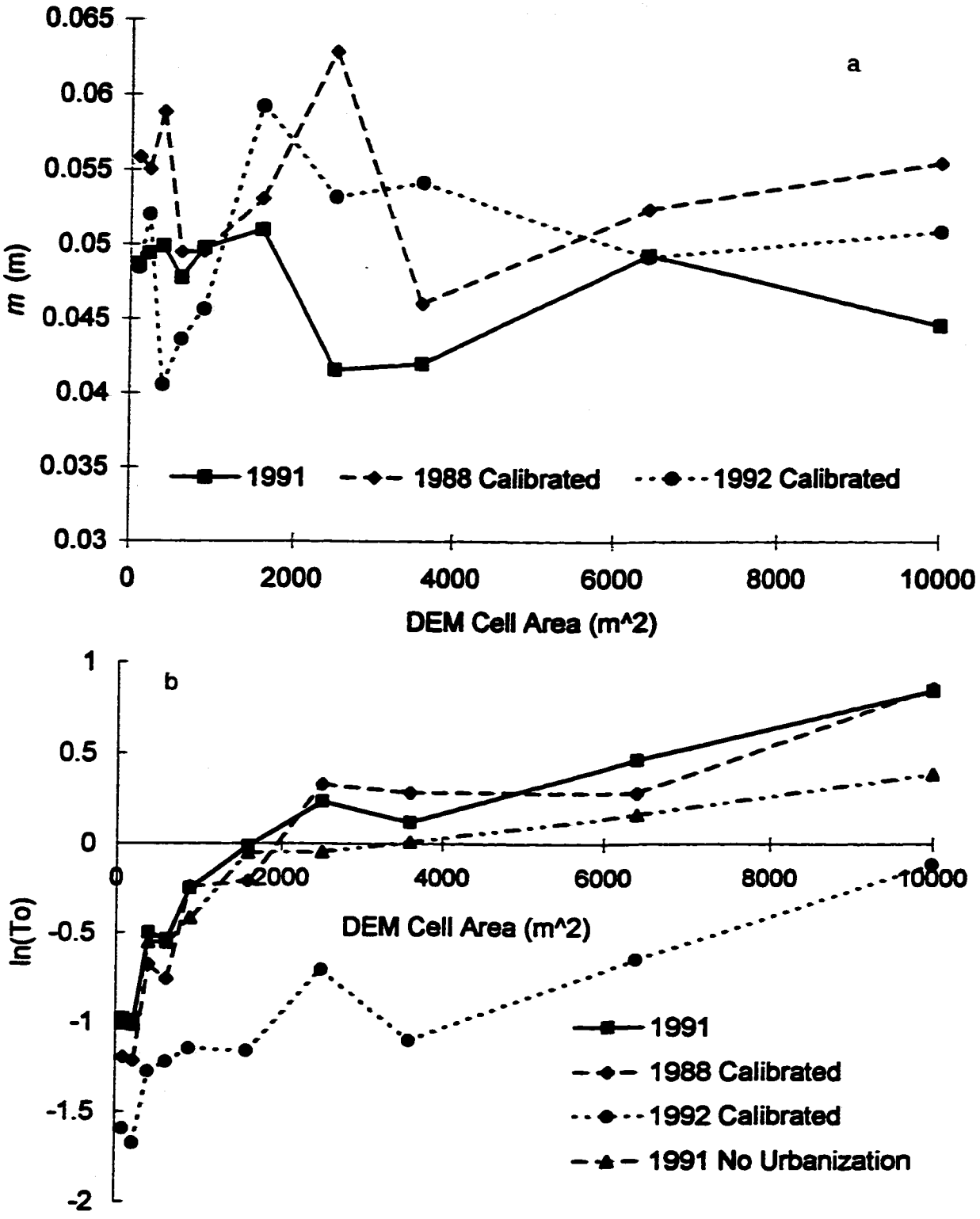

Figure 6.20: a) Recession *m* vs. DEM cell area and b) *ln(To)* versus DEM cell area.

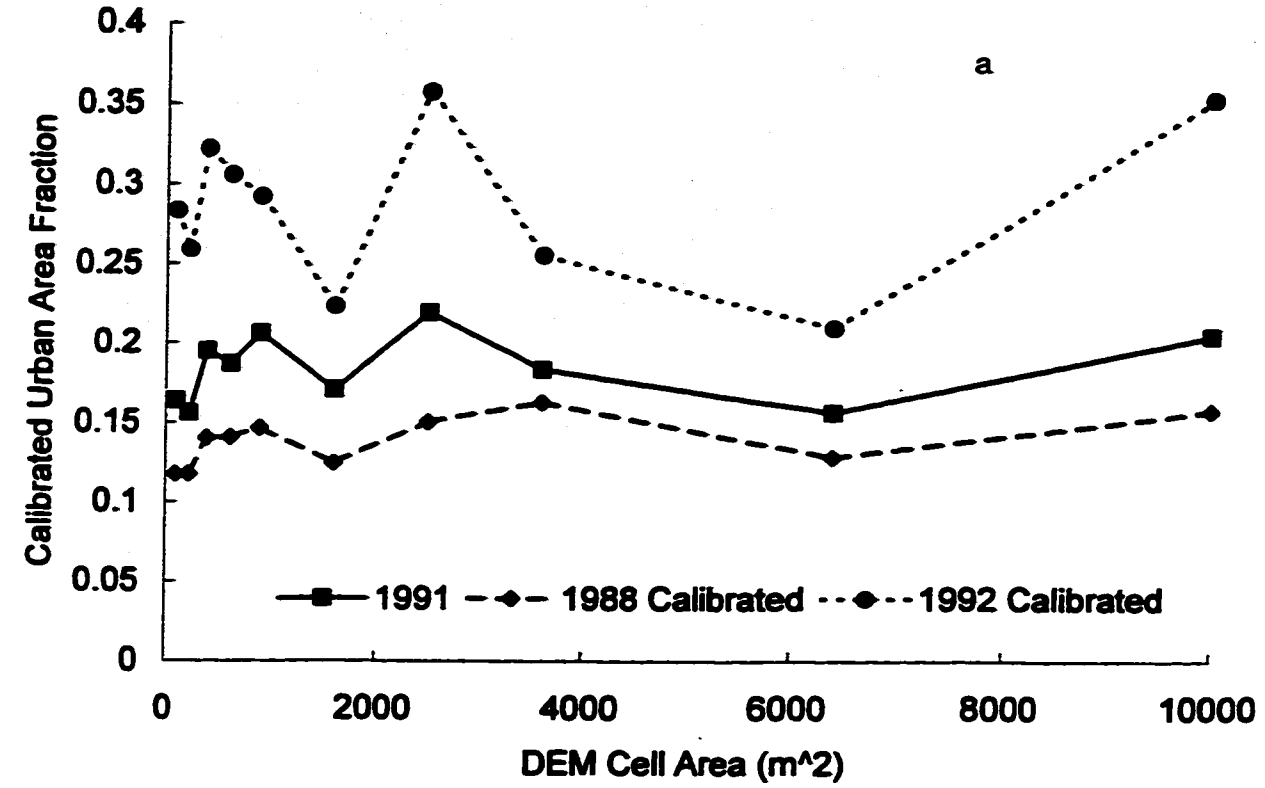

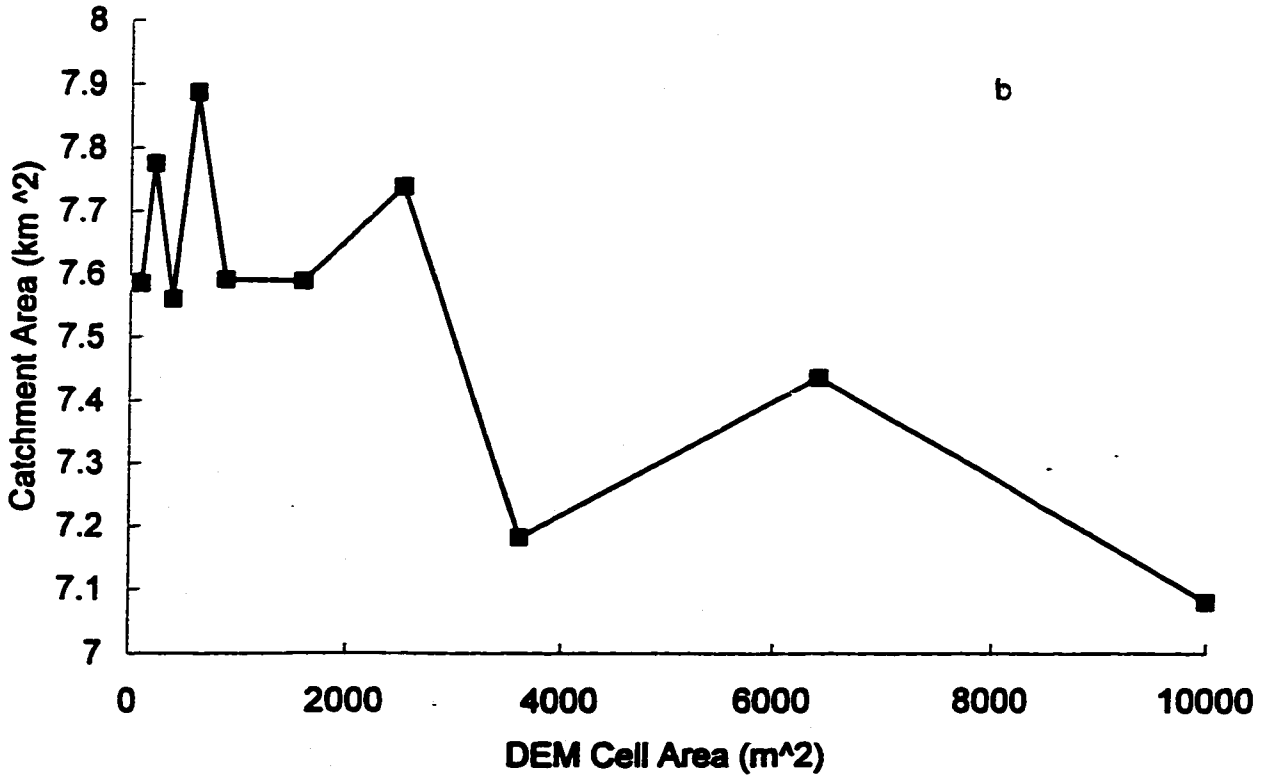

Figure 6.21:a) *uacp* versus DEM cell area and b) catchment area versus DEM cell area.

CHAPTER 7 FURTHER IMPROVEMENTS TO TOPURBAN

7.1 Introduction

This chapter looks at improving TOPURBAN and modifies it accordingly in Section 7.2 where TOPURBAN v. 2 is developed. All six series are used to test this model in comparison to the previous version. Water Survey of Canada statistics are also used to provide an indication of model fit. Section 7.3 introduces QualHYMO - a conventional model of hydrology for both continuous series and for single events. QualHYMO is "conventional" in that it assumes that runoff during rainfall is only generated through infiltration excess and it does so over the entire basin. This model will be compared to TOPURBAN v. 2 on the continuous series data and the single events.

7.2 Re-evaluation of the Role of Urban Flow in the Continuous Series

From examining Figures 6.2 to 6.5, and Figures 6.15 and 6.17, one can see that the recession following peak flows is not simulated well by TOPURBAN. Furthermore, the characteristic recession that is not modeled well occurs for all levels of flow. Figure 7.1 shows the division of flow between direct urban flow (as it was modeled by TOPURBAN), and the predicted saturation excess flow contribution in 1991. The baseflow contribution is not shown. The figure shows that saturation excess overland flow simply does not contribute to every rain event. Since TOPURBAN was devised so that the urban component contributes to runoff during all rain events, it is concluded that this characteristic recession is a function of the urban component. Storage ponds that collect urban runoff are part of a water resource management plan to mitigate the effects of urban development on runoff in the Ancaster area. While numerous small ponds exist, there are three major ones located at the foot of residential areas in the subcatchments of Maple Lane, Golf Links and Wilson St.

(Philips Planning and Engineering Ltd. 1987). It was noted earlier that TOPURBAN did not account for any storage effects in urban runoff. Therefore, an urban storage function that can produce the observed recession will be implemented in TOPURBAN. From the literature review in Section 2.2.5, both Viessman (1970) and Nash (1957) propose that a linear storage model is a perfectly suitable model of urban runoff. The following revisions to TOPURBAN were devised to model these linear storage effects.

7.2.1 TOPURBAN version 2

The test periods were set up to begin after a dry period. Based on this, assume that all the urban storage has been depleted at the start of the simulation. Define two new parameters: $S_{uQ}{}^{\tau}$ and $Q_{uS}{}^{\tau}$. The first parameter is the amount of water held in urban storage at time τ(m) and the second parameter is the outflow from storage (m/hr) at time τ. Therefore, initial conditions exist where,

$$S_{uQ}^{0} = 0 \tag{7.1}$$

$$Q_{uS}^{0} = 0 \tag{7.2}$$

The general equation of continuity is applied where,

$$S_{uQ}^{\tau+1} = S_{uQ}^{\tau} - Q_{uS}^{\tau} + I^{\tau} \tag{7.3}$$

and as before,

$$I^{\tau} = P^{\tau} A f_{UA} uacp \tag{7.4}$$

And the outflow is equal to,

$$Q_{uS}^{\tau} = Q_{uS}^{I} e^{-\tau/zk} \tag{7.5}$$

where zk is a recession constant (hrs). The equations above are applied at each time step τ, which is a counter that is set to 1 if $P^t \neq 0$ at time t, and increases continuously throughout time by 1 until the next rain event where it is set to 1 again. Therefore, $P^{\tau} = P^{(t-\tau-1)}$ and if $P^t \neq 0$ then,

$$Q_{uS}^{I} = \frac{S_{uQ}^{I}}{zk} \tag{7.6}$$

These equations were placed into the TOPURBAN code and the original mechanism for runoff generation in which,

$$Q_{urb}^{t} = P^{t} A f_{UA} uacp \tag{7.7}$$

was left in place so that the model could continue to simulate the peak flows accurately. Note that in this scenario, the maximum contribution to urban overland flow at any moment is,

$$max\, Q_{uS}^{t} = (1 + \frac{1}{zk}) P^{t} A f_{UA} uacp \tag{7.8}$$

These equations together create TOPURBAN version 2. Henceforth, the version of TOPURBAN described previously to Chapter 7 will be referred to as TOPURBAN v. 1.

TOPURBAN v. 2 was applied to each of the six data series available. Furthermore, TOPURBAN v. 1 was applied to the periods in 1989, 1990 and 1993 which were not included in the aggregation study of Chapter 6. The catchment characteristics used

were those derived from the 50 m DEM. The results are given in the next section.

7.2.2 Modeling with TOPURBAN version 2

The following results were obtained after calibrating TOPURBAN v.2 and where necessary, v. 1 on the data series. Figures 7.2 to 7.7 show the resulting predicted and observed discharges. Table 7.1 lists the resulting parameters and Table 7.2 provides the Nash and Sutcliffe Efficiencies that resulted from the calibration.

Table 7.1: TOPURBAN v. 1 and v. 2 calibrated parameters.

Year		*m* (m)	*Ko* (m/hr)	Sr_{max} (m)	*uacp*	*zk* (hrs)
1988	v. 1	0.063	22	0.026	0.15	
Dry	v. 2	0.044	28	0.033	0.12	8
1989	v. 1	0.063	16	0.035	0.35	
Med.	v. 2	0.065	17	0.072	0.32	21
1990	v. 1	0.068	20	0.049	0.22	
Wet	v. 2	0.053	37	0.060	0.21	20
1991	v. 1	0.042	30	0.024	0.22	
Dry	v. 2	0.040	30	0.027	0.19	21
1992	v. 1	0.053	9	0.266	0.36	
Wet	v. 2	0.052	9	0.294	0.25	13
1993	v. 1	0.060	9	0.031	0.24	
Med.	v. 2	0.090	4	0.093	0.28	21

Version 1 and 2 values of F_{RV} and Sr^0 are the same for all series.
All values of F_{CHV} are equal to 0.242, corresponding to a flow rate of 920m/hr.

	1989	1990	1993
F_{RV}	0.224 (851 m/hr)	0.400 (1520 m/hr)	0.047 (179 m/hr)
Sr^0 (m)	0.004	0.020	0.0001

Notice that in the table above, the parameters do not change greatly for *Ko* or *uacp*

between versions. There is however, some change in Sr_{max} for several of the years and there is significant change in m between versions for 1993. What is interesting about Table 7.1 is that for the calibration year 1991, very little changed between the parameters.

Table 7.2: Nash E values for TOPURBAN v. 1 and v. 2.

Year	Calibrated Nash E TOPURBAN v. 1	Calibrated Nash E TOPURBAN v. 2
1988 (Dry)	0.69	0.74
1989 (Med)	0.73	0.76
1990 (Wet)	0.74	0.82
1991 (Dry)	0.75	0.80
1992 (Wet)	0.85	0.87
1993 (Med)	0.84	0.89

In all cases, the Nash Efficiency increased. This is primarily due to the fact that the newer version is better able to model the recession limb of the hydrographs for individual rain events by incorporating the release from the urban storage. Figure 7.2 shows a much better prediction of recession for 1988 when compared visually to Figure 6.15 using version 1. The prediction of peak flows however, does not improve. In Figure 7.3, the recession is again modeled well for 1989, however TOPURBAN version 2 overestimates all low peaks and underestimates the highest peak in the series. The 1990, 1991 and 1992 data series in Figures 7.4, 7.5 and 7.6, respectively all show similar types of over and under predictions with a closely modeled recession and baseflow. The figure for 1993 however, shows a rather good prediction of both high and low flows with differences in peak flows being generally less than 10%.

7.2.2.1 Discussion

For every simulation with TOPURBAN version 2, values of *uacp* decreased with the exception of 1993. Furthermore, between the two versions, the values of Sr_{max} would increase marginally. This would imply a decrease in the peak flows as does a decrease in *uacp*. To compensate, *m* tended to decrease with the exception of 1989 and 1993. When *m* tended to increase, *Ko* tended to increase. But by and large, *Ko* tended to stay the same. The greater changes resulted in *m* and Sr_{max} which tend to govern low flows in their recession and inhibit flow during dry periods.

Figure 7.8 is an illustration of the flow dissected into its individual components for 1991. It clearly shows that saturation excess overland flow contributes to large flows and at points where the water table is likely to be high. Again, small storm flows are dominated by the urban area contributions. Equation (7.8) provides the maximum peak flow possible from the urban areas and this implies that the urban area fraction contributing to peak flow is 1.13*uacp* for the period in 1988, 1.08*uacp* for 1992, and approximately 1.05*uacp* for all the other periods. However, Equations (7.4) and (7.7) together imply that in version 2, the overall contribution of urban runoff volume is double what it would be in version 1. This means that one half of the urban area discharges overland flow directly to the creek and the other half routes overland flow through a linear storage. This in turn implies that in actuality, the average fraction of impervious surface area is double the value of *uacp*. Instead of the catchment being 3% impervious on average, it is actually 6% impervious. This is closer in value to the original assumption by MacLaren (1990) to assume an overall impervious surface area of roughly 8% in their watershed study of Spencer Creek.

The values in the period of 1992 also did not change a great deal except that the value of *uacp* was brought down to approximately 0.25 which is much closer in value to the other values of *uacp* for the other years. The increase in urban peak flow from

Equation (7.8) is marginal and is not as high as the values predicted by version 1. There is little correlation between wet and dry years. The parameter *m* seems to remain stable between 0.04 and 0.068 except for version 2 in 1993. It is difficult to assess the correct parameter for the hydraulic conductivity because, as one can see, there is a distinct correlation and parameter interaction between the values of hydraulic conductivity and the values of *uacp*. Notice that in 1989 and 1992 which are medium and wet years, respectively, the values of *uacp* are high relative to the other values in the table, yet the values of hydraulic conductivity are low. There seems to be some parameter interaction in these cases and that the hydraulic conductivity is compensating for reduced values in *uacp* and vice versa. Essentially, the smaller the values of *uacp,* the more likely a decrease is observed.

Table 7.3 Division of flow among runoff generating mechanisms.

Year	% Urban Flow	% Base Flow	% Sat. Excess Flow
1988 v.1	8.2	89.2	2.6
Dry v.2	13.5	84.4	2.1
1989 v.1	24.5	71.0	4.5
Avg. v.2	43.1	55.0	1.9
1990 v.1	12.4	85.2	2.4
Wet v.2	23.1	75.6	1.3
1991 v.1	18.2	76.9	4.9
Dry v.2	17.3	80.6	2.1
1992 v.1	22.1	66.8	11.1
Wet v.2	28.6	61.4	10.0
1993 v.1	10.4	79.4	10.2
Avg. v.2	22.8	69.8	7.4

In all cases for the above table, the percentage of urban volume increased by the

simple fact that TOPURBAN v.2 doubles the percentage of urban contribution and the saturation excess volume contribution decreased between versions for the same reason. There is a great deal of parameter interaction here, but one may draw the conclusion for the first four years, which might be characterized as together relatively dry, that the baseflow contributes approximately 70%, the urban contribution is approximately 25% and the saturation excess component is approximately 5%. The year of 1993 is an average year but may be considered as slightly on the wet side. Both 1993 and 1992 had saturation excess contributions that were anywhere from 7 to 11%. The very wet year of 1992 had one of the highest contributions of saturation excess overland flow which was expected. Very little changed in the modeling process between versions 1 and 2 for 1992 for the simple reason that the very wet year produced conditions that minimized the urban contribution. The values of *m*, *Ko* and Sr_{max} do not change significantly at all. The parameter *uacp* decreases but the decrease in urban flow is compensated by the effects of *zk*. When examining this table in conjunction with Table 7.1, the percentage of saturation excess contribution seems to be related to the hydraulic conductivity which is lower for higher values of saturation excess contribution.

Figures 7.9 and 7.10 are bubble plots of the triplets of parameters for 10 of the 12 simulations (1992 data were not included in these analyses). In these bubble plots, one parameter is plotted against another while a third variable (the one marked on the graph) is illustrated in the size of the bubble. Figure 7.10 shows the parameter *uacp* plotted against one of the other three major parameters and the next most sensitive parameter is shown as the bubble size. The three sub-figures show that there is little correlation between *uacp* and the other three most sensitive parameters as the R^2 values are very low. While some general trend is observed, it is weak, thus indicating little parameter interaction between *uacp* and the other major parameters. However, Figure 7.9 a), b) shows a high correlation between the variables *Ko* and Sr_{max} with *m*. There seems to be a low correlation between *Ko* and Sr_{max}. It is

believed that the inclusion of urban storage should not increase problems with parameter interaction. The point of these bubble plots is to indicate some parameter space that may arise between the four parameters with $zk = 20$. These plots should indicate quadruplets of possible parameters for different years.

7.2.3 Evaluating TOPURBAN version 1 and 2

Up until now, the model simulations have been assessed with the objective function and the Nash and Sutcliffe Efficiency. However, predicting peak and average daily flows is also an important assessment, and Water Survey of Canada Statistics can be used to evaluate the two models. These statistics include the minimum and maximum peak discharges, average daily flows, and average monthly flows. The two models were compared with regard to these statistics for all six series in the following six tables. The flows in columns four and five of the tables are shown as follows: flow @ predicted time index, followed by flow at observed time index in brackets. Version 1 values of percent differences are above version 2 values.

Consider Table 7.4 on the following page. The table states that in year 1988, the observed minimum hourly flowrate for the entire series was 0.012 cms. This occurred at the 1056th hour of the series. TOPURBAN version 1 predicted a minimum hourly flow of 0.030 cms to occur at the 1239th hour. The hourly flow predicted at the 1056th hour was 0.031 cms. Similarly, version 2 predicted the minimum hourly flowrate in the entire series as 0.027 cms at the 1228th hour and a flowrate of 0.028 cms was predicted for the 1056th hour. The percent difference between the observed minimum and the minimum hourly flow rate predicted by version 1 was 158%; and the percent difference between the observed minimum and the minimum predicted by version 2 is 133%.

Table 7.4: Minimum hourly flows (cms) and percent differences.

Year	Observed	Time Index	v. 1	v. 2	% Diff.
1988	0.012	1056	0.030 @1239 (0.031)	0.027@1228 (0.028)	158 133
1989	0.014	239	0.024 @ 448 (0.025)	0.024 @ 423 (0.025)	79
1990	0.031	1577	0.039 @ 2021 (0.044)	0.034 @ 2002 (0.039)	42 26
1991	0.024	661	0.029 @ 3711 (0.06)	0.027 @ 3711 (0.058)	150 142
1992	0.03	1279	0.032 @1411 (0.033)	0.033 @ 1386 (0.034)	10 13
1993	0.04	2561	0.035 @ 3755 (0.054)	0.038 @ 4099 (0.058)	35 45

In general, both models are unable to predict the minimum flows observed in all six series; however, both models perform best in 1992 which is the wettest year and when flows were generally high. It also performs poorest in the driest year of 1988. TOPURBAN v.2 performs better than v.1 but as one can see from the graphs, the predicted low never occurs at the observed low. The relatively large percent differences seen in the two dry years 1988 and 1991 is consistent with observations in the literature that TOPMODEL has difficulty modeling very low flows in dry periods and the development of TOPURBAN versions 1 and 2 do not address the modeling component that deals with abstraction over long periods of time.

Table 7.5: Maximum hourly flows (cms) and percent differences.

Year	Observed	Time Index	v.1	v.2	% Diff.
1988	0.735	1257	0.664 @ 1574 (0.449)	0.613@1574 (0.471)	-39 -36
1989	3.568	450	1.845	1.746	-48 -52
1990	1.54	2232	1.140	1.093	-26 -29
1991	0.702	1087	0.659 @ 1088 (0.503)	0.648 @ 1088 (0.548)	-28 -22
1992	2.385	1529	2.000 @ 1534 (1.702)	2.092 @ 1534 (1.630)	-29 -32
1993	2.882	946	2.677 @ 945 (2.589)	3.028	-10 5

In predicting maximum flows, both models are split in terms of performing better or worse than the other. The overall best performance is in 1993 where TOPURBAN version 2 is the better model. But in general both models seem to under-predict maximum flows by roughly 30%.

Table 7.6: Minimum daily flows (cms) for entire series.

Year	Discharge	Start Index	v.1	v.2
1988	0.014	1080	0.030 @ 1224	0.027 @ 1224
1989	0.016	264	0.024 @ 408	0.025
1990	0.035	1656	0.039 @ 1992	0.034 @ 1992
1991	0.032	2856	0.029 @ 3696	0.027 @ 3696
1992	0.032	1128	0.034 @ 1272	0.035 @ 1152
1993	0.044	2256	0.035 @ 3744	0.038 @ 4080

The observed discharges in the table above are the minimum daily average flow rate

in m^2/s. Again, minimum daily flow (the 24 hour period with the lowest observed flow) was poorly predicted and minimum values simply did not coincide between predicted and observed times. This is for the same reason as before, that both versions have difficulty predicting low baseflow levels. For this reason, no percent differences were computed because results would be similar between this table and Table 7.4. The percent difference between v.2 and the observed series for 1989 at index 264 was 56%

Table 7.7: Maximum daily flows (cms) for entire series and percent.

Year	Discharge	Start Hour	v.1	v.2	% Diff.
1988	0.228	1272	0.162 @ 1584	0.185	-19
1989	0.492	456	0.324	0.363	-34, -26
1990	0.356	2256	0.244	0.289	-25, -19
1991	0.256	1656	0.217	0.257	-15, 0.4
1992	0.714	1536	0.620	0.670	-13, -6
1993	1.13	960	0.839	0.95	-26, -16

Maximum observed daily flow was predicted much better in that the days of observed and predicted daily flow coincided often. TOPURBAN v. 2 performed better than version 1 in general for reasons that TOPURBAN v. 2 incorporated greater volumes of flow

Table 7.8: Monthly average flows (cms) and percent differences.

Year	June	July	Aug.	Sept.	Oct.
1988 Obs.	0.025	0.036			
v.1	0.038 (52%)	0.041 (14%)			
v.2	0.036 (44%)	0.040 (11%)			
1989			0.054	0.036	0.062
v.1			0.050 (-7%)	0.043 (19%)	0.051 (-18%)
v.2			0.058 (7%)	0.047 (31%)	0.060 (-3%)
1990	0.064	0.058	0.069	0.053	0.079
v.1	0.073 (14%)	0.057 (-2%)	0.060 (-13%)	0.059 (11%)	0.077 (-3%)
v.2	0.075 (15%)	0.059 (2%)	0.064 (-8%)	0.057 (8%)	0.080 (1%)
1991	0.055	0.068	0.057	0.045	0.063
v.1	0.067 (18%)	0.073 (7%)	0.066 (16%)	0.045	0.047 (-25%)
v.2	0.066 (20%)	0.077 (13%)	0.064 (12%)	0.043 (-4%)	0.043 (-32%)
1992	0.051	0.115			
v.1	0.048 (-6%)	0.108 (-6%)			
v.2	0.050 (-2%)	0.119 (3%)			
1993	0.152	0.065	0.052	0.063	0.080
v.1	0.126 (-17%)	0.092 (42%)	0.061 (17%)	0.051 (19%)	0.062 (-23%)
v.2	0.136 (-11%)	0.084 (30%)	0.063 (21%)	0.063	0.064 (-25%)

TOPURBAN v. 2 predicts higher flow rates than does TOPURBAN v. 1 and for this reason, depending on the degree of over or under-prediction, v. 2 will perform better than v. 1 and vice versa. There is no generality in better or worse performance with regard to the month, and a model's performance in a given month may depend on the rain events that occurred within that month and whether the model was under-predicting high rain events or over-predicting low ones. TOPURBAN version 2 does slightly better than version 1.

Table 7.9: Mean Period Flow (cms) and percent differences.

Year	Observed	v.1	% Diff.	v.2	% Diff.
1988	0.034	0.043	26	0.042	24
1989	0.048	0.051	6	0.053	10
1990	0.066	0.067	2	0.068	3
1991	0.061	0.061	0	0.061	0
1992	0.079	0.076	-4	0.082	-3
1993	0.083	0.078	-6	0.082	-1

In the table above, the two models are again split in their performance against each other. Version 2 not surprisingly does predict higher flow, so it tends to do well in 1992 and 1993. The observations in the previous 5 tables show that TOPURBAN v. 2 fares better in most cases than TOPURBAN v. 1 but does so in predicting larger flows. As TOPURBAN v. 2 has difficulty in predicting low flows, TOPURBAN v. 1 actually seems to fare equally well when computing average flows over longer periods of time.

7.2.2.3 Recommended Parameter Values

Variability between years does exist for some of the calibrated parameters; but there should be some recommendation of parameter values for future use. The two easiest parameters to select seem to be those dealing with the urban areas. The value of *zk* should be selected at roughly 20. The value of *uacp* does fluctuate between 0.12 and 0.36. Some of these low values can be explained by the low value of *zk* (particularly in the case of 1988 which would increase the peaks). But the average value of *uacp* is approximately 0.25. It was noticed that in Section 6.5.2.1, the rough calibration of Sr_{max} in a mass balance over a seven year period was 0.084 m. The lower values in the table will reflect the midsummer conditions and not conditions over the very long term. The very high value of Sr_{max} for 1992 is a manifestation of the

meteorological conditions of that year. While this is an important point when considering the impacts of climate change on watershed response, the fact remains that the data series of 1992 is a very short one and is not an indication of the long periods of time on which a model should be calibrated. Table 7.10 below is a list of the number of points in each data series and totals of input data. Both the very wet and very dry years are short in comparison to the other years. This was in part due to instrument malfunction that occurred frequently in both of these years. Three very long series of data exist for a wet (1990), dry (1991) and average year (1993) and the parameters from these years should be given greater weight than parameters in other years. Furthermore, Table 7.9 reveals that total runoff volumes were best predicted in those three years of the six available.

Table 7.10: Total precipitation, potential evapotranspiration and flows for each series.

Year	Total P (m)	Total ET (m)	Total Q (m)	No. of Points in Series
1988 (Dry)	0.1297	0.4382	0.0299	1863
1989 (Avg.)	0.2939	0.3708	0.0633	2794
1990 (Wet)	0.4158	0.5640	0.1161	3791
1991 (Dry)	0.3208	0.6367	0.1113	3888
1992 (Wet)	0.2721	0.2075	0.0735	2000
1993 (Avg.)	0.4089	0.6434	0.1607	4128

Version 2 is recommended over version 1 because of its general ability to predict higher flows. Table 7.11 lists recommended parameter values considered suitable for the Ancaster Creek Catchment. The parameters found in the median row are considered applicable to most meteorological conditions but two other sets have been added to account for extreme conditions: dry (parameters derived from the very dry period calibration of 1988) and wet (parameters based on the 1992 calibration during

very wet conditions).

Table 7.11: Recommended TOPURBAN version 2 parameters.

Condition	m (m)	Ko (m/hr)	Sr_{max} (m)	$uacp$*	v_{RV} (m/hr)
Dry	0.040	30	0.027	0.21	270
Median	0.090	4	0.093	0.28	180
Wet	0.052	9	0.294	0.25	180

*Note that $uacp = 0.25$ implies a percentage of imperviousness = 8%
$zk = 21$
$v_{CHV} = 920$ m/hr
$Sr^0 \approx 0.0$ m

Each row in Table 7.11 should be considered a ***parameter set*** and each parameter in a set does not hold very significant physical meaning when considered alone. Therefore, caution should be exercised when attempting to institute a value different from the set without regard to the other parameter values in the set.

There are a handful of other dissertation studies that used TOPMODEL concepts. The authors were also forced to make revisions to the model in order to account for some specific watershed quality. The following differences in Nash and Sutcliffe Efficiencies were observed before and after their revisions.

Table 7.12: Comparison of Model Enhancements.

Dissertation Author	Nash E before model revision	Nash E after model revision
Lamb (1996)	0.89 (900 hours)	0.91
Chairat (1993)	< 0.0 (4 events ~ 100 to 175 hrs)	0.49, 0.69, 0.76, 0.77
Quinn (1991)	0.0 (1000 hours)	0.87
Valeo (1998)	0.75 (3888 hours)	0.80

The revision made by Lamb (1996) involved modeling baseflow recession by two curves at different times instead of just one. The model was applied over a rather short time period and only a 0.02 difference in Nash E resulted. Chairat modified TOPMODEL to incorporate agricultural tile drainage, but it is the opinion of this author that Chairat (1993) should not have used TOPMODEL, because the simulated flow in the revised model was completely dominated by the tile drainage and there was very little contribution from TOPMODEL stores. Quinn (1991) made significant improvements to the model to account for very deep soils. The author feels that the application of TOPURBAN over the very long time series and the resulting high Nash E values for both model revisions are significant improvements and contributions to using TOPMODEL concepts in a wide variety of applications.

7.3 Calibration and Verification of a Traditional Hortonian Flow Model

Another way to evaluate TOPURBAN v. 2 is by comparing it to one of the more widely used conventional models in Southern Ontario. The model chosen for this comparison is QualHYMO. This model was chosen because it was used in the Spencer Creek Watershed study by MacLaren Plansearch Ltd. (1990) that included the area of Ancaster Creek.

7.3.1 QualHYMO

QualHYMO (OMOE 1985) is a continuous hydrological model that is based on the model HYMO by Williams and Hahn (1973) and is especially suited to rural basins that are undergoing urbanization. The original HYMO model was intended for direct runoff prediction from rural areas under single events and uses an SCS loss procedure. QualHYMO uses the same basic input as HYMO but was developed for continuous simulation of flow and pollutant levels. It is also capable of detention pond or river routing over a period of indefinite length. Essentially, the basin's rural

and impervious areas are completely decoupled and modeled completely separately. The effective precipitation is then convoluted to a hydrograph using the Nash Unit Hydrograph method for impervious areas and the William's Unit Hydrograph for the pervious areas. The final hydrograph is the sum of these two hydrographs. The relevant model equations are given below.

7.3.1.1 Effective Rainfall in Pervious Areas (Losses)

The effective volume of runoff after abstractions in the pervious areas is V_p^t at time t,

$$V_p^t = \frac{(P^t - ABS_p^t)^2}{(P^t - ABS_p^t + S_*^t)} \tag{7.9}$$

V_p^t is the cumulative depth of runoff (mm), P^t is the cumulative depth of precipitation (mm), ABS_p^t is the initial abstraction (mm) from the pervious area and S_*^t is a loss parameter (mm). This equation is known as the SCS relation for rural abstraction. The parameters S_*^t and ABS_p^t are updated by the model for each event to account for initial soil moisture conditions where S_*^t is a function of the Antecedent Precipitation Index (*API*). The *API* concept was originally devised by Linsley et al. (1982) as a way of accounting for soil moisture conditions before a storm. The equation is,

$$S_*^t = S_{min} + (S_{max} - S_{min})e^{-S_k API^t} \tag{7.10}$$

where the API^t is described by the following relation,

$$API^{t+1} = API_k API^t + P^t \tag{7.11}$$

where API^t is the antecedent moisture condition (mm) at time t, API_k is a constant with a typical value of 0.9. The API increases with rainfall and high values indicate high moisture conditions with small values of S_*^t, and low values of API^t indicate high values of S_*^t and dry conditions. This is a simple model where the constant API_k in a sense determines the "memory" of the system. S_{min} and S_{max} represent the range of S_*^t (mm) and S_k is a calibration parameter. The parameters S_{min} and S_{max} can be estimated from the SCS AMC I (Soil Conservation Service Antecedent Moisture Condition I) and AMC III values of the SCS Curve Number (CN), respectively. OMOE (1985) maintains that this "pseudo-continuous" model appears to be suited to planning studies.

The model uses hydrologic parameters that are well understood but the main concept introduced by the model is the link between Equations (7.10) and (7.11). ABS_p^t is modified by reducing it by the incoming precipitation. Once it reaches zero, it remains zero until a dry period occurs. During dry periods, ABS_p^t increases until the maximum value is reached. ABS_p^t can go from 0 to the maximum value in 24 hours of dryness. The authors agree this is "reasonable but arbitrary." The input rainfall series is really modeled as one large rainfall event with several inter-event dry periods. Losses are computed on the basis of S_*^t which is chosen at the beginning of an event at time t. The model assumes a new S_*^t value for each rainfall period when preceded by at least four dry hours. If the dry period is less than four hours than the previous rainfall is lumped in as part of the event and the previous value of S_*^t is used.

7.3.1.2 Effective Rainfall in Impervious Areas (Losses)

In impervious areas, the cumulative depth of runoff is given by,

$$V_i^t = (P^t - ABS_i^t) R_i \tag{7.12}$$

where ABS_i^t is the impervious area's initial abstraction which is updated in the same way as ABS_p^t. R_i is a constant volumetric runoff coefficient that describes the amount of urban area that is contributing to the flow, and is a user specified input.

7.3.1.3 Discharge in Pervious Areas

The discharge rate in pervious areas, Q_p^t, is given using the Williams Unit Hydrograph Method (Williams and Hahn 1973). This method is the original method used in HYMO. Convolution of the unit hydrograph produces the desired Hydrograph and the following equations can be used,

$$t_p = 0.97A^{0.4}HT^{-0.2}L^{0.2}$$
$$k_W = 4.50A^{0.4}HT^{-0.8}L^{0.4} \qquad \text{Slopes} < 5\% \qquad (7.13a)$$

$$t_p = 1.74A^{0.3}HT^{-0.3}L^{0.2}$$
$$k_W = 1.48A^{0.3}HT^{-0.4}L^{0.4} \qquad \text{Slopes 5\%-10\%} \qquad (7.13b)$$

$$t_p = 0.97A^{0.04}HT^{-0.2}L^{0.2}$$
$$k_W = 4.50A^{0.04}HT^{-0.8}L^{0.4} \qquad \text{Slopes} > 10\% \qquad (7.13c)$$

t_p is the predicted time to peak (hr), k_W is a recession parameter (hr), A is the drainage area (km^2), HT is the difference in elevation between the catchment divide and the outlet along the drainage length (m), and L is the hydraulic length of longest drainage path (km). The unit hydrograph is divided into three parts for computation. The three equations are given below,

$$u = u_p(t/t_p)^{n_W-1}e^{(1-n_W)(t/t_p-1)} \qquad (7.14)$$

Where u is the discharge (cms), u_p is the peak discharge (cms), t_p is the time to peak in hours and n_W is a dimensionless parameter. This equation is valid from the

beginning of the flow rise, to the inflection point of the hydrograph at t_{io}. For the stage of the hydrograph from t_{io} to $(t_{io}+k_W)$, the recession depletion is given by,

$$u = u_o e^{\frac{t_{io} - t}{k_W}} \tag{7.15}$$

And from $(t_{io}+k_W)$ to ∞, the relevant expression is,

$$u = u_1 e^{\frac{t_{io} + 2k_W - t}{3k_W}} \tag{7.16}$$

Where u_1 is the discharge at $(t_{io}+k_W)$. Also,

$$u_p = \frac{B_W A V_p}{t_p} \tag{7.17}$$

Where B_W is an additional watershed parameter which is some function of n_W and is derived by graphical means. Again, A is the catchment area and V_p is the cumulative runoff as in Equation (7.9) Notice that in these equations for the unit hydrograph, the superscript denoting the time step has been dropped.

7.3.1.4 Discharge in Impervious Areas

The Nash Unit Hydrograph Method (Nash 1957) shown in Section 2.2.5 is used to model the flow generated over impervious surfaces. Recall that it has two parameters, a recession constant k_N (hr) and the number of linear reservoirs in the cascade, n_N.

7.3.1.5 Baseflow

The model uses a simple relation to compute baseflow in which the groundwater storage is a single reservoir. The baseflow at time t is computed as,

$$Q_b^t = Q_{min} + \frac{A k_b k_2 V_b^t}{1000} \tag{7.19}$$

Where k_b is the baseflow recession constant (mm/(mm seconds)), k_2 is a parameter that accounts for deep losses to storage, V_b^t is the depth of water in the groundwater reservoir (mm), Q_b^t is the predicted baseflow at time t (cms) and Q_{min} is the minimum baseflow possible (cms). The factor of 1/1,000 is used because A is in units of m^2. The parameters Q_{min}, k_b and k_2 are all input by the user and V_b^t can be estimated from the following,

$$V_b^t = \frac{V_i^t + V_{bo}[1 - k_b(\Delta t/2)]}{1 + k_b(\Delta t/2)} \tag{7.20}$$

where Δt is the time step (s) and V_{bo} is the initial value of storage depth (mm). The depth of water infiltrated over the time step is V_i^t and is equal to the rainfall less runoff and initial abstractions. The parameters k_b, k_2, Q_{min} and V_{bo} are all specified by the user.

7.3.1.6 Channel Routing and Other Model Modifications

Modifications made to the original QualHYMO computer model by the consultants at MacLaren Plansearch include the Muskingum-Cunge method for channel routing, and the specification of the initial value of API. By examining the meteorological data over many years, MacLaren Plansearch determined that the initial API for rain events that were exceeded 85% of the time is 10.5 mm; the initial API for rain events that were exceeded 50% of the time is 21.8 mm and rain events that were exceeded only 15% of the time have an initial API of 37.7 mm. The 85% initial API corresponds to AMC I conditions, the 50% initial API corresponds to AMC II conditions, and the 15% initial API corresponds to AMC III conditions. Therefore,

the following relationship holds,

$$S_{*(X_p)} = \frac{25400}{CN(X_p)} - 254 \tag{7.21}$$

where $S_{*(Xp)}$ is the S_* corresponding to exceedence percentage (X_p) and $CN(X_p)$ is the CN of the appropriate type (I, II or III) depending on the exceedence percentage. This in combination with Equation (7.10) provides two equations and two unknowns thus allowing one to solve for S_{min} and S_{max}.

The following parameters must be specified by the user and the list indicates how they may be obtained and if they should be calibrated. The table lists only the primary parameters.

Table 7.13: QualHYMO Parameters.

Parameter	Symbol	Source
Basin area	A	Specified a priori from maps
Fraction of basin area that is impervious	$FRIMP$	Same as above
Nash UH constant	k_N	Calibrated
Nash UH constant	n_N	Calibrated
Impervious area abstractions	ABS_i	Assumed value
Impervious area runoff coefficient	R_i	Assumed value
Williams and Hahn constant	k_W	Calibrated but estimates can be obtained a priori with topographic maps
Williams and Hahn constant	n_W	same as above
Pervious area loss parameter	S_{min}	Specified a priori but may need some calibration if based on CN
Pervious area loss parameter	S_{max}	Specified a priori but may need some calibration if based on CN
Pervious area loss calibration parameter	S_k	Calibration parameter
Pervious area loss coefficient	API_k	Assumed value
Pervious area abstractions	ABS_p	Assumed value
Initial value of groundwater storage	V_{bo}	Assumed value
Baseflow constant	k_b	Assumed value specified a priori from gauge readings
Baseflow constant	k_2	same as above
Minimum baseflow	Q_{min}	same as above
Channel routing parameters such as rating curve, channel slopes, lengths and Manning's n		Specified by the user from topographic maps and water flow studies.

Of the list above, outside of the channel routing, there are a total of 17 parameters that must be specified and of these, anywhere from one to six parameters will require calibration.

7.3.2 Comparison Between TOPURBAN and QualHYMO

Parallels can be drawn between those important parameters in TOPURBAN and those in QualHYMO. The following list gives the TOPURBAN equivalent to the QualHYMO parameters.

Table 7.14: Parameter comparisons between QualHYMO and TOPURBAN v. 2.

Parameter	QualHYMO	TOPURBAN v. 2
Urban area fraction	*FRIMP*	f_{UA}
Urban area runoff coefficient	R_i	*uacp*
Urban area abstractions	ABS_i^t	*uacp*, Sr_{max}, Sr_i^t
Nash number of reservoirs	n_N	*1.0*
Nash recession constant	k_N	*zk*
Pervious area abstractions	ABS_p^t	Sr_{max}, Sr_i^t
Williams and Hahn Unit Hydrograph	n_W, k_W	f_{RV}
Loss parameters	S_{min}, S_{max}, *and* S_k	*Ko, m*
Antecedent Precipitation Index	*API*, API_k	S_i^t
Baseflow parameters	Q_{min}, V_{bo}, k_b, k_2	*m*, Q_o

Notice that some parameters in TOPURBAN play more than one role in QualHYMO. The parameters that are calibrated in TOPURBAN are not necessarily calibrated in QualHYMO and vice versa.

The QualHYMO model was applied to the six series of data. Originally, the parameters used by MacLaren in their watershed study of Spencer Creek were used in these six applications but it was soon obvious that the choice of parameters made

for that study were completely unreasonable. Figure 7.11 shows the subcatchments delineated by ARC/INFO using the same subcatchment outlets as MacLaren Plansearch Ltd. The number given to each subcatchment corresponds to the MacLaren numbering system. Some of the parameters were obtained using ARC/INFO including the length of each subcatchment, the height used in the Williams and Hahn equation, the fraction of impervious area (*FRIMP*) and the curve number. A short AML (Arc Macro Language) program was written (shown in Appendix A31) to compute curve numbers with ARC/INFO. This program computes a curve number based on the average subcatchment soil type, land use, and percentage of imperviousness. The same assumption that MacLaren Plansearch used in their watershed study was used in the QualHYMO applications regarding the percentage of imperviousness in urban areas; this being 40%. Furthermore, the values of S_{min} and S_{max} were then computed using Equations (7.21) and (7.10). The following table shows some of the parameters that were used in the QualHYMO applications.

Table 7.15: QualHYMO parameter values.

Subcat. No.	Subcat. Area (Ha)	*FRIMP*	Height (m)	Length (km)	*CN*	S_{min} (mm)	S_{max} (mm)
363	140.25	0.136	13.25	2.3	69	44.3	1033.4
362	235.50	0.020	14.57	1.9	68	46.4	1082.4
364	104.75	0.248	19.06	1.3	76	31.1	726.4
366	65.25	0.157	23.14	1.4	75	32.9	766.7
365	65.50	0.053	24.49	1.4	75	32.9	766.7
367	67.50	0.141	25.41	1.4	77	29.4	687.1
368	114.75	0.588	26.73	1.6	79	26.2	611.4

Appendix A32 shows the input file for the 1991 series. The model was calibrated manually which was very difficult and time consuming; hence, the model was only

calibrated on the 1991 data series. The resulting calibrating parameters were then used on the other data series to produce the Nash and Sutcliffe Efficiencies shown in Table 7.16 below.

Table 7.16: Nash efficiencies for QualHymo during verification periods.

Year	Nash E
1988	-2.03
1989	-0.31
1990	-0.66
1991 (Calibrated)	0.37
1992	0.66
1993	0.78

The most influential parameters in the calibration were those dealing with the Nash Unit Hydrograph that dealt directly with the urban areas. The calibrated Nash UH parameters were $n_N = 1.028$ and $k_N = 1.2$ hours. The resulting predicted and observed series are shown in Figures 7.12 to 7.17.

The original QualHYMO model that was obtained by the author was modified to allow for calibration of two multiplication factors: one for each of the Williams and Hahn UH constants. These were found to only affect the flow contributed by the rural areas and were left at the optimum values that were originally determined in the MacLaren Plansearch Study. It is interesting to note that the majority of flow in Figures 7.12 to 7.17 is urban flow. While the entire basin contributes to flow at all times, the enormous abstraction of 15 mm was found to eliminate contributions from rural areas for many rain events. But this value was left as is because it did in some cases produce better values of Nash and Sutcliffe Efficiencies. Because the model only required a 24 hour dry period for the abstraction to reach a maximum value, the abstraction was almost always 15 mm prior to any rain event. Modifying the curve

number produced very small changes as well as the originally specified calibration parameter S_k (equal to 0.14).

Recall that if the Nash E value is less than 0.0, then a model that can only predict the average of the observed series is a better predictor of observed values than the model that produced the Nash E value of 0.0. If it is exactly 1.0 then the model predicts observations exactly. The literature does not seem to associate qualitative descriptions such as "good" or "poor" to specific values of Nash E, but a Nash E value of 0.7 is certainly much better than a Nash E value of 0.3. For the purposes of this discussion, Nash E values less then zero indicate a "very poor" model performance, Nash E values between 0.0 and 0.5 are considered "poor", Nash E values between 0.5 and 0.7 indicate "acceptable performance", values between 0.7 and 0.85 are considered "good", while values of Nash E above 0.85 are deemed "excellent".

Table 7.16 shows a very poor calibrated Nash E for most years, an acceptable Nash E for 1992 and a good Nash E for 1993. The series of 1991, 1990 and 1993 are considered to be the best test series for the models in this dissertation. The performance on the wet year of 1990 was very poor, although it showed a good performance in 1992. The best performance by the model is in 1993 in which it produces a Nash E of 0.78 using the 1991 calibrated parameters. From examining the figures however, the model visually does very well in simulating the baseflow and the observed recessions in 1993. But, as all the figures show, QualHYMO over-predicts all peak flows by as much as 100% in some cases. This overestimation is a manifestation of both the rural and urban contributions. One of the reasons 1993 makes such a good test year is that it starts with a relatively dry period with a few small rain events. So much of this flow is baseflow, which the QualHYMO model does an excellent job of simulating but single events are poorly modeled by QualHYMO in comparison to TOPURBAN. Therefore, an examination of the

performance of these models on single events is required.

7.4 Applications to Single Events

QualHYMO's intended use in the MacLaren Plansearch study was to model the flows for the 100 year return storm and the regional storm, Hurricane Hazel. During the process of determining these flows, the models are calibrated on relatively small events. Therefore, both models are tested in this section on their ability to accurately simulate single events. A true test of a single event model, is that given the right antecedent moisture conditions, the model calibrated on one single event should perform equally as well on a second event with roughly similar antecedent conditions. In Section 7.4.1, a closer inspection of TOPURBAN v. 1 and v.2 for predicting time to peak, peak discharge and event water volume are examined for each of the six applications of the previous section. Then in Section 7.4.2, TOPURBAN v. 2 and QualHYMO are each calibrated on a single event and then applied on a second event using the same calibrated parameters.

7.4.1 TOPURBAN Single Event Modeling

All events with rainfall greater than 10 mm were selected from the six data series to evaluate TOPURBAN v. 1 and v. 2. The evaluations were made on the observed and predicted time to peak, peak discharge, and total volume of water for the event. The next three tables (Tables 7.17 to 7.19) provide the results of applying both versions of TOPURBAN to these events. In the first table, a description of the rain event is given in terms of its distribution. If it is spiked, then the rain event is characterized by a very sudden rise and drop in precipitation levels. If it is double peaked then the rain event undergoes a rise and fall and then another rise and fall before the entire rain event is over. And finally, in a bell shaped curve, the hyetograph has a long duration with a gradual rise and falling of values. The predicted times to peak were

similar between TOPURBAN v. 1 and v. 2, therefore, only one set of values is shown in the table below.

Table 7.17: Comparison between predicted and observed values of time to peak (t_p).

Event/ Description/Time Index on Figure			Observed t_p (hrs)	Predicted t_p (hrs)
1988-1	spike	1250	1.0	1.0
1988-2	double peak	1257	1.0	3.0 (1.0)
1988-3	spike	1574	1.0	1.0
1989-1	spike	450	1.0	1.0
1989-2	bell shape	1847	4.0	4.0
1990-1	spike	1031	1.0	1.0
1990-2	bell shape	2026	4.0	4.0
1990-3	spike	2232	0.0	0.0
1990-4	spike	2658	0.0	0.0
1991-1	double peak	1085	6.0 (4.0)	7.0 (4.0)
1991-2	bell shape	2087	4.0	3.0
1992-1	bell shape	1289	5.0	5.0
1992-2	double peak	1529	5.0 (10.0)	10.0 (5.0)
1993-1	bell shape	946	9.0	9.0
1993-2	bell shape	1057	5.0	9.0

Values in brackets are the time to peak of the lesser peak if a double peak occurred. In general, the table shows that TOPURBAN does very well in predicting the time to peak of spiked and bell shaped curves. It does not fare so well on the three double peak events. The time to peak predicted by TOPURBAN is a direct result of the channel routing flow factor which in TOPURBAN assumes a constant flow at all times. It is likely that this is not always entirely reasonable.

Table 7.18: Comparison between predicted and observed peak values given in cms.

Event	Observed Peak	Predicted Peak v. 1	% Diff.	Predicted Peak v. 2	%Diff.
1988-1	0.51	0.27	-47	0.27	-47
1988-2	0.74	0.45	-39	0.47	-36
1988-3	0.43	0.64	49	0.60	40
1989-1	3.57	1.85	-48	1.75	-51
1989-2	1.28	1.39	9	1.24	-3
1990-1	0.49	0.51	4	0.50	2
1990-2	0.86	0.68	-21	0.67	-22
1990-3	1.54	1.14	-26	1.09	-29
1990-4	0.55	0.47	-15	0.47	-15
1991-1	0.70	0.50	-29	0.55	-21
1991-2	0.43	0.37	-14	0.33	-23
1992-1	0.87	0.56	-36	0.46	-47
1992-2	2.40	1.70	-29	1.63	-32
1993-1	2.88	2.59	-10	3.028	5
1993-2	1.60	1.25	-22	1.20	-25

In this table, TOPURBAN v. 1 and v. 2 are split in terms of ability to predict peak flow for each of the rain events in a single year and there are minor differences between simulated results of versions 1 and 2. No one version is able to provide consistent predictions. Predictions are best in 1990, 1991 and 1993 which are the longest of the six data series. This may imply that accurate TOPURBAN event modeling may depend on calibrations using long continuous series. The following table details differences in the predicted and observed volumes

Table 7.19: Comparison between predicted and observed values of hydrograph volumes.

Event and Start and End Indices	Observed Volume m^3	Volume v. 1	% Diff.	Volume v. 2	% Diff.
1988-1& 2 (1240-1270)	20,475	14,837	-28	17,604	-14
1988-3 (1570-1610)	17,516	17,138	-2	20,288	16
1989-1 (447-490)	61,565	33,510	-46	46,810	-24
1989-2 (1840-1860)	26,475	24,525	-7	26,025	-2
1990-1 (1028-1045)	11,791	9,922	-16	12,433	5
1990-2 (2023-2033)	12,315	11,073	-10	11,853	-4
1990-3 (2230-2047)	23,022	16,200	-30	18,690	-19
1990-4 (2658-2668)	6,087	6,577	8	7,770	28
1991-1 (1082-1120)	25,515	20,325	-20	24,000	-6
1991-2 (2080-2110)	15,300	11,888	-22	15,915	4
1992-1 (1286-1300)	19,980	15,523	-22	16,500	-17
1992-2 (1525-1540)	61,464	52,328	-15	54,638	-11
1993-1 (939-960)	94,425	71,648	-24	79,455	-16
1993-2 (1054-1070)	47,040	50,100	7	50,850	8

The table indicates a better performance by TOPURBAN version 2 over version 1 which is not surprising as version 2 naturally produces greater flow generation. In terms of overall volume, version 2 is considered better.

7.4.2 Comparison to QualHYMO's Performance on Single Events

QualHYMO's event performance is compared to TOPURBAN by considering a calibration on a single event and applying the calibrated model to a second event with similar soil moisture levels. Figure 7.18 shows the application of TOPURBAN v.2 and QualHYMO on a double-peaked event. Two QualHYMO calibrations are shown where one produces the correct time to peak but has a lower Nash E. While the Nash E of the TOPURBAN model is almost perfect, QualHYMO still produces a good Nash E. The parameters used in TOPURBAN v. 2 were, $m = 0.0307$, $uacp = 0.34$, $zk = 6$, $Ko = 55$, and $Sr_{max} = 0.096$. All other TOPURBAN parameters are those of the 1993 calibrated values. The initial value of *API* was raised to 18.5 mm for QualHYMO in this event but all else remains the same. Figure 7.19 shows the application of these two calibrated models to the second event. The Nash Efficiencies were 0.64 for TOPURBAN and 0.08 for QualHYMO. This is an excellent illustration of why QualHYMO is unable to model a second event in a series of a similar year and only several days later. The TOPURBAN model still produces a respectable result.

7.4.3 Applying TOPURBAN v.2 to Hurricane Hazel and Other Storms

To investigate the role of the soil medium and the urban component in peak flows and single events, TOPURBAN v.2 was applied to storms with 2, 5, 10, 25, 50, and 100 year return frequencies. The rainfall hyetographs used are shown in A33. The hyetograph for Hurricane Hazel is also included. The test used the parameters of Table 7.11 belonging to the wet year. This was done to consider worst case

conditions. The parameters are listed below.

$m = 0.052$ m	$Sr_{max} = 0.297$ m	$T_d = 1.0$ hr/m
$Ko = 9$ m/hr	$uacp = 0.25$	$zk = 21$ hrs
$v_{RV} = 180$ m/hr	$v_{CHV} = 920$ m/hr	$Q_o = 0.0000153$ m
$Sr^0 \sim 0.0$ m		

In this test, there are no losses due to evapotranspiration and Q_o was set to the 1993 baseflow value. In each of the storms, the percentage of saturation excess contributing area was recorded and plotted against the return period. This plot is shown in Figure 7.20. The equation representing the best fit line to this plot is,

$$A_c = 5.7 \ln(RT) + 14.4 \qquad (7.22)$$
$$R^2 = 0.94$$

where A_c is the percentage of the soil medium contributing to flow and RT is the return period of the rain event. As the percentage of urban land contributing to flow is always the same - roughly 8%, then Equation (7.22) above can be re-written as,

$$A_c = 5.7 \ln(RT) + 21.2 \qquad (7.23)$$

in which A_c is now the *total catchment* contributing area. This equation implies that a storm with a 500 year return period (that is, $RT = 500$ in this simplistic analysis) would have a total catchment contributing area of 57%.

A test was conducted using TOPURBAN v. 2 with the parameters above, Hurricane Hazel rainfall data, channel flow routing turned off and two overland flow routing conditions: $v_{RV} = 180$ m/hr and $v_{RV} = 1520$ m/hr. These two flow speeds were chosen because they cover the range of speeds found in the calibration of the six series and

result in slightly different peak flows. Figure 7.21 shows the resulting hydrographs. A peak flow of 40 m^3/s resulted for the overland speed of 180 m/hr and a peak flow of 84 m^3/s was predicted in the test that used a flow speed of 1520 m/hr. The flow volume predicted by the model (hydrograph area over a 24 hour period starting from hour 37 in order to leave out the first 36 hours preceding Hurricane Hazel) was 1.1 million cubic metres. The percentage of contributing area from saturation excess overland flow was 90%.

The peak flowrate predicted by MacLaren Plansearch Ltd. in its study of the Spencer Creek Watershed was approximately 63 m^3/s for this catchment when using the original input file that was used in the study. The predicted hydrograph volume was 2.25 million cubic metres. When the QualHYMO input file for 1993 was used with the Hurricane Hazel data, a value of 24 m^3/s was predicted and a hydrograph volume of 0.6 million cubic metres was obtained. These hydrographs are also shown in Figure 7.21. Notice from the graph that the time to peak is different between this study and the one done by MacLaren Plansearch Ltd., and this is due to the fact that the latter study used a channel flow routing scheme. The peak flow predicted for Hurricane Hazel by MacLaren Plansearch Ltd. is within the range predicted by TOPURBAN v.2; however, the values obtained by these two studies were obtained through radically different theory. If we were to assume that a value close to 63 m^3/s is the true flow for Hurricane Hazel for this catchment, then the simulation by QualHYMO which performed very well in 1993 was insufficient in predicting the Hurricane Hazel flow. The QualHYMO simulation used in the Spencer Creek Watershed Study may be considered an entirely different model for all intents and purposes because the input files were so different. This reiterates the fact that this Hortonian Flow model is not representative of the flow mechanisms in the catchment.

7.5 Summary

This chapter began by modifying TOPURBAN v.1 to incorporate a linear reservoir representation of urban storage. This modification created TOPURBAN v.2 which essentially doubled the contribution of the urban component to flow volume. This version of the model performed on average, 5% better in Nash E value then its predecessor. TOPURBAN v.1 and v.2 were compared in a variety of ways including through Water Survey of Canada statistics, and their ability to predict single event peak discharge, time to peak and hydrograph volume. TOPURBAN v.2 in general improved the overall performance in terms of volume and maximum peak flowrate predictions. The model is quite good at predicting time to peak, but has difficulty in predicting high flowrates. Recommended parameter sets were suggested for use with TOPURBAN v. 2 in the Ancaster Creek area. TOPURBAN v. 2 is recommended over version 1 with only the parameters m, Ko and Sr_{max} as calibration parameters. The user may consider a coarse initial calibration of F_{RV}.

QualHYMO was executed on the six data series and performed poorly on four of the six series. It did perform fairly well on the 1992 and 1993 data but it could never reach the same efficiencies as TOPURBAN v. 2. QualHYMO did a very good job of predicted baseflow rates but had very high predictions of peak flow far and above the under-predictions of TOPURBAN. QualHYMO did poorly in predicting single event peak flow after being calibrated on another event with similar antecedent moisture conditions in 1993. TOPURBAN on the other hand fared quite well. Furthermore, the application of QualHYMO and TOPURBAN on Hurricane Hazel rain data revealed that QualHYMO can predict similar values of TOPURBAN flow for this event, but does so only through a majority of contribution from the urban areas where the Nash parameters are very small.

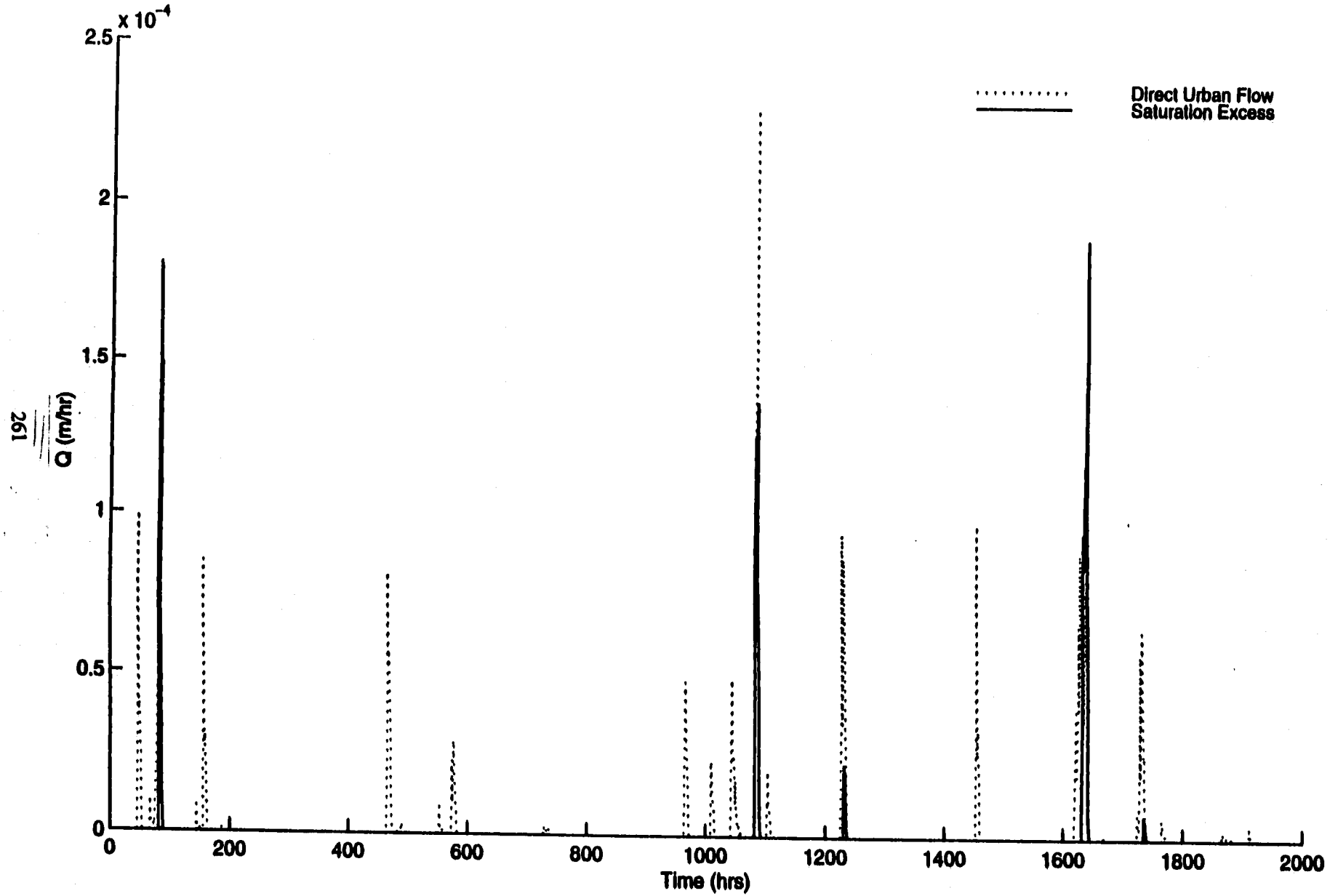

Figure 7.1: TOPURBAN's division of overland flow between urban and non-urban areas for 1991.

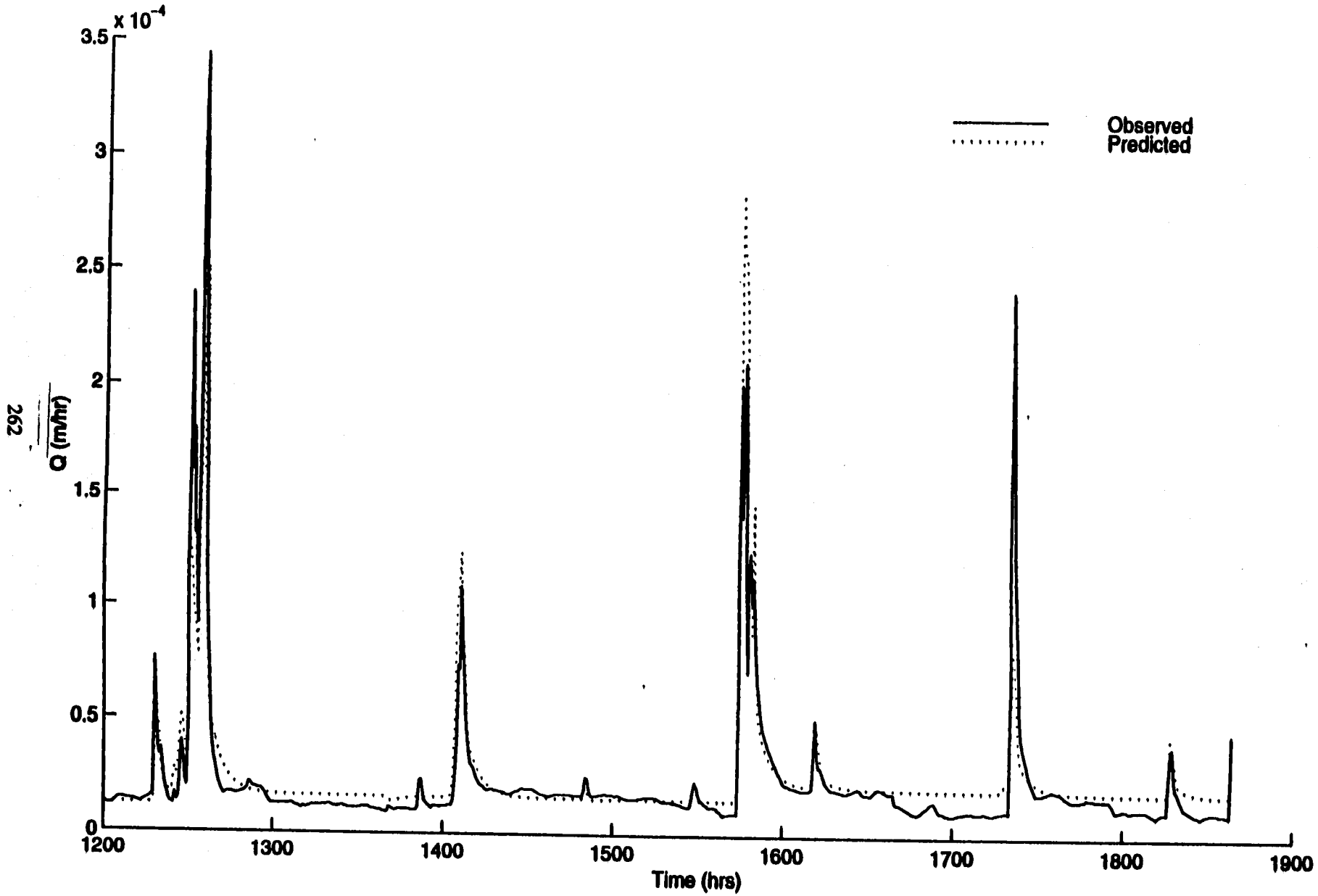

Figure 7.2: Observed vs. TOPURBAN v. 2 predicted flowrates for 1988.

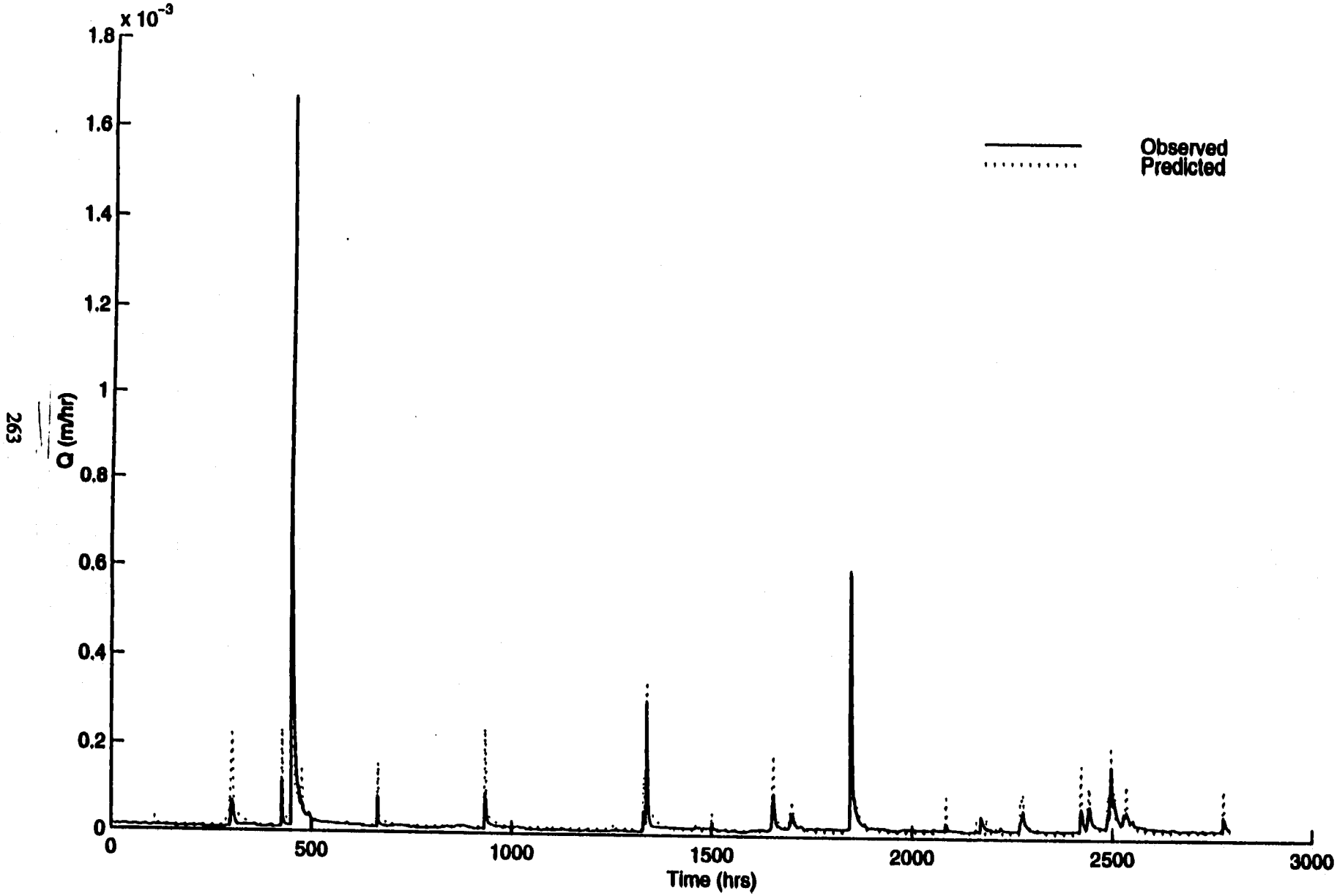

Figure 7.3: Observed vs. TOPURBAN v. 2 predicted flowrates for 1989.

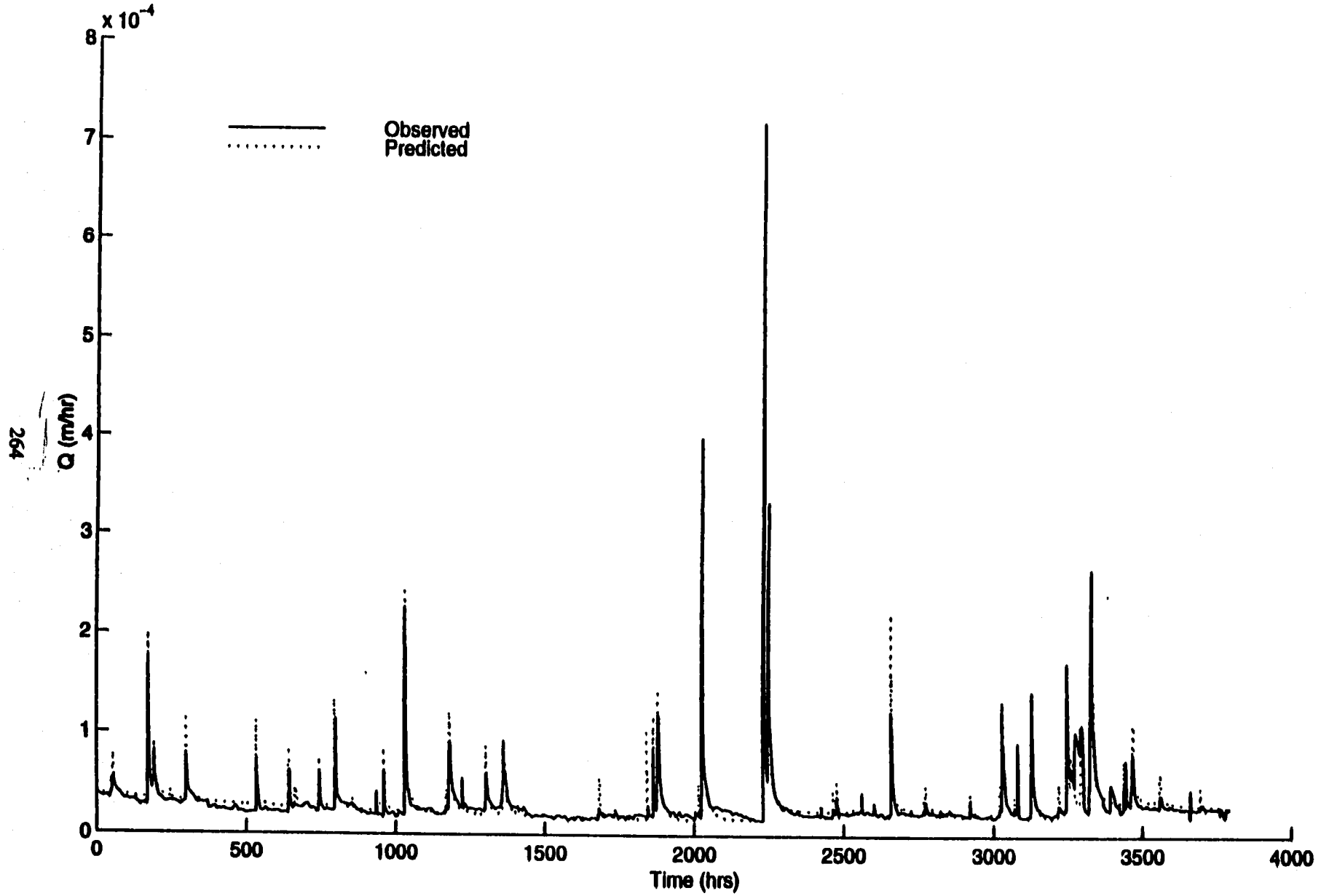

Figure 7.4: Observed vs. TOPURBAN v. 2 predicted flowrates for 1990.

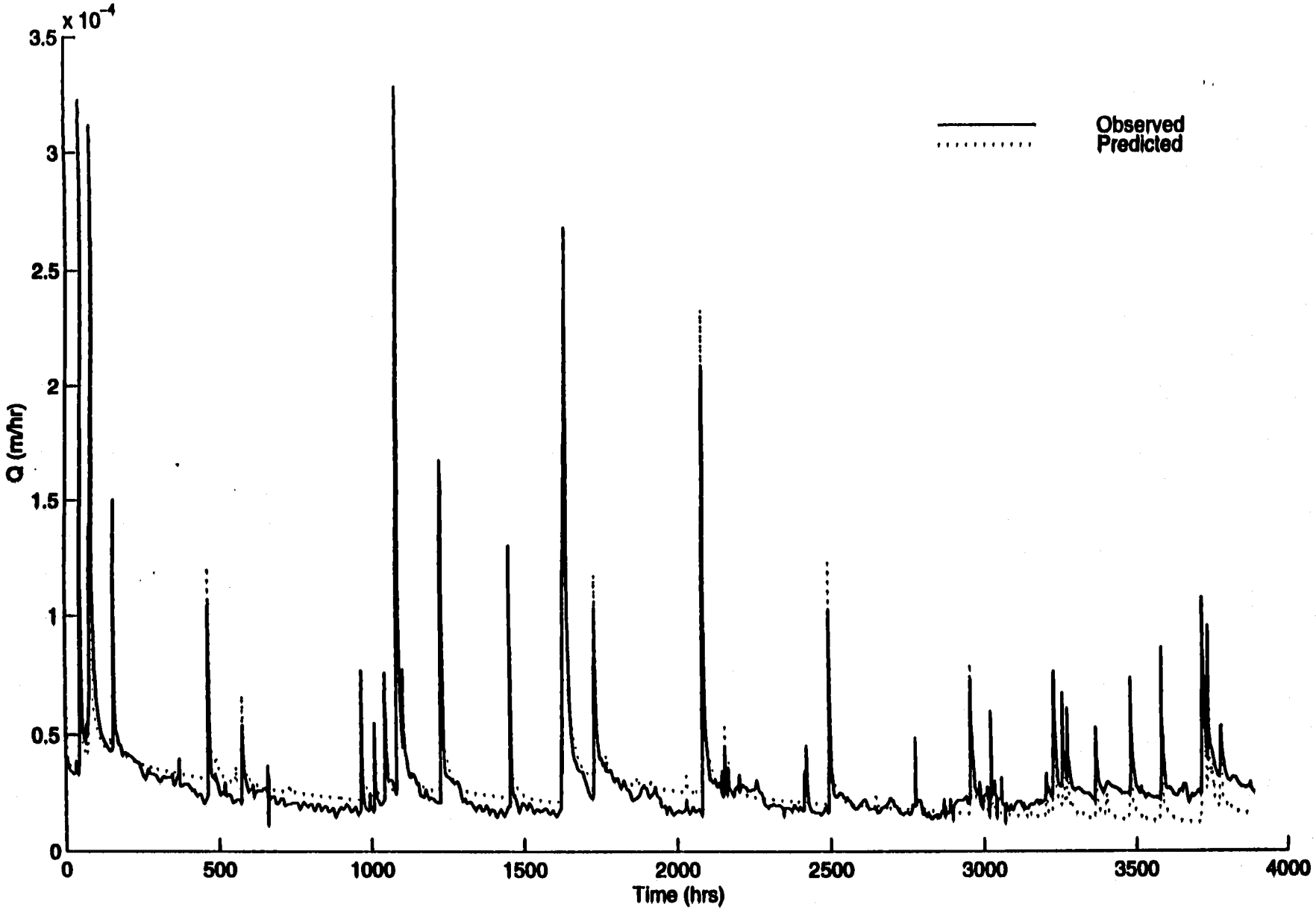

Figure 7.5: Observed vs. TOPURBAN v. 2 predicted flowrates for 1991.

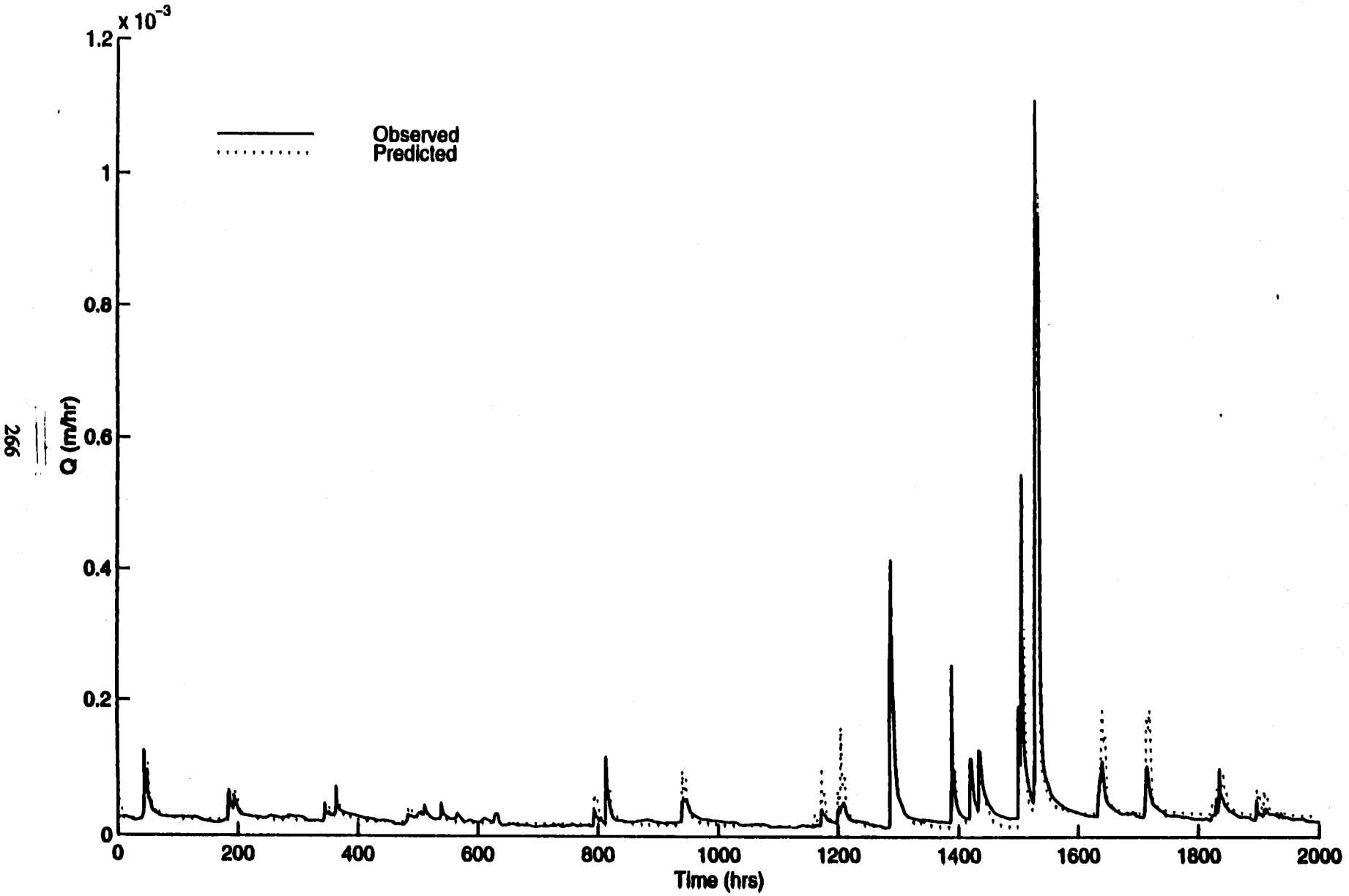

Figure 7.6: Observed vs. TOPURBAN v. 2 predicted flowrates for 1992.

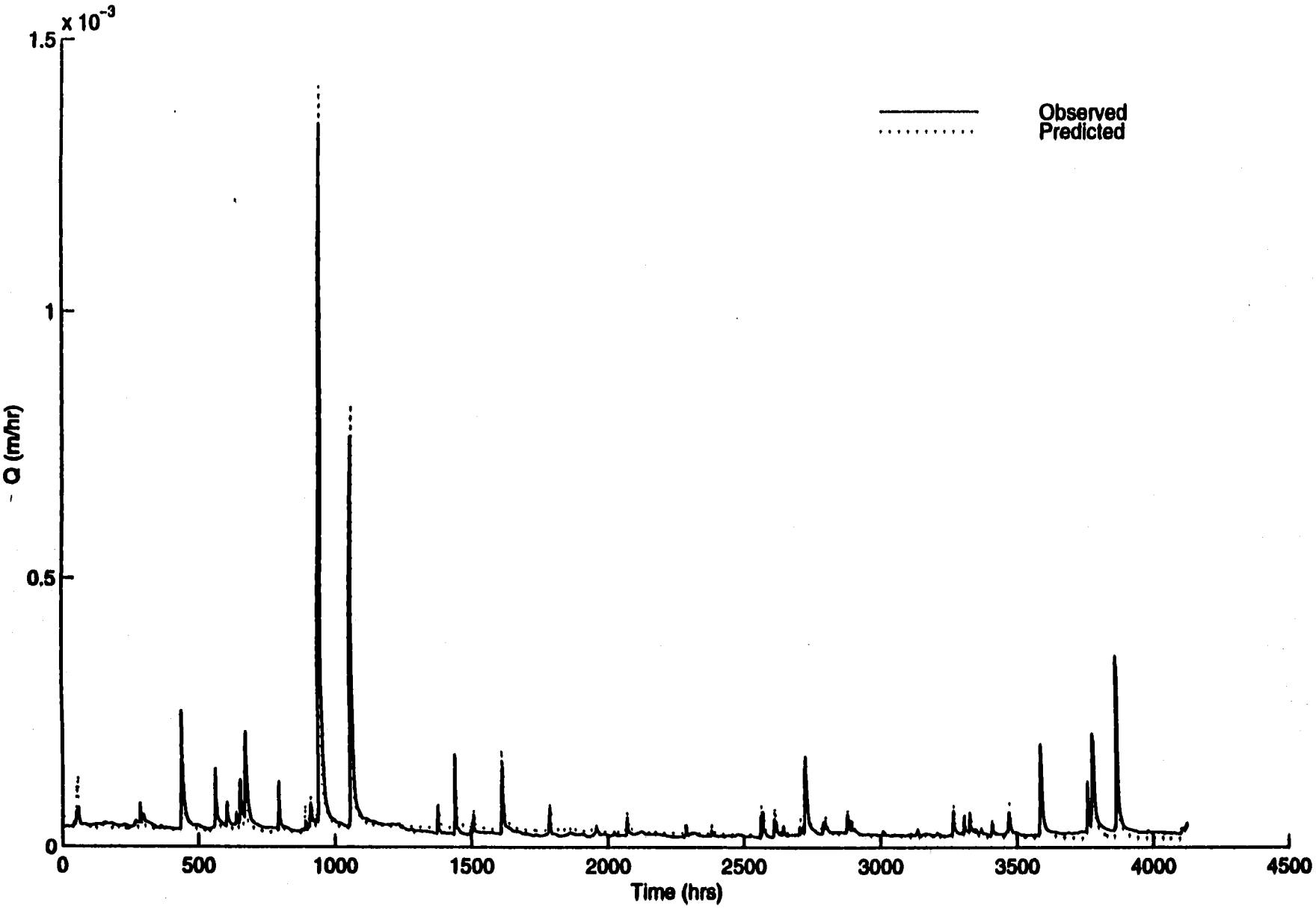

Figure 7.7: Observed vs. TOPURBAN v. 2 predicted flowrates for 1993.

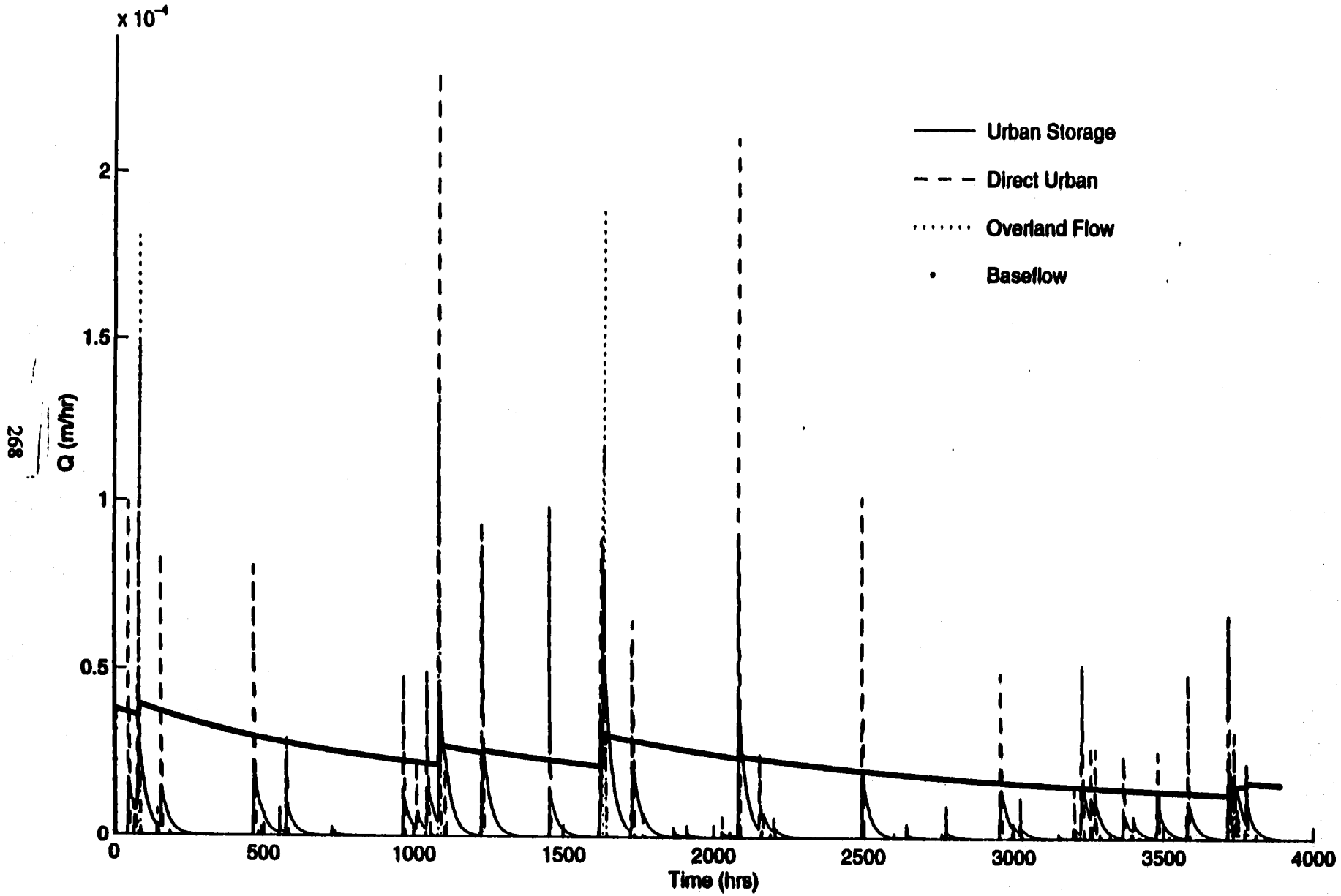

Figure 7.8: Flowrate contributions from the various runoff mechanisms in TOPURBAN v.2.

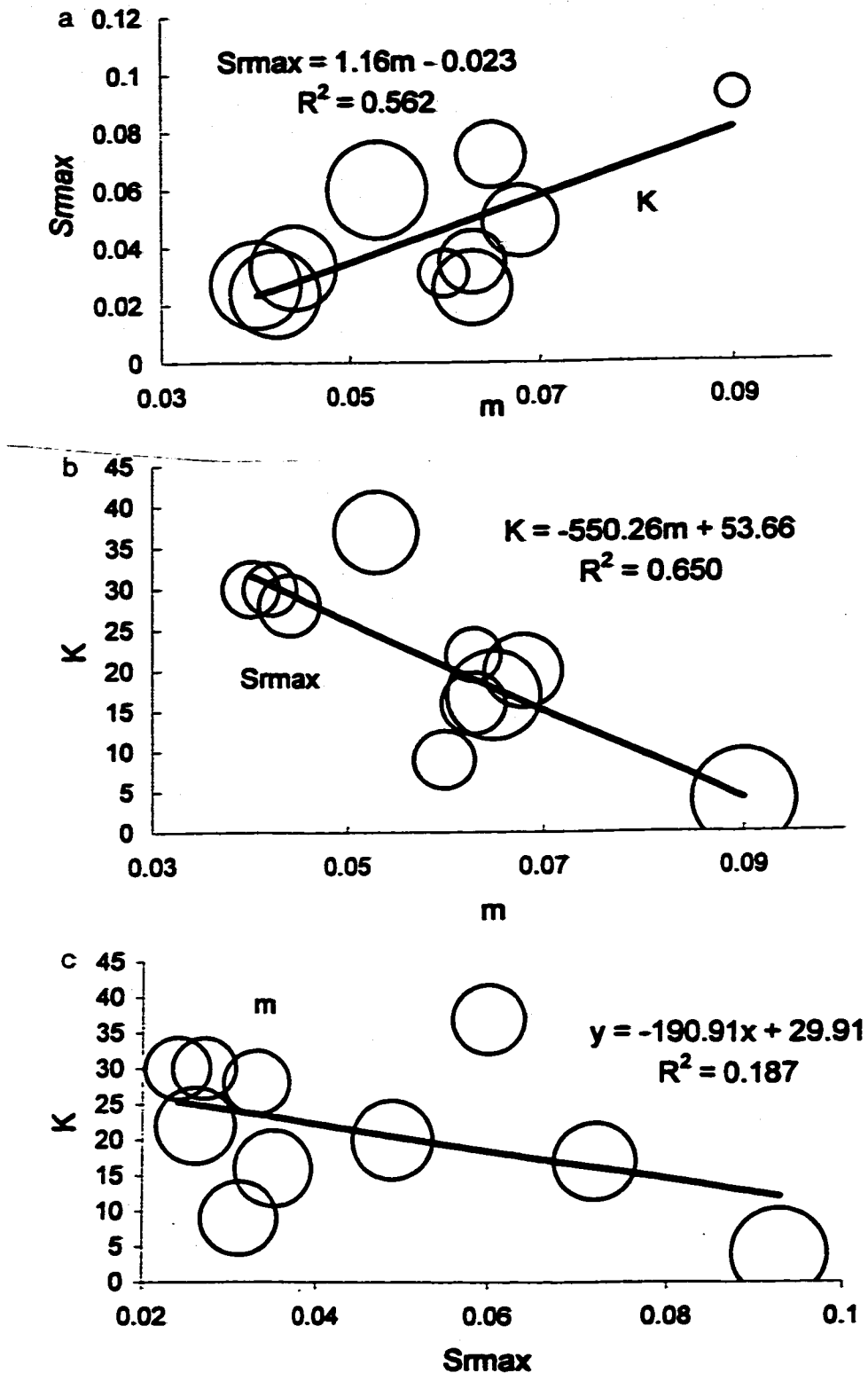

Figure 7.9: Bubble plots of parameter triplets a) Sr_{max}, m and Ko; b) Ko, m and Sr_{max}; c) Ko, Sr_{max} and m.

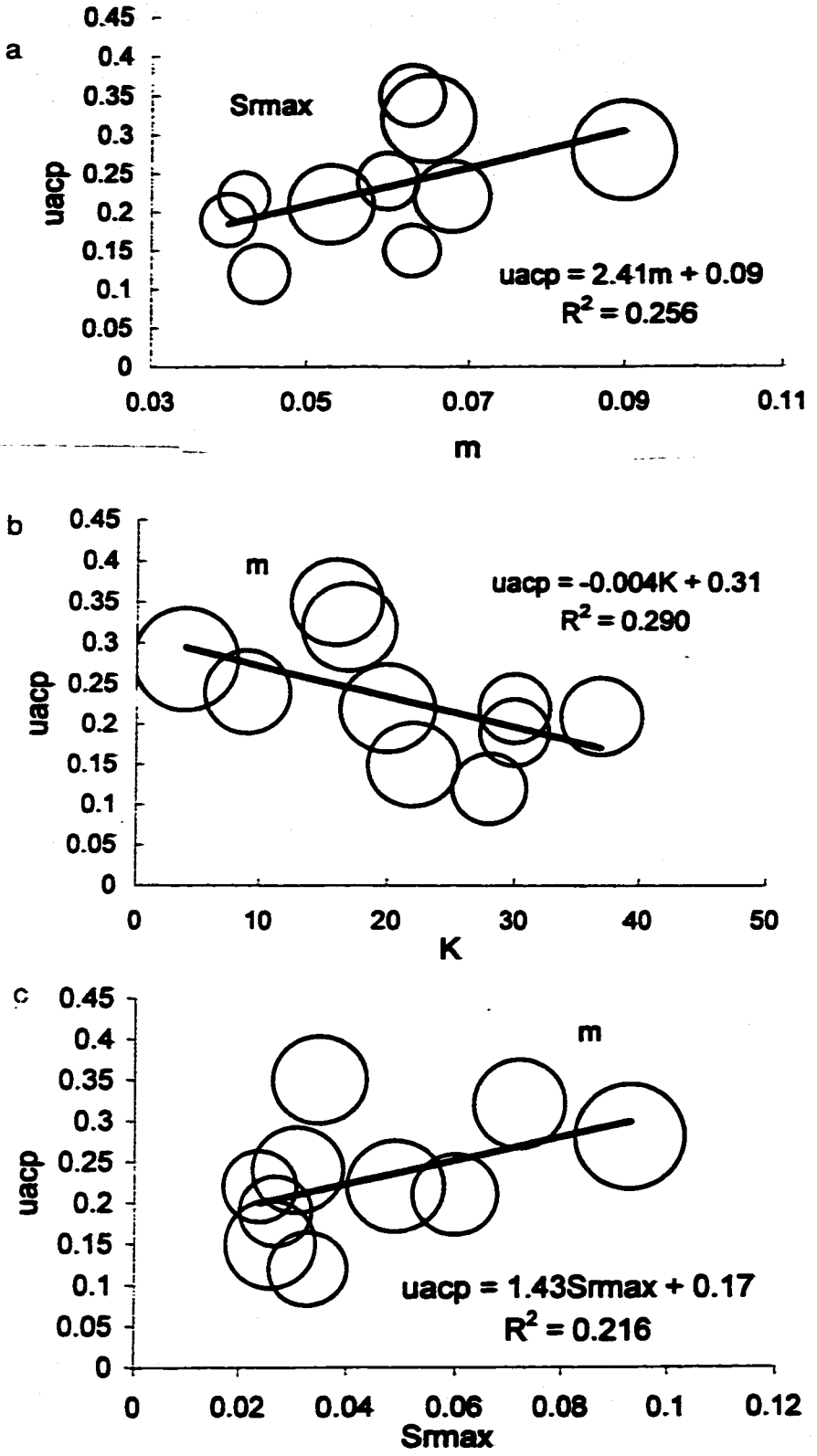

Figure 7.10: Bubble plots of parameter triplets a) *uacp*, *m* and Sr_{max}; b) *uacp*, *Ko* and *m*; c) *uacp*, Sr_{max} and *m*.

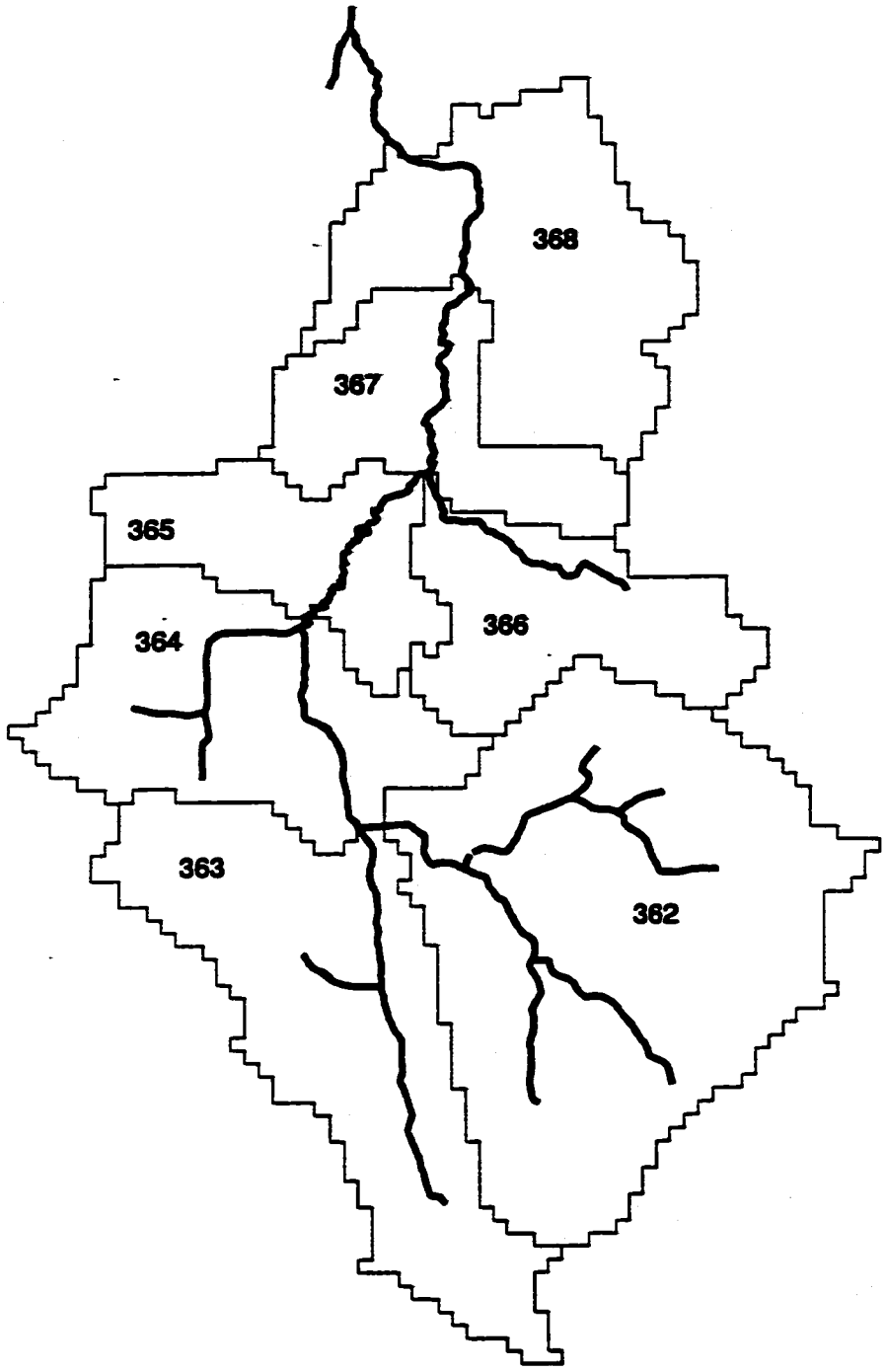

Figure 7.11: Subcatchment delineation using MacLaren (1990) pour points.

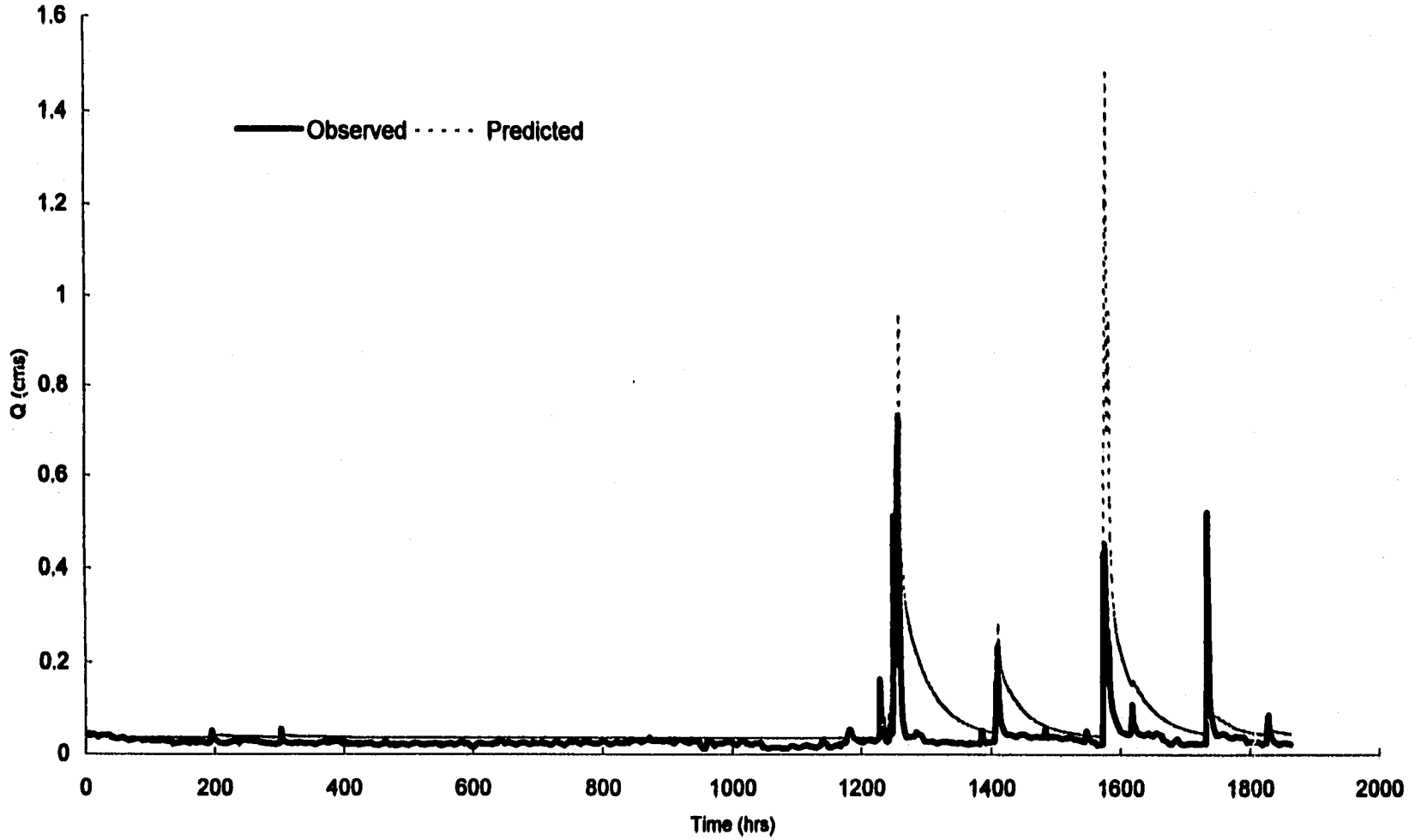

Figure 7.12: Observed vs. QualHYMO predicted flowrates for 1988.

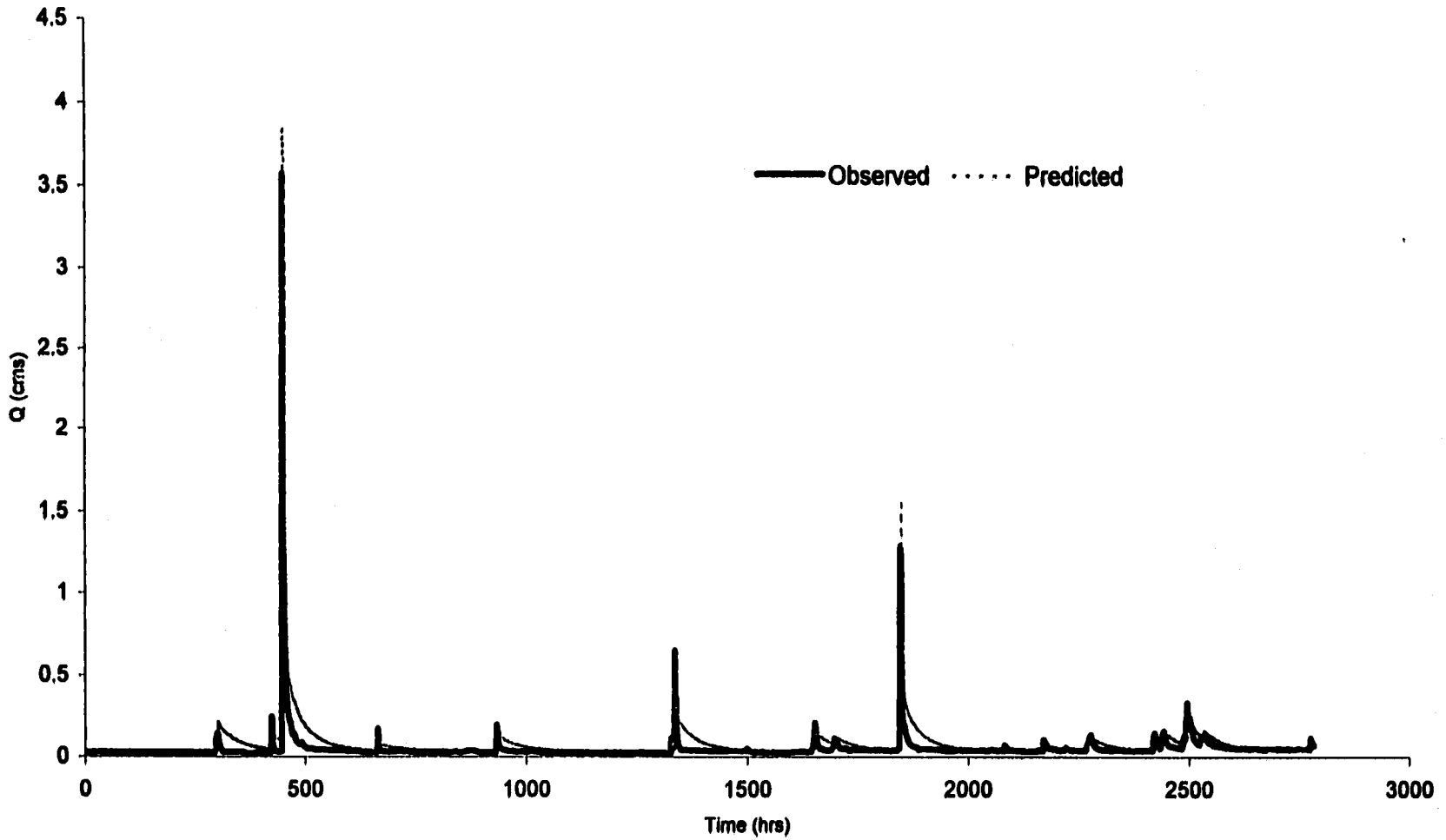

Figure 7.13: Observed vs. QualHYMO predicted flowrates for 1989.

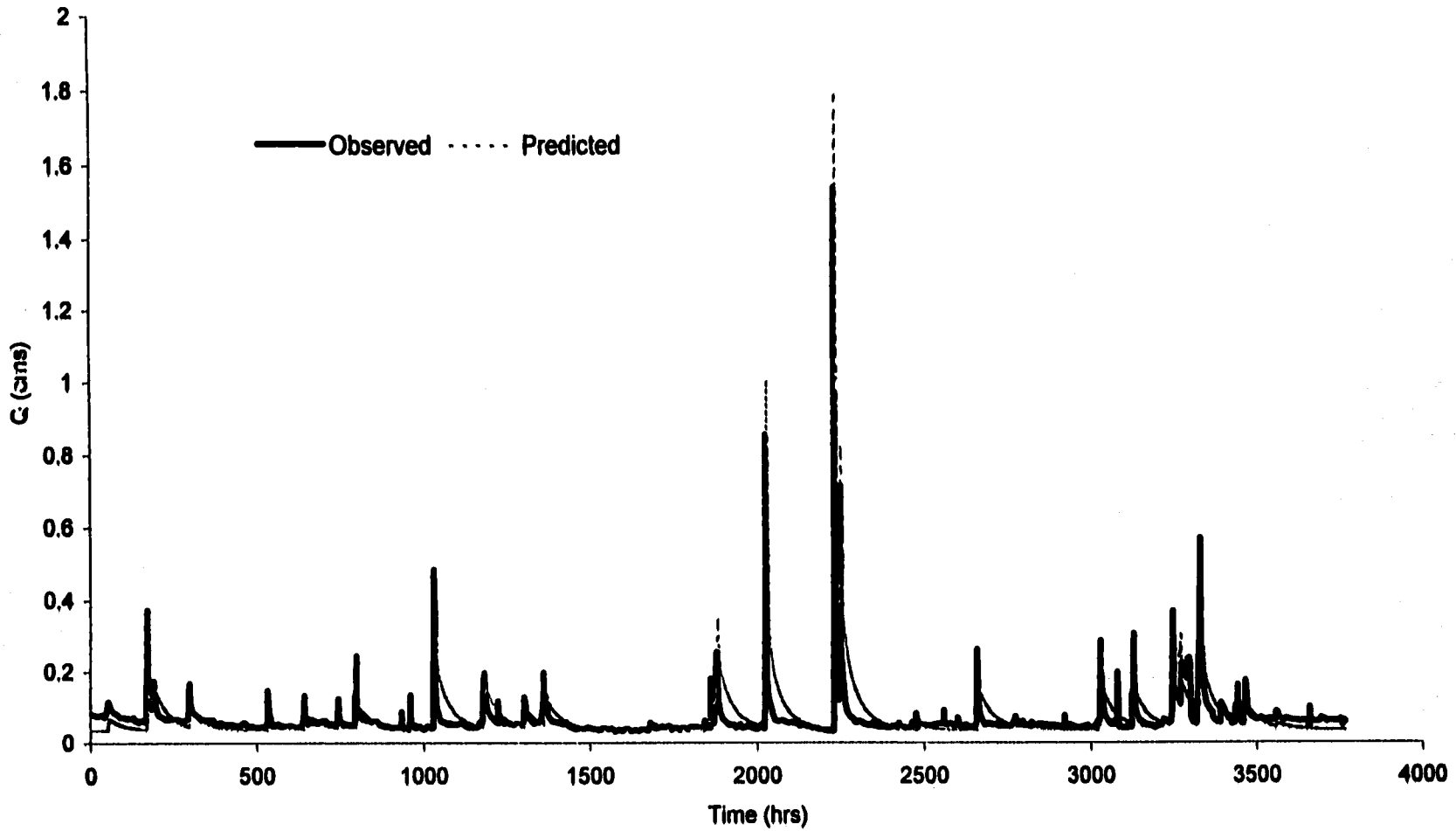

Figure 7.14: Observed vs. QualHYMO predicted flowrates for 1990.

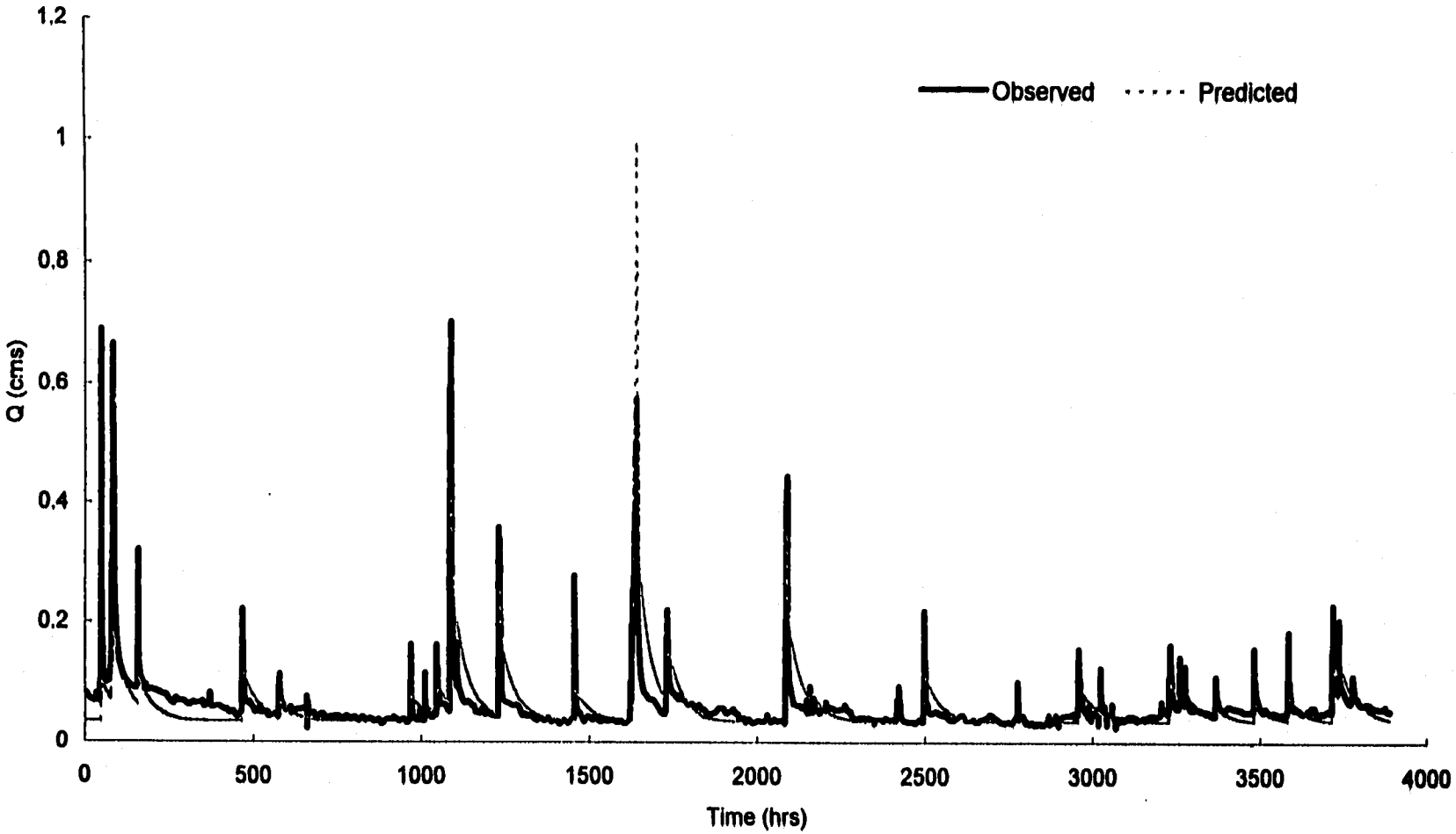

Figure 7.15: Observed vs. QualHYMO predicted flowrates for 1991.

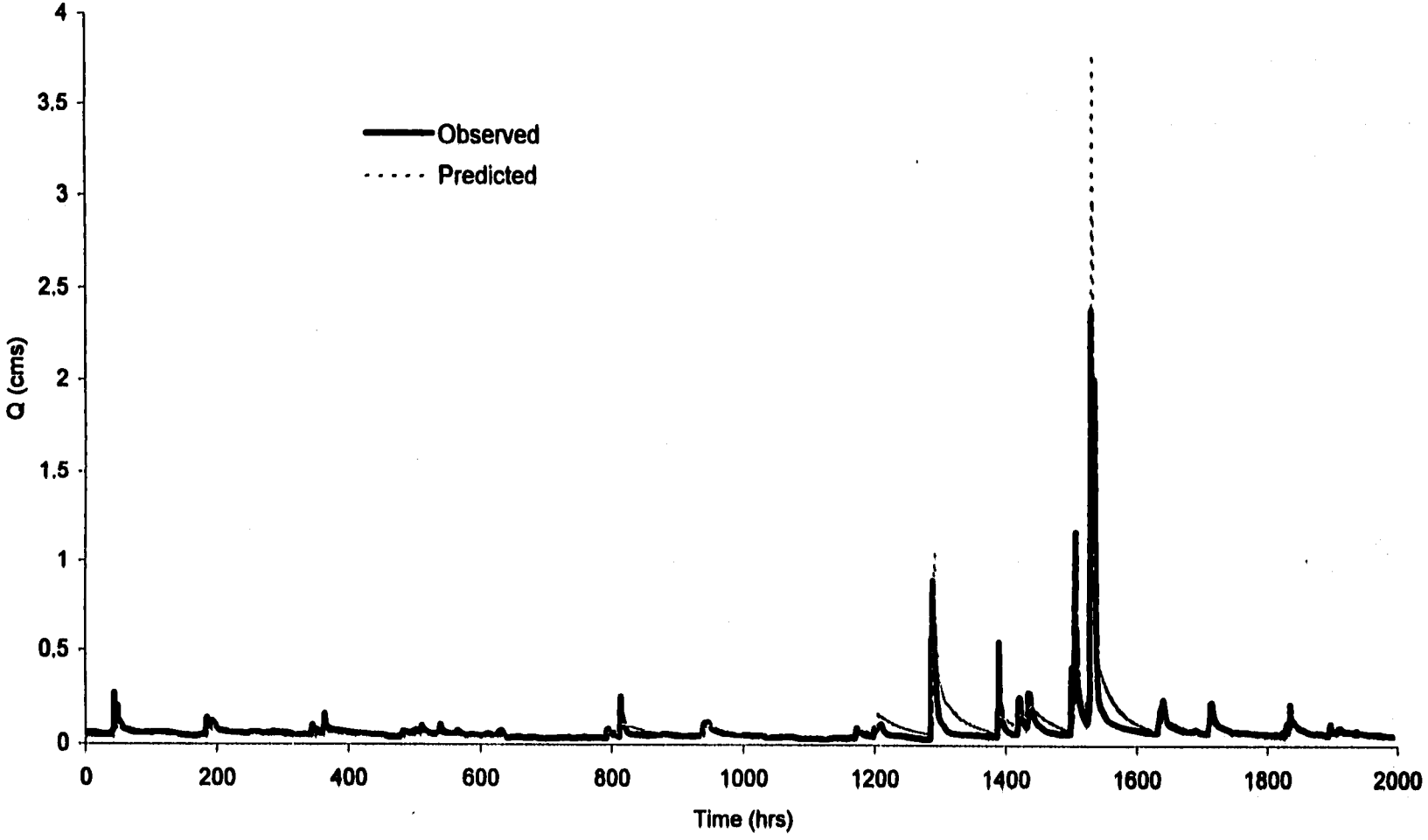

Figure 7.16: Observed vs. QualHYMO predicted flowrates for 1992.

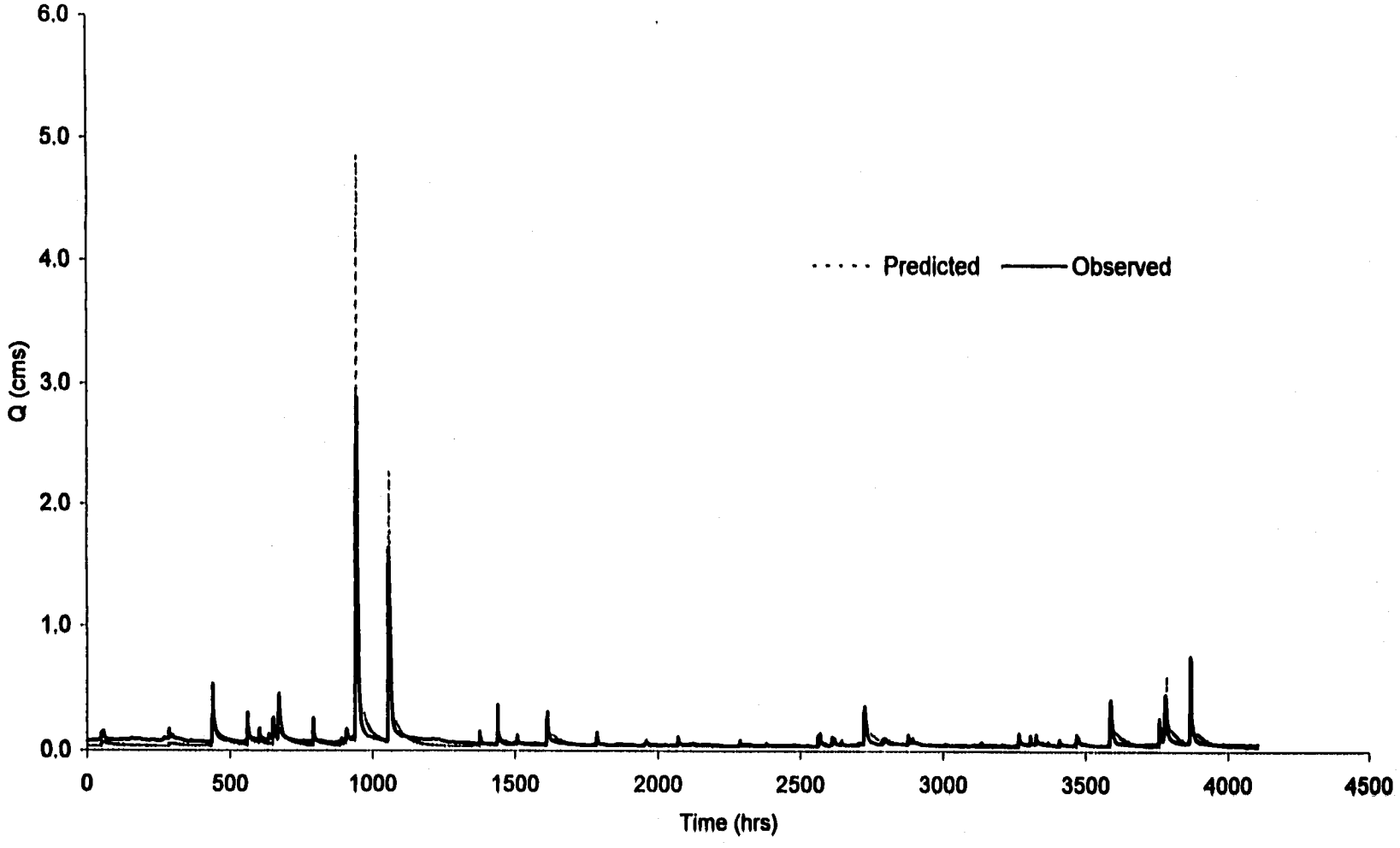

Figure 7.17: Observed vs. QualHYMO predicted flowrates for 1993.

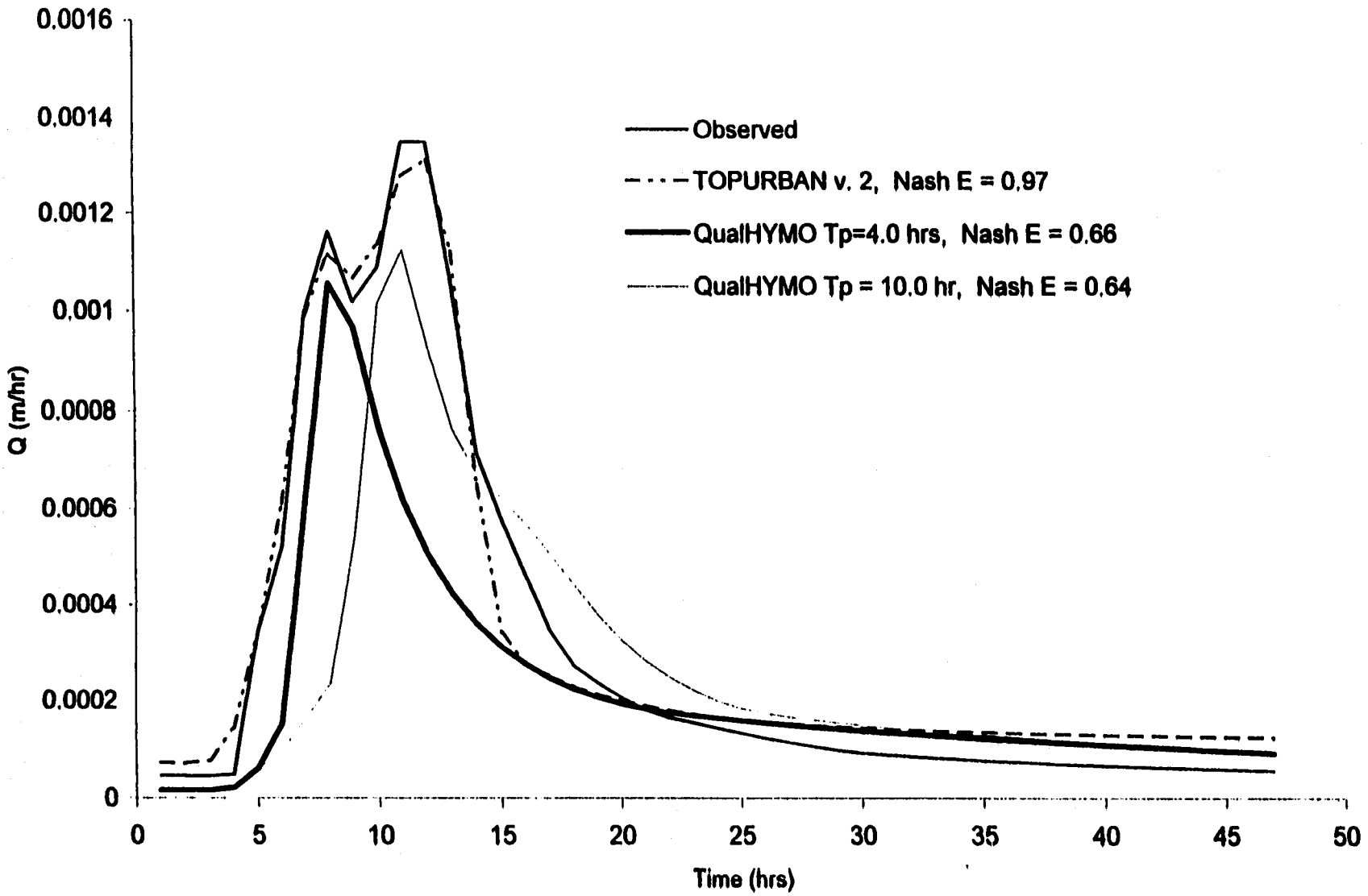

Figure 7.18: TOPURBAN v. 2 vs. QualHYMO for single event #1.

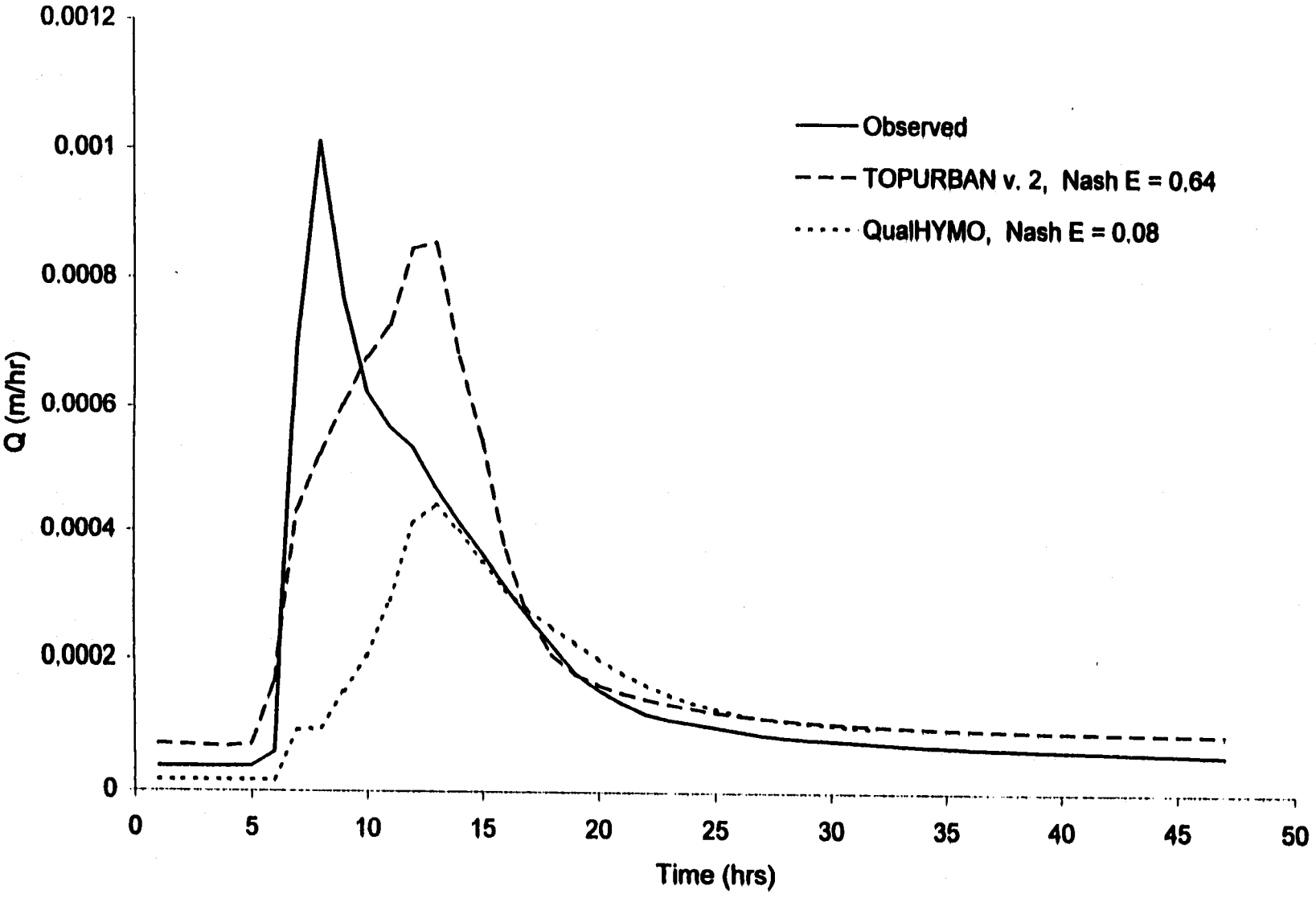

Figure 7.19: TOPURBAN v. 2 vs. QualHYMO for single event # 2.

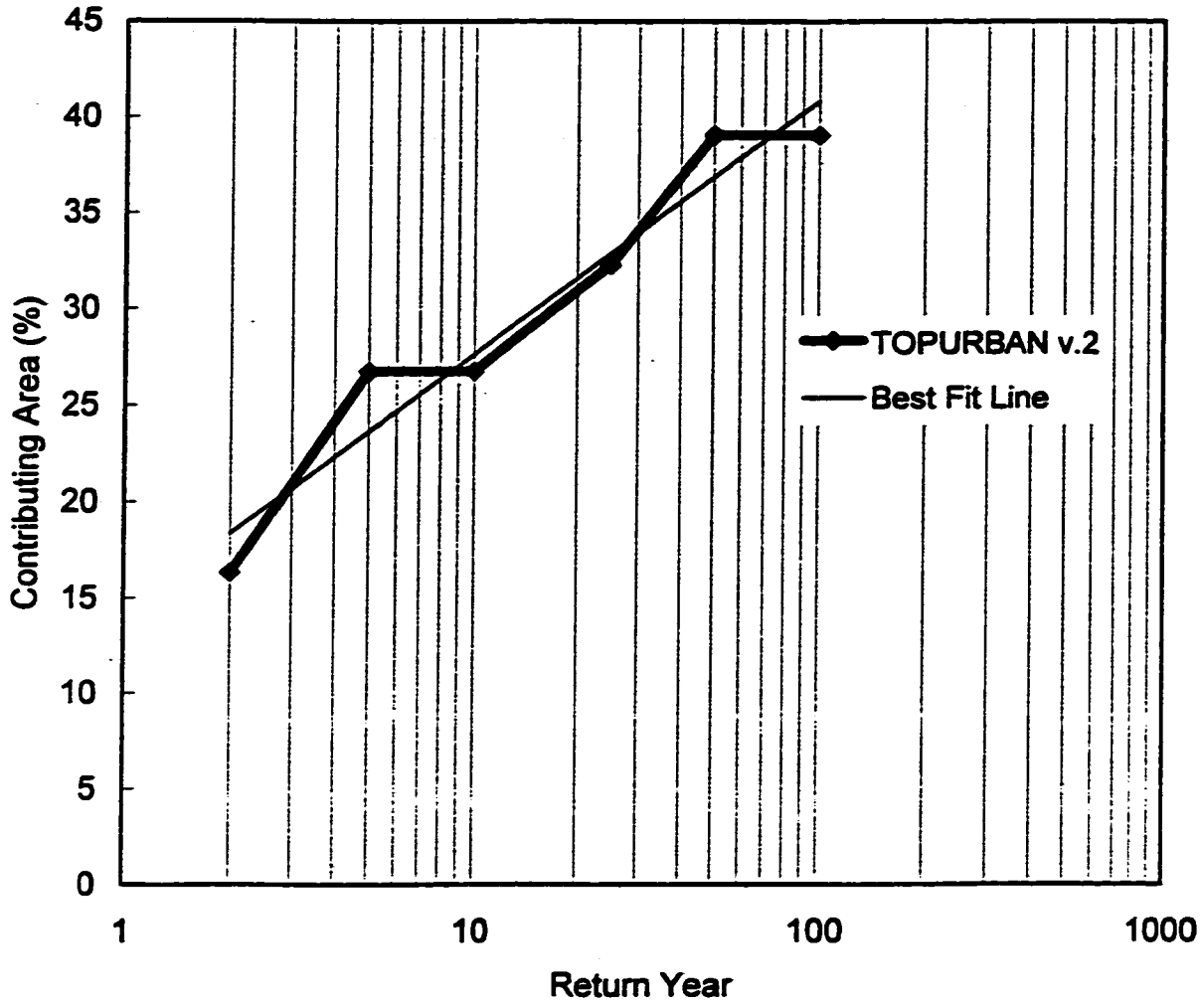

Figure 7.20: Source area vs. return period.

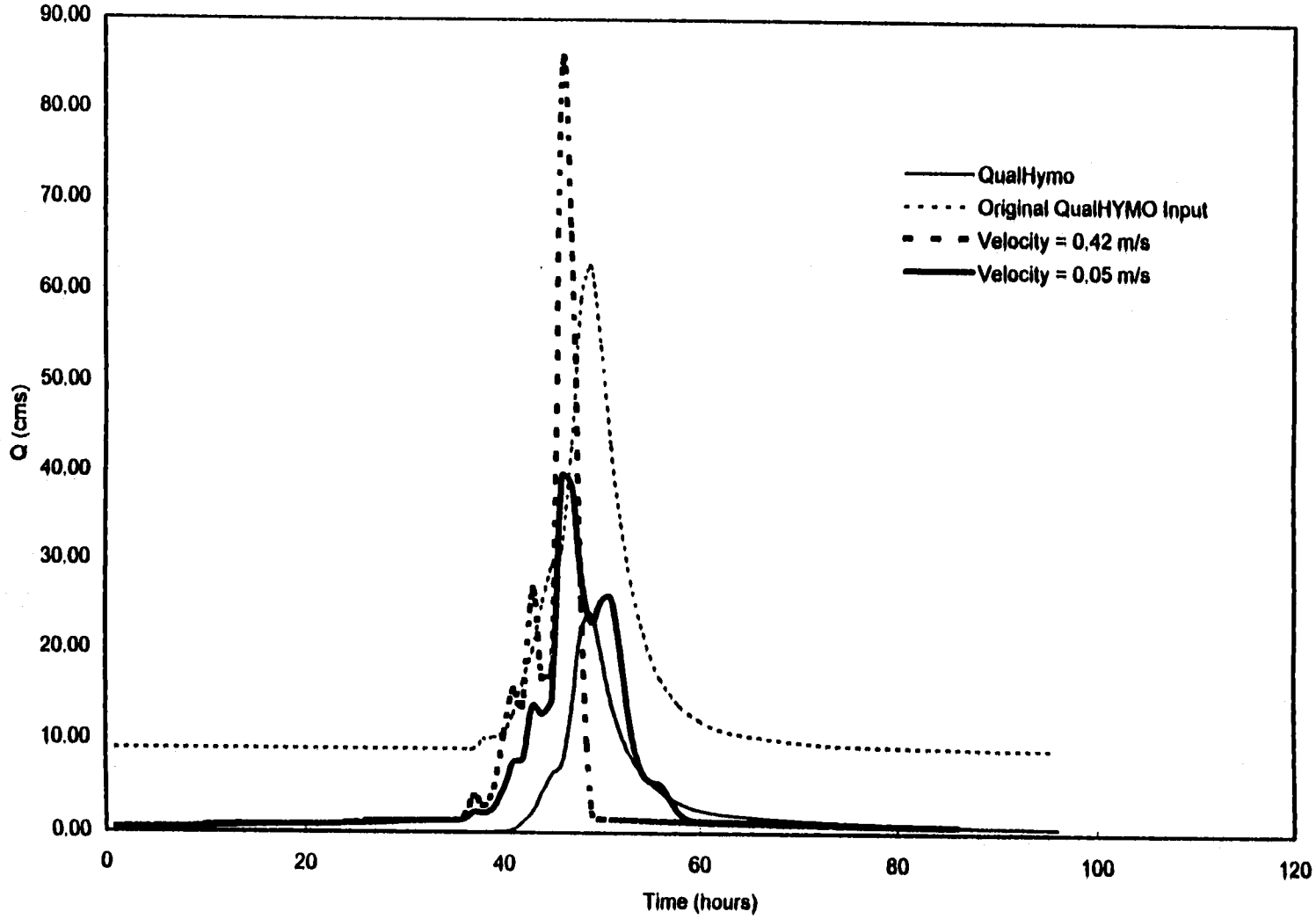

Figure 7.21: Hurricane Hazel Hydrographs.

CHAPTER 8 SUMMARY, CONCLUSIONS AND RECOMMENDATIONS

A plethora of hydrologic models exist for runoff prediction and they range from the most simplistic black box models with lumped parameter modeling to comprehensive physically-based models that account for heterogeneity and have numerous parameters. Both models have their advantages and disadvantages but neither is appropriate in a wide range of situations. Furthermore, traditional methods of runoff generation have subscribed to a Hortonian mechanism in which infiltration excess forms over the entire basin for all rain events after abstractions. In response to the deficiencies in these models, a relatively new class of models have emerged to account for the formation of variable source areas that are conceptual, and avoid the problems of physically-based models. The number of models of this type is small but one model in particular has been getting widespread attention because of its parametrically parsimonious approach to runoff generation from variable source areas. TOPMODEL can be applied in a distributed or semi-distributed way, and of the handful of parameters it employs, only a few require calibration. These parameters are derived from physically-based concepts and are theoretically measurable in the field.

Models such as TOPMODEL are, because of their nature, reserved for runoff generation in the medium of soil and are intended for use at the hillslope scale. But often, watersheds will have some degree of urbanization that can have enormous effects on observed flowrates. The conventional model of treating urbanization in watershed modeling is to completely decouple it from the non-urban portion of the watershed. This effectively removes not only the surface but the subsurface soil medium which can transmit flow. Saturation excess runoff is the rise of water table from below and depends on subsurface flow processes. If we are to properly account for variable sources of saturation excess, then urban areas should be incorporated in the modeling in a more meaningful way instead of completely decoupling the urban

component from the watershed. The objective of this research is to incorporate urban areas in TOPMODEL concepts.

8.1 Summary and Novel Contributions of this Dissertation

Chapter 2 presented the reader with an understanding for the differences in black-box, physically-based and conceptual models, as well as a more formal review of several well-established computer models of hydrology. The models were reviewed based on their technique for generating runoff, their treatment of heterogeneity and the number of parameters requiring calibration. The literature showed that few conceptual models address the concerns of hillslope hydrology and that urban and non-urban components of a catchment are decoupled entities in the hydrological process. The TOPMODEL concept was selected as the conceptual model of hillslope hydrology for this research. The theory was reviewed as well as the model's performance in real-world applications. It has earned a reputation for accurately modeling the soil contribution to flow in several cases. Following these reviews, the dissertation then proceeded to provide several novel contributions to the area of variable-source area modeling. They include the following:

8.1.1 Incorporating Urban Areas into TOPMODEL Concepts

Urban areas were incorporated in two ways in TOPMODEL: 1) in the formation of the topographic index which defines the propensity of a point to contribute to saturation excess overland flow, and 2) in an urban runoff generating mechanism that completely directed the flow to the stream. These two modifications created TOPURBAN v. 1 and involved increasing the number of parameters by one. The modifications to the topographic index generally lowered the average topographic index of the catchment by reducing those values in urban areas to lower values. Version 1 of TOPURBAN did not consider abstractions or urban storage. This

model increased the Nash and Sutcliffe efficiency of the modeling process from less than 50% to 75%. When no change was made to the formation of the topographic index, TOPURBAN could not perform as well as with the topographic index distribution that incorporated urban areas.

TOPURBAN v.1 was modified to incorporate a linear reservoir representation of urban storage. TOPURBAN v.2 essentially doubled the contribution of the urban component to flow volume. This version of the model performed on average, 5% better in Nash E value than its predecessor. TOPURBAN v.2 in general improved the overall performance in terms of volume and maximum peak flowrate predictions. The model is quite good at predicting time to peak, but has difficulty in predicting high flowrates.

8.1.2 Comparing TOPURBAN v. 2 to QualHYMO

TOPURBAN v. 2 was compared to the conventional Hortonian model QualHYMO on six data series, two separate single events, and the Hurricane Hazel regional storm. QualHYMO performed well on two series but in neither case did it reach the same efficiencies as TOPURBAN v. 2. QualHYMO had very high predictions of peak flow; far and above the under-predictions of TOPURBAN. QualHYMO did poorly in predicting single event peak flow after being calibrated on another event with similar antecedent moisture conditions in 1993; however, TOPURBAN fared better. Furthermore, applications of QualHYMO and TOPURBAN on Hurricane Hazel rain data revealed that QualHYMO can predict similar values of TOPURBAN flow for this event, but does so only through a majority of contribution from the urban areas where the Nash parameters are very small.

8.1.3 Aggregation Phase of Research

The aggregation study of this research examined different DEM sizes and calibrated a hydrological model using parameters derived for each of these DEMs on three separate years. A very wet year (1992), a very dry year (1988) and a moderately dry year (1991) were selected. The dry year of 1991 had many small rain events and one of the longer complete series and that is why it was also included in the aggregation study. A total of 21 different parameters including Nash and Sutcliffe Efficiency, the final optimized value of the objective function, peak flow predictions, minimum flow predictions, and hydrograph volumes were used to evaluate which DEM led to the calculation of parameters that provided the best fit of data against observed values. The research concluded that for the area in Ancaster, a 50 m cell size of Digital Elevation Model is suitable and provides the best fit of predicted to observed data.

8.1.4 Parameter Recommendations and Return Period Storms

TOPURBAN parameter sets were recommended for the three most influential parameters of the model in Section 7.2.2.3. These parameters can be used to provide a good starting point for hydrologic modeling in the area, but a calibration of the three parameters *m*, *Ko*, and Sr_{max} is recommended. There is some parameter interaction observed between *m*, *Ko*, *uacp* and Sr_{max}; however, reliability can be assured in the recommended parameters for this area. Using the parameters for the wet condition, a relationship was developed to relate the percentage of catchment area that is contributing to saturation excess overland flow to the return period of the event. The relationship states that the percentage of contributing area of catchment (including the urban component) is approximately six times the Naperian logarithm of the return period, plus approximately 20%.

8.2 Conclusions

The conclusions of this dissertation are the following:

1. An accurate and adequate representation of the urban component of a semi-urbanized watershed can be easily incorporated in a TOPMODEL conceptual framework without having to decouple the urban component from the non-urban component of the watershed.

2. A simple modification of the formation of the topographic index and the inclusion of up to two new parameters that do not require calibration can be incorporated to accurately model all runoff generating mechanisms in the catchment.

3. A recommended DEM size for the Ancaster Creek catchment is 50 m. The 50 m DEM was derived from Ontario Base Maps at a scale of 1:10,000 and this DEM size is also recommended for similar areas in Southern Ontario with similar levels of relief.

4. TOPURBAN v. 2 which incorporated urban storage performed better than TOPURBAN v. 1. It only included one additional parameter but effectively implied that the degree of impervious surface in Ancaster Creek catchment that is contributing to flow for all rain events is 8%.

5. TOPURBAN in general had some difficulty in certain cases predicting high peak flows but was able to predict peak flows to within roughly 10 - 20% for the last three years of the six year study. TOPURBAN did poorly on the very dry year of 1988. However, regardless of the quality assurance that was instigated in the data collection and assembling phase of this research, it is suspected that numerous errors exist in both the hydrometric and rainfall data of this year. When data was being assembled,

it was found that instrument malfunction often occurred during rain events. It is believed that errors exist in the 1988 data, the 1989 data and the 1992 data. For this reason greater weight should be given to 1990, 1991 and 1993 data series. The model generally performed better in these three years.

6. TOPURBAN version 2 outperformed a conventional model of infiltration excess in which the entire catchment contributes to flow. QualHYMO performed poorly on 4 of the six data series. Of the two data series it did perform well on, it could not perform as well as TOPURBAN. Furthermore, when TOPURBAN and QualHYMO were each calibrated to a single event, QualHYMO could not model a second event with similar antecedent moisture conditions as well as TOPURBAN. This may be an indication that TOPURBAN is modeling the flow process in a way that QualHYMO cannot.

7. The Hurricane Hazel predicted peak flowrate by TOPURBAN was between 40 and 84 m^3/s for the study area in this research. This range is comparable to the peak flowrate predicted by MacLaren Plansearch Ltd. using QualHYMO which is 63 m^3/s. However, this flowrate predicted by MacLaren is mostly due to the urban flow component, whereas in TOPURBAN, the majority of flow is generated by the soil. When the calibrated QualHYMO model parameters were used in an application with Hurricane Hazel rain data, the predicted flow rate was 24 m^3/s.

8.3 Recommendations for Future Research

The following tasks are recommended for future research,

1. Apply TOPURBAN v.2 to a greater number of data series that include accurate data in wet, dry and average years, in order to continually verify the model.

2. Apply TOPURBAN on other catchments in the area with varying degrees of urbanization, varying relief and varying basin size. This will verify the model for a wide variety of regions in Southern Ontario.

3. Implement a snow-melt component in order to model TOPURBAN year round. Therefore, an accurate value of maximum root zone size may be obtained in the calibration.

4. Implement a more sophisticated loss component in TOPURBAN such that losses due to interception are considered separately from losses due to evapotranspiration.

By following up on these research recommendations, integrated urban and rural flow modeling can be achieved by physically representing the runoff generating mechanisms in the catchment.

REFERENCES

Abbott, M.B., Bathurst, J.C., Cunge, J.A., O'Connell, P.E. and Rasmussen, J. (1986). "An introduction to the European Hydrological System - Systeme Hydrologique European, 'SHE', 1. History and philosophy of a physically-based distributed modeling system", *Journal of Hydrology*, **87**, pp. 45-59.

Abrahamse, M. (1997). Personal Communication. Environment Canada, Guelph, Ontario.

Ambroise, B., Beven, K.J. and Freer, J. (1996). "Toward a generalization of the TOPMODEL concepts: Topographic indices of hydrological similarity", *Water Resources Research*, **32**, (7), pp. 2135-2145.

Anderson, M.G. and Burt, T.P. (1985). "Modeling strategies", in Hydrological Forecasting, ed. by M.G. Anderson and T.P. Burt, John Wiley & Sons, pp. 1-13.

Aronoff, S. (1991). Geographic Information Systems: A Management Perspective, WDL Publications, Ottawa, Ontario.

Bathurst, J.C. (1986). "Physically-based distributed modelling of an upland catchment using the Systeme Hydrologique Europeen", *Journal of Hydrology*, **87**, pp.79-102.

Bathurst, J.C., Wicks, J.M. and O'Connell, P.E. (1995). The SHE/SHESED basin scale water flow and sediment transport modelling system", in Computer Models of Watershed Hydrology, ed. by V.P. Singh, Water Resources Publications, Highlands Ranch, Colorado, pp. 563-594.

Becker, A. and Nemec, J. (1987). "Macroscale hydrologic models in support to climate research", in The Influence of Climate Change and Climatic Variability on the Hydrologic Regime and Water Resources, Proceedings of the Vancouver Symposium, IAHS Publication no. 168.

Bergstrom, S. (1995). "The HBV model", in Computer Models of Watershed Hydrology, ed. by V.P. Singh, Water Resources Publications, Highlands Ranch, Colorado, pp. 443-476.

Betson, R.P. and Marius, J.B. (1969). "Source areas of storm runoff", *Water Resources Research*, **5**, (3), pp. 574-582.

Beven, K.J. (1982). "On subsurface stormflow, an analysis of response times", *Hydrological Sciences Journal*, **27**, pp.505-521.

Beven, K.J. (1984). "Infiltration into a class of vertically non-uniform soils", *Hydrological Sciences Journal*, **29**, (4), pp. 425-434.

Beven, K.J. (1986a). "Runoff production and flood frequency in catchments of order n: An alternative approach", in Scale Problems in Hydrology, ed. by V.K. Gupta, I. Rodriguez-Iturbe and E.F. Wood, pp. 107-131.

Beven, K.J. (1986b). "Hillslope runoff processes and flood frequency characteristics", in Hillslope Processes, ed. by A.D. Abrahams, Allen & Unwin, Boston, pp. 187-202.

Beven, K.J. (1987a). "Towards a new paradigm in hydrology", Water for the Future:Hydrology in Perspective, Proceedings of the Rome Symposium, IAHS publ. no. 164, pp. 393-403.

Beven, K.J. (1987b). "Towards the use of catchment geomorphology in flood frequency predictions", *Earth Surface Processes and Landforms*, **12**, pp. 69-82.

Beven, K.J. (1989a). "Interflow", in Unsaturated Flow in Hydrologic Modeling, Theory and Practice., ed. by H.J. Morel-Seytoux, Kluwer Academic Publishers, The Netherlands, pp. 191-219.

Beven, K.J. (1989b). "Changing ideas in hydrology - the case of physically-based models", *Journal of Hydrology*, **105**, pp.157-172.

Beven, K.J. (1991a). "Scale considerations", in Recent Advances in the Modeling of Hydrologic Systems, ed. by D.S. Bowles and P.E. O'Connell, Kluwer Academic Publishers, The Netherlands, pp. 357-371.

Beven, K.J. (1991b). "Spatially distributed modeling: conceptual approach to runoff prediction", in Recent Advances in the modeling of Hydrologic Systems, ed. by D.S. Bowles and P.E. O'Connell, Kluwer Academic Publishers, The Netherlands, pp. 373-387.

Beven, K.J. (1995). "Linking parameters across scales: subgrid parameterization and scale dependent hydrological models", *Hydrological Processes*, **9**, pp. 507-525.

Beven, K.J. and Kirkby, M.J. (1979). "A physically-based variable contributing area model of basin hydrology", *Hydrological Sciences Journal*, **24**, (1), pp.43-69.

Beven, K.J. and German, P. (1982). "Macropores and waterflow in soils", *Water Resources Research*, **18**, (5), pp. 1311-1325.

Beven, K.J. and Wood, E.F. (1983). "Catchment geomorphology and the dynamics of runoff contributing areas", *Journal of Hydrology*, **65**, pp.139-158.

Beven, K.J., Kirkby, M.J., Schofield, N. and Tagg, A.F. (1984). "Testing a physically-based flood forecasting model (TOPMODEL) for three U.K. catchments", *Journal of Hydrology*, **69**, pp.119-143.

Beven, K.J., Calver, A. and Morris, E.M. (1987). "The Institute of Hydrology distributed model", *Rep. 98*, Institute of Hydrology, Wallingford, U.K.

Beven, K.J., Lamb, R., Quinn, P., Romanowicz, R. and Freer, J. (1995). "TOPMODEL", in Computer Models of Watershed Hydrology, ed. by V.P. Singh, Water Resources Publications, Highlands Ranch, Colorado, pp. 627-668.

Blackie, J.R. and Eeles, C.W.O. (1985). "Lumped catchment models", in Hydrological Forecasting, ed. by M.G. Anderson and T.P. Burt, John Wiley & Sons, Ltd., Chichester, UK., pp. 311-344

Bruneau, P., Gascuel-Odoux, C., Robin, P., Merot, Ph. and Beven, K.J. (1995). "Sensivity to space and time resolution of a hydrological model using digital elevation data", *Hydrological Processes*, **9**, pp. 69-81.

Burman, R. and Pochop, L.O. (1994). Evaporation, Evapotranspiration and Climatic Data,. Elsevier Science B.V., The Netherlands.

Burnash, R.J.C. (1995). "The NWRS river forecast system - catchment modelling", in Computer Models of Watershed Hydrology, ed. by V.P. Singh, Water Resources Publications, Highlands Ranch, Colorado, pp. 311-366.

Burt, T.P. and Butcher, D.P. (1985). "Topographic controls of soil moisture distributions", *Journal of Soil Science*, **36**, pp. 469-486.

Calver, A. and Wood, W.L. (1995). "The Institute of Hydrology distributed model", in Computer Models of Watershed Hydrology, ed. by V.P. Singh, Water Resources Publications, Highlands Ranch, Colorado, pp. 595-626.

Carson, M.A. and Sutton, E.A. (1971). "The hydrologic response of the Eaton River Basin, Quebec", *Journal of Earth Sciences*, **8**, (102), pp. 102-115.

Chairat, S. (1993). "Adapting a physically based hydrologic model with a Geographic Information System for runoff prediction in a small watershed", Doctoral Thesis, Department of Civil Engineering, Purdue University, West Lafayette, Indiana.

Chorely, R.J. (1978). "The Hillslope Hydrological Cycle", in Hillslope Hydrology by M.J. Kirkby, ed., John Wiley & Sons, Ltd., Chichester, Great Britain, pp.1-42.

Chow, V.T., Maidment, D.R., Mays, L.W. (1988). Applied Hydrology, McGraw-

Hill, Inc., New York, N.Y.

Clark, C.O. (1945). "Storage and unit hydrograph", *Trans. Am. Soc. Civ. Engrs.*, **110**, pp. 14616-1446.

Cordova, J.R. and Rodriguez-Iturbe, I. (1983). "Geomorphoclimatic estimation of extreme flow probabilities", *Journal of Hydrology*, **65**, pp. 159-173.

Crawford, N.H. and Linsley, R.K.,Jr. (1966). "Digital simulation in hydrology: Stanford Watershed Model IV", *Technical Report No. 39*, Department of Civil Engineering, Stanford University, Stanford, California.

Cruise, J.F. and Contractor, D.N. (1980). "Unit hydrographs for urbanizing watersheds", *Journal of the Hydraulics Division*, Proceedings of the American Society of Civil Engineers, **106**, (HY3), pp. 440-445.

Donigian, A.S. Jr., Bicknell, B.R. and Imhoff, J.C. (1995). "Hydrological Simulation Program - Fortran (HSPF)", in Computer Models of Watershed Hydrology, ed. by V.P. Singh, Water Resources Publications, Highlands Ranch, Colorado, pp. 395-442.

Dunne, T. (1978). "Field studies of hillslope flow processes", in Hillslope Hydrology by M.J. Kirkby, ed., John Wiley & Sons, Ltd., Chichester, Great Britain, pp. 227-293.

Dunne, T. and Black, R.D. (1970a). "Partial area contributions to storm runoff in a small New England watershed", *Water Resources Research*, **6**, (5), pp. 1296-1311.

Dunne, T. and Black, R.D. (1970b). "An experimental investigation of runoff production in permeable soils", *Water Resources Research*, **6**, (2), pp. 478-490.

Dunne, T., Moore, T.R. and Taylor, C.H. (1975). "Recognition and prediction of runoff-producing zones in humid regions", *Hydrology Science Bulletin*, **20**, pp. 305-327.

Durand, P., Robson, A. and Neal, C. (1992). "Modelling the hydrology of submediterranean Montane catchments (Mont-Lozere, France) using TOPMODEL: initial results", *Journal of Hydrology*, **139**, pp. 1-14.

Environment Canada. (1993a). "Active Hydrometric Stations, Ontario", Environmental Monitoring Branch, Environment Canada, Guelph, Ontario.

Environment Canada. (1993b). Canadian Climate Normals, 1961-1990, Atmospheric Environment Service, Ottawa, Canada.

ESRI. (1990). Understanding GIS, The ARC/INFO Method, Revision 6,

Environmental Systems Research Institute, Inc,. Redlands, California.

Famiglietti, J.S. and Wood, E.F. (1994a). "Multiscale modeling of spatially variable water and energy balance processes", *Water Resources Research*, **30**, (11), pp. 3061-3078.

Famiglietti, J.S. and Wood, E.F. (1994b). "Application of multiscale water and energy balance models on a tall grass prairie", *Water Resources Research*, **30**, (11), pp. 3079-3093.

Famiglietti, J.S. and Wood, E.F. (1994c). "Effects of spatial variability and scale in areally averaged evapotranspiration", *Water Resources Research*, **31**, (3), pp. 699-712.

Feldman, A.D. (1995) "HEC-1 Flood Hydrograph Package", in Computer Models of Watershed Hydrology, ed. by V.P. Singh, Water Resources Publications, Highlands Ranch, Colorado, pp. 119-150.

Fleming, G. (1975). Computer Simulation Techniques in Hydrology, American Elsevier Publishing Company, Inc., New York, N.Y.

Fleming, G. (1979). "Deterministic Models in Hydrology", Food and Agriculture Organization of the United Nations, FAO Irrigation and Drainage Paper No. 32, Rome, pp. 80.

Franchini, M. and Pacciani, M. (1991). "Comparative analysis of several conceptual rainfall-runoff models", *Journal of Hydrology*, **122**, pp.161-219.

Franchini, M., Wendling, J., Obled C. and Todini, E. (1996). "Physical interpretation and sensitivity analysis of the TOPMODEL", *Journal of Hydrology*, **175**, pp.293-338.

Freeze, R.A. (1972). "Role of subsurface flow in generating surface runoff, 2: upstream source areas", *Water Resources Research*, **8**, (5), pp. 1272-1283.

Freeze, R.A. (1974). "Streamflow generation", *Reviews of Geophysics and Space Physics*, **12**, (4), pp. 627-647.

Freeze, R.A. and Harlan, R.L. (1969). "Blueprints for a physically-based digitally simulated hydrologic response model", *Journal of Hydrology*, **58**, pp.205-221.

Grayson, R.B., Moore, I.D. and McMahon, T.A. (1992). "Physically-based hydrologic modeling, 2. Is the concept realistic", *Water Resources Research*, **26**, (10), pp. 2659-2666.

Grayson, R.B., Bloschl, G. and Moore, I.D. (1995). "Distributed parameter hydrologic modelling using vector elevation data: THALES and TAPES-C", in

Computer Models of Watershed Hydrology, ed. by V.P. Singh, Water Resources Publications, Highlands Ranch, Colorado, pp. 669-696.

Gregory, K.J. and Walling, D.E. (1973). Drainage Basin Form and Process A geomorphologial approach, John Wiley & Sons, New York, N.Y.

Gupta, V.K., Rodriguez-Iturbe, I. and Wood, E.F. (1986). Scale Problems in Hydrology, D. Reidel Publishing Company, Dordrecht, Holland.

Hall, M.J. (1984). Urban Hydrology, Elsevier Applied Sci., UK.

Heeps, D.P. and Mein, R.G. (1974). "Independent comparison of three urban runoff models." *Journals of the Hydraulics Division*, Proceedings of the American Society for Civil Engineers, **100**, (HY7), pp. 995-1009.

Hohner, B.K. (1996). Private Communication. Ontario Land Resource Unit, Greenhouse and Processing Crops Research Centre, Guelph, Ontario.

Hornberger, G.M., Beven, K.J., Cosby, B.J. and Sappington, D.E. (1985). "Shenandoah watershed study: calibration of a topography-based, variable contributing area hydrological model to a small forested catchment", *Water Resources Research*, **21**, (12), pp.1841-1850.

Horton, R.E. (1933). "The role of infiltration in the hydrologic cycle", *Transactions of the American Geophysical Union*, **1**, pp. 446-460.

Horvat, T. (1996). "Summary of Hurricane Fran storm event", Memorandum to Water Management and Environmental Impact Advisory Board, Hamilton Region Conservation Authority, Dundas, Ontario, 6 pp.

Huber, W.C. (1995). "EPA storm water management model-SWMM", in Computer Models of Watershed Hydrology, ed. by V.P. Singh, Water Resources Publications, Highlands Ranch, Colorado, pp. 783-808.

Hutchinson, M.F. (1989). "A new procedure for gridding elevation and stream line data with automatic removal of spurious pits", *Journal of Hydrology*, **106**, pp. 211-232.

Institute of Hydrology. (1980). "Low flow studies", Report No. 3, Wallingford, Oxon, UK. 27, pp.

Iorgulescu, I. and Jordan, J.P. (1994). "Validation of TOPMODEL on a small Swiss catchment", *Journal of Hydrology*, **159**, pp.255-273.

Islam, S. (1996). "Why bother for 0.0001% of Earth's water? Challenges for soil moisture research", EOS, **77**, (43), pp. 420.

Jordan, J.P. (1994). "Spatial and temporal variability of stormflow generation

process on a Swiss catchment", *Journal of Hydrology*, **153**, pp. 357-382.

Karrow, P.F. (1963). "Pleistocene geology of the Hamilton-Galt area", Ontario Department of Mines, Field Report 16, 68 pp.

Kirkby, M.J., ed. (1978). Hillslope Hydrology, John Wiley & Sons, Ltd., Chichester, Great Britain.

Kite, G. W. (1975). "The SLURP Model", in Computer Models of Watershed Hydrology, ed. by V.P. Singh, Water Resources Publications, Highlands Ranch, Colorado, pp. 521-562.

Knisel, W.G. and Williams, J.R. (1995). "Hydrology components of CREAMS and GLEAMS models", in Computer Models of Watershed Hydrology, ed. by V.P. Singh, Water Resources Publications, Highlands Ranch, Colorado, pp. 1069-1112.

Lamb, R. (1996). "Distributed hydrological prediction using a generalised TOPMODEL concepts," Doctoral Thesis, University of Lancaster, UK.

Leavesley, G.H. and Stannard, L.G. (1995). "The precipitation-runoff modelling system - PRMS", in Computer Models of Watershed Hydrology, ed. by V.P. Singh, Water Resources Publications, Highlands Ranch, Colorado, pp. 281-310.

Linsley, R.K. (1967). "The relation between rainfall and runoff", *Journal of Hydrology*, **5**, pp. 297-311.

Linsley, R.K. Jr., Kohler, M.A., Paulhus, J.L.H. (1982). Hydrology for Engineers, McGraw-Hill, New York, N.Y.

Loague, K. (1990). "R-5 revisted, 2: Reevaluation of a quasi-physically based rainfall-runoff model with supplemental information", *Water Resources Research*, **26**, (5), pp. 973-987.

MacLaren (1990). "Spencer Creek Watershed Hydrology Study Volumes I and II", Report to the Hamilton Region Conservation Authority by MacLaren Plansearch, Ontario.

Marsalek, J., Dick, T.M., Wisner, P.E. and Clarke, W.G. (1975). "Comparative evaluation of three urban runoff models", *Water Resources Bulletin*, American Water Resources Association, **11**, (2), pp. 306-328.

Mathews, J.H. (1987). Numerical Methods for Computer Science, Engineering, and Mathematics, Prentice-Hall International, London.

McBride, R. (1996). Personal Communication. Land Resources Science, University of Guelph, Guelph, Ontario.

Merot, Ph., Ezzahar, B., Walter, C. and Aurousseau, P. (1995). "Mapping waterlogging of soils using digital terrain models", *Hydrological Processes*, **9**, pp. 27-34.

Moin, S.M.A and Shaw, M.A. (1986). "Canada/Ontario flood damage reduction program, Regional flood frequency analysis for Ontario streams, Vol. 2 Multiple Regression Method", Canadian Center for Inland Waters, Environment Canada, Burlington, Ontario, 87 pp.

Nash, J.E. (1957). "The form of the instantaneous unit hydrograph", *International Association of Scientific Hydrology Publication*, **45**, (3), pp. 114-21.

Nash, J.E. and Sutcliffe, J.V. (1970). "River flow forecasting through conceptual models, Part I - a discussion of principles", *Journal of Hydrology*, **10**, pp. 282-290.

Nyberg, L. (1996). "Spatial variability of soil water content in the covered catchment at Gardsjon, Sweden", *Hydrological Process,* **10**, pp. 89-103.

Obled, C., Wedling, J. and Beven, K.J. (1994). "The sensitivity of hydrological models to spatial rainfall patterns: an evaluation using observed data", *Journal of Hydrology*, **159**, pp. 305-333.

O'Loughlin, E.M. (1981). "Saturation regions in catchments and their relations to soil and topographic properties", *Journal of Hydrology*, **53**, pp.229-246.

O'Loughlin, E.M. (1986). "Prediction of surface saturation zones in natural catchments by topographic analysis", *Water Resources Research*, **22**, (5), pp. 794-804.

O'Loughlin, G., Huber, W. and Chocat, H. (1996). "Rainfall-runoff proceses and modeling", *Journal of Hydraulic Research*, **34**, (6), pp. 733-751.

OMOE (Ontario Ministry of the Environment). (1985). "QualHYMO Manual", Environment Canada, Ottawa, Ontario.

Ontario Ministry of Natural Resources. (1985). Flood Plain Management in Ontario - Technical Guidelines. Ottawa, Ontario.

Ontario Department of Mines. (1969). Southern Ontario Drift Thickness Series, Map 2043, Hamilton Area.

Philips Planning & Engineering Ltd. (1987). "Master drainage plan, Town of Ancaster", Project 86003 for the Hamilton Region Conservation Authority, Burlington, Ontario.

Presant, E.W., Wicklund, R.E. and Matthews, B.C. (1965). "The soils of

Wentworth County", Report No. 32 of the Ontario Soil Survey, Canada Department of Agriculture and Ontario Department of Agriculture, Ottawa, Ontario.

Quinn, P.F. (1991). "The Role of Digital Terrain Analysis in Hydrological Modelling", PhD Dissertation, Lancaster University, Lancaster, U.K.

Quinn, P.F. and Beven, K.J. (1993). "Spatial and temporal predictions of soil moisture dynamics, runoff, variable source areas and evapotranspiration for Plynlimon, Mid-Wales", *Hydrological Processes*, **7**, pp. 425-448.

Quinn, P.F., Beven, K.J. and Lamb, R. (1995). "The ln(a/tanβ) index: how to calculate it and how to use it within the TOPMODEL framework", *Hydrological Process*, **9**, pp. 161-182.

Rao, R.A., Delleur, J.W. and Sarma, B.S.P. (1972). "Conceptual hydrological models for urbanizing basins", *Journal of Hydraulics Division, Proceedings of the ASCE*, HY7, pp. 1205-1220.

Robson, A.J., Whitehead, P.G. and Johnson, R.C. (1993). "An application of a physically based semi-distributed model to the Balquidder catchments", *Journal of Hydrology*, **145**, pp.357-370.

Romanowicz, R., Beven, K.J. and Moore, R. (1993). "GIS and distributed hydrological models." in Geographic Information Handling ed. by P.M. Mather, John Wiley & Sons, Ltd., pp 197-205.

Royal Botanical Gardens. (1995). "Annual Meteorological Summary", Hamilton, Ontario.

Rutter, A.J., Marton, A.J. and Robins, P.C. (1975). "A predictive model of rainfall interception in forests. II: Generalization of the model and comparison with observations in some coniferous and hardwood stands", *Journal of Applied Ecology*, **12**, pp. 367.

Sherman, L.K. (1932). "Stream flow from rainfall by the unit graph method", *Engineering News-Record*, **108**, pp. 501-505.

Singh, V.P. (1989a). Hydrologic Systems, Vol. I., Rainfall-Runoff Modelling, Prentice-Hall, Englewood Cliffs, New Jersey.

Singh, V.P. (1989b). Hydrologic Systems, Vol. II., Watershed Modelling, Prentice-Hall, Englewood Cliffs, New Jersey.

Singh, V.P. ed. (1995). Computer Models of Watershed Hydrology, Water Resources Publications, Highlands Ranch, Colorado.

Singh, V.P. and Chowdhury, P.K. (1986). "Comparing some methods of estimating mean areal rainfall", *Water Resources Bulletin*, **22**, (2), pp. 275-82.

Sivapalan, M., Beven, K.J. and Wood, E.F. (1987). "On hydrologic similarity 2. A scaled model of storm runoff production", *Water Resources Research*, **23**, (12), pp. 2266-2278.

Sklash, M.G. and Farvolden, R.N. (1979). "The role of groundwater in storm runoff", *Journal of Hydrology*, **43**, pp.45-65.

Smith, M. (1990). "Report on the expert consultation on revision of FAO methodologies for crop water requirements", Land and Water Development Division, Food and Agriculture Organization of the United Nations, Rome, Italy.

Smith, R.E., Goodrich, D.C., Woolhiser, D.A. and Unkrich, C.L. (1995). "KINEROS-A KINematic Runoff and EROsion model", in Computer Models of Watershed Hydrology, ed. by V.P. Singh, Water Resources Publications, Highlands Ranch, Colorado, pp. 697-732.

Soil Conservation Service. (1972). National Engineering Handbook, Section 4, Hydrology, US Department of Agriculture, Washington, D.C.

Song, Z. and James, L.D. (1992). "An objective test for hydrologic scale", *Water Resources Bulletin*, **28**, (15), pp. 833-844.

Sorooshian, S. and Gupta, V.K. (1995). "Model Calibration", in Computer Models of Watershed Hydrology, ed. by V.P. Singh, Water Resources Publications, Highlands Ranch, Colorado, pp. 23-68.

Speers, D.D. (1995). "SSARR Model", in Computer Models of Watershed Hydrology, ed. by V.P. Singh, Water Resources Publications, Highlands Ranch, Colorado, pp. 367-394.

Sugawara, M. (1995). "Tank Model", in Computer Models of Watershed Hydrology, ed. by V.P. Singh, Water Resources Publications, Highlands Ranch, Colorado, pp. 165-214.

Troch, P.A., Smith, J.A., Wood, E.F. and de Troch, F.P. (1994). "Hydrologic controls of large floods in a small basin: central Appalachian case study", *Journal of Hydrology*, **156**, pp. 285-309.

Troendle, C.A. (1985). "Variable source area models", in Hydrological Forecasting, ed. by M.G. Anderson and T.P. Burt, John Wiley & Sons Ltd., New York, N.Y. pp. 347-403

US Geological Survey. (1992). "Standards for Digital Elevation Models", National

Mapping Program Technical Instructions, United States Department of Interior, National Mapping Division, Reston, Virginia.

US Geological Survey. (1993). "Digital Elevation Models, Data Users Guide 5", United States Department of Interior, Reston, Virginia.

Viessman, W. (1966). "The hydrology of small impervious areas", *Water Resources Research*, **2**, (3), pp. 405-412.

Viessman, W. (1970). "Urban storm runoff relations", *Water Resources Research*, **6**, (1), pp. 275-279.

Viessman, W., Lewis, G.L. and Knapp, J.W. (1989). Introduction to Hydrology, 3rd ed., Harper Collins Publishers, New York, N.Y.

Waters, D., Jenkins, A., Staples, J. and Donald, A.P. (1991). "The importance of hydrological source areas in terrestrial limnology", *J.IWEM*, (5), pp. 336-341.

Watt, W.E. (1989). Hydrology of Floods in Canada A Guide to Planning and Design, National Research Council, Ottawa, Ont.

Weyman, D.R. (1970). "Throughflow on hillslopes and its relation to the stream hydrograph." *Bull. Int. Assoc. Sci. Hydrol.*, **2** (6), pp. 25-33.

Whipkey, R.Z. (1965). "Subsurface stormflow from forested slopes", *Bull. Int. Assoc. Sci. Hydrol.*, **10**, (2), pp. 74-85.

Williams, J.R. (1995). "The EPIC model", in Computer Models of Watershed Hydrology, ed. by V.P. Singh, Water Resources Publications, Highlands Ranch, Colorado, pp. 909-1000.

Williams, J.R. and Hahn, R.W. Jr. (1973). "HYMO: Problem-Oriented Computer Language for Hydrologic Modeling Users Manual", Agricultural Research Service, U. S. Department of Agriculture, ARS-S-9.

Wolock, D.M., Hornberger, G.M., Beven, K.J. and Campbell, W.G. (1989). "The relationship of catchment topography and soil hydraulic characteristics to lake alkalinity in the Northeastern United States", *Water Resources Research*, **25**, (5), pp. 829-837.

Wolock, D.M. and Horberger, G.M. (1991). "Hydrological Effects of Changes in Levels of Atmospheric Carbon Dioxide", *Journal of Forecasting*, **10**, pp.105-116.

Wolock, D.M. and Price, C.V. (1994). *Water Resources Research*, **30**, (11), pp. 3041-3052.

Wolock, D.M and McCabe, G.J.Jr. (1995). "Comparison of single and multiple

flow direction algorithms for computing topographic parameters for TOPMODEL", *Water Resources Research*, **31**, (5), pp. 1315-1324.

Wood, E.F., Sivaplan, M., Beven, K.J. and Band, L. (1988). "Effects of spatial variability and scale with implications to hydrologic modelling", *Journal of Hydrology*, **102**, pp. 29-47.

Wood, E.F., Sivapalan, M. and Beven, K.J. (1990). "Similarity and scale in catchment storm response", *Reviews of Geophysics*, **28**, (1), pp. 1-18.

Zhang, W. and Montgomery, D.R. (1994). "Digital elevation model grid size, landscape representation, and hydrologic simulations", *Water Resources Research*, **30**, (4), pp. 1019-1028.

Zhao, R.J. and Liu, X.R. (1995). "The Xinanjiang Model", in Computer Models of Watershed Hydrology, by V.P. Singh, Water Resources Publications, Highlands Ranch, Colorado, pp. 215-232.

APPENDICES

A0: List of symbols used in the Appendices.

English Alphabet (uppercase followed by lowercase letters)

A	catchment or subcatchment area (m^2)
A_k	fraction of area flowing through channel segment l_k
A_s	moisture content in a soil column (m)
A_z	moisture content in a soil column when saturated to a height (Z-z) (m)
AR_k	histogram ordinate in overland flow routing scheme
B	channel width (m)
C	Muskingum-Cunge routing constant
C_1, C_2, C_3	Muskingum-Cunge routing coefficients
Cdelta	slope vapour pressure curve ($kPa°C^{-1}$)
D	Muskingum-Cunge channel constant
D_{ji}	distance between rain gauge i and element j (m)
D_{min}, D_{max}	evaluation statistics (see Section 6.2.3 for a full description)
E	potential evapotranspiration array (m/day)
ER	extraterrestrial radiation ($Mjm^{-2}d^{-1}$)
F_{RV}	overland flow velocity factor
F_{CHV}	channel flow velocity factor
FLG	channel routing flag
G	soil heat flux ($Mjm^{-2}d^{-1}$)
I_j	inflow hydrograph at time j
Ko	hydraulic conductivity (m/hr)
N_E	number of elements
N_R	number of rain gauges
N_{RV}	number of internal channel segments
N_h	number of hours through which flow is routed
O_j	outflow hydrograph at time j
P	atmospheric pressure (kPa)
P_i	depth of rainfall at gauge i (m)
R_j	depth of rainfall at element j (m)
$R_{x,y}$	depth of rainfall at element (x,y) (m)
$\bar{R}$	average depth of rainfall on catchment (m)
RNH	minimum daily relative humidity array (%)
RXH	maximum daily relative humidity array (%)

S	soil moisture deficit (m)
S_o	bed slope
Sr_{max}	maximum size of root zone (m)
Sr_o	initial size of root zone deficit (m)
SN	hours of sunshine array (hr)
Q_k	runoff generated at time t (m/hr)
Q_k^t	fraction of flow that arrives at time (k+t-1) (m/hr)
Q_o	initial subcatchment discharge (m/hr)
T_d	unsaturated zone time delay constant (hr/m)
T_k	length of time it takes to travel through segment l_k
T_{RV}	travel time of overland flow through catchment (hr)
V	volume of rainfall on catchment (m^3)
W	average windspeeds array (m/s)
X	wedge storage constant
YNT	minimum daily temperature array (°C)
Z	depth of soil column (m)
ZXT	maximum daily temperature array (°C)
a_j	area of element j (m^2)
aw	adjust wind speeds (m/s)
ambda	latent heat of vapour (°C)
c	kinematic wave celerity (m/s)
delta	solar declination (rad)
dres	relative earth-sun distance
ea	saturation vapour pressure (kPa)
ed	actual vapour pressure (kPa)
gamma	psychometric constant ($kPa°C^{-1}$)
i	rain gauge index
j	element index or day index
k	time index or channel segment index
k_M	Muskingum-Cunge lag constant
$\ln(a/\tan\beta)$	topographic index
l_k	channel subdivision length (m)
m	recession parameter (m)
q	channel flow per unit channel width (m^2/s)
rnc	net radiation at crop surface ($MJm^{-2}d^{-1}$)
rnl	net longwave radiation ($MJm^{-2}d^{-1}$)

rns	net shortwave radiation ($MJm^{-2}d^{-1}$)
rsf	relative sunshine fraction
shr	sunset hour angle (rad)
t	time (hr)
uacp	urban area calibration parameter
v_j	volume of rainfall falling on element j (m^3)
vpd	vapour pressure deficit (kPa)
v_{CHV}	user defined channel velocity (m/hr)
v_{RV}	user defined overland flow velocity (m/hr)
w_i	weight applied to rain gauge
z	depth in soil column to saturated zone (m)
zk	urban storage recession constant (hr)

Greek Alphabet (upper case followed by lower case letters)

Δx	channel segment length (m)
Δt	time step (hr)
Σ	evaluation statistics (see Section 6.2.3 for a full description)
$\Sigma 1$	evaluation statistics (see Section 6.2.3 for a full description)
θ_r	residual volumetric moisture content
θ_r	volumetric moisture content in saturated part of column

A1: Relationship between soil moisture and depth to water table.

Assume that when a column is completely saturated, that A_s is the amount of moisture in the column in meters. Then,

$$A_s = Z\,\theta s \tag{A1.1}$$

where θs is the volumetric moisture content in the saturated column (no units) and Z is the depth of the column. Let A_z be the moisture content in the column when the column is saturated up to a height of $(Z - z)$. Then,

$$A_z = (Z - z)\,\theta s + z\,\theta r \tag{A1.2}$$

where θr is the residual volumetric moisture content in the depth z (i.e., that section at the top which is unsaturated). Now the soil moisture deficit of the column S is equal to the difference between A_s and A_z, therefore,

$$S = A_s - A_z \tag{A1.3}$$

$$S = Z\theta s - [(Z - z)\,\theta s + z\,\theta r] \tag{A1.4}$$

$$S = (\theta s - \theta r)\,z \tag{A1.5}$$

A2: Overland flow routing method used in TOPMODEL.

This section describes the overland flow routing method used in the TOPMODEL version of this dissertation. This method is modeled after Clark's (1945) Time-Area method and involves a number of equations.

Divide the subcatchment or catchment into N_{RV} channel segments, where each segment has a length l_k (m) and the fraction of subcatchment area draining into that segment is A_k. The user selects an overland flow speed v_{RV}. Then histogram ordinates AR_k are constructed to distribute the runoff generated at time t, Q^t, through N_h number of hours,

$$Q_k^t = Q^t AR_k \tag{A2.1}$$

where the flow Q_k^t (m) arrives at time $(t+k-1)$ and,

$$N_h = \frac{T_{RV}}{\Delta t} \tag{A2.2}$$

T_{RV} (hr) is described in Equation (4.5) and Δt is the time step used in the model. If T_k is the time it takes for the flow to travel down segment l_k then naturally,

$$T_k = \frac{l_k}{v_{RV}} \tag{A2.3}$$

And the histogram ordinates are computed using the following,

```
loop over i
jΔt = [integer (T_RV) - integer(T_1)] + iΔt
loop over k
when jΔt ≤ T_k
```

$$AR_i = A_{k-1} + (A_k - A_{k-1})\frac{(j\Delta t - T_{k-1})}{(T_k - T_{k-1})} \tag{A2.4}$$

```
end k loop
end i loop
```

A3: Sample TOPOGRID input file.

While in ARC type in the following command,

```
SETENV GRIDALLOCSIZE 80
```

The following AML (Arc Macro Language) program runs TOPOGRID and shows the input parameters used. Those terms not in bold are user specified and may be either parameters or file names.

```
TOPOGRID ANCDEM10 10
RESET
ENFORCE ON
DATATYPE CONTOUR
ITERATIONS 40
MARGIN 0.0
TOLERANCES 0.015 2.0 5.0
XYZLIMITS 580200.75 780644.062 586982.312 788141.375
POINT SPOTS ZVALUE
CONTOUR CONTOUR_C ZVALUE
STREAM WRIVERS
OUTPUTS ASINK10 ADRAIN10 AF10.TXT
END
```

Then while in GRID correct DEM errors by using the FILL command,

FILL ANCDEM10 ANCDEMOUT **SINKS**

A4: Derivation of RDS method for a Digital Elevation Model.

By the RDS method (Singh 1990b), for a basin descretized into small but finite elements, the depth of rainfall (m) at element *j* at location *(x,y)* is equal to,

$$R_{x,y} = \frac{\sum_{i=1}^{N_R} \frac{P_i}{D_{ji}^2}}{\sum_{i=1}^{N_R} \frac{1}{D_{ji}^2}} = R_j \qquad \text{(A4.1)}$$

where N_R is the number of rain gauges surrounding the basin; D_{ij} is the distance (m) between the gauge *i* and the element *j* at location (x,y); and P_i is the rainfall measured at gauge *i* (m). If V is the total volume of rain falling on the catchment (m^3) and A is the catchment area (m^2), then the average value of rainfall is,

$$\bar{R} = \frac{V}{A} \qquad \text{(A4.2)}$$

If v_j is the volume of rainfall (m^3) on element *j* at location *(x,y)* then,

$$V = \sum_{j=1}^{N_E} v_j \qquad \text{(A4.3)}$$

where N_E is the number of elements or cells in the catchment. If the area of each element is a_j (m^2) , then,

$$\bar{R} = \frac{\sum_{j=1}^{N_E} v_j}{\sum_{j=1}^{N_E} a_j} = \frac{\sum_{j=1}^{N_E} R_j a_j}{\sum_{j=1}^{N_E} a_j} \qquad \text{(A4.4)}$$

therefore,

$$\bar{R} = \frac{\sum_{j=1}^{N_E} \left(\frac{\sum_{i=1}^{N_R} \frac{P_i}{D_{ji}^2}}{\sum_{i=1}^{N_R} \frac{1}{D_{ji}^2}} \right) a_j}{\sum_{j=1}^{N_E} a_j} \qquad \text{(A4.5)}$$

In the case of a DEM created by `TOPOGRID`, all the a_j are equal then,

$$\sum_{j=1}^{N_E} a_j = a + a + a + a + \ldots\ldots = aN_E \qquad \text{(A4.6)}$$

Therefore,

$$\bar{R} = \frac{a \sum_{j=1}^{N_E} \left(\frac{\sum_{i=1}^{N_R} \frac{P_i}{D_{ji}^2}}{\sum_{i=1}^{N_R} \frac{1}{D_{ji}^2}} \right)}{aN_e} \qquad \text{(A4.7)}$$

$$\bar{R} = \frac{1}{N_E} \sum_{j=1}^{N_E} \left(\frac{\sum_{i=1}^{N_R} \frac{P_i}{D_{ji}^2}}{\sum_{i=1}^{N_R} \frac{1}{D_{ji}^2}} \right) \qquad \text{(A4.8)}$$

If you group the terms in Equation A4.8 and sum terms with the common P_i, then the following equation is easily deduced,

$$w_i = \frac{1}{N_E} \sum_{j=1}^{N_E} \frac{\frac{1}{D_{ji}^2}}{\sum_{i=1}^{N_R} \frac{1}{D_{ji}^2}} \qquad \text{(A4.9)}$$

and,

$$\bar{R} = \sum_{i=1}^{N_R} w_i P_i \qquad \text{(A2.10)}$$

A5: ARC/INFO commands used to implement RDS method.

Begin with a point coverage of rain gauges. Select each rain gauge in turn and save it to a separate point coverage. Therefore, if the point coverage which shows the location of rain gauge A is called **A** then, the following AML will compute rain gauge weights w_i shown in Equation A4.9, using ARC/INFO.

Step 1: Convert the point coverage **A** with the location of rain gauge A to grid **AGRD** (after the cell size has been set to the desired DEM size using SETCELL). Run the following commands for every rain gauge.

```
AGRD = POINTGRID(A)
```

Step 2: Using the EUCDISTANCE function create **EUD_A** such that each cell has the distance between the indicator cell (the location of the rain gauge A) in **AGRD** and every other cell in **AGRD**.

```
EUD_A = EUCDISTANCE(AGRD)
```

Step 3: Clip out the catchment boundary in **EUD_A** by using the CON command (note that # in the command below would be the value of those cells that are non zero in **CATCHMENT**, that is, the value of those cells that are within the catchment boundary). Set all cells inside the catchment boundary to the value of **EUD_A** and all values outside the catchment boundary to 0.

```
E_A = CON(CATCHMENT == #, EUD_A, 0)
```

Step 4: Calculate the inverse of each cell value and multiply by the cell area.

```
INV_A = (1 DIV E_A) * 10000
```

Step 5: Square the grid **INV_A**.

```
INP_A = POW(INV_A, 2)
```

Step 6: Add all the **INP_** grids that were created in the line above for each rain gauge.

```
DENOM = INP_A + ......
```

Step 7: Compute the following quantity.

```
NUM = INP_A / DENOM
```

Step 8: Set the following scalar value.

```
W_A = SCALAR(0)
```

Step 9: Run the following DOCELL loop that sums all the values in **NUM** in order to obtain the weight **(W_A)** in Equation A4.9 For rain gauge A.

```
DOCELL
     W_A = += NUM
ENDCELL
```

A6: Equations used in computing potential evapotranspiration using the Penman-Monteith method.

The listing below is part of FORTRAN computer program, so the equations will not be numbered.

E array holds the potential evapotranspiration values (m/hr); *ZXT* array holds the daily maximum temperature values (°C); *YNT* array holds the daily minimum temperature values (°C); *SN* array holds the hours of sunshine per day; *RXH* array holds the daily maximum relative humidity values (%); *RNH* array holds the daily minimum relative humidity values (%); *W* array holds the average wind speeds (m/s).

Step 1: Compute the number of the day of the year that is provided by the user (`Nstart`). Assign *j*, as the index of each day, beginning with the start of the series (`Nstart`) and ending with the number of days (`Ndays`) which is also provided by the user..

```
Start Loop on j from Nstart to Ndays
j = j + 1
```

Step 2: Solar Declination *delta* (rad)

```
delta = 0.409*SIN(0.0172*float(j) - 1.39)
```

Step 3: Relative Distance Earth-Sun *dres*

```
dres = 1 + 0.033*COS(0.0172*float(j))
```

Step 4: Sunset Hour Angle *shr* (rad)

```
shr = ACOS(-TAND(float(LAT))*TAN(float(delta)))
```

Step 5: Extraterrestrial Radiation *ER* ($MJm^{-2}d^{-1}$)

```
ER = 37.6 *dres*(shr*SIND(float(LAT))*SIN(float(delta))
+COSD(float(LAT))*COS(float(delta))*SIN(float(shr)))
```

Step 6: Relative Sunshine Fraction *rsf*

```
rsf = SN(i) / (7.64*shr)
```

Step 7: Net Shortwave Radiation *rns* ($MJm^{-2}d^{-1}$)

```
rns = 0.77*(0.25+0.5*rsf)*ER
```

Step 8: Latent heat of vapour *ambda* (°C)

```
T = (YNT(i) + ZXT(i))/2
ambda = 2.501 - (0.002361*T)
```

Step 9: Atmospheric Pressure *P* (kPa)

```
TO = 273 + T
P = 101.3*((TO - 0.0065*ELEV)/TO)**5.26
```

Step 10: Psychometric Constant *gamma* ($kPa°C^{-1}$)

```
gamma = 0.00163*P/ambda
```

Step 11: Saturation Vapour Pressure *ea* (kPa)

```
eax = 0.611*exp(17.27*ZXT(i)/(ZXT(i)+237.3))
ean = 0.611*exp(17.27*YNT(i)/(YNT(i)+237.3))
ea = (eax + ean)/2
```

Step 12: Actual Vapour Pressure *ed* (kPa)

```
ed = RXH(i)*ean/200 + RNH(i)*eax/200
```

Step 13: Slope vapour pressure curve *Cdelta* ($kPa°C^{-1}$)

```
Cdelta = 4098*ea/(T + 237.3)**2
```

Step 14: Net longwave radiation *rnl* ($MJm^{-2}d^{-1}$)

```
rnl = 0.00000000245*(0.9 * rsf +0.1)*(0.34 -0.14*SQRT(ed))
*((ZXT(I)+273)**4 +(YNT(i)+273)**4)
```

Step 15: Net radiation at crop surface *rnc* ($MJm^{-2}d^{-1}$)

```
rnc = rns - rnl
```

Step 16: Vapour pressure deficit *vpd* (kPa)

```
vpd = (eax + ean)/2 - ed
```

Step 17: Soil flux (daily temp fluctuations and effective soil depth of 0.18m) *G* ($MJm^{-2}d^{-1}$)

```
Tg = T - (ZXT(i-1)+YNT(i-1))/2
G = 0.38*(Tg)
```

Step 18: Adjust wind speed (measured at 10 m) to 2 m height *aw* (m/s)

```
aw = 0.75*W(i)
```

Step 19: Evapotranspiration values (m/day)

```
evap = (0.408*Cdelta*(rnc - G) + gamma*(900/(T+273
))*aw*(ea-ed))/(Cdelta + gamma*(1+0.34*aw))
```

Now convert the daily values to hourly values using sine curves (make necessary changes for leap years).

```
Cum = -1
Fac = 1 + SIN(6.283185*Float(j)/366. - 1.570796)
DET = evap
DStart = 10 - 2.5*Fac
Dlength = 6 + 4*Fac
DFin = DStart + DLength
Loop over IT from 1 to 24
   Frac = (IT*DT-DStart)/DLength
   CUMT = - COS(Frac*3.14159265)
   E(IT) = (0.5 * DET*(CUMT - CUM))/1000
   CUM = CUMT
   End loop over IT
End loop over j
```

A7: Muskingum-Cunge routing equations.

The wedge storage constant X is computed as,

$$X = \frac{1}{2}\left(1 - \frac{q}{S_o c \Delta x}\right) \qquad 0 \le X \le \frac{1}{2} \tag{A7.1}$$

where q is the channel flow per unit channel width (m^2/s), S_o is the bed slope, c is the kinematic wave celerity (m/s) and Δx is the channel segment width (m), and the lag constant k_M

$$k_M = \frac{\Delta x}{c} \tag{A7.2}$$

$$C = \frac{c \Delta t}{\Delta x} \tag{A7.3}$$

$$D = \frac{q}{S_o c \Delta x} \tag{A7.4}$$

$$2X = (1 - D) \qquad C = \frac{\Delta t}{k_M} \tag{A7.5}$$

where C is a routing constant, D is a channel constant and Δt is the computation time step. The routing coefficients, C_1, C_2 and C_3 are,

$$C_1 = \frac{1 - C + D}{1 + C + D} \qquad C_2 = \frac{1 + C - D}{1 + C + D} \qquad C_3 = \frac{-1 + C + D}{1 + C + D} \tag{A7.6}$$

$$O_j = C_1 O_{j-1} + C_2 I_{j-1} + C_3 I_j \tag{A7.7}$$

Where O_j is the outflow hydrograph at time index j and I_j is the inflow hydrograph at time index j. The following parameters were derived through the use of information in the ARC/INFO database using the ARC/INFO software:

Table A7.1: Various subcatchment parameters and topographic characteristics.

DEM	S_o		
	Hwy 403 to Maple Lane $\Delta x = 850.92$ m B = 2.6 m	Maple Lane to Golf Links $\Delta x = 1060.98$ m B = 2.9 m	Golf Links to Wilson St. $\Delta x = 1692.70$ m B = 3.5 m
10	0.032	0.023	0.027
15	0.028	0.019	0.021
20	0.027	0.018	0.019
25	0.029	0.021	0.021
30	0.027	0.020	0.022
40	0.023	0.019	0.020
50	0.023	0.019	0.018
60	0.026	0.022	0.023
80	0.023	0.019	0.017
100	0.027	0.021	0.016

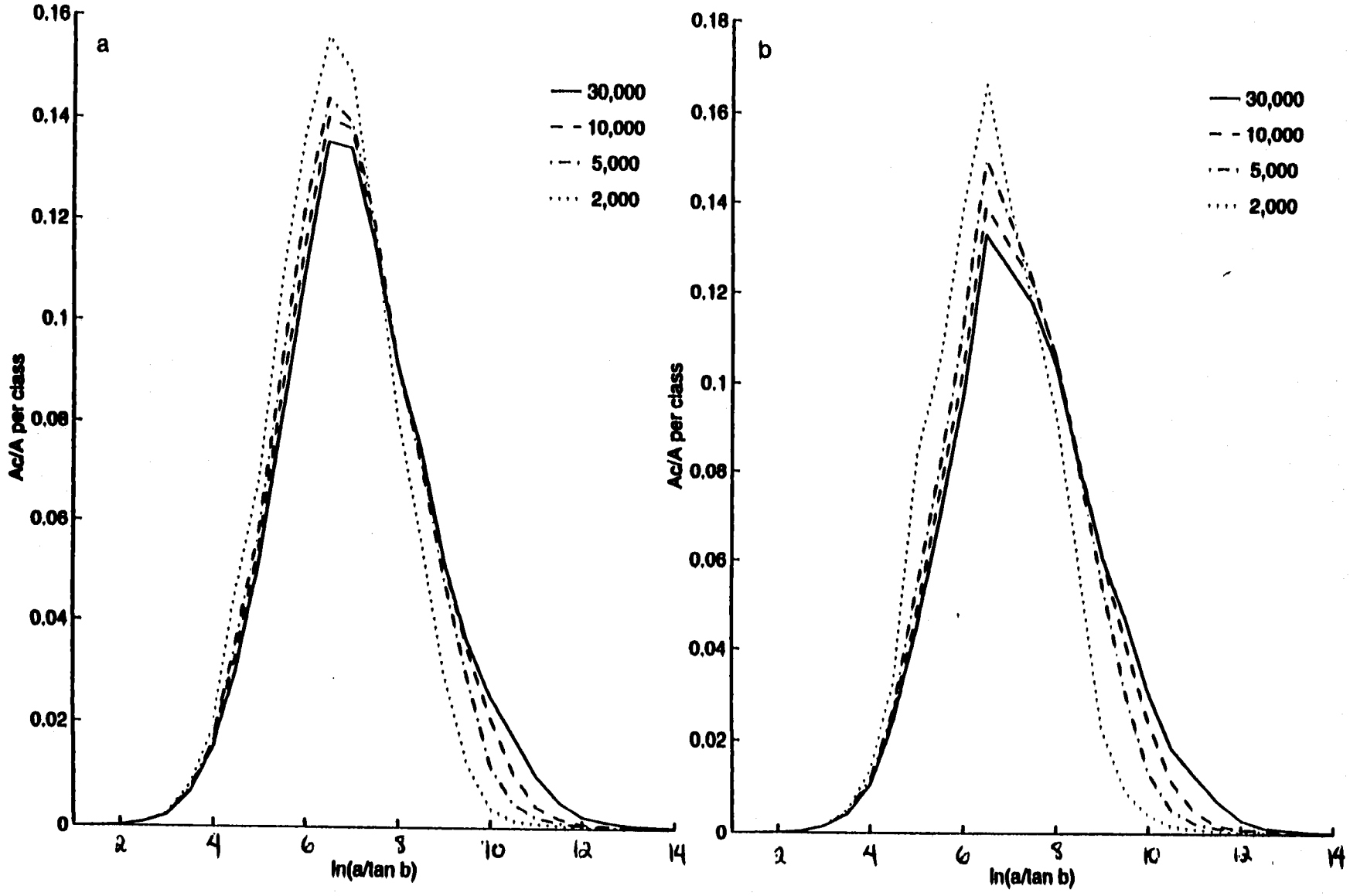

A8: Topographic Index Distribution for various river threshhold treatment levels for a) 10 m DEM and b) 15 m DEM.

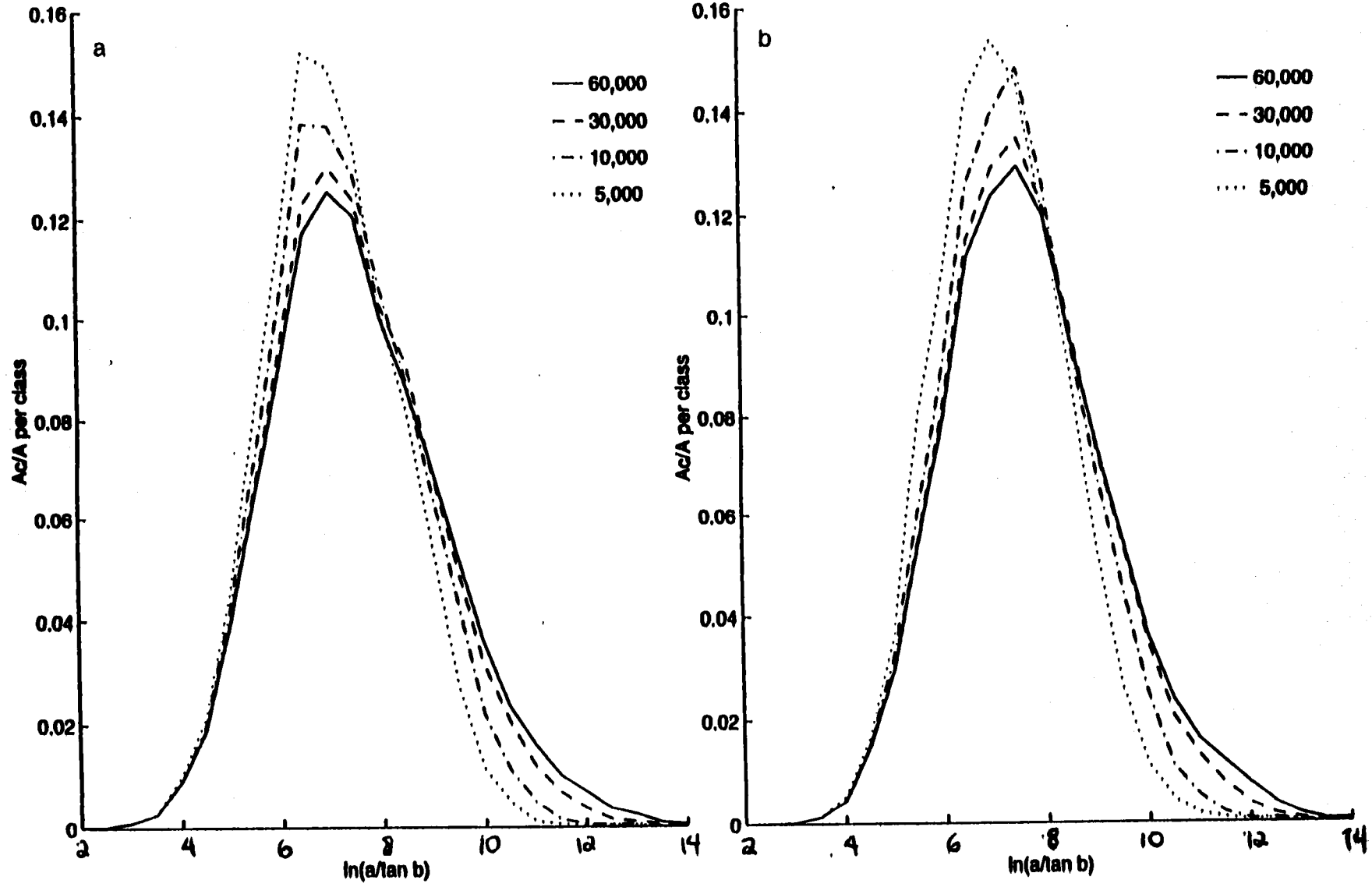

A9: Topographic Index Distribution for various river threshhold treatment levels for a) 20 m DEM and b) 25 m DEM.

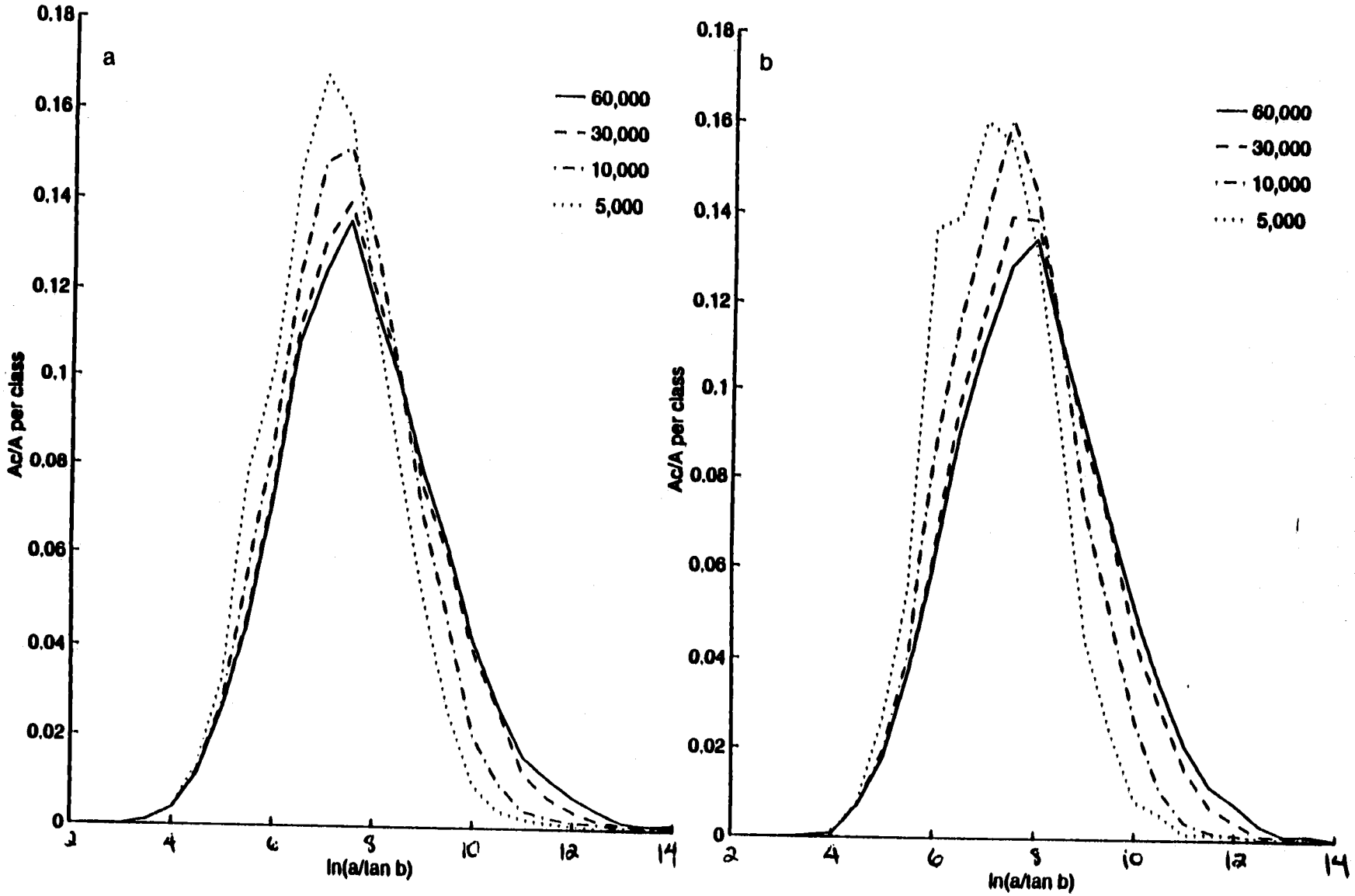

A10: Topographic Index Distribution for various river threshhold treatment levels for a) 30 m DEM and b) 40 m DEM.

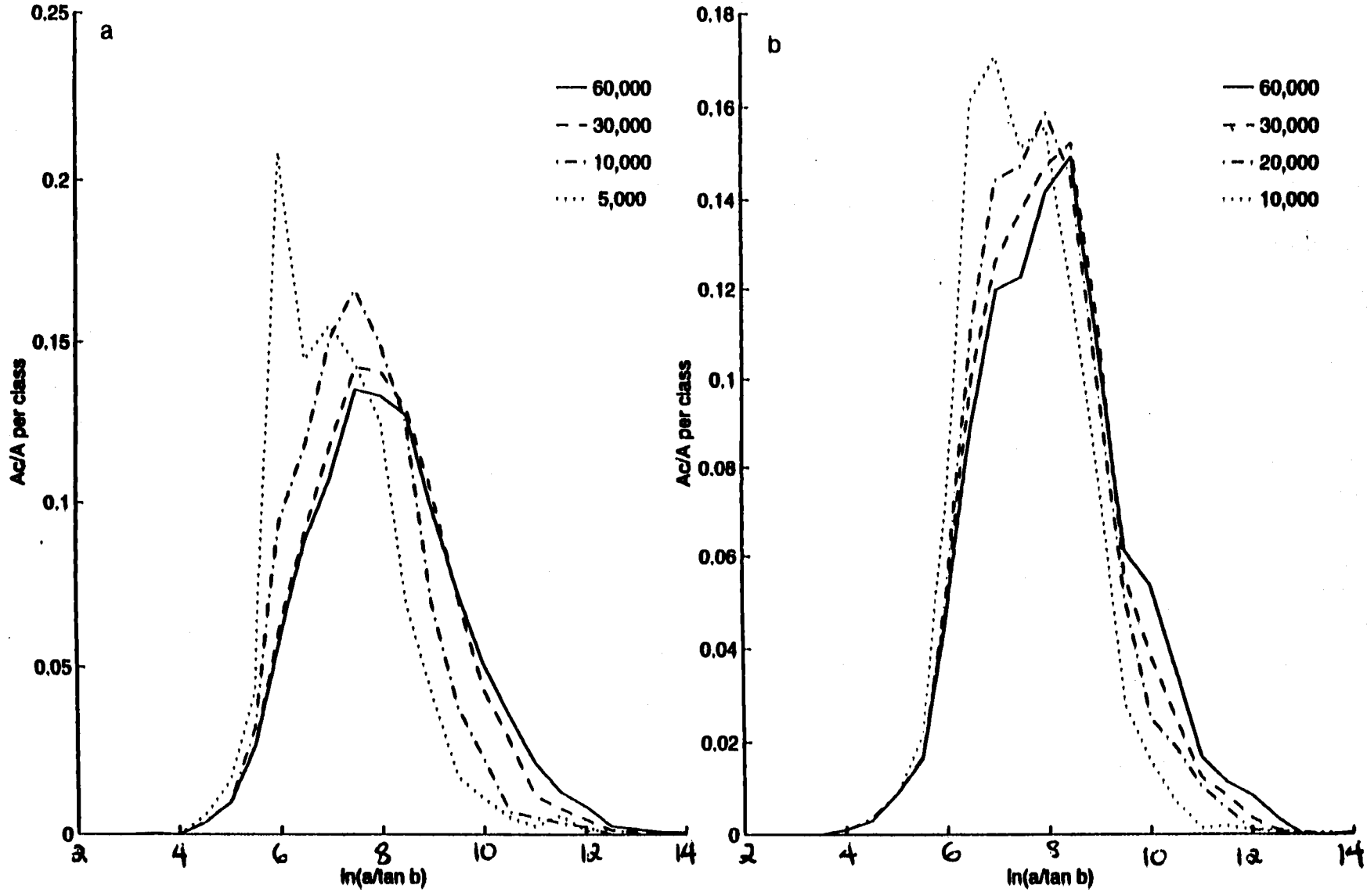

A11: Topographic Index Distribution for various river threshhold treatment levels for a) 50 m DEM and b) 60 m DEM.

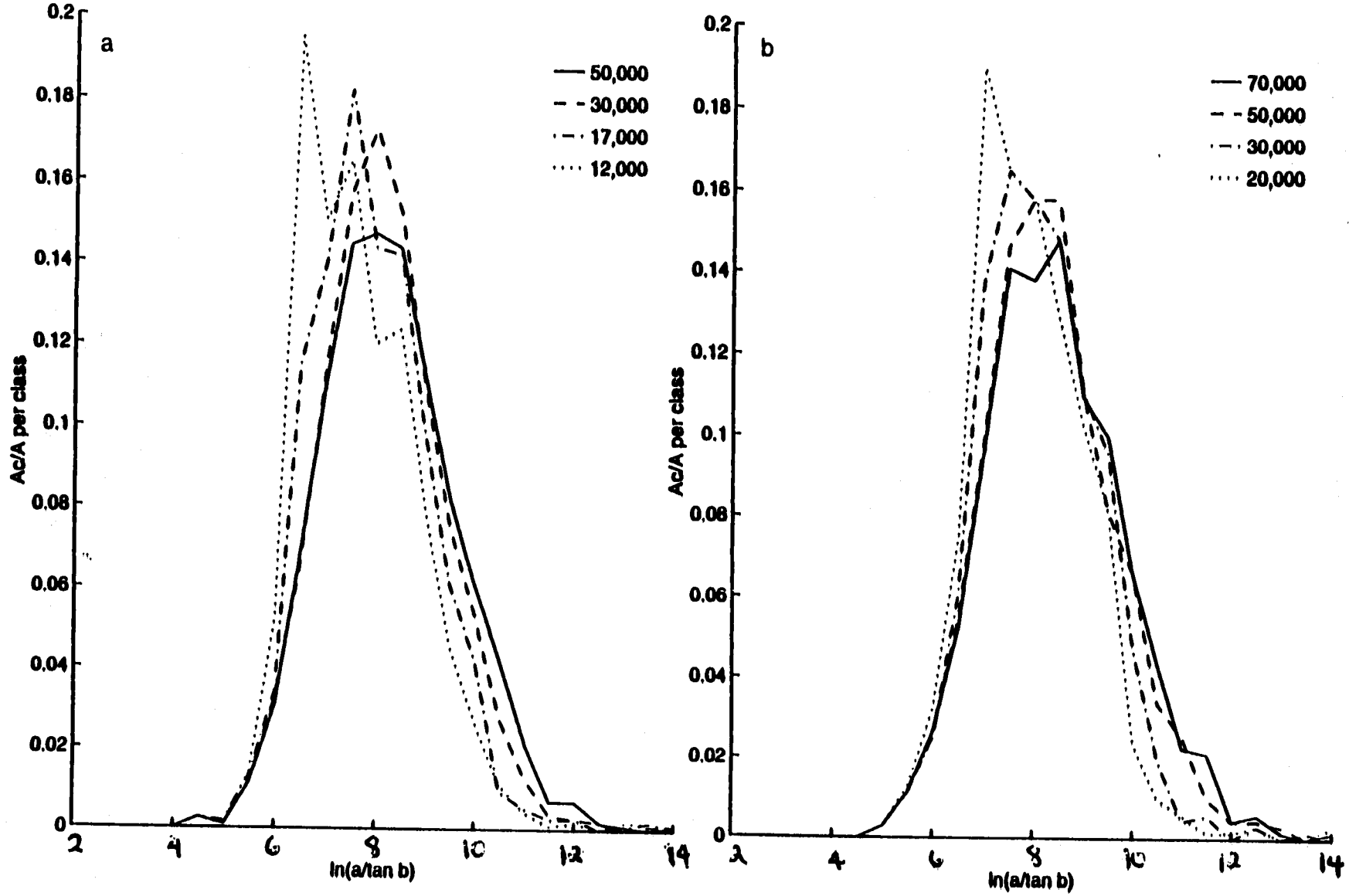

A12: Topographic Index Distribution for various river threshhold treatment levels for a) 80 m DEM and b) 100 m DEM.

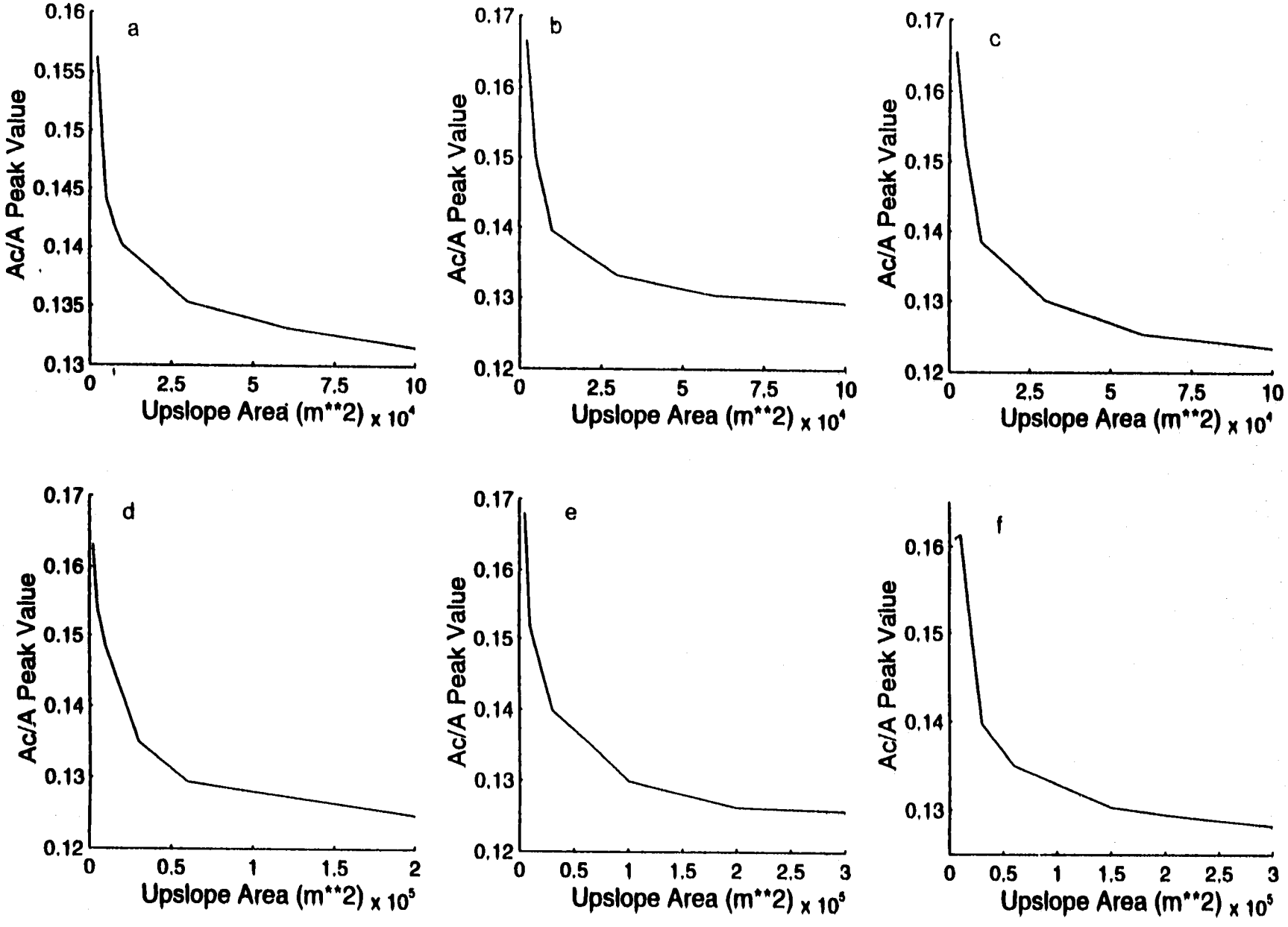

A13: Fraction of land area per topographic index class vs upslope area for DEMS of a) 10; b) 15; c) 20; d) 25; e) 30 and f) 40 m.

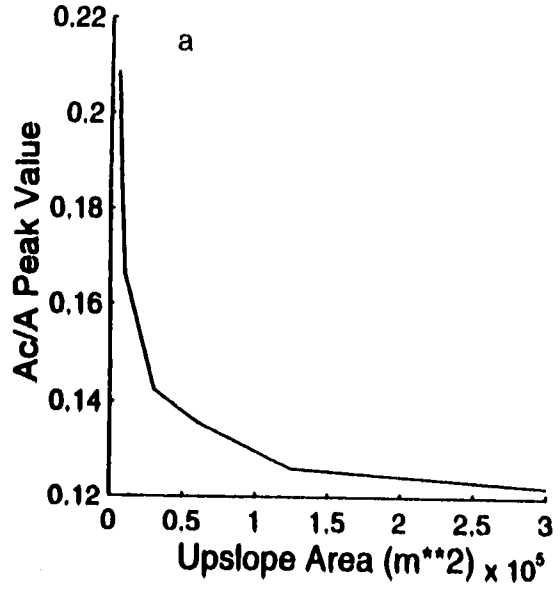

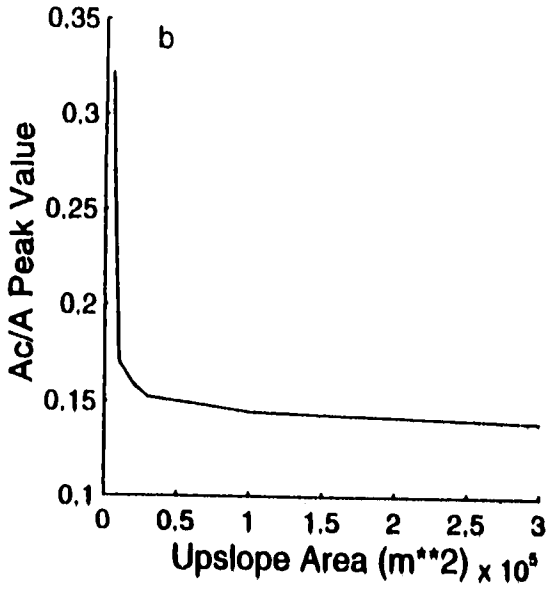

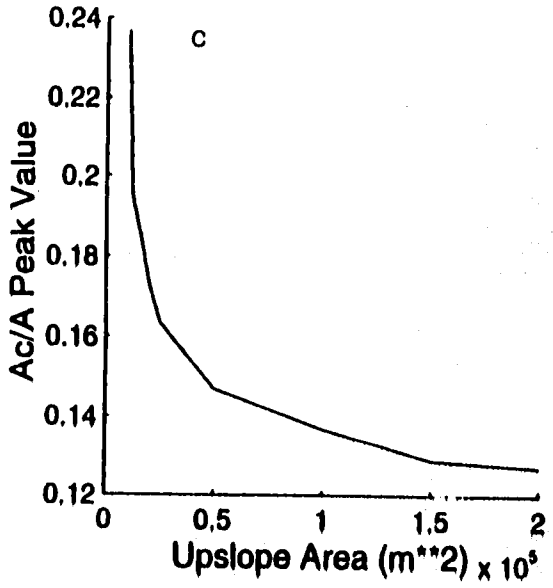

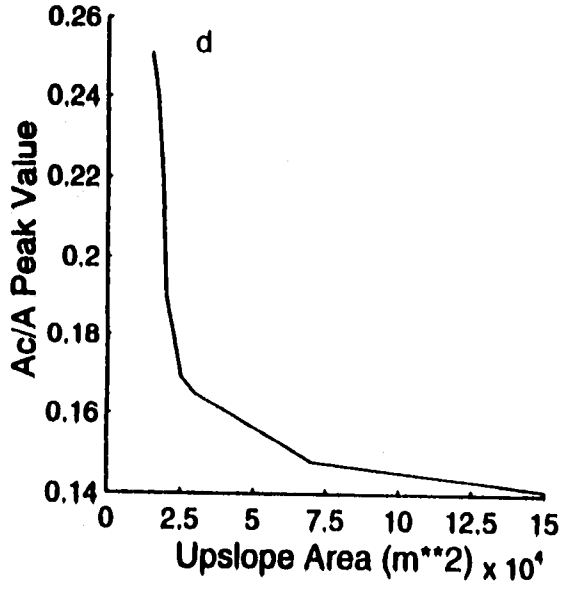

A14: Fraction of land area per topographic index class vs upslope area for DEMS of a) 50; b) 60; c) 80 and d) 100 m.

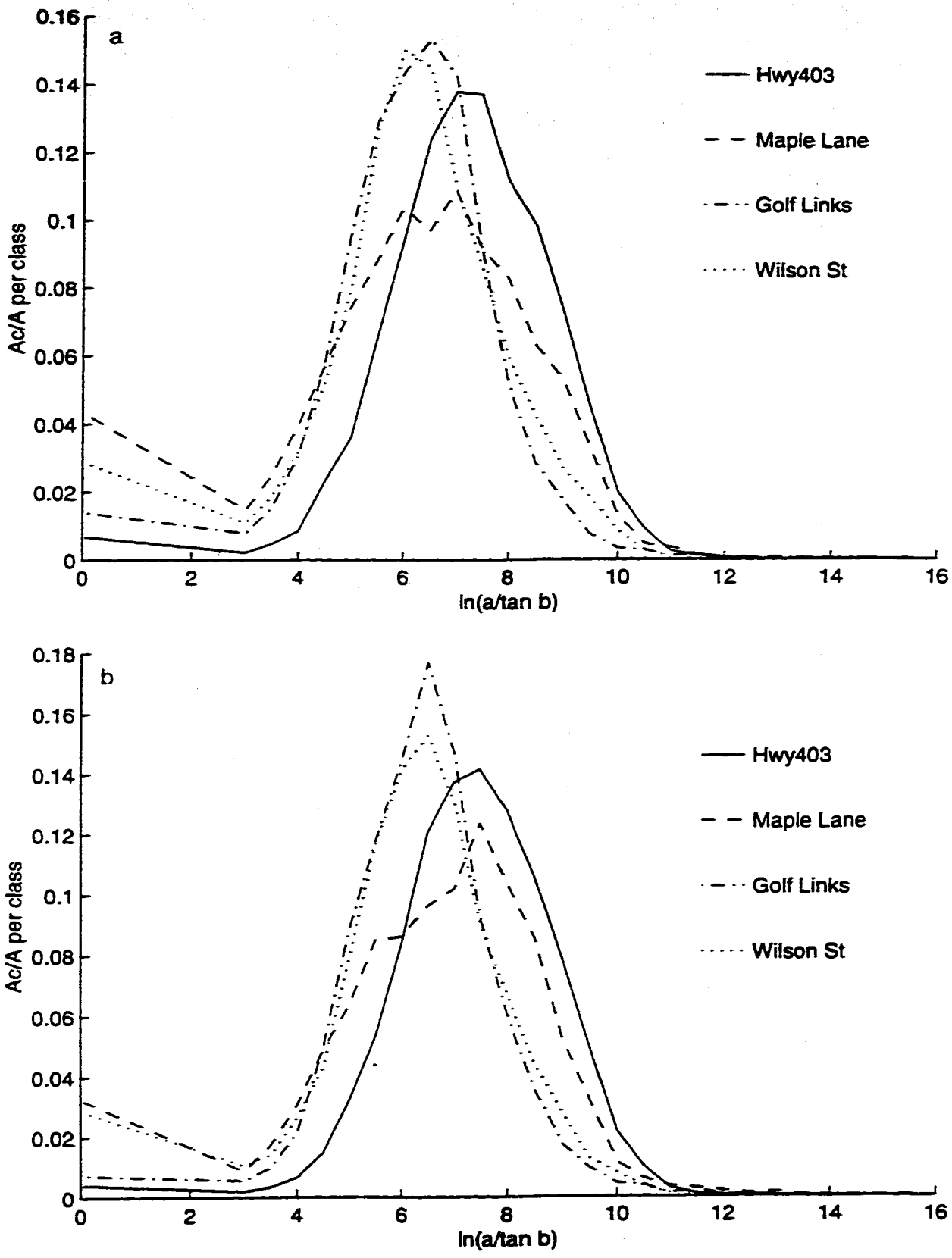

A15: Distribution of topographic index for each subcatchment for a) 10 m DEM and b) 15 m DEM.

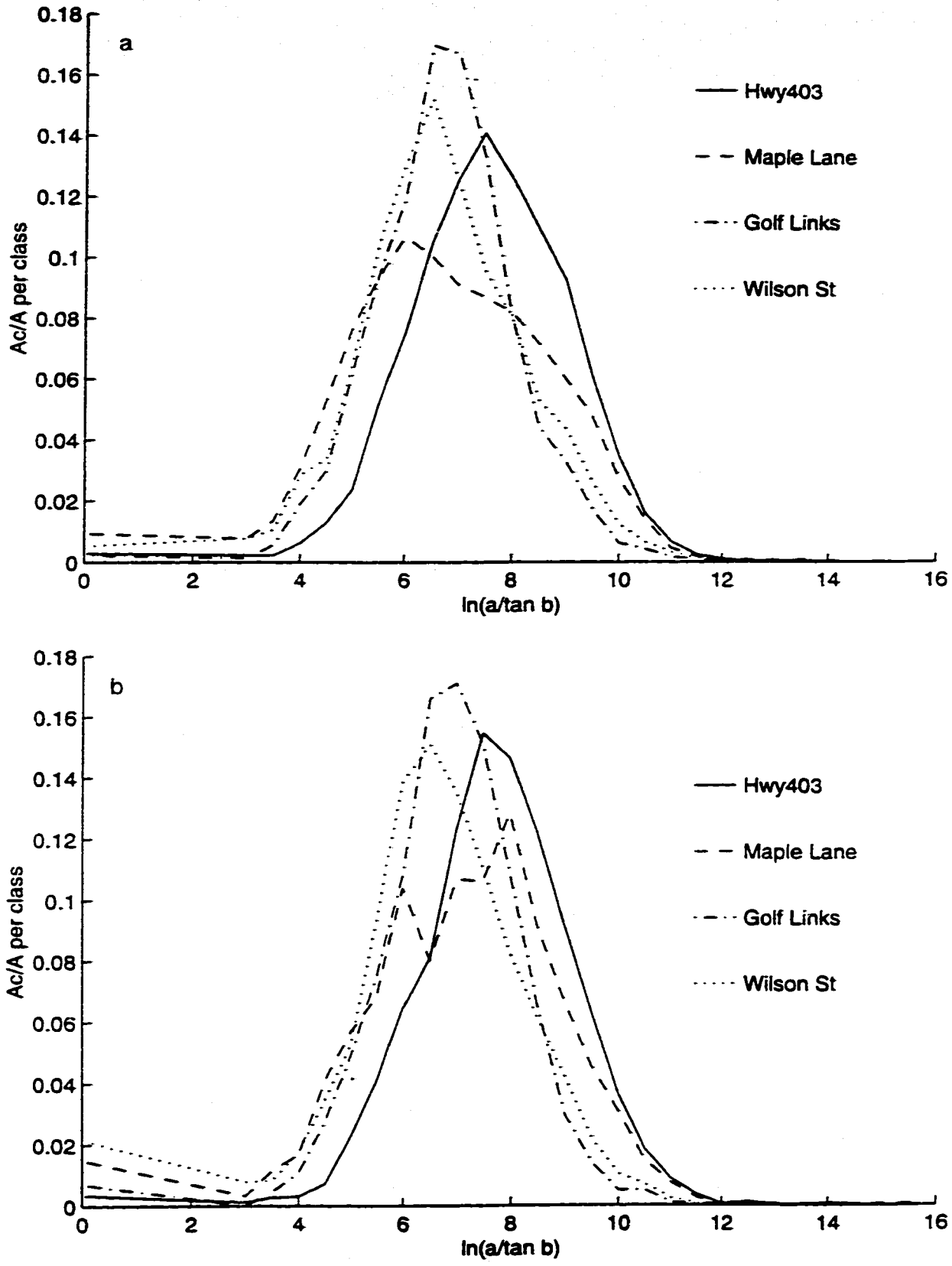

A16: Distribution of topographic index for each subcatchment for a) 20 m DEM and b) 25 m DEM.

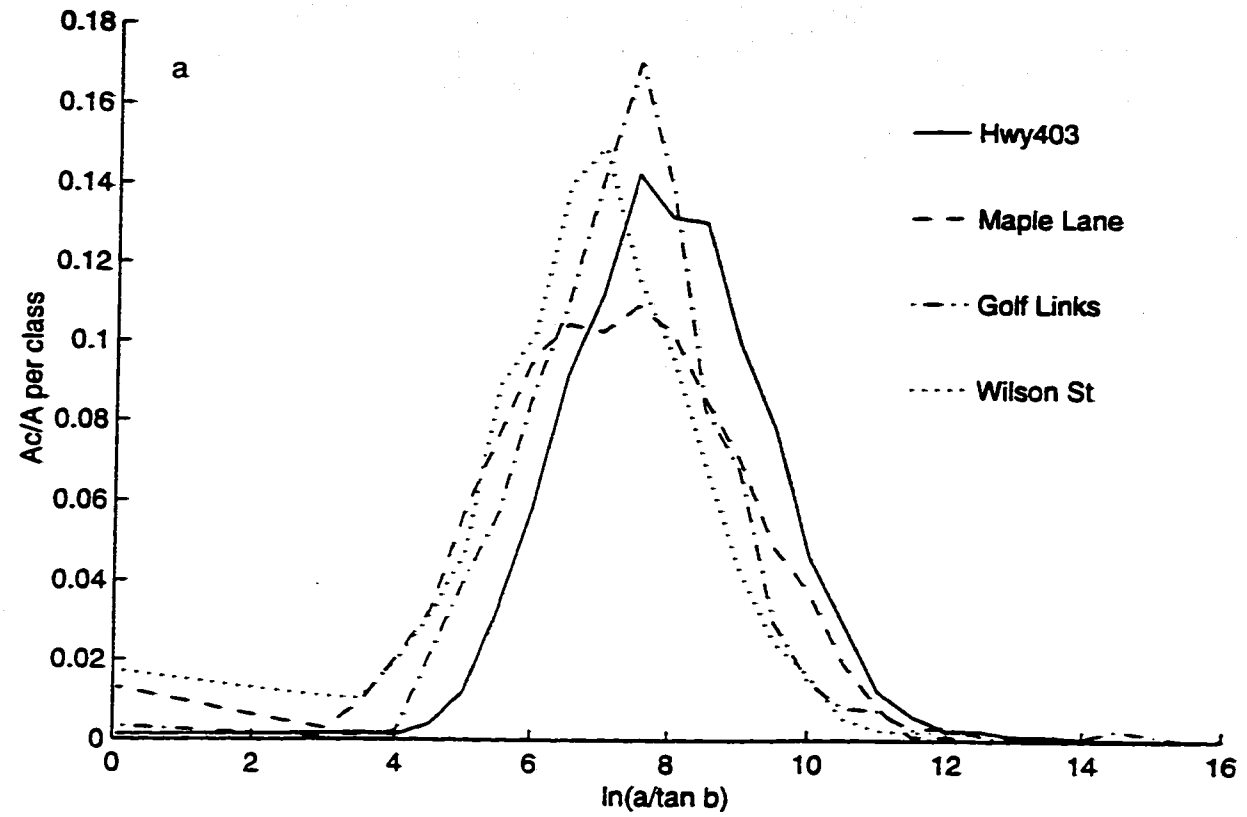

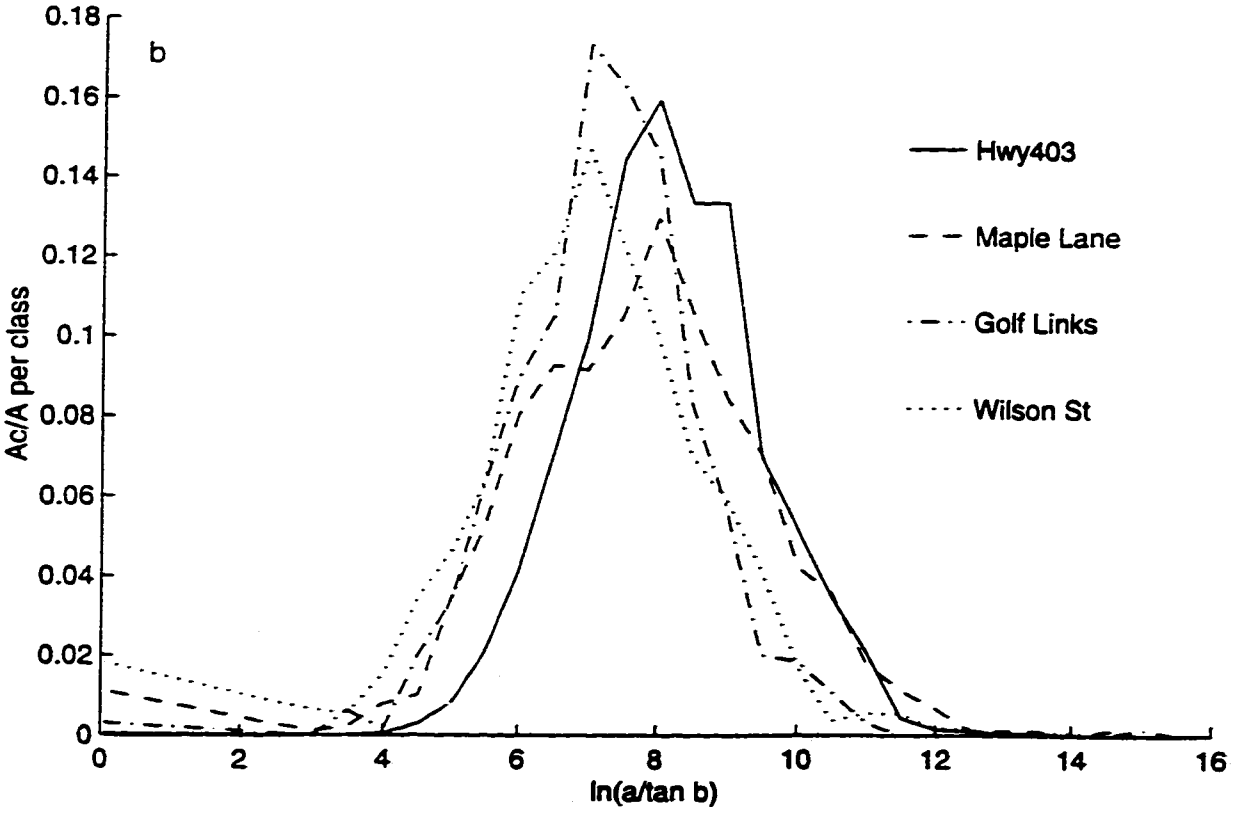

A17: Distribution of topographic index for each subcatchment for a) 30 m DEM and b) 40 m DEM.

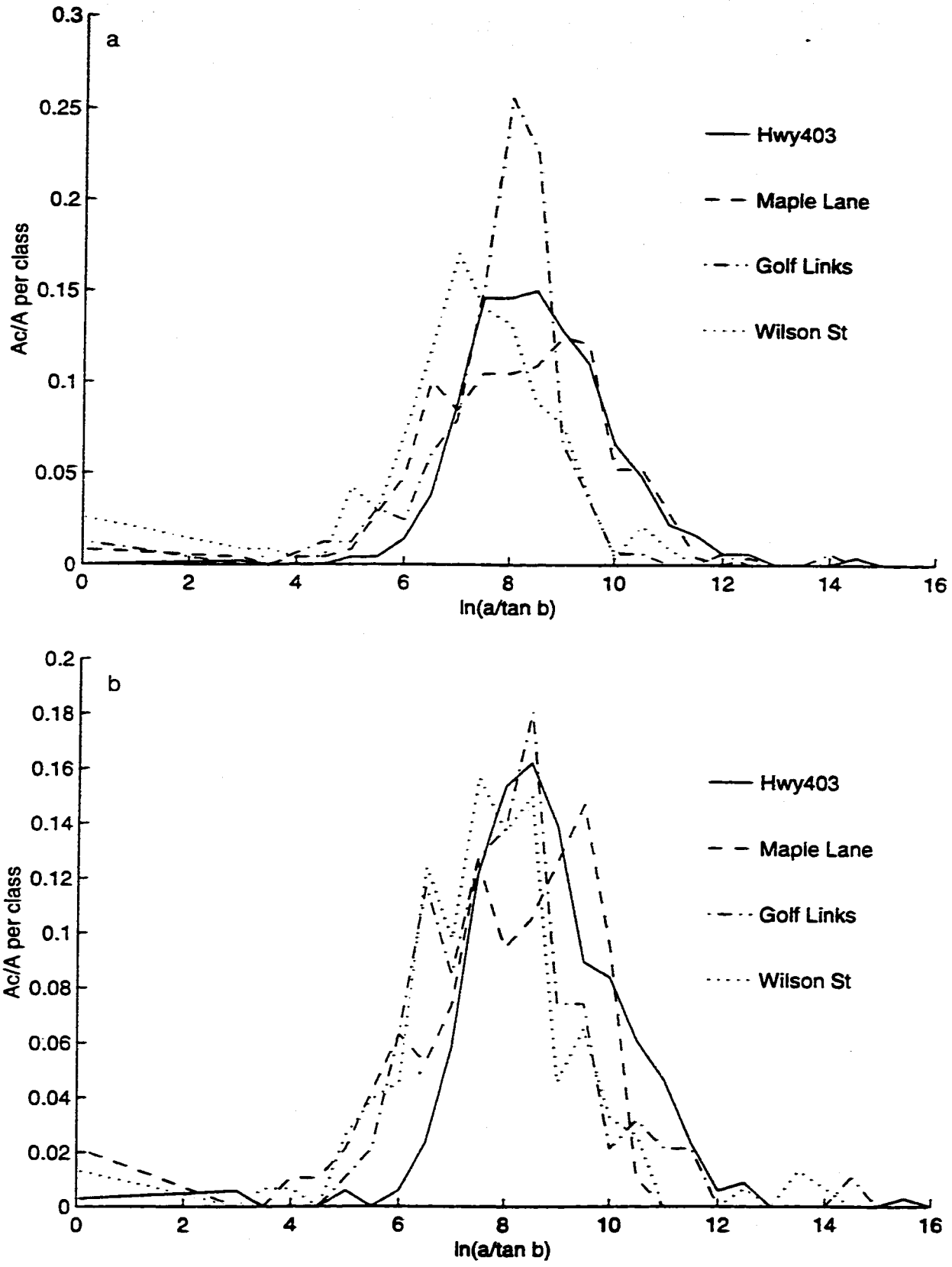

A18: Distribution of topographic index for each subcatchment for a) 50 m DEM and b) 60 m DEM.

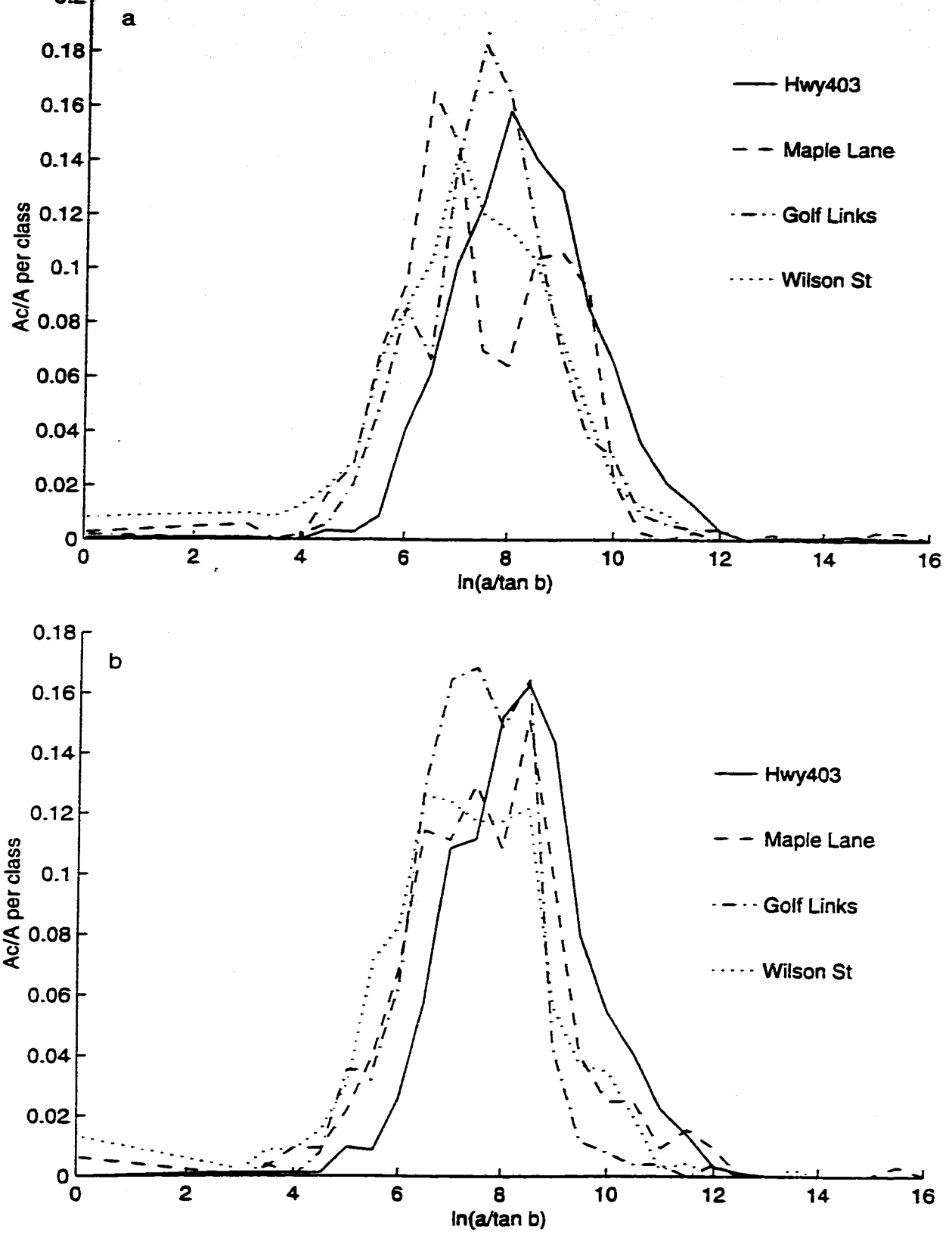

A19: Distribution of topographic index for each subcatchment for a) 80 m DEM and b) 100 m DEM.

A20: TOPURBAN sample input files.

Batch File: `TOPMOD.RUN`

```
Ancaster Creek
in10_91.dat
sb10_91.dat
ot10_91.dat
opter.dat
1 0
```

This batch file is the very first file that is accessed by TOPURBAN and tells the model where to find specific information. The meteorological and hydrometric data is contained in `in10_91.dat`, the subcatchment characteristics are contained in `sb10_91.dat`, the output file is `ot10_91.dat`. The parameters are found in `opter.dat`. The last line has two flags: the first details the amount of output and the second tells the model whether or not to optimize the parameters.

Input File: `in10_91.dat`

```
3888 1.0 4
   0.0000000   0.0000000   0.0000380
   0.0000000   0.0000000   0.0000380
   0.0000000   0.0000000   0.0000384
   0.0000000   0.0000000   0.0000399
   0.0000000   0.0000000   0.0000399
   0.0000000   0.0000158   0.0000394
   0.0000000   0.0001497   0.0000384
   0.0000000   0.0002997   0.0000380
```

The first line in this file contains the number of time steps, the time step length in hours and the number of subcatchments. This is then followed by the precipitation, potential evapotranspiration and flowrates on each line for each time step.

Subcatchment Characteristics File: `sb10_91.dat`

```
Hwy403
32 0.4325 0.0284
   0.00000  18.00000
   0.00000  17.50000

   0.00468   3.50000
   0.00214   3.00000
   0.00679   0.05000
0.000038 1 3 3800.0 3800.0  90505025.0
0.0 3604.6 0.34 4112.7 1.0 4571.0
Maple Lane
32 0.1692 0.3390
   0.00000  18.00000
   0.00000  17.50000

   0.02511   3.50000
   0.01463   3.00000
   0.04303   0.05000
0.000038 1 1 3800.0 3800.0  112628672.0
0.0 2753.7
Golf Links
32 0.1574 0.0959
   0.00000  18.00000
   0.00008  17.50000

   0.01547   3.50000
   0.00782   3.00000
   0.01396   0.05000
0.000038 1 1 3800.0 3800.0   79587021.0
```

This file contains information for each subcatchment. The first line has the subcatchment name; second line is the number of $ln(a/tan\beta)$ classes, followed by the fraction of total catchment area for this subcatchment followed by the fraction of subcatchment area that is urbanized. The next series of lines contain the fraction of subcatchment area for each class. The last two lines for each subcatchment contain the following information,
Q_o, FLG, N_{RV}, v_{RV}, v_{CHV}, A^*B/S_o
A_k, l_k (for $k = 1$ to N_{RV}). Note that $FLG = 1$ for channel routing, else 0.

```
0.0 1692.7
Wilson St
32 0.2409 0.3133
   0.00000  18.00000
   0.00000  17.50000

   0.01890   3.50000
   0.01083   3.00000
   0.02852   0.05000
0.000038 0 3 3800.0 3800.0   1.0
0.00 0.0 0.28 562.9 1.00 1692.7
```

Parameter File: `opter.dat`

```
1
0.0484  4.0  1.0 0.224 0.0004
1 0.95  0.50 0.50
0.047 0.242 0.28  20.0
0.000000000003  50  100
    0.0476042  3.07537  0.28736   0.2630429   0.241051  9.76035
    0.0547096  3.81828  0.279114  0.2166150  0.275744  13.7858
    0.0484330  4.19618  0.283499   0.224416  0.317345  18.9907
    0.0497605  4.38021  0.282474   0.226109  0.261587   12.3764
    0.0793432  4.04947  0.240373   0.04359  0.293311   14.4008
    0.0691298  2.51821  0.142689   0.047955   0.317348  18.9909
    0.0693609  2.3208   0.0775368  0.0421356  0.29548   17.0483
```

The parameter file contains the following information:
No. of runs
m, Ko, T_d, Sr_{max}, Sr_o
Infiltration Excess Terms
F_{RV}, F_{CHV}, $uacp$, zk
tolerance, min. no. of iter., max. no. of iter.
Initial estimates of parameters in the optimization

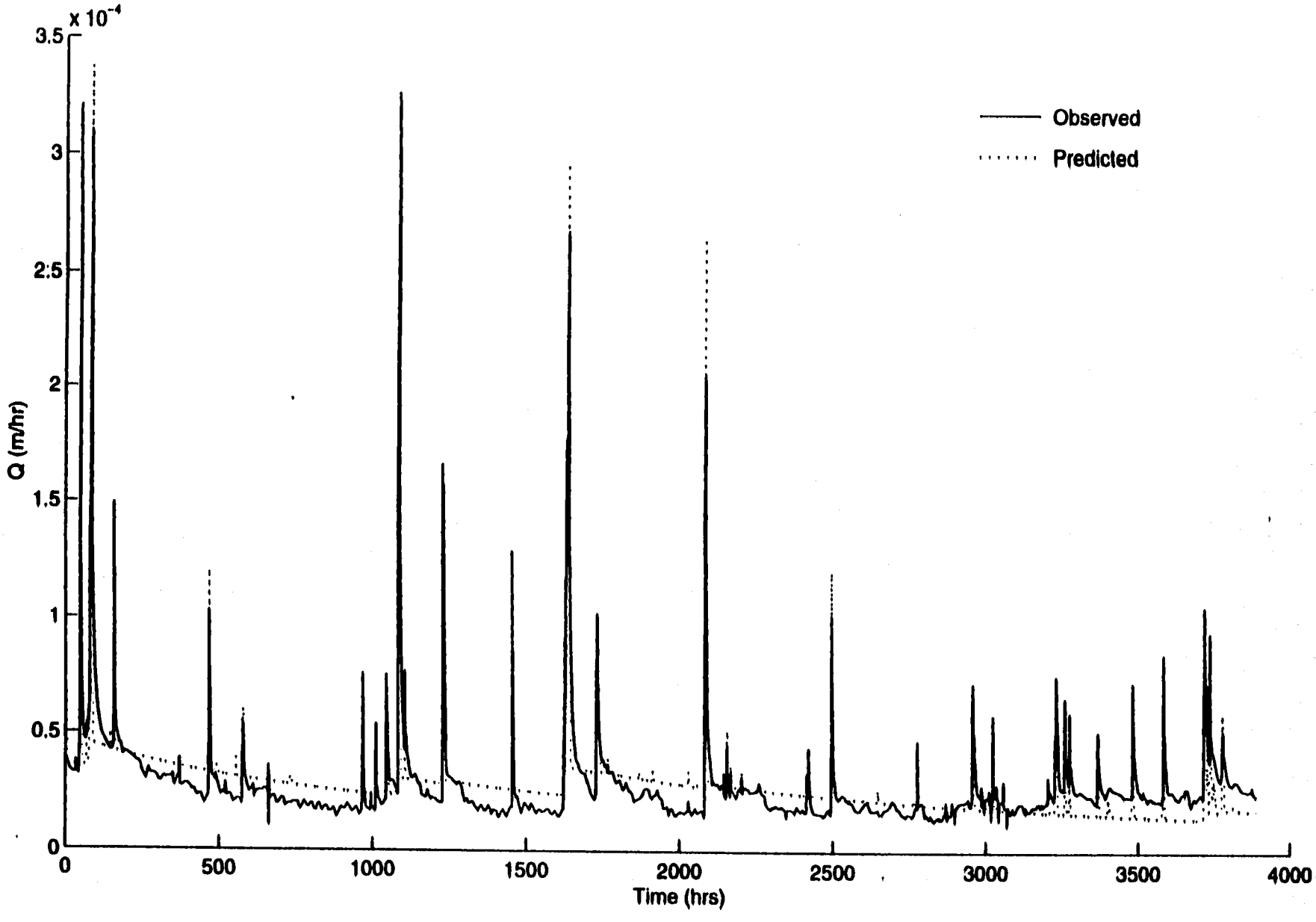

A21: Observed vs. predicted flowrates for the 15 m DEM in 1991.

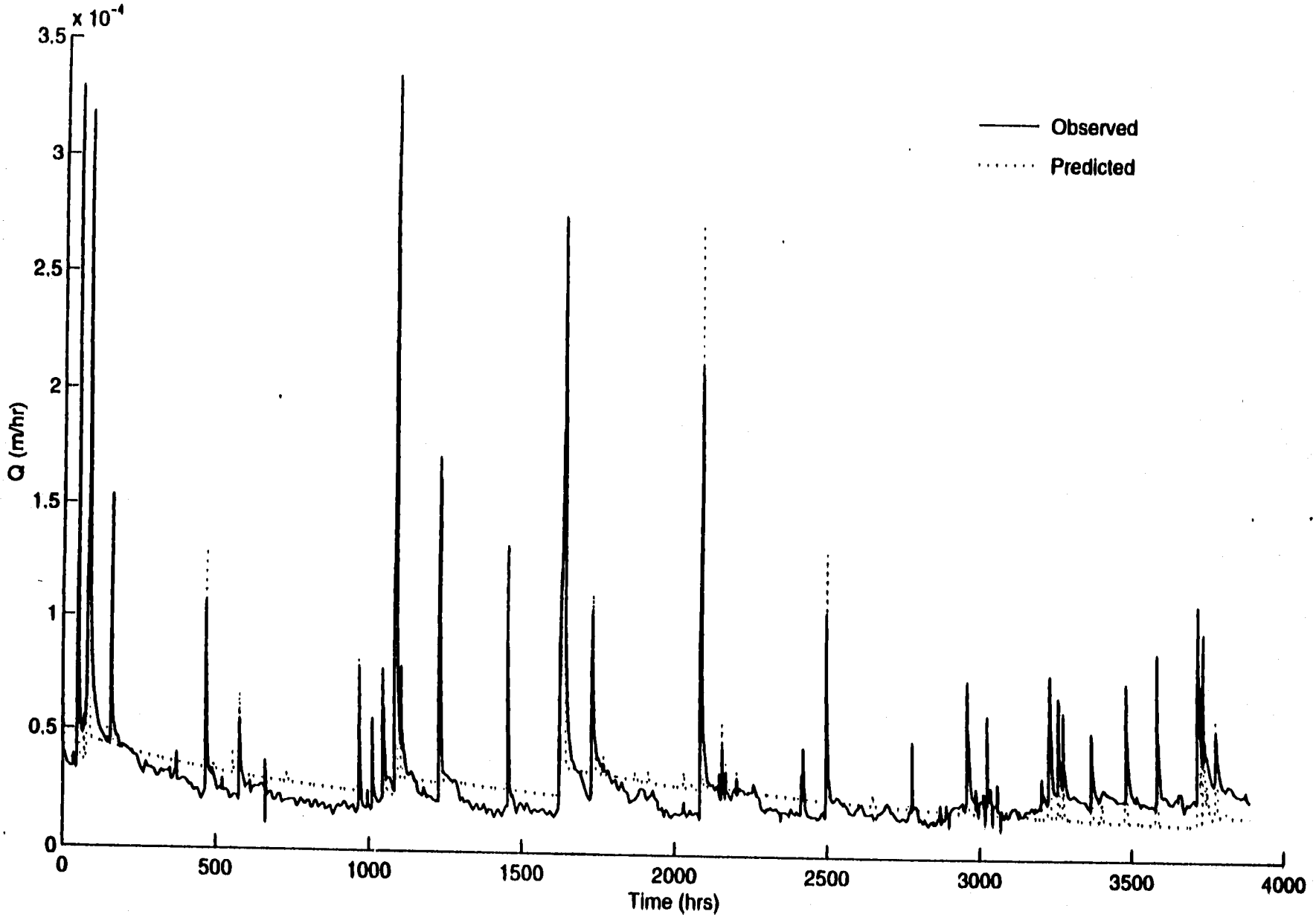

A22: Observed vs. predicted flowrates for the 20 m DEM in 1991.

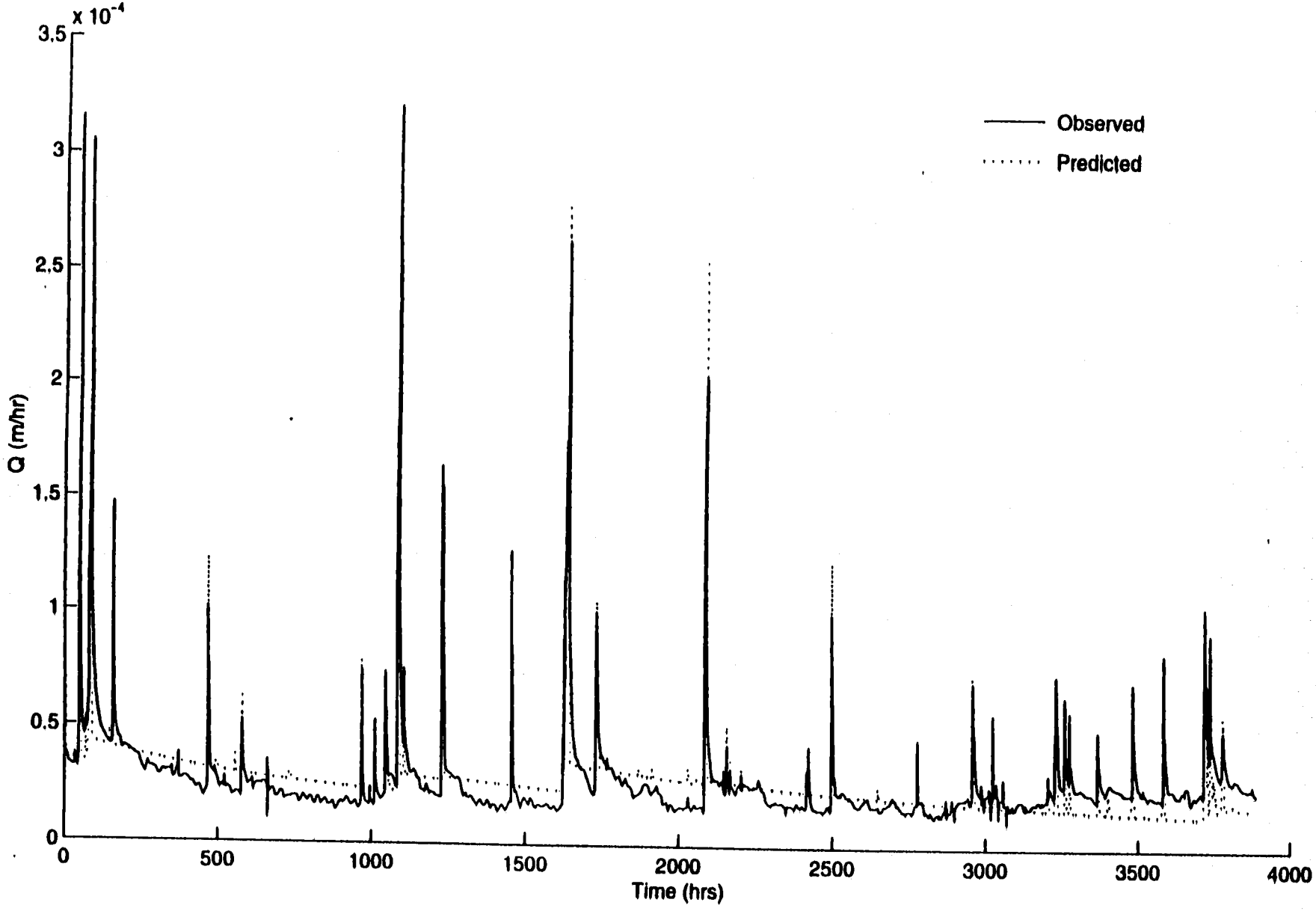

A23: Observed vs. predicted flowrates for the 25 m DEM in 1991.

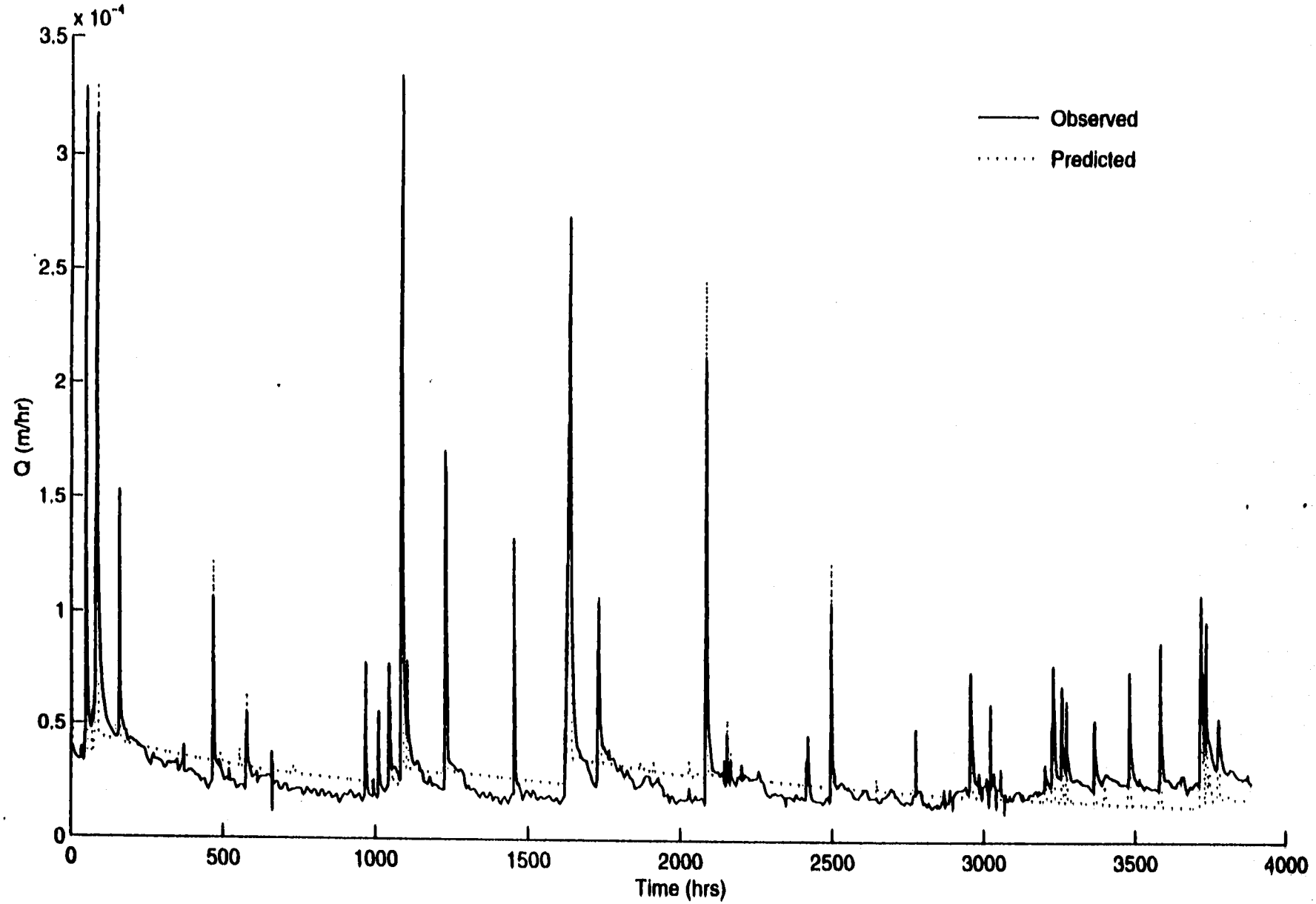

A24: Observed vs. predicted flowrates for the 30 m DEM in 1991.

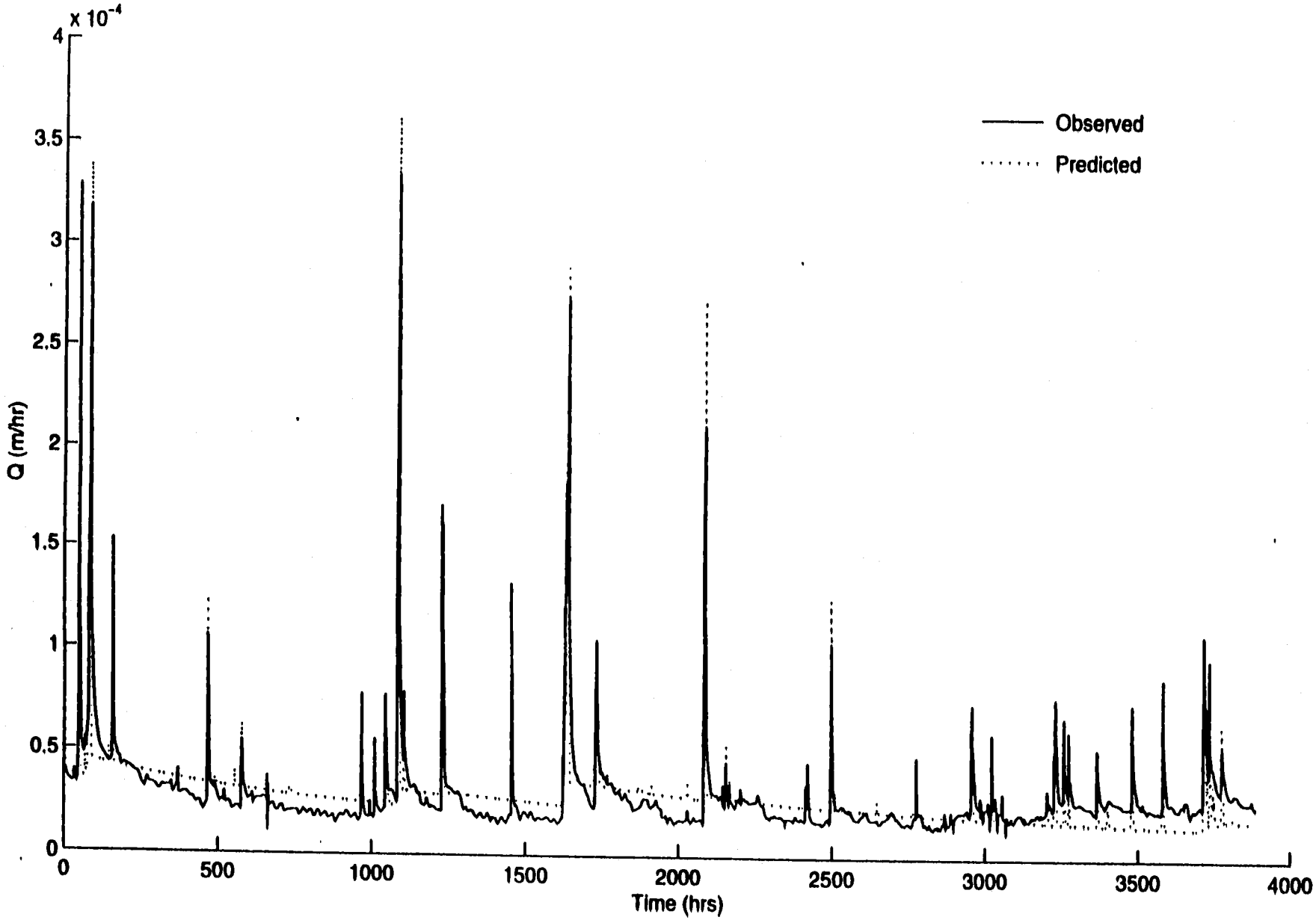

A25: Observed vs. predicted flowrates for the 40 m DEM in 1991.

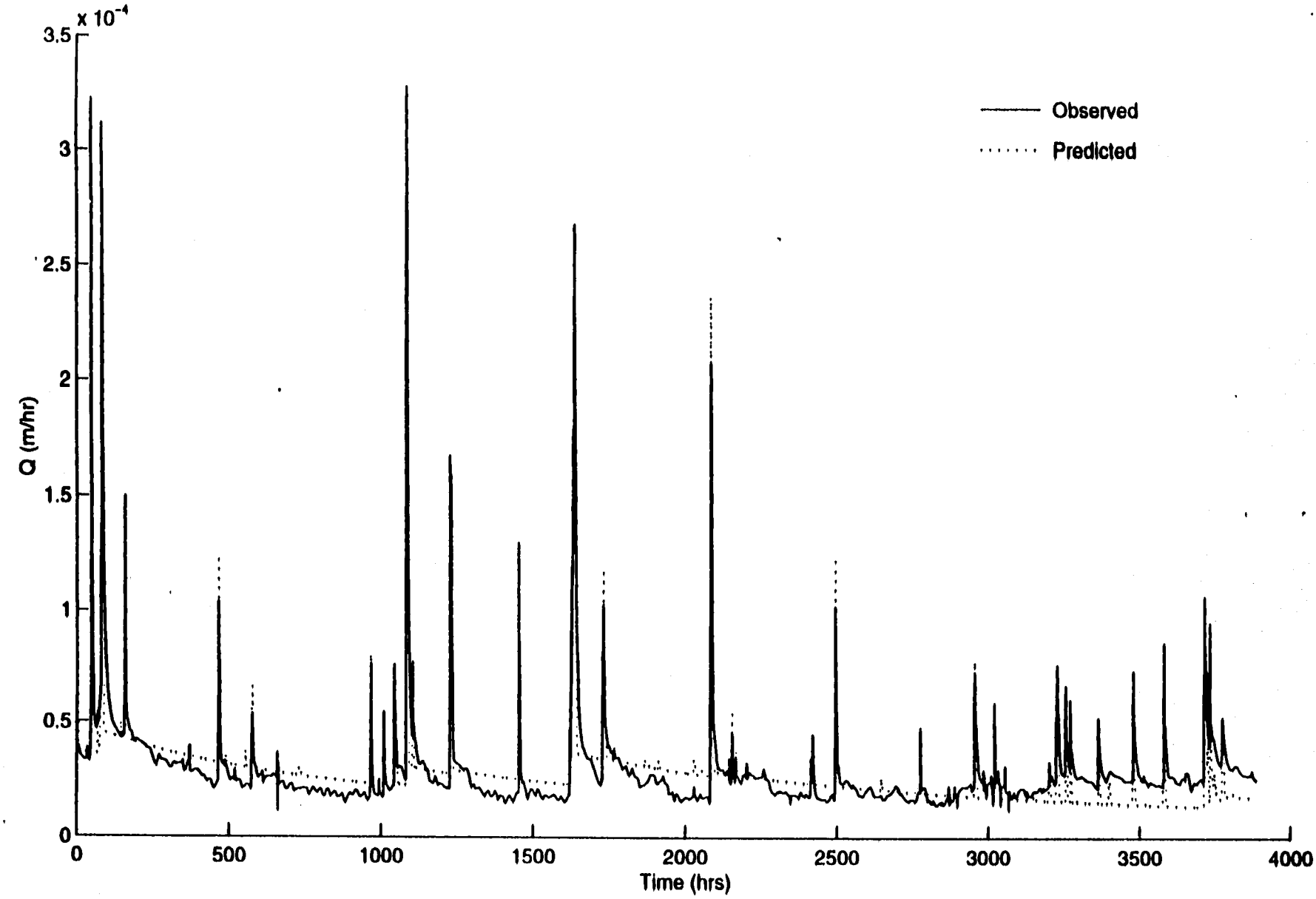

A26: Observed vs. predicted flowrates for the 50 m DEM in 1991.

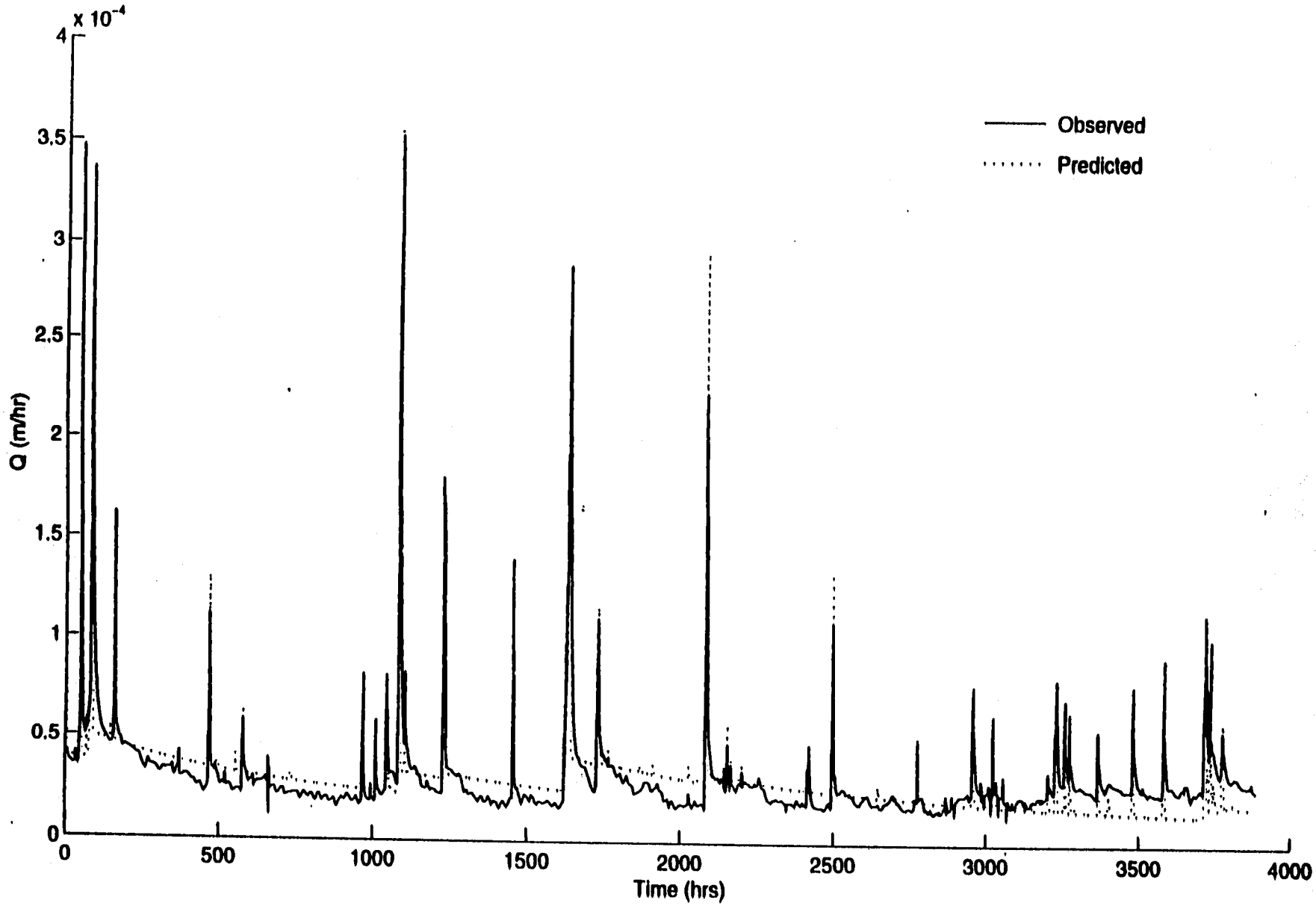

A27: Observed vs. predicted flowrates for the 60 m DEM in 1991.

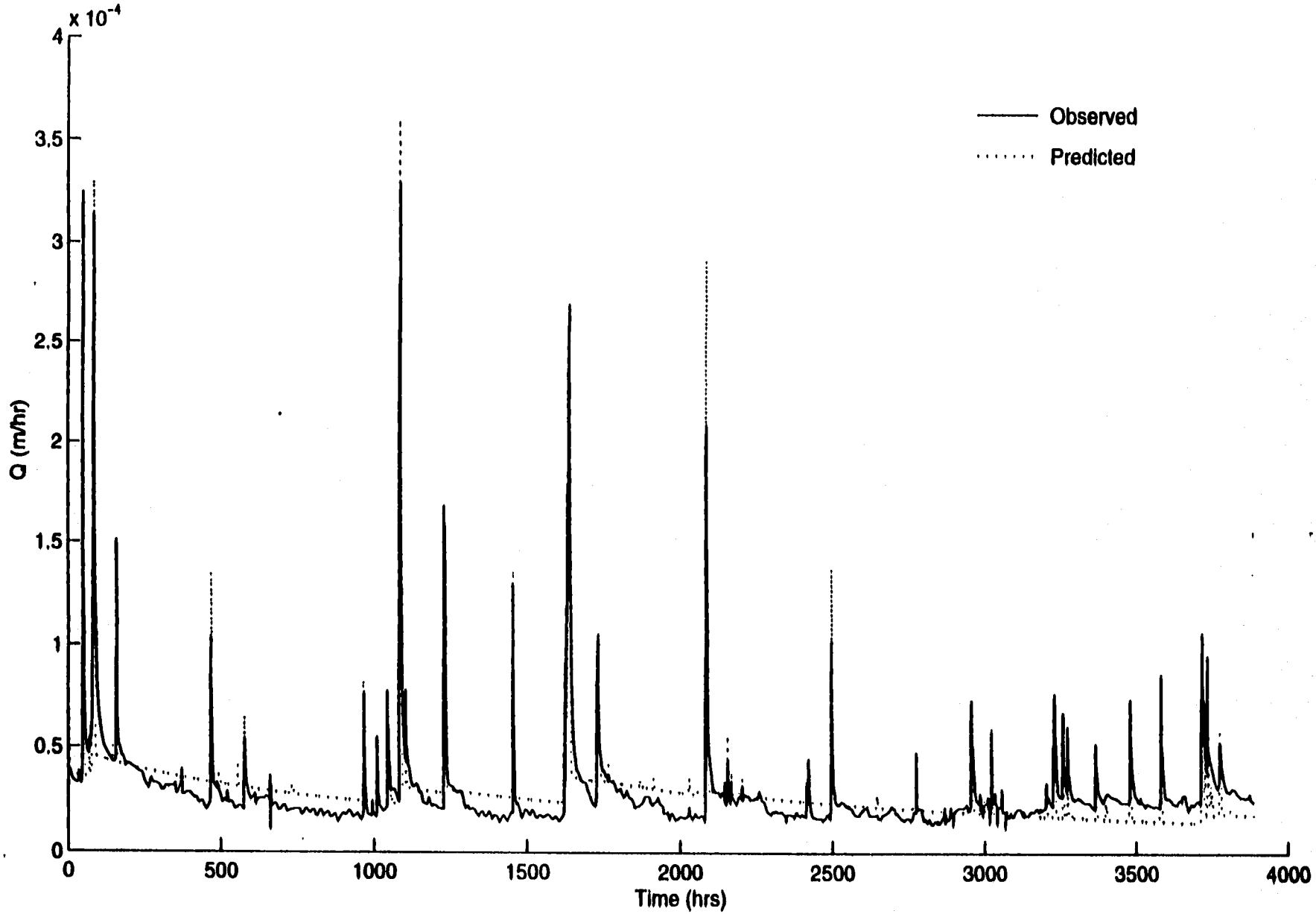

A28: Observed vs. predicted flowrates for the 80 m DEM in 1991.

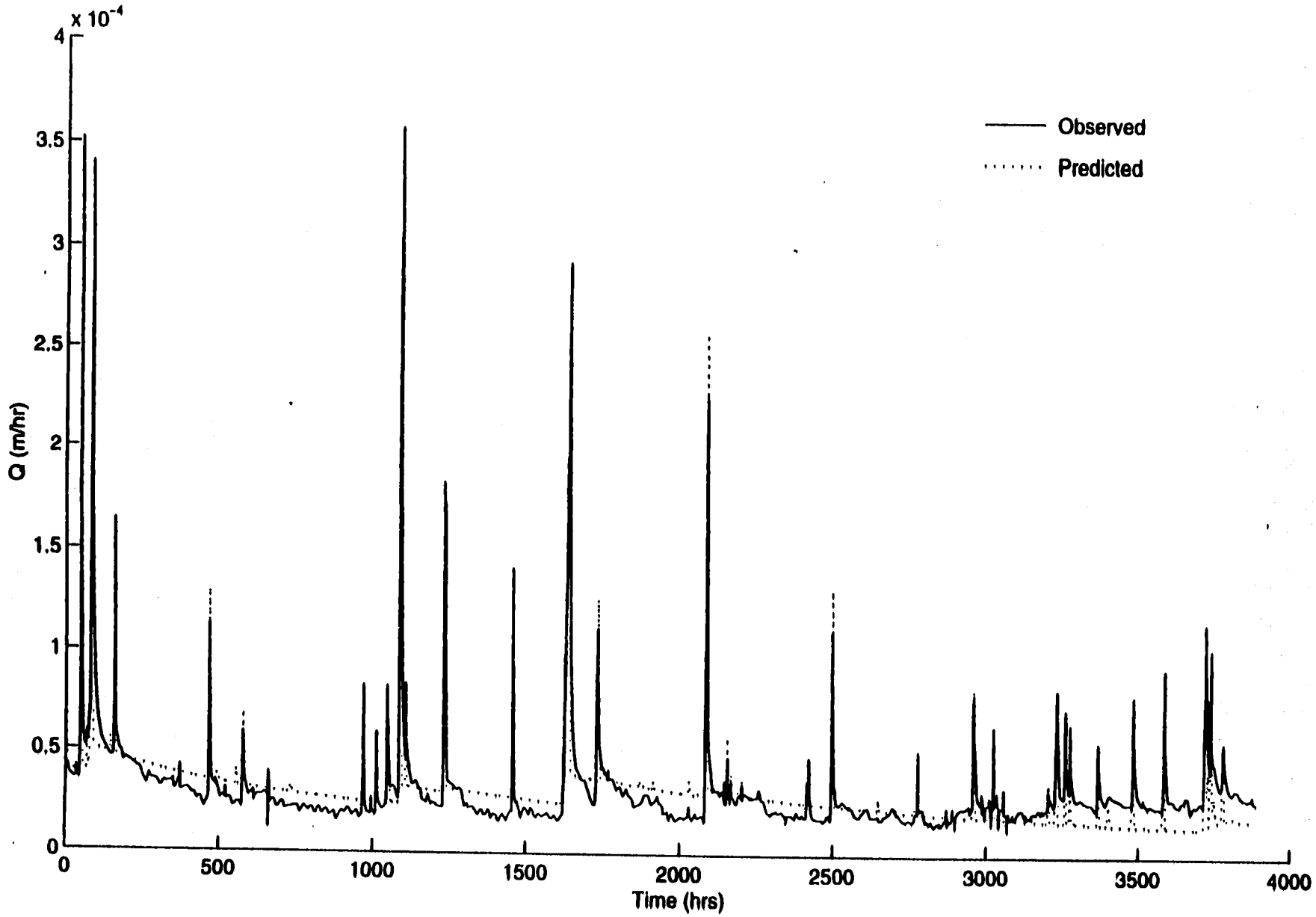

A29: Observed vs. predicted flowrates for the 100 m DEM in 1991.

A30: Statistics for evaluating TOPURBAN with DEM size in 1988 and 1991.

Table A30.1: Statistics for TOPURBAN performance on the dry year 1988.

DEM	$\Sigma x10^{-8}$	$\Sigma 1x10^{-3}$	D_{max}	D_{min}	D_{avg}	$\sigma^2 x10^{-9}$
10	8.6703	7.878	71.174	6.451	34.756	5.78
15	28.018	14.726	98.263	1.4286	61.718	18.7
20	8.081	7.499	68.071	5.9101	33.584	5.39
25	7.549	7.556	65.942	1.5155	36.303	5.03
30	7.179	6.791	65.144	2.088	31.255	4.79
40	8.948	7.7844	70.894	6.923	33.862	5.97
50	7.0829	6.826	63.663	0.421	32.551	4.72
60	10.064	8.020	67.662	4.089	34.3053	6.71
80	8.7215	7.556	70.142	6.0584	35.321	5.81
100	8.451	7.224	64.845	1.0271	30.955	5.63

Table A30.2: Statistics for TOPURBAN performance on the wet year 1991.

DEM	$\Sigma x10^{-8}$	$\Sigma 1x10^{-3}$	D_{max}	D_{min}	D_{avg}	$\sigma^2 x10^{-9}$
10	1.01970	1.17823	246.519	3.00722	43.8655	3.92192
15	1.10078	1.22712	230.019	1.87147	45.2915	4.23377
20	0.970085	1.14744	228.030	2.03917	42.5448	3.73110
25	0.857762	1.07514	215.747	1.71566	41.7170	3.29909
30	1.22885	1.24921	156.731	2.95937	41.4588	4.72635
40	1.47055	1.39824	170.961	9.06020	45.9309	5.65598
50	0.839944	1.03535	191.804	0.643445	40.5749	3.23055
60	1.67766	1.48738	191.094	5.47792	47.3646	6.45254
80	1.28351	1.32555	220.068	7.64153	47.1571	4.93657
100	1.30248	1.28728	206.041	1.80996	44.2243	5.00953

A31: Proceedure for computing curve numbers using ARC/INFO.

Step 1: Intersect the polygon soils coverage (Figure 4.2) with the polygon coverage of the subbasins (Figure 7.10) to create another polygon coverage called **MACSOIL**.

Step 2: Go to **TABLES** and add an item called **DRN** to **MACSOIL.PAT** using the `ADDITEM` command.

Step 3: `SELECT` all polygons with the "**DRAIN_1**" attribute in **MACSOIL.PAT** equal to "**WELL**". These are the well draining soils so assign them a **DRN** value of 1. Similarly, the 3 other types of soils in the soils coverage were assigned the following values: Imperfectly and variably draining soils were assigned a value of 2, and both poorly and very poorly draining soils were assigned a value of 4. This procedure was necessary as a numeric value was required to describe the drainage in future steps.

Step 4: Convert the polygon coverage to a grid called **D-TEMP** with cell size of 50 m using `POLYGRID` and only preserving the attribute **DRN**

Step 5: Create **CN** Using a `DOCELL` loop and a series of `IF` commands on the grid **D-TEMP**, with the following assignments:

D-TEMP = 1 → CN = 72
D-TEMP = 2 → CN = 82
D-TEMP = 3 → CN = 87
IF D-TEMP = 1 & (Subcatchment Number = 363 or 363) → CN = 65
IF D-TEMP = 2 & (Subcatchment Number = 363 or 363) → CN = 75
IF D-TEMP = 3 & (Subcatchment Number = 363 or 363) → CN = 82

Step 6: Assume that urban areas are 40% impervious as in MacLaren (1990). Let **URB** be a grid where cells having a value of 1 indicate an urban area, and 0 otherwise. Then if **URB** = 1, assign the corresponding cell in **CN** a value of

```
CN = CN * 0.6 + 0.4*98
```

where the impervious areas have been assigned a curve number value of 98.

Step 7: Compute the final curve numbers for each subcatchment by using the `ZONALMEAN` command:

```
CNAVG = ZONALMEAN(MACSHEDS, CN)
```

where **CNAVG** is the grid of average curve numbers for each subcatchment, and **MACSHEDS** is the grid containing the subcatchments (a grid of the polygon coverage shown in Figure 7.10).

The curve number assignments shown in steps 5, 6 and 7 were adopted from the MacLaren Plansearch's study on the Spencer Creek Watershed (Vol. II).

Table A31.1: Curve Number (AMC II) for Existing Landuse

Land Use	Soil A	Soil B	Soil C
Urban Pervious	72	82	87
Row Crops	65	75	82

The assumption was made that in the soils map, well draining soils were of soil type A; variable and imperfectly draining soils were of soil type B; and poorly draining soils were soil type C. The row crop land use was chosen for subcatchments 363 and 362 shown in Figure 7.10. It was felt that these subcatchments contained very little urbanization and some farming of the "row crop" type.

A32: QualHYMO Input File for 1991.

```
1234567890 *./-
21
START                  1 25
STORE                  2  4
GENERATE               3 27
PRINT SPAN             4 10
PLOT SPAN              5 10
ADD SERIES             6  4
POND                   7310
REACH                  8310
CALIBRATE              9310
POLLUTANT RATES       10  9
SPLIT SERIES          11310
DUMP PRINT            12  1
EXCEEDANCE CURVES     13310
DUMP PLOT             14  9
FINISH                15  0
COMPUTE RATING CURVE  16310
COMPUTE TRAVEL TIME   17  5
STORE TRAVEL TIME     18100
ROUTE                 19  4
PRINT PEAK            20  2
ROUTE MC              21 10
** ANCASTER CREEK WATERSHED
** QUALHYMO MODEL - DISCRETIZED SUBCATCHMENTS
** CALIBRATION RUN   SEPT. 1997
**
** SUMMER MODEL - FUTURE CONDITIONS -
**
START                  SIMULATE FROM  91 05 23 TO 91 10 31
                       RAIN RECORDS ON FILE 9
                       WATER SURVEY FLOW RECORDS ON FILE 10
                       CASE=1 (API METHOD)
**
** ANCASTER CREEK
**
GENERATE              IDOUT=3 ISER=362 DT= 1.00 HR
                      DA=235.5 HA AB=0 FRIMP=0.0202
                      IMPERVIOUS DATA***
                      AA=1 KORH=1.028 TPORL=1.2 HRS
                      ABSIMP=2. MM RIMP=0.95
                      PERVIOUS DATA***
                      AA=2  KORH=14.6 TPORL=1.9
                      SMIN=46.4 SMAX=1082.4 MM SK=0.14
                      APIK=0.9 APII=10.5
                      ABSER=15. MM SVOL = 15. MM  SLOSKI=0.000025
                      SLOSK=0.0 BASMIN=0.01068 CMS
                      BASET=0.0 SNOFAC=-1 PACDEP=0
PRINT PEAK             ID=3 NPEAK=1
GENERATE              IDOUT=2 ISER=363 DT= 1.00 HR
                      DA=140.25 HA AB=0 FRIMP=0.1355
                      IMPERVIOUS DATA***
                      AA=1 KORH=1.028 TPORL=1.2 HRS
                      ABSIMP=2. MM RIMP=0.95
                      PERVIOUS DATA***
                      AA=2  KORH=13.3 TPORL=2.3
                      SMIN=44.3 SMAX=1033.4 MM SK=0.14
                      APIK=0.9 APII=10.5
                      ABSER=15. MM SVOL = 15. MM  SLOSKI=0.000025
                      SLOSK=0.0 BASMIN=0.00636 CMS
                      BASET=0.0 SNOFAC=-1 PACDEP=0
PRINT PEAK             ID=2 NPEAK=1
ADD SERIES             ID=4 ISER=154 IDI=2 IDII=3
PRINT PEAK            ID=4  NPEAK=1
*<<<<<<<<<<<<<<<<<<<<<<<<<<<<<<<<<<<< ROUTING REACH 31 >>>>>>>>>>>>>>>>>>>>>>>>>>>>>>>>
*
COMPUTE RATING CURVE ID=1  VALLEY SECTION= 31.0 WHICH IS DIVIDED INTO 3 SECTIONS
                      ELEVATION >  MIN=232.8 M    MAX=237.3   M
                      SLOPE >     CHANNEL=0.00350   FLOODPLAIN=0.00350
```

```
                    N=0.05 DIST=30.5 N=-.035 DIST=33.5 N= .05  DIST=57.2
                     DIST      ELEV      DIST      ELEV      DIST      ELEV
                      0.       237.3       5.3     234.7      16.8     234.1
                     30.5      233.8      30.5     233.2      32.0     232.8
                     33.5      233.2      33.5     233.8      42.2     234.0
                     51.2      234.5      52.9     235.3      55.1     235.8
                     57.2      237.3
COMPUTE TRAVEL TIME ID= 2     REACH NO = 31  NO OF VALLEY SECTIONS= 1
                    LENGTH= 855.            SLOPE= 0.0035
ROUTE MC            ID=2      HYD NO=1031  INFLOW HYD ID= 4
                    LENGTH = 855. SLOPE = .0035 RATING CURVE ID = 1
                    SECTIONS =4  PCODE = 0
PRINT PEAK          ID=2 NPEAK=1
GENERATE            IDOUT=3 ISER=364 DT= 1.00 HR
                    DA=104.8 HA AB=0 FRIMP=0.2482
                    IMPERVIOUS DATA***
                    AA=1 KORH=1.028 TPORL=1.2 HRS
                    ABSIMP=2. MM RIMP=0.95
                    PERVIOUS DATA***
                    AA=2  KORH=19. TPORL=1.3
                    SMIN=31.1 SMAX=726.4 MM SK=0.14
                    APIK=0.9 APII=10.5
                    ABSER=15. MM SVOL = 15. MM  SLOSKI=0.000025
                    SLOSK=0.0 BASMIN=0.004752 CMS
                    BASET=0.0 SNOFAC=-1 PACDEP=0
PRINT PEAK           ID=3 NPEAK=1
ADD SERIES           ID=4 ISER=155 IDI=2 IDII=3
PRINT PEAK          ID=4  NPEAK=1
*<<<<<<<<<<<<<<<<<<<<<<<<<<<<<<<< ROUTING REACH 32 >>>>>>>>>>>>>>>>>>>>>>>>>>>>
*
COMPUTE RATING CURVE ID=1  VALLEY SECTION= 32.0 WHICH IS DIVIDED INTO 3 SECTIONS
                     ELEVATION >  MIN=229.9 M    MAX=234.4   M
                     SLOPE >     CHANNEL=0.00580   FLOODPLAIN=0.00580
                     N=0.05 DIST=54. N=-.035 DIST=87.6 N= .05  DIST=107.6
                      DIST      ELEV      DIST      ELEV      DIST      ELEV
                       0.       237.7      10.9     233.0      32.1     230.6
                      54.0      230.8      57.9     230.4      57.9     229.9
                      58.6      229.9      59.3     229.9      59.9     230.5
                      74.6      230.7      87.6     230.9      97.2     232.0
                     107.6      234.4
COMPUTE TRAVEL TIME ID= 2     REACH NO = 32  NO OF VALLEY SECTIONS= 1
                    LENGTH= 770.            SLOPE= 0.0058
ROUTE MC            ID=2      HYD NO=1032  INFLOW HYD ID= 4
                    LENGTH = 770. SLOPE = .0058 RATING CURVE ID = 1
                    SECTIONS =4  PCODE = 0
PRINT PEAK          ID=2 NPEAK=1
GENERATE            IDOUT=3 ISER=365 DT= 1.00 HR
                    DA=65.5 HA AB=0 FRIMP=0.0534
                    IMPERVIOUS DATA***
                    AA=1 KORH=1.028 TPORL=1.2 HRS
                    ABSIMP=2. MM RIMP=0.95
                    PERVIOUS DATA***
                    AA=2  KORH=24.5 TPORL=1.4
                    SMIN=32.9 SMAX=766.7 MM SK=0.14
                    APIK=0.9 APII=10.5
                    ABSER=15. MM SVOL = 15. MM  SLOSKI=0.000025
                    SLOSK=0.0 BASMIN=0.00296 CMS
                    BASET=0.0 SNOFAC=-1 PACDEP=0
PRINT PEAK           ID=3 NPEAK=1
ADD SERIES           ID=4 ISER=156 IDI=2 IDII=3
PRINT PEAK          ID=4  NPEAK=1
GENERATE            IDOUT=2 ISER=366 DT= 1.00 HR
                    DA=65.25 HA AB=0 FRIMP=0.1571
                    IMPERVIOUS DATA***
                    AA=1 KORH=1.028 TPORL=1.2 HRS
                    ABSIMP=2. MM RIMP=0.95
                    PERVIOUS DATA***
                    AA=2  KORH=23.1 TPORL=1.4
                    SMIN=32.9 SMAX=766.7 MM SK=0.14
                    APIK=0.9 APII=10.5
                    ABSER=15. MM SVOL = 15. MM  SLOSKI=0.000025
                    SLOSK=0.0 BASMIN=0.00296 CMS
```

```
                    BASET=0.0 SNOFAC=-1 PACDEP=0
PRINT PEAK           ID=2 NPEAK=1
ADD SERIES           ID=3 ISER=157 IDI=2 IDII=4
PRINT PEAK          ID=3  NPEAK=1
*<<<<<<<<<<<<<<<<<<<<<<<<<<<<<<<< ROUTING REACH 33 >>>>>>>>>>>>>>>>>>>>>>>>>>>>>>>>
*
COMPUTE RATING CURVE ID=1  VALLEY SECTION= 33.0 WHICH IS DIVIDED INTO 3 SECTIONS
                     ELEVATION >  MIN=224.4 M    MAX=229.8    M
                     SLOPE >     CHANNEL=0.00320   FLOODPLAIN=0.00320
                     N=0.05 DIST=43.5 N=-.035 DIST=49.7 N= .05  DIST=284.1
                      DIST      ELEV      DIST      ELEV      DIST      ELEV
                       0.       229.8      13.6     228.1      17.5     226.5
                      34.9      226.1      43.5     225.7      44.8     224.7
                      47.1      224.4      49.4     224.5      49.7     225.5
                     110.1      225.6     140.1     225.8     170.1     226.3
                     265.1      227.5     284.1     228.3

COMPUTE TRAVEL TIME ID= 2     REACH NO = 33  NO OF VALLEY SECTIONS= 1
                    LENGTH= 785.              SLOPE= 0.0032
ROUTE MC            ID=2      HYD NO=1033  INFLOW HYD ID= 3
                    LENGTH = 785. SLOPE = .0032 RATING CURVE ID = 1
                    SECTIONS =4  PCODE = 0
PRINT PEAK          ID=2 NPEAK=1
GENERATE            IDOUT=3 ISER=367 DT= 1.00 HR
                    DA=67.5 HA AB=0 FRIMP=0.1407
                    IMPERVIOUS DATA***
                    AA=1 KORH=1.028 TPORL=1.2 HRS
                    ABSIMP=2. MM RIMP=0.95
                    PERVIOUS DATA***
                    AA=2  KORH=25.4 TPORL=1.4
                    SMIN=29.4 SMAX=687.1 MM SK=0.14
                    APIK=0.9 APII=10.5
                    ABSER=15. MM SVOL = 15. MM  SLOSKI=0.000025
                    SLOSK=0.0 BASMIN=0.0030623 CMS
                    BASET=0.0 SNOFAC=-1 PACDEP=0
PRINT PEAK           ID=3 NPEAK=1
ADD SERIES           ID=4 ISER=158 IDI=2 IDII=3
PRINT PEAK          ID=4  NPEAK=1
*<<<<<<<<<<<<<<<<<<<<<<<<<<<<<<<< ROUTING REACH 34 >>>>>>>>>>>>>>>>>>>>>>>>>>>>>>>>
*
COMPUTE RATING CURVE ID=1  VALLEY SECTION= 34.0 WHICH IS DIVIDED INTO 3 SECTIONS
                     ELEVATION >  MIN=221.7 M    MAX=225.    M
                     SLOPE >     CHANNEL=0.00860   FLOODPLAIN=0.00860
                     N=0.05 DIST=52.5 N=-.035 DIST=56.4 N= .05  DIST=155.0
                      DIST      ELEV      DIST      ELEV      DIST      ELEV
                       0.       225.0      24.0     222.8      35.0     222.3
                      52.5      222.5      53.5     221.8      54.0     221.7
                      55.3      221.9      56.4     222.2      56.5     222.6
                      84.0      222.8      155.     225.0
COMPUTE TRAVEL TIME ID= 2     REACH NO = 34  NO OF VALLEY SECTIONS= 1
                    LENGTH= 870.              SLOPE= 0.0086
ROUTE MC            ID=2      HYD NO=1034  INFLOW HYD ID= 4
                    LENGTH = 870. SLOPE = .0086 RATING CURVE ID = 1
                    SECTIONS =4  PCODE = 0
PRINT PEAK          ID=2 NPEAK=1
GENERATE            IDOUT=3 ISER=368 DT= 1.00 HR
                    DA=114.75 HA AB=0 FRIMP=0.5882
                    IMPERVIOUS DATA***
                    AA=1 KORH=1.028 TPORL=1.2 HRS
                    ABSIMP=2. MM RIMP=0.95
                    PERVIOUS DATA***
                    AA=2  KORH=26.7 TPORL=1.6
                    SMIN=26.2 SMAX=611.4 MM SK=0.14
                    APIK=0.9 APII=10.5
                    ABSER=15. MM SVOL = 15. MM  SLOSKI=0.000025
                    SLOSK=0.0 BASMIN=0.00521 CMS
                    BASET=0.0 SNOFAC=-1 PACDEP=0
PRINT PEAK           ID=3 NPEAK=1
ADD SERIES           ID=4 ISER=159 IDI=2 IDII=3
PRINT PEAK          ID=4  NPEAK=1
DUMP PRINT          ID=4
FINISH
```

A33: Precipitation used in return period studies.

The following storm depths and distributions were obtained from the Ontario Ministry of Natural Resources (1985) for the RBG for a 12 hour storm.

Distribution for the 2 year to 100 year return storms:

Hour	Fraction	Hour	Fraction
1	0.13	7	0.02
2	0.24	8	0.01
3	0.22	9	0.01
4	0.15	10	0.00
5	0.13	11	0.00
6	0.09	12	0.00

Storm depths for a given return frequency (mm):

Return Frequency	Depth
2	42.8
5	57.6
10	67.4
25	79.6
50	88.7
100	97.7

Hurricane Hazel rainfall for drainage areas equal to or less than 25 km^2

Hour	Rainfall (mm)
First 36	73
37	6
38	4
39	6
40	13
41	17
42	13
43	23
44	13
45	13
46	53
47	38
48	13
Total	285